https://ntrs.nasa.gov/search.jsp?R=19940020866 2020-06-16T13:56:34+00:00Z

NASA Contractor Report 188271

National Aeronautics and Space Administration (NASA)/American Society for Engineering Education (ASEE) Summer Faculty Fellowship Program - 1993

Volume 1

William A. Hyman, Editor
Texas A&M University
College Station, Texas

Stanley H. Goldstein, Editor
University Programs Office
Lyndon B. Johnson Space Center
Houston, Texas

Grant NGT 44-001-800

National Aeronautics and Space Administration
Lyndon B. Johnson Space Center

1993

Preface

The 1993 Johnson Space Center (JSC) National Aeronautics and Space Administration (NASA)/American Society for Engineering Education (ASEE) Summer Faculty Fellowship Program was conducted by Texas A&M University and JSC. The program at JSC, as well as the programs as other NASA centers, was funded by the Office of University Affairs, NASA Headquarters, Washington, D.C. The objectives of the program, which began nationally in 1964 and at JSC in 1965, are

1. To further the professional knowledge of qualified engineering and science faculty members

2. To stimulate an exchange of ideas between participants and NASA

3. To enrich and refresh the research and teaching activities of participants' institutions

4. To contribute to the research objectives of the NASA centers

Each faculty fellow spent at least 10 weeks at JSC engaged in a research project in collaboration with a NASA/JSC colleague. This document is a compilation of the final reports on the research projects done by the faculty fellows during the summer of 1993. Volume 1 contains reports 1 through 18 and Volume 2 contains reports 19 through 35.

PRECEDING PAGE BLANK NOT FILMED

Contents

PRECEDING PAGE BLANK NOT FILMED

Contents
(continued)

Contents
(concluded)

N94- 25349

DATA ANALYSIS AND INTERPRETATION OF LUNAR DUST EXOSPHERE

Final Report

NASA/ASEE Summer Faculty Fellowship Program--1993

Johnson Space Center

Prepared By:	George A. Andrews, Jr.
Academic Rank:	Assistant Professor of Physics
University & Department:	LeTourneau University Division of Natural Sciences Longview, Texas 75607
NASA\JSC	
Directorate:	Space and Life Sciences
Division:	Solar System Exploration
Branch:	Space Science
JSC Colleague:	Andrew Potter, Ph.D.
Date Submitted:	August 13, 1993
Contract Number	NGT-44-001-800

ABSTRACT

The lunar horizon glow observed by Apollo astronauts and recorded during the Surveyor missions is believed to result from the scattering of sunlight off lunar fines suspended in a dust layer above the lunar surface. For scale heights of tens of kilometers, theory and astronaut's observations suggest that the size of the dust particles will be smaller than 0.1 microns in radius and will act as Rayleigh scatters. This means that the dust scattered light will be 100% polarized at a 90 degree scattering angle and will depend on wavelength to the inverse fourth power ("bluing"). Believing these signatures to be observable from ground based telescopes, observational data in the form of CCD images has been collected from McDonald Observatory's 36" telescope and the reduction and analysis of this data is the focus of the present report.

INTRODUCTION

Evidence for electrically charged lunar fines above the moon's surface was recorded by the LEAM experiments conducted on the Moon [Berg et al., 1976]. In these experiments, charged particles were detected by three detectors with peak activity occurring with the passage of the daylight/dark terminator. In addition, Surveyor photographs taken at sunset [Rennilson and Criswell, 1974] and the Lunokhod-2 detection of "lunar twilight" brightness [Severny at el., 1974], as well as observations sketched and reported by astronauts just before sunrise, provide powerful evidence for the existence of light-scattering dust particles in the vicinity of the terminator.

If the scattering particles have a size that is smaller than about one sixth of the incident wavelength, the intensity of the scattered light depends on wavelength to the inverse fourth power and is classified as Rayleigh scattering. Hence, shorter wavelength (blue) light will be preferentially scattered. In addition, this light will be nearly 100% polarized when the moon is near first and third quarter with the degree of polarization decreasing with an increase or decrease of the moon's phase. This decrease in polarization is expected since an increase in phase corresponds to a decrease in the scattering angle between the incident and reflected rays.

In this report, we summarize the results and analysis of observations taken at various wavelengths of light at four different lunar sites using the 36 inch reflecting telescope at the McDonald observatory.

REDUCTION & ANALYSIS

The Signal

Light arriving at the telescope from the moon's surface is expected to consist of four components: 1) sunlight scattered directly off the surface, 2) "earthshine" back-scattered off the moon's surface, 3) luminescence from the lunar soil and 4) light scattered from dust above the lunar surface. While the magnitude of the luminescent light can be substantial [Kopal 1966], its occurrence is transient in nature and tends to be confined both in locality and to emission of photons possessing longer wavelengths; hence, in our hunt for dust, we can reasonably ignore this source.

From the before-mentioned probes and observations, the dust particles causing lunar horizon glow (LHG) would be expected to have a maximum contrast with background sources of light up to a few tens of kilometers from the terminator in the anti-sun (dark side) direction. Thus, within this region, scattered sunlight from the bright moon will be held to a minimum; however, there will be some light from the bright moon scattered

from the earth's atmosphere into the telescope, but this light will be approximately the color of scattered moonlight and should reflect lunar polarization effects for each wavelength.

The percent polarization of the signal is defined as

$$P(\%) = 100 (I_{\perp} - I_{\parallel} / I_{\perp} + I_{\parallel})$$

where $I_{\perp}$ is the intensity of the light measured with the polarizer perpendicular to the scattering plane (defined as the plane containing the incident sun ray and the reflected moon ray) and $I_{\parallel}$ is the intensity of the light measured with the polarizer oriented parallel to the scattering plane. Dollfus [Dollfus 1970] has established that the polarization of red light reflected from the bright moon is on average one half that of blue light. Hence, in the vicinity of the terminator, any relative increase in the intensity and polarization of blue light compared to longer wavelengths *greater* than that which has been observed on the bright moon can be taken as indicative of the existence of submicron dust. It is interesting to note that in 1860 Secchi [Secchi 1859], observed a "small difference" in polarization between "the illuminated edge and the area which is adjacent to the edge of the shadow." In addition, Lyot [Lyot 1929] reported that "near the terminator, the polarization goes through a significant increase...." While both of these references refer to the bright side of the terminator, it is not at all improbable that high altitude dust may be the cause of these observed increases in polarization!

Estimates of the brightness of the "bluing" were produced by Herbert Zook on the bases the brightness of the LHG reported by the astronauts (Zook and McCoy, 1991, and private communication). In this report only polarization effects will be discussed since time does not permit the inclusion of estimates of the absolute brightness derivable from the data. The absolute brightness of the signal can be calculated from calibration frames taken of the star β Virgo 4550.

The data frames were corrected to remove spurious signals arising from the CCD bias and pixel to pixel variations. The CCD bias noise was removed to first order by subtracting the "overscan" section of the chip. Any residual noise was further removed by averaging several "zero" frames (images taken with zero exposure time) and subtracting this average from the data. The pixel to pixel variation was eliminated by "flatfielding" each frame with the appropriate flatfield image created by the "dome flat" method familiar to astronomers. Each wavelength and polarization angle has an associated flatfield image.

RESULTS

Figure 1 reveals an image of the moon indicating the location of the four sites that were analyzed. The locations and selenographic coordinates of the sites are as follows: site 1, 15° north latitude and 5° east longitude in Mare Vaporum; site 2, 35° north latitude and

Figure 1.- Location of four sites studied; 1) Mare Vaporum, 2) Mare Imbrium/Caucasus mountains, 3) Mare Imbrium and 4) Oceanus Procellarum.

8° east longitude at the edge of Mare Inbrium and the lower end of the Caucasus mountains; site 3, 23° north latitude and 30° west longitude in Mare Inbrium; site 4, 18° north latitude and 42° west longitude in Oceanus Procellarum.

Site 1.

Figure 2 shows an image of the Moon's surface located in Mare Vaporum. In this image, the terminator is clearly seen with a bright peak reflecting sun light in the upper left hand corner of the frame within the dark side of the terminator. Due to reflective optics in the telescope, this image is actually reversed top-to-bottom so that on the moon, the peak is located in the lower right hand corner. The distances spanned by the image is approximately equal to 279km normal to the terminator and 383km parallel to the terminator. The actual "raw" data spanned distances of 415km in both the parallel and perpendicular directions, but due to edge effects and numerical interpolation associated with the registering of the perpendicular frame with the parallel frame, the data was "trimmed". The letters "A" and "B" will be discussed below.

Examination of the bright side of the terminator revels topographical surface structure at the extreme upper and lower edges of the image. The highland mountains are thousands of meters high and scatter light so as to inhibit illumination of any dust among or behind them. The center portion of the image, however, represents a smooth mare region in Mare Vaporum. It is hypothesized that it is in these relatively smooth low lying areas that dust, existing tens of kilometers into the exosphere, will be detected.

Figures 3-a and 3-b represent horizontal, or east-west polarizations sections (slices) of the image of Mare Vaporum found in figure 2. These are plots of percentage of polarization as a function of distance. The units of distance are in number of pixels (1 pixel = 3.24km). Three different wavelengths are plotted on each graph with the wavelengths indicated on the plot. The multiplicative factors operating on the wavelengths seen in the key represent scale factors required to "normalize" the longer (redder) wavelengths to the shortest blue wavelength. The reason for these scale factors is to look for ***blue enhanced relative*** polarization in the area just past the terminator. Finally, each line represents an average of eleven lines taken east-west across the terminator with the approximate position of the terminator and the direction of the sun explicitly marked in each plot.

Figure 3-a depicts lines taken across the terminator at position "A" marked in figure 2. This position apparently represents the most mountain free east-west slice across the image. In figure 3-a, it is evident that the polarization of the 404nm light exhibits a marked enhancement just past the terminator as compared to the 486nm and 656nm light! While the 486nm light shows a slight enhancement over the 656nm, the enhancement is much

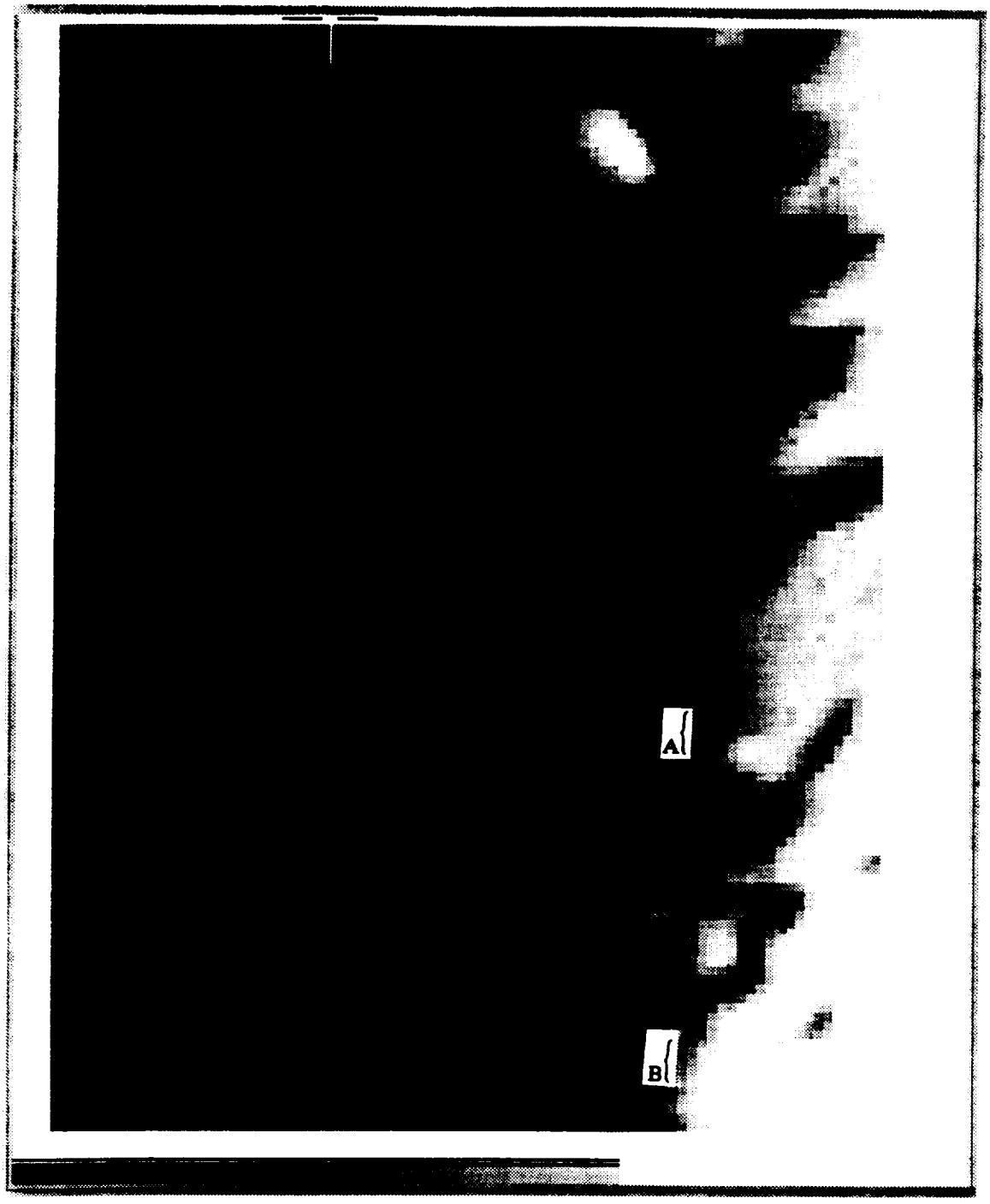

Figure 2.- Mare Vaporum; 15 degrees north latitude and 5 degrees east longitude.

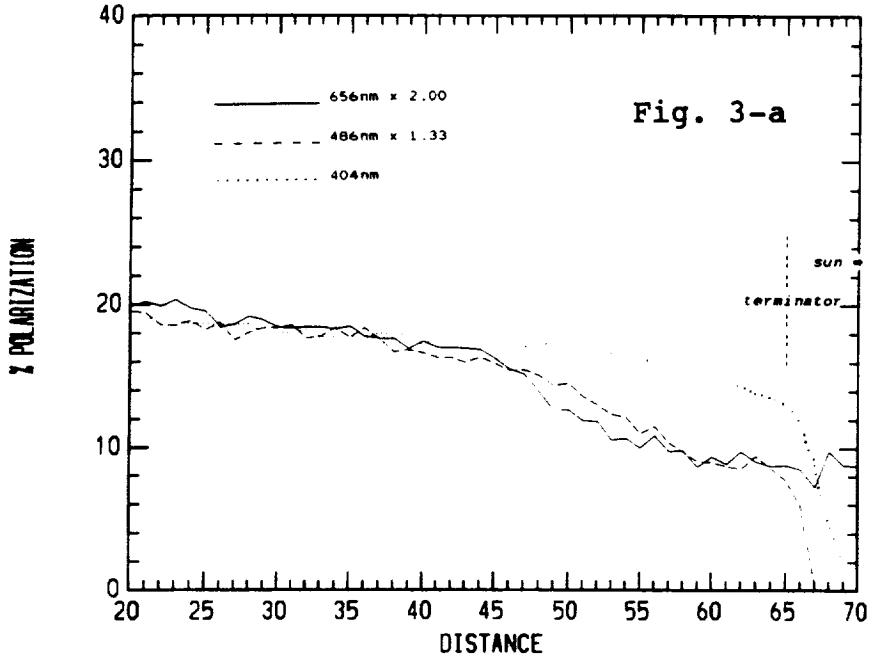

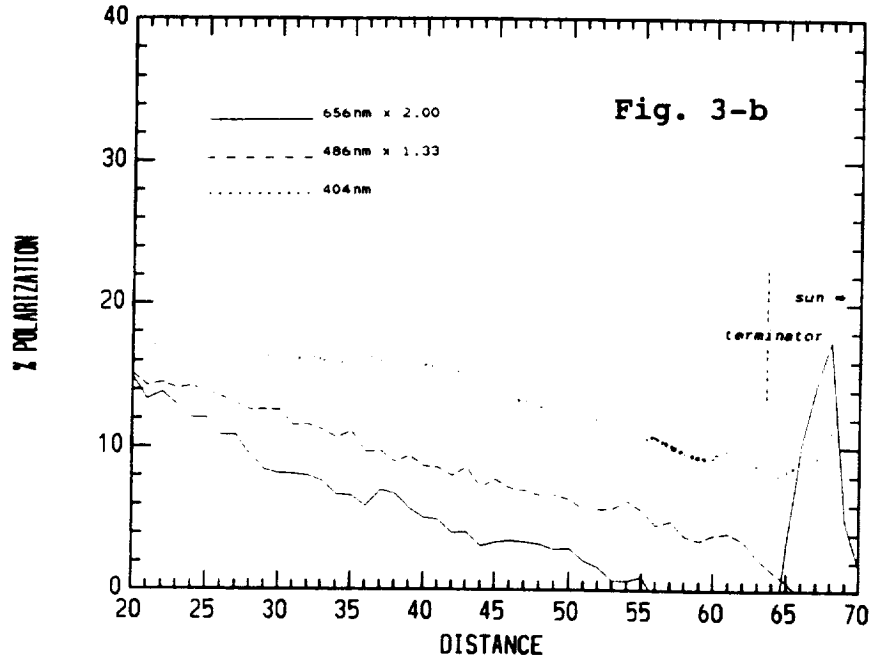

Figure 3.- a) Polarization curves for Mare Vaporum site; 3-a corresponds to the region marked with the letter "A" in figure 2 and 3-b corresponds to the region marked "B".

less than the 404nm light over the 486. Since submicron dust would favor the bluer light in a highly nonlinear way ("inverse lambda to the forth"), this "nonlinear" relationship between subsequent ratios of wavelengths can only be understood in terms of Rayleigh scattered light! It should be noted that further quantitative work on the functional relationship between the intensity and wavelength will be completed at a later date.

Figure 3-b depicts lines taken across the terminator at position "B" marked in figure 2 which is behind the highlands. In this figure, the polarization enhancement of the blue to the red is still seen but is not as strong and a "spreading" of the curves is also evident. This spreading and decrease in enhancement may be interpreted as being caused by decreased sun light due to the shadows of the highlands.

Site 2.
Figure 4 shows an image of the Moon's surface located on the eastern edge of Mare Imbrium with the tip of the Caucasus Mountains visible in the lower right hand corner. This image was taken during the same night as the Mare Vaporum site 1 above, so the light scattering angle is approximately the same.

Polarization plots are shown in figures 5-a and 5-b where figure 5-a represents the area marked "A" in figure 4 and figure 5-b depicts the area marked "B". The average polarization of the 404nm light shows an increase by about 10% compared to the average polarization of the Mare Vaporum plots. While this is probably due to differences in the geological and topographical make up of the lunar terrain [see Gehrels 1964], artifacts of the data processing can not yet be ruled out. Further work is needed to determine the cause and will be done at a future date. In figure 5-a, the enhanced polarization of the 404nm light over the longer wavelengths is evident whereas in figure 5-b it is not. Again, the pattern of increased polarization within topographically smooth areas as compared to mountainous regions is observed.

Site 3.
Site three involves an area of the Moon's surface located on the south-western edge of Mare Imbrium. This site was imaged three nights later so the phase of the moon (hence the scattering angle) has decreased. At this site most of the Mare is topographically smooth. It is thus expected that the enhanced blue polarization phenomenon should reveal itself all along the dark side of the terminator. This is indeed the case as figures 6-a and 6-b reveal, where these figures represent the average of eleven lines taken across the terminator at two different locations.

Site 4.
Our last image was taken of Oceanus Procellarum on the final night of observations when

Figure 4.- Mare Imbrium and Caucasus Mountains; 35 degrees north latitude and 8 degrees east longitude.

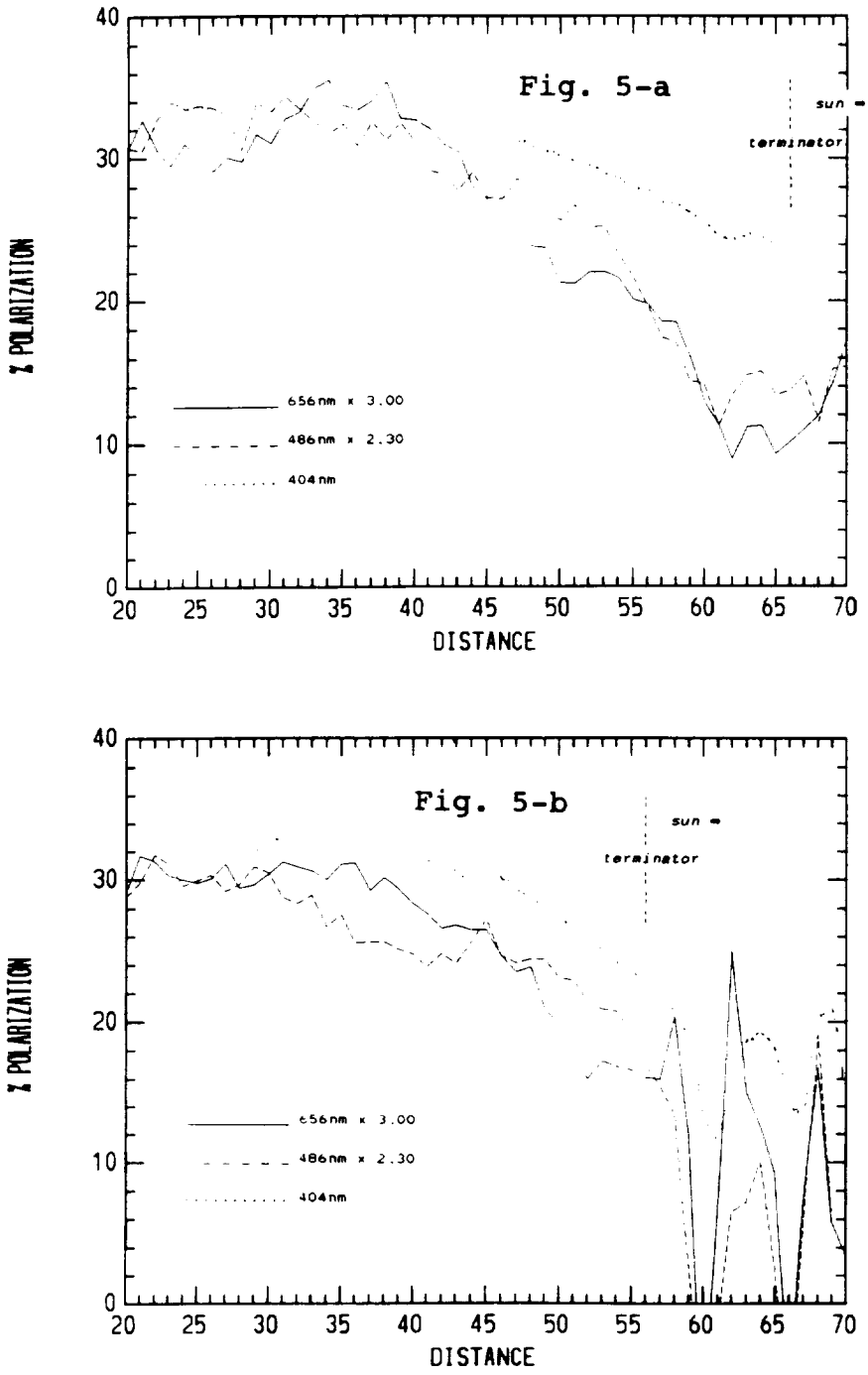

Figure 5.- a) Polarization curves for Mare Imbrium/Caucasus Mtns. site; 5-a corresponds to the region marked with the letter "A" in figure 4 and 5-b corresponds to the region marked "B".

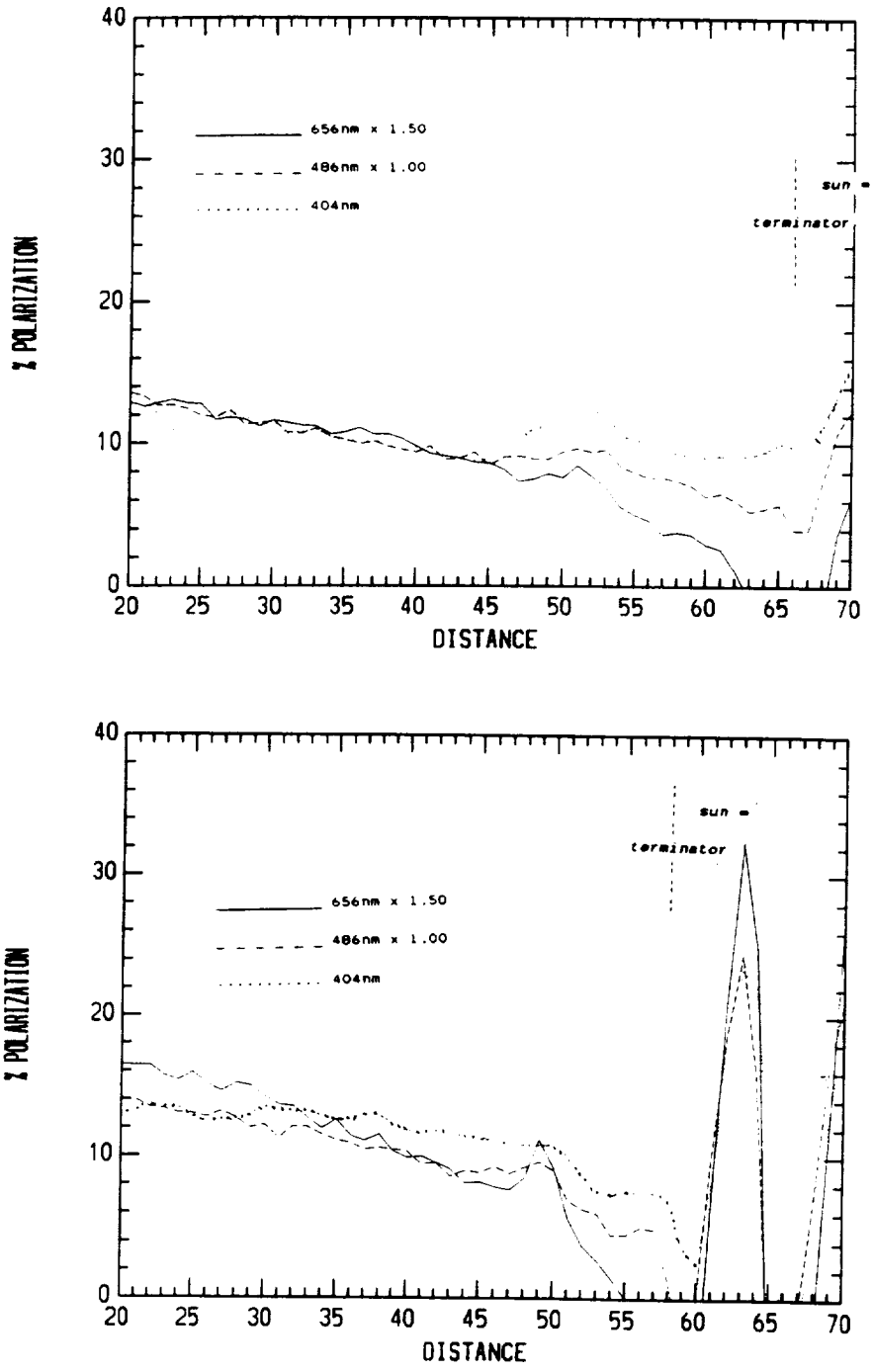

Figure 6.- Polarization curves for Mare Imbrium site.

the phase of the moon decreased further. At this phase angle, the scattering angle is such that polarization due to Rayleigh scattering should be decreased to 0.25. While no quantitative numbers are as yet available, the representative polarization plot found in figure 7 in fact reveals a slight polarization effect but definitely less than the earlier nights.

Conclusion and Summary

This report resents preliminary results of polarization-versus-wavelength analyses of CCD images of four lunar sites looking for evidence of a lunar horizon glow. The polarization trends that would occur due to Rayleigh-scattered light in the region of the dark side of the terminator are, indeed observed. It is our conclusion that very fine submicron dust is being ejected into the lunar exosphere causing sun light to scatter and thereby create the lunar horizon glow phenomenon.

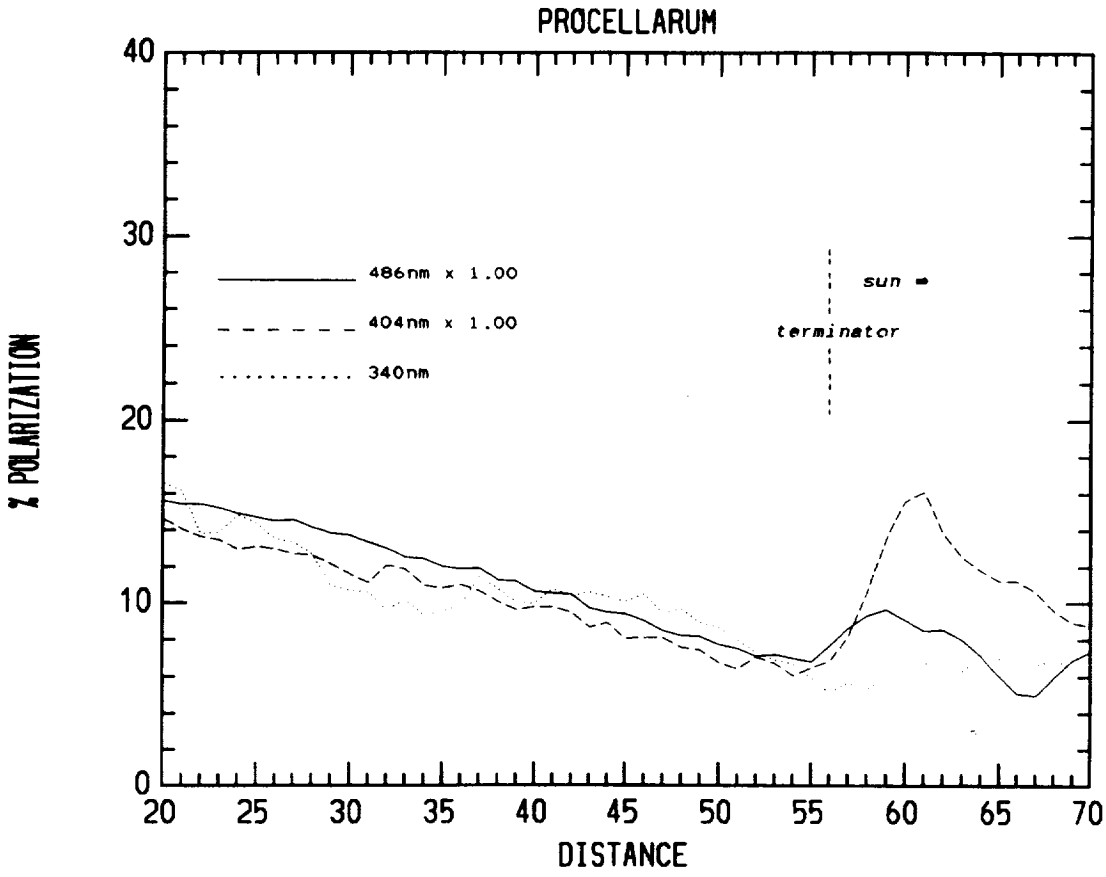

Figure 7.- Polarization curves for Oceanus Procellarum site.

Berg,O.E., H.Wolf, and J.Rhee, Lunar soil movement registered by Apollo 17 cosmic dust experiment., *Interplanetary Dust and Zodiacal Light* (H.Elsasser and H.Fechtig, eds.) Springer-Verlag, New York, 233-237, 1976.

Dollfus,A. and Bowell,E., Polarimetric Properties of the Lunar Surface and its Interpretation, *Astron. & Astrophys.* **10**, 29-53, 1971.

Gehrels,T., Coffeen,T., and Owings,D., Wavelength Dependence of Polarization.III. The Lunar Surface, *The Astronomical Journal*, Vol. **69**, Number 10, 1964.

Kopal,Z., Astrophysics and Space Sciences Library, *An Introduction to The Study of The Moon* **4**, D.Reidel, New York, 1966.

Lyot,B., Research on the Polarization of Light from Planets and from some Terrestrial Substances, *Ann. Obs. Meudon*, **8**, 1929,

Seferny,A.B., I.I.Terez, and A.M.Zvereva, The measurements of sky brightness of Lunokhok-2, *The Moon* **14** 123-128, 1975.

Secchi, *Monthly notices*, **19**, p290, 1859, *Astronomie populaire*, **52**, p93, 1860.

Zook,H.A. and McCoy,J.E., Large Scale Horizon Glow and a High Altitude Lunar Dust Exosphere, *J. Geophys. Res.* **18**, 2117-2120, 1991.

N94-25350

MODELING THE SHUTTLE REMOTE MANIPULATOR SYSTEM–ANOTHER FLEXIBLE MODEL

Final Report

NASA/ASEE Summer Faculty Fellowship Program–1993

Johnson Space Center

Prepared By:	Alan A. Barhorst
Academic Rank:	Assistant Professor
University & Department	Texas Tech University
	Department of Mechanical Engineering
	Lubbock, Texas 79409-1021

NASA/JSC	
Directorate:	Engineering
Division:	Structures and Mechanics
Branch:	Loads and Structural Dynamics
JSC Colleague:	Dave Hamilton
Date Submitted:	August 13, 1993
Contract Number:	NGT-44-001-800

ABSTRACT

High fidelity elastic system modeling algorithms are discussed. The particular system studied is the Space Shuttle Remote Manipulator System (RMS) undergoing full articulated motion. The model incorporates flexibility via a methodology the author has been developing. The technique is based in variational principles, so rigorous boundary condition generation and weak formulations for the associated partial differential equations are realized, yet the analyst need not integrate by parts. The methodology is formulated using vector–dyad notation with minimal use of tensor notation, therefore the technique is believed to be affable to practicing engineers. The objectives of this work are to:

1. Determine the efficacy of the modeling method.
2. Determine if the method affords an analyst advantages in the overall modeling and simulation task.

Generated out of necessity were *Mathematica* algorithms that quasi-automate the modeling procedure and simulation development. The project was divided into sections as follows:

1. Model development of a simplified manipulator.
2. Model development for the full-freedom RMS including a flexible movable base on a six degree of freedom orbiter. A rigid-body is attached to the manipulator end-effector.
3. Simulation development for item 2.
4. Comparison to the currently used model of the flexible RMS in the Structures and Mechanics Division of NASA JSC.

At the time of the writing of this report, items 3 and 4 above were not complete.

INTRODUCTION

Material bodies are inherently of a distributed mass and elasticity nature. Analyst have realized this fact since the early days and developed tools to model these distributed effects [1]. Engineers, challenged with the task of making devices work in a reliable, energy efficient, and inexpensive manner, have been gradually increasing the fidelity of their models by incorporating the distributed properties. The ability to study these high fidelity models grows with the increasing computational capabilities of inexpensive computers.

The literature is teeming with ever-improving ways to model the distributed effects [1]. There are a diverse cross-section of techniques. Some are intuitive to a design engineer [2, 3, 4, 5], while others are mathematically elegant but beyond the training of many practicing engineers [6, 7]. The purpose of this study is to examine the efficacy of the author's attempt at developing a rigorous yet usable method for modeling complicated systems [5].

METHODOLOGY

Present Capabilities

Based on discussions,[1] the author understands that the fidelity of the model for the present Shuttle Remote Manipulator System (RMS) simulation is limited to small amplitude vibrations about any "snap shot" configuration of the system. This limitation manifests itself because of the linear finite element (NASTRAN) model used as the progenitor for the modal basis functions. Therefore, RMS slewing maneuver studies are not within the fidelity of the linear model. There exist techniques which allow an analyst to study the slewing maneuvers of systems like the RMS, but these modeling techniques are computationally expensive and/or hard to understand [1], therefore they are not always implemented by practicing engineers. The author believes the technique discussed below gives analysts a familiar yet powerful modeling tool.

New Capabilities

The main motivating factor for the development of another modeling method was the need to easily derive complete models of complex elastic systems [1, 4, 8, 9, 10, 11, 12]. Although the method discussed herein is still relatively mathematically intense (compared to an equal number of rigid bodies), it has a predisposition for symbolic manipulation. Another impetus for this work is that a simple method may make it possible to bring rigorous flexible system modeling out of the academic domain and into use by product designers. Another catalyst for this effort is that a simple (ultimately an automated) method will make it possible for researchers to rapidly regenerate models based on new continuum assumptions.

The approach is variational in nature. It retains most of the attributes of the analytical approach (i.e. Hamilton's principle), but eliminates most of the pitfalls, such as the need to use Lagrange multipliers for constraints, and excessive algebra. The methodology is vector

[1] Orientation meetings with various engineers from the Structures and Mechanics Division of JSC.

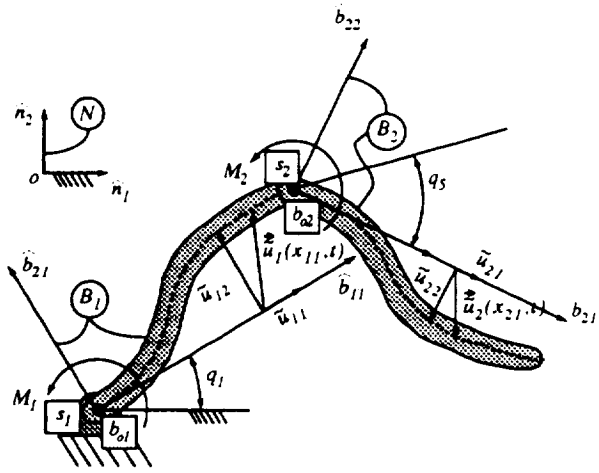

Figure 1: Two Link Flexible Manipulator

based and requires the analyst to perform operations comparable to the operations required for implementing Lagrange's equations. However, it is claimed that the net algebra with the method herein will be less than the net algebra associated to Hamilton's principle or Lagrange's equations. Analysts familiar with Kane's [13] form of d'Alembert's principle will find the technique affable. The complete derivation of the method is shown elsewhere [1, 5].

SIMPLIFIED MANIPULATOR MODEL

Preamble

In this section the equations of motion for a flexible two-link planar manipulator will be derived. This section is included for demonstrative purposes. The procedure that is used on the full RMS model is used on a somewhat simpler model so the reader can follow the steps involved. This simpler system was chosen because: a) it is non-trivial due to its distributed elasticity, b) its planar nature allows for heuristic equation verification, and c) Hamilton's principle can be readily applied to it. This example will demonstrate some of the qualities of the new methodology, such as: a) its systematic nature, b) its resulting closed form equations, and c) automatic boundary condition generation.

The system is shown in figure 1. The domain of each beam is one dimensional. The independent coordinates are x_{11} and x_{21} measured from the root of beam B_1 and B_2, respectively, along the undeformed neutral axis of each beam. The "special" point of beam B_1 is labeled s_1 (the pivot) and s_2 (the joint between the two beams) is for beam B_2. The coordinate frames, denoted with B_1 and B_2, are attached as shown in figure 1. At the root of each beam (B_1 and B_2) there are massless hubs to which torques M_1 and M_2 are applied. The angular position of frames B_1 and B_2 are q_1 and q_5. Beam deflections are measured with $\tilde{u}_{11}(x_{11},t)\hat{b}_{11}$ and $\tilde{u}_{21}(x_{21},t)\hat{b}_{21}$ (elongation), and with $\tilde{u}_{12}(x_{11},t)\hat{b}_{12}$ and $\tilde{u}_{22}(x_{21},t)\hat{b}_{22}$ (flexure), as shown in figure 1. The beams have mass per unit length ρ, total lengths are

L_1 and L_2, cross sectional area A, area moment of inertia $\mathcal{I}$, and Young's modulus E. It is assumed that large deflections and rotational inertia is pertinent, but not shear deformation. Therefore, the beams are modeled with Rayleigh beam theory. The cross-sections of each beam are assumed symmetric about the neutral axis. The intrinsic mass moment of inertia of the cross-section will be taken as $\vec{\vec{I}}_{i_o} = \rho\mathcal{I}\hat{i}_3\hat{i}_3$. $\hat{i}_3$ is normal to the plane of the problem.

Kinematics

The geometry of the motion for the system is as follows. The position vectors of interest are:

$$
\begin{aligned}
{}^{o}\vec{r}^{s_1} &= 0 && (1)\\
{}^{o}\vec{r}^{i_{o_1}} &= {}^{s_1}\vec{r}^{i_{o_1}} = (x_{11} + \tilde{u}_{11})\,\hat{b}_{11} + \tilde{u}_{12}\hat{b}_{22} && (2)\\
{}^{o}\vec{r}^{s_2} &= (L_1 + q_2')\,\hat{b}_{11} + q_3'\hat{b}_{12} && (3)\\
{}^{s_2}\vec{r}^{i_{o_2}} &= (x_{21} + \tilde{u}_{21})\,\hat{b}_{21} + \tilde{u}_{22}\hat{b}_{22} && (4)\\
{}^{o}\vec{r}^{i_{o_2}} &= (L_1 + q_2')\,\hat{b}_{11} + q_3'\hat{b}_{12} + (x_{21} + \tilde{u}_{21})\,\hat{b}_{21} \\
&\quad + \tilde{u}_{22}\hat{b}_{22} && (5)
\end{aligned}
$$

The angular velocity of frame B_1 and B_2 and intermediate frames (in the cross-section) I_1 and I_2 are:

$$
\begin{aligned}
{}^{\mathcal{N}}\vec{\omega}^{B_1} &= u_1\hat{b}_{13} && (6)\\
{}^{\mathcal{N}}\vec{\omega}^{B_2} &= (u_1 + u_4' + u_5)\,\hat{b}_{13} && (7)\\
{}^{\mathcal{N}}\vec{\omega}^{I_1} &= \left(u_1 + \frac{\partial^2\tilde{u}_{12}}{\partial x_{11}\partial t}\right)\hat{b}_{13} && (8)\\
{}^{\mathcal{N}}\vec{\omega}^{I_2} &= \left(u_1 + u_4' + u_5 + \frac{\partial^2\tilde{u}_{22}}{\partial x_{21}\partial t}\right)\hat{b}_{23} && (9)
\end{aligned}
$$

The generalized and pseudo-generalized (denoted with a $'$) coordinates and velocities are defined as:

$$u_1 = \dot{q}_1,\ u_5 = \dot{q}_5 \qquad (10)$$

$$q_2' = \tilde{u}_{11}(L_1, t),\ q_3' = \tilde{u}_{12}(L_1, t),\ q_4' = \frac{\partial\tilde{u}_{12}(L_1, t)}{\partial x_{11}} \qquad (11)$$

$$
\begin{aligned}
&u_2' = \dot{q}_2' = \frac{\partial\tilde{u}_{11}(L_1, t)}{\partial t},\ u_3' = \dot{q}_3' = \frac{\partial\tilde{u}_{12}(L_1, t)}{\partial t},\\
&u_4' = \dot{q}_4' = \frac{\partial^2\tilde{u}_{12}(L_1, t)}{\partial x_{11}\partial t} && (12)
\end{aligned}
$$

The absolute velocity of the point s_1 and s_2 are also required. Since the system is rotating about s_1:

$$^{o}\vec{v}_{\mathcal{N}}^{s_1} = 0 \tag{13}$$

and

$$^{o}\vec{v}_{\mathcal{N}}^{s_2} = (u_2' - u_1 q_3')\,\hat{b}_{11} + (u_3' + u_1\,(L_1 + q_2'))\,\hat{b}_{12} \tag{14}$$

where the pseudo-coordinates and pseudo-speeds have been defined above.

The absolute acceleration of the differential beam elements for beam B_1 and B_2 can be written as:

$$\begin{aligned} ^{o}\vec{a}_{\mathcal{N}}^{i_{o_1}} &= \left(\frac{\partial^2 \tilde{u}_{11}}{\partial t^2} - \dot{u}_1 \tilde{u}_{12} - 2u_1 \frac{\partial \tilde{u}_{12}}{\partial t} - (x_{11} + \tilde{u}_{11})\,u_1^2\right)\hat{b}_{11} \\ &+ \left(\frac{\partial^2 \tilde{u}_{12}}{\partial t^2} + (x_{11} + \tilde{u}_{11})\,\dot{u}_1 + 2u_1 \frac{\partial \tilde{u}_{11}}{\partial t} - \tilde{u}_{12} u_1^2\right)\hat{b}_{12} \end{aligned} \tag{15}$$

and

$$\begin{aligned} ^{o}\vec{a}_{\mathcal{N}}^{i_{o_2}} &= \left(\dot{u}_2' - \dot{u}_1 q_3' - 2u_1 u_3' - (L_1 + q_2')\,u_1^2\right)\hat{b}_{11} \\ &+ \left(\dot{u}_3' + (L_1 + q_2')\,\dot{u}_1 + 2u_1 u_2' - q_3' u_1^2\right)\hat{b}_{12} \\ &+ \left(\frac{\partial^2 \tilde{u}_{21}}{\partial t^2} - (\dot{u}_1 + \dot{u}_4' + \dot{u}_5)\,\tilde{u}_{22} - \right. \\ &\left. 2\,(u_1 + u_4' + u_5)\,\frac{\partial \tilde{u}_{22}}{\partial t} - (x_{21} + \tilde{u}_{21})\,(u_1 + u_4' + u_5)^2\right)\hat{b}_{21} \\ &+ \left(\frac{\partial^2 \tilde{u}_{22}}{\partial t^2} + (x_{21} + \tilde{u}_{21})\,(\dot{u}_1 + \dot{u}_4' + \dot{u}_5)\right. \\ &\left. + 2\,(u_1 + u_4' + u_5)\,\frac{\partial \tilde{u}_{21}}{\partial t} - \tilde{u}_{22}\,(u_1 + u_4' + u_5)^2\right)\hat{b}_{22} \end{aligned} \tag{16}$$

respectively. For this problem i_{oe} for each beam is at the centroid of the cross-section.

The methodology also requires the calculations of the "preferred directions" for the variations (pseudo and ordinary), namely the partial speeds. They are determined by inspection of the velocity equations and given in table 1. The partial velocities for the field equations are given as:

$$\begin{aligned} \frac{\partial^{B_1}\vec{\omega}^{I_1}}{\partial \tilde{u}_{12,1t}} &= \hat{b}_{13}, & \frac{\partial^{B_2}\vec{\omega}^{I_2}}{\partial \tilde{u}_{22,1t}} &= \hat{b}_{23} \\ \frac{\partial^{s_1}\vec{v}_{B_1}^{i_1}}{\partial \tilde{u}_{11,t}} &= \hat{b}_{11}, & \frac{\partial^{s_1}\vec{v}_{B_1}^{i_1}}{\partial \tilde{u}_{12,t}} &= \hat{b}_{12} \\ \frac{\partial^{s_2}\vec{v}_{B_2}^{i_2}}{\partial \tilde{u}_{21,t}} &= \hat{b}_{21}, & \frac{\partial^{s_2}\vec{v}_{B_2}^{i_2}}{\partial \tilde{u}_{22,t}} &= \hat{b}_{22} \end{aligned} \tag{17}$$

	${}^{o}\vec{v}_{\mathcal{N}}^{s_1}$	${}^{o}\vec{v}_{\mathcal{N}}^{s_2}$	${}^{\mathcal{N}}\vec{\omega}^{B_1}$	${}^{\mathcal{N}}\vec{\omega}^{B_2}$
$\frac{\partial}{\partial u_1}$	0	$-q_3'\hat{b}_{11} + (L_1 + q_2')\,\hat{b}_{12} + q_6\hat{b}_{23}$	$\hat{b}_{13}$	$\hat{b}_{23}$
$\frac{\partial}{\partial u_2'}$	0	$\hat{b}_{11}$	0	0
$\frac{\partial}{\partial u_3'}$	0	$\hat{b}_{12}$	0	0
$\frac{\partial}{\partial u_4'}$	0	0	0	$\hat{b}_{23}$
$\frac{\partial}{\partial u_5}$	0	0	0	$\hat{b}_{23}$

Table 1: Partial Velocities for Pseudo and Regular Coordinates

The strain energy density functions for the beams B_i $(i = 1, 2)$ are (assuming large deflections):

$$\bar{V}_i = \frac{1}{2}EA\left(\frac{\partial \tilde{u}_{i1}}{\partial x_{i1}} + \frac{1}{2}\left(\frac{\partial \tilde{u}_{i2}}{\partial x_{i1}}\right)^2\right)^2 + \frac{1}{2}E\mathcal{I}\left(\frac{\partial^2 \tilde{u}_{i2}}{\partial x_{i1}^2}\right)^2 \tag{18}$$

The torques applied to the massless hubs are:

$$\vec{T}_1 = M_1\hat{b}_{13} \quad \text{and} \quad \vec{T}_2 = M_2\hat{b}_{23} \tag{19}$$

on B_1 and B_2, respectively. The equations of motion can now be written down.

Ordinary Differential Equations

The ordinary differential equations, governing the angular positions are:

$$\begin{aligned} 0 = &\frac{\partial {}^{o}\vec{v}_{\mathcal{N}}^{s_1}}{\partial u_1} \cdot \left[\vec{F}_{B_1} - \vec{I}_{B_1}\right] + \frac{\partial {}^{\mathcal{N}}\vec{\omega}^{B_1}}{\partial u_1} \cdot \left[\vec{T}_{B_1} - \vec{J}_{B_1}\right] \\ &+ \frac{\partial {}^{o}\vec{v}_{\mathcal{N}}^{s_2}}{\partial u_1} \cdot \left[\vec{F}_{B_2} - \vec{I}_{B_2}\right] + \frac{\partial {}^{\mathcal{N}}\vec{\omega}^{B_2}}{\partial u_1} \cdot \left[\vec{T}_{B_2} - \vec{J}_{B_2}\right] \end{aligned} \tag{20}$$

for u_1, and

$$\begin{aligned} 0 = &\frac{\partial {}^{o}\vec{v}_{\mathcal{N}}^{s_1}}{\partial u_5} \cdot \left[\vec{F}_{B_1} - \vec{I}_{B_1}\right] + \frac{\partial {}^{\mathcal{N}}\vec{\omega}^{B_1}}{\partial u_5} \cdot \left[\vec{T}_{B_1} - \vec{J}_{B_1}\right] \\ &+ \frac{\partial {}^{o}\vec{v}_{\mathcal{N}}^{s_2}}{\partial u_5} \cdot \left[\vec{F}_{B_2} - \vec{I}_{B_2}\right] + \frac{\partial {}^{\mathcal{N}}\vec{\omega}^{B_2}}{\partial u_5} \cdot \left[\vec{T}_{B_2} - \vec{J}_{B_2}\right] \end{aligned} \tag{21}$$

for u_5. The partial velocities are defined in table 1. The forces and torques (applied and inertia) are defined as:

$$\vec{F}_e = \int_{\Omega_f} \left(\mathcal{H}_e\vec{F}_{he} + \mathcal{D}_e\vec{F}_{de}\right) d\Omega_e$$

$$+\int_{\partial\Omega_e}\left(\mathcal{H}_e\vec{F}_{he}+\mathcal{D}_e\vec{F}_{de}\right)d\sigma_e$$

$$\vec{I}_e=\int_{\Omega_e}\rho_e{}^{o}\vec{a}_{\mathcal{N}}^{\,*I_e}\,d\Omega_e$$

$$\vec{T}_e=\int_{\Omega_e}\Big[{}^{s_e}\vec{r}^{\,i_{oe}}\times\left(\mathcal{H}_e\vec{F}_{he}+\mathcal{D}_e\vec{F}_{de}\right)+\mathcal{H}_e\vec{T}_{he}+\mathcal{D}_e\vec{T}_{de}\Big]\,d\Omega_e$$

$$+\int_{\partial\Omega_e}\Big[{}^{s_e}\vec{r}^{\,i_{oe}}\times\left(\mathcal{H}_e\vec{F}_{he}+\mathcal{D}_e\vec{F}_{de}\right)+\mathcal{H}_e\vec{T}_{he}+\mathcal{D}_e\vec{T}_{de}\Big]\,d\sigma_e$$

$$\vec{J}_e=\int_{\Omega_e}\Big[{}^{s_e}\vec{r}^{\,i_{oe}}\times\rho_e{}^{o}\vec{a}_{\mathcal{N}}^{\,*I_e}+{}^{i_{oe}}\vec{r}^{\,*I_e}\times\rho_e{}^{o}\vec{a}_{\mathcal{N}}^{\,i_{oe}}+\vec{\vec{I}}_{i_{oe}}\cdot{}^{\mathcal{N}}\vec{\alpha}^{\,I_e}+{}^{\mathcal{N}}\vec{\omega}^{\,I_e}\times\vec{\vec{I}}_{i_{oe}}\cdot{}^{\mathcal{N}}\vec{\omega}^{\,I_e}\Big]d\Omega_e$$

The final form of the differential equation are found by taking the indicated dot products and are not displayed here.

Partial Differential Equations

The field equations governing elongation and bending for B_1, are:

$$\begin{aligned}0 &= \frac{\partial}{\partial x_{11}}\left(\frac{\partial\bar{V}_1}{\partial\tilde{u}_{11,1}}\right)-\rho^{o}\vec{a}_{\mathcal{N}}^{\,i_{o_1}}\cdot\hat{b}_{11}\\ &= \frac{\partial}{\partial x_{11}}\left[EA\left(\frac{\partial\tilde{u}_{11}}{\partial x_{11}}+\frac{1}{2}\left(\frac{\partial\tilde{u}_{12}}{\partial x_{11}}\right)^2\right)\right]\\ -\rho&\left(\frac{\partial^2\tilde{u}_{11}}{\partial t^2}-\dot{u}_1\tilde{u}_{12}-2u_1\frac{\partial\tilde{u}_{12}}{\partial t}-(x_{11}+\tilde{u}_{11})\,u_1^2\right)\end{aligned}\qquad(22)$$

for elongation, and:

$$\begin{aligned}0=&\frac{\partial}{\partial x_{11}}\left(\frac{\partial\bar{V}_1}{\partial\tilde{u}_{12,1}}\right)-\frac{\partial^2}{\partial x_{11}^2}\left(\frac{\partial\bar{V}_1}{\partial\tilde{u}_{12,11}}\right)-\rho^{o}\vec{a}_{\mathcal{N}}^{\,i_{o_1}}\cdot\hat{b}_{12}\\ &+\frac{\partial}{\partial x_{11}}\left[\hat{b}_{13}\cdot\left(\vec{\vec{I}}_{i_{o_1}}\cdot{}^{\mathcal{N}}\vec{\alpha}^{\,I_1}+{}^{\mathcal{N}}\vec{\omega}^{\,I_1}\times\vec{\vec{I}}_{i_{o_1}}\cdot{}^{\mathcal{N}}\vec{\omega}^{\,I_1}\right)\right]\\ &=\frac{\partial}{\partial x_{11}}\left[EA\left(\frac{\partial\tilde{u}_{11}}{\partial x_{11}}+\frac{1}{2}\left(\frac{\partial\tilde{u}_{12}}{\partial x_{11}}\right)^2\right)\frac{\partial\tilde{u}_{12}}{\partial x_{11}}\right]\\ &-\frac{\partial^2}{\partial x_{11}^2}\left(EI\frac{\partial^2\tilde{u}_{12}}{\partial x_{11}^2}\right)\end{aligned}$$

$$
\begin{aligned}
&-\rho\left(\frac{\partial^2\tilde{u}_{12}}{\partial t^2}+2u_1\frac{\partial\tilde{u}_{12}}{\partial t}+\left(x_{11}+\tilde{u}_{11}\right)\dot{u}_1-\tilde{u}_{12}u_1^2\right)\\
&+\frac{\partial}{\partial x_{11}}\left[\left(\dot{u}_1+\frac{\partial^3\tilde{u}_{12}}{\partial x_{11}\partial t^2}\right)\rho\mathcal{I}\right.\\
&\left.+\rho\mathcal{I}\left(u_1+\frac{\partial^2\tilde{u}_{12}}{\partial x_{11}\partial t}\right)^2(\hat{b}_{13}\cdot\hat{i}_{13})(\hat{b}_{13}\times\hat{i}_{13})\cdot\hat{b}_{13}\right]
\end{aligned}
\tag{23}
$$

for bending.

At $x_{11}=0$, the boundary conditions for B_1 are:

$$
\tilde{u}_{11}=\tilde{u}_{12}=\tilde{u}_{12,1}=0 \tag{24}
$$

The boundary conditions at $x_{11}=L_1$ for B_1 are:

$$
\frac{\partial\bar{V}_1}{\partial\tilde{u}_{11,1}}=EA\left(\frac{\partial\tilde{u}_{11}}{\partial x_{11}}+\frac{1}{2}\left(\frac{\partial\tilde{u}_{12}}{\partial x_{11}}\right)^2\right)=g'_{11} \tag{25}
$$

for elongation, with:

$$
\begin{aligned}
g'_{12} &= \hat{b}_{13}\cdot\left(\vec{\bar{I}}_{i_{o_1}}\cdot{}^{\mathcal{N}}\vec{\alpha}^{I_1}+{}^{\mathcal{N}}\vec{\omega}^{I_1}\times\vec{\bar{I}}_{i_{o_1}}\cdot{}^{\mathcal{N}}\vec{\omega}^{I_1}\right)\\
&\quad+\frac{\partial\bar{V}_1}{\partial\tilde{u}_{12,1}}-\frac{\partial}{\partial x_{11}}\left(\frac{\partial\bar{V}_1}{\partial\tilde{u}_{12,11}}\right)\\
&= \left(\dot{u}_1+\frac{\partial^3\tilde{u}_{12}}{\partial x_{11}\partial t^2}\right)\rho\mathcal{I}\\
&\quad+\rho\mathcal{I}\left(u_1+\frac{\partial^2\tilde{u}_{12}}{\partial x_{11}\partial t}\right)^2(\hat{b}_{13}\cdot\hat{i}_{13})(\hat{b}_{13}\times\hat{i}_{13})\cdot\hat{b}_{13}\\
&\quad+EA\left(\frac{\partial\tilde{u}_{11}}{\partial x_{11}}+\frac{1}{2}\left(\frac{\partial\tilde{u}_{12}}{\partial x_{11}}\right)^2\right)\frac{\partial\tilde{u}_{12}}{\partial x_{11}}\\
&\quad-\frac{\partial}{\partial x_{11}}\left(E\mathcal{I}\frac{\partial^2\tilde{u}_{12}}{\partial x_{11}^2}\right)
\end{aligned}
\tag{26}
$$

for shear, and

$$
\frac{\partial\bar{V}_1}{\partial\tilde{u}_{12,11}}=E\mathcal{I}\frac{\partial^2\tilde{u}_{12}}{\partial x_{11}^2}=k'_{12} \tag{27}
$$

for bending moment. The intrinsic forcing terms of the boundary conditions at $x_{11}=L_1$ are defined as:

$$
g'_{11} = \frac{\partial^o\vec{v}_{\mathcal{N}}^{\,B_1}}{\partial u'_2}\cdot\left[\vec{F}_{B_1}-\vec{I}_{B_1}\right]+\frac{\partial{}^{\mathcal{N}}\vec{\omega}^{\,B_1}}{\partial u'_2}\cdot\left[\vec{T}_{B_1}-\vec{J}_{B_1}\right]
$$

$$+\frac{\partial^o \vec{v}_{\mathcal{N}}^{s_2}}{\partial u_2'} \cdot \left[\vec{F}_{B_2} - \vec{I}_{B_2}\right] + \frac{\partial^{\mathcal{N}} \vec{\omega}^{B_2}}{\partial u_2'} \cdot \left[\vec{T}_{B_2} - \vec{J}_{B_2}\right] \tag{28}$$

and

$$\begin{aligned} g_{12}' &= \frac{\partial^o \vec{v}_{\mathcal{N}}^{s_1}}{\partial u_3'} \cdot \left[\vec{F}_{B_1} - \vec{I}_{B_1}\right] + \frac{\partial^{\mathcal{N}} \vec{\omega}^{B_1}}{\partial u_3'} \cdot \left[\vec{T}_{B_1} - \vec{J}_{B_1}\right] \\ &+\frac{\partial^o \vec{v}_{\mathcal{N}}^{s_2}}{\partial u_3'} \cdot \left[\vec{F}_{B_2} - \vec{I}_{B_2}\right] + \frac{\partial^{\mathcal{N}} \vec{\omega}^{B_2}}{\partial u_3'} \cdot \left[\vec{T}_{B_2} - \vec{J}_{B_2}\right] \end{aligned} \tag{29}$$

and

$$\begin{aligned} k_{12}' &= \frac{\partial^o \vec{v}_{\mathcal{N}}^{s_1}}{\partial u_4'} \cdot \left[\vec{F}_{B_1} - \vec{I}_{B_1}\right] + \frac{\partial^{\mathcal{N}} \vec{\omega}^{B_1}}{\partial u_4'} \cdot \left[\vec{T}_{B_1} - \vec{J}_{B_1}\right] \\ &+\frac{\partial^o \vec{v}_{\mathcal{N}}^{s_2}}{\partial u_4'} \cdot \left[\vec{F}_{B_2} - \vec{I}_{B_2}\right] + \frac{\partial^{\mathcal{N}} \vec{\omega}^{B_2}}{\partial u_4'} \cdot \left[\vec{T}_{B_2} - \vec{J}_{B_2}\right] \end{aligned} \tag{30}$$

The field equations for the second member (B_2) are:

$$\begin{aligned} 0 &= \frac{\partial}{\partial x_{21}} \left(\frac{\partial \bar{V}_2}{\partial \tilde{u}_{21,1}}\right) - \rho^o \vec{a}_{\mathcal{N}}^{i_{o_2}} \cdot \hat{b}_{21} \\ &= \frac{\partial}{\partial x_{21}} \left[EA\left(\frac{\partial \tilde{u}_{21}}{\partial x_{21}} + \frac{1}{2}\left(\frac{\partial \tilde{u}_{22}}{\partial x_{21}}\right)^2\right)\right] \\ &-\rho\left[\dot{u}_2' - \dot{u}_1 q_3' - 2u_1 u_3' - u_1^2\left(L_1 + q_2'\right)\right]\left(\hat{b}_{11} \cdot \hat{b}_{21}\right) \\ &-\rho\left[\dot{u}_3' + \dot{u}_1\left(L_1 + q_2'\right) + 2u_1 u_2' - u_1^2 q_3'\right]\left(\hat{b}_{12} \cdot \hat{b}_{21}\right) \\ &-\rho\left[\frac{\partial^2 \tilde{u}_{21}}{\partial t^2} - \left(\dot{u}_1 + \dot{u}_4' + \dot{u}_5\right)\tilde{u}_{22}\right. \\ &\left.-2\left(u_1 + u_4' + u_5\right)\frac{\partial \tilde{u}_{22}}{\partial t} - \left(u_1 + u_4' + u_5\right)^2\left(x_{21} + \tilde{u}_{21}\right)\right] \end{aligned} \tag{31}$$

for elongation, and:

$$\begin{aligned} 0 &= \frac{\partial}{\partial x_{21}} \left(\frac{\partial \bar{V}_2}{\partial \tilde{u}_{22,1}}\right) - \frac{\partial^2}{\partial x_{21}^2} \left(\frac{\partial \bar{V}_2}{\partial \tilde{u}_{22,11}}\right) - \rho^o \vec{a}_{\mathcal{N}}^{i_{o_2}} \cdot \hat{b}_{22} \\ &+\frac{\partial}{\partial x_{21}} \left[\hat{b}_{23} \cdot \left(\vec{\bar{I}}_{i_{o_2}} \cdot {}^{\mathcal{N}}\vec{\alpha}^{I_2} + {}^{\mathcal{N}}\vec{\omega}^{I_2} \times \vec{\bar{I}}_{i_{o_2}} \cdot {}^{\mathcal{N}}\vec{\omega}^{I_2}\right)\right] \\ &= \frac{\partial}{\partial x_{21}} \left[EA\left(\frac{\partial \tilde{u}_{21}}{\partial x_{21}} + \frac{1}{2}\left(\frac{\partial \tilde{u}_{22}}{\partial x_{21}}\right)^2\right)\frac{\partial \tilde{u}_{22}}{\partial x_{21}}\right] \end{aligned}$$

$$
\begin{aligned}
&-\frac{\partial^2}{\partial x_{21}^2}\left(EI\frac{\partial^2 \tilde{u}_{22}}{\partial x_{21}^2}\right)\\
&-\rho\left[\dot{u}_2' - \dot{u}_1 q_3' - 2u_1 u_3' - u_1^2\left(L_1 + q_2'\right)\right]\left(\hat{b}_{11}\cdot\hat{b}_{22}\right)\\
&-\rho\left[\dot{u}_3' + \dot{u}_1\left(L_1 + q_2'\right) + 2u_1 u_2' - u_1^2 q_3'\right]\left(\hat{b}_{12}\cdot\hat{b}_{22}\right)\\
&-\rho\left[\frac{\partial^2 \tilde{u}_{22}}{\partial t^2} + \left(\dot{u}_1 + \dot{u}_4' + \dot{u}_5\right)\left(x_{21} + \tilde{u}_{21}\right)\right.\\
&\left.+2\left(u_1 + u_4' + u_5\right)\frac{\partial \tilde{u}_{21}}{\partial t} - \left(u_1 + u_4' + u_5\right)^2 \tilde{u}_{22}\right]\\
&+\frac{\partial}{\partial x_{21}}\left[\left(\dot{u}_1 + \dot{u}_4' + \dot{u}_5 + \frac{\partial^3 \tilde{u}_{22}}{\partial x_{21}\partial t^2}\right)\rho I\right.\\
&\left.+\rho I\left(u_1 + u_4' + u_5 + \frac{\partial^2 \tilde{u}_{22}}{\partial x_{21}\partial t}\right)^2\left(\hat{b}_{23}\cdot\hat{i}_{23}\right)\left(\hat{b}_{23}\times\hat{i}_{23}\right)\cdot\hat{b}_{23}\right]
\end{aligned}
\tag{32}
$$

for bending.

The boundary conditions for B_2 at $x_{21} = 0$ are:

$$
\tilde{u}_{21} = \tilde{u}_{22} = \tilde{u}_{22,1} = 0 \tag{33}
$$

The boundary conditions at $x_{21} = L_2$ are:

$$
0 = EA\left(\frac{\partial \tilde{u}_{21}}{\partial x_{21}} + \frac{1}{2}\left(\frac{\partial \tilde{u}_{22}}{\partial x_{21}}\right)^2\right) \tag{34}
$$

$$
\tag{35}
$$

for elongation, and:

$$
\begin{aligned}
0 = &\left(\dot{u}_1 + \dot{u}_4' + \dot{u}_5 + \frac{\partial^3 \tilde{u}_{22}}{\partial x_{21}\partial t^2}\right)\rho I\\
&+\rho I\left(u_1 + u_4' + u_5 + \frac{\partial^2 \tilde{u}_{22}}{\partial x_{21}\partial t}\right)^2\left(\hat{b}_{23}\cdot\hat{i}_{23}\right)\left(\hat{b}_{23}\times\hat{i}_{23}\right)\cdot\hat{b}_{23}\\
&+EA\left(\frac{\partial \tilde{u}_{21}}{\partial x_{21}} + \frac{1}{2}\left(\frac{\partial \tilde{u}_{22}}{\partial x_{21}}\right)^2\right)\frac{\partial \tilde{u}_{22}}{\partial x_{21}} - \frac{\partial}{\partial x_{21}}\left(EI\frac{\partial^2 \tilde{u}_{22}}{\partial x_{21}^2}\right)
\end{aligned}
\tag{36}
$$

for shear, and:

$$
0 = EI\frac{\partial^2 \tilde{u}_{22}}{\partial x_{21}^2} \tag{37}
$$

for moment.

Initial conditions for q_1, q_5, u_1, u_5, $\tilde{u}_{11}$, $\tilde{u}_{12}$, $\tilde{u}_{21}$, $\tilde{u}_{22}$, $\frac{\partial \tilde{u}_{11}}{\partial t}$, $\frac{\partial \tilde{u}_{12}}{\partial t}$, $\frac{\partial \tilde{u}_{21}}{\partial t}$, and $\frac{\partial \tilde{u}_{22}}{\partial t}$ must also be specified. The kinematic differential equations for q_1 and q_5 are given in equation 10.

Discussion

As can be seen by the presentation above, the methodology facilitates the process of writing equations of motion for complex systems. One can see that the rigorous natural boundary conditions that are generated via variational principles are present but the analyst does not have to integrate by parts. For comparison of the technique with Hamilton's principle see [14] relative to the problem above. For more complex systems, such as those exhibiting nonholonomic constraints, see [1, 15]. For systems undergoing contact/impact, in a hybrid parameter fashion, see [1, 16, 17].

Apparently some of the lingering questions are whether or not the method is attractive to practicing engineers and can the symbolic form of the equations be put in a form suitable for simulation. The author claims yes to the later question and only time will tell on the former question. Massaging the equations into a simulation are the topic of the next section.

With regards to getting numbers from the equations, it is possible to put the equations in a weak form so that the complicated boundary conditions are absorbed into an integrated form of the partial differential equations. Then one has only to choose an appropriate function for the test function used to cast the problem in its weak form. For problems like the manipulator above, Rayleigh-Ritz discretization is probably sufficient. For more complicated continuum bodies, finite element discretization is probably appropriate provided the analyst work with the problem in its weak form so the appropriate boundary conditions are included.

RMS MODEL

Model Description

The main subject of this report is the application of the method described above to the Space Shuttle RMS. The RMS is modeled as a system of rigid and continuously elastic bodies, a hybrid parameter mechanical system. The system is broken down as follows (see figure 2).

The orbiter is taken as a six degree of freedom rigid body. The RMS base (assumed to be rigid and labeled B) is attached to the orbiter via small displacement small angle springs which approximate the elastic nature of the orbiter. The RMS shoulder yaw motor and housing are assumed to be a rigid body (body Sy). Connected to Sy via a nonlinear spring and motor control action is the RMS shoulder pitch body Sp with its actuator. Attached to Sp is the first elastic boom. This boom, as with all booms in this model, is assumed to be a continuum in which y and z deflections along with axial rotation are modeled. The beam model is a Rayleigh beam (intrinsic cross-sectional inertia incorporated) with small deflections. The next body in the chain is the elbow pitch motor and housing. It is attached through a nonlinear actuator to rigid body EL. Attached to EL is the next flexible boom, modeled like the first boom. Attached to the second boom is the wrist pitch motor and housing. It is attached to body P. Boom three is anchored by body P. Boom three is elastic and modeled as described before. At the tip of boom 3 is the motor and housing for the wrist yaw action. The wrist yaw body is rigid and labeled Y. Attached to the yaw body through a nonlinear actuator is the wrist roll motor and housing. This is followed by the

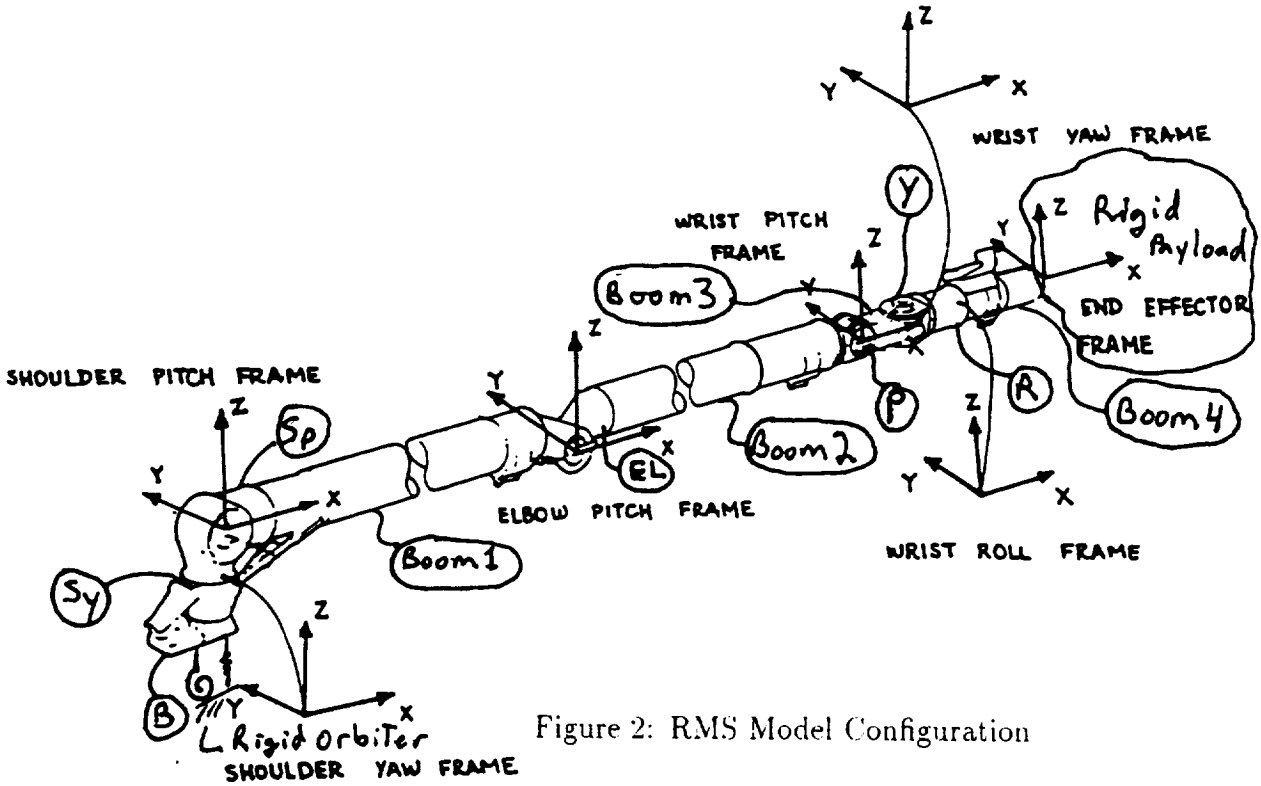

Figure 2: RMS Model Configuration

fourth elastic boom (the end effector). Attached to the end effector is a rigid payload.

Closed Form Model

In order to attempt writing a closed form model for a system as complicated as the RMS described above, a symbolic manipulating assistant is desired. The author has access to *Mathematica* so this is the tool that was utilized. Before getting into the description of the algorithms developed, justification for the effort will be outlined.

Why should an analyst develop closed form models when there exist other tools that seem to adequately model these systems? The author believes that using tools that are traditionally from the structural analysis realm such as NASTRAN models unnecessarily limit the model to the linear motion about some configuration. It is felt that if the approach of writing complete models first (then reducing to linear if desired) is feasible, in a timely manner, then engineers will utilize these more exact models. In order to facilitate the clock, computer aided modeling is desired; *Mathematica* is an excellent tool for this process. Another advantage to working directly with the closed form model is that the "zero times zero" multiplications that arise in straight out matrix models are avoided. Also repetitive multiplications and additions are readily recognized and can be assigned to a memory location for instant recall. This tight code will make running these complicated models more feasible.

Mathematica Algorithms

Mathematica algorithms were developed to mimic the procedure outlined in the previously discussed simplified model of the RMS. The standard notation for *Mathematica* was adjusted so as to mimic engineering vector notation. Then algorithms were developed that recognize the vector dot and cross products, the triple products, and other identities. Differentiation of vectors in multiple coordinate frames was defined. Standard order for the symbols was defined so symbolic cancelation was facilated. Function that aid in the gathering of terms, the distribution of terms, and general manipulation were developed. At this point these

algorithms are used via a *Mathematica* notebook running on a NeXT computer. They are not limited to this computer system because the notebooks are portable across multiple computer systems. An example of how one enters symbols for manipulation is shown in the appendix.

RMS Model Status

Presently the modeling procedure is not complete. All stages of the development are complete up to the point where the actual differential equations suitable for output to FORTRAN format are formed. All the appropriate d'Alembert forces and torques have been calculated along with the appropriate partial velocities, and the weak formulation. Unfortunately the approach taken thus far is very memory hungry so the workstation is using a lot of virtual memory which is time consuming. Refinements to the procedure and algorithms are made in real time and the memory and time consumption problems are being reduced.

Model Shake Down

Comparisons of the aforementioned model with existing models will be made upon completion of the modeling procedure. It is intended that the efficacy of the technique and model will be tested via metrics such as accuracy, calculation speed, and generality.

SUMMARY

The rudimental aspects of a procedure to rigorously model complicated systems in a timely manner have been developed. The modeling technique is based on a variational principle based approach for writing the equations of motion, augmented with computer aided modeling algorithms written in *Mathematica* code. The tools developed are being applied to a complicated RMS model in order to establish the efficacy of the modeling technique. The technique shows promise because of its rigor, but the details of the computer aided algorithms need refinement. Numerical studies have yet to be performed.

REFERENCES

[1] A. A. Barhorst, *On Modeling the Dynamics of Hybrid Parameter Multiple Body Mechanical Systems.* PhD thesis, Texas A & M University, College Station, Texas, 1991.

[2] D. R. Glandorf, "Equations of motion for the station control simulator, memo 23338," Tech. Rep., Lockheed EMSCO, December 1986.

[3] T. R. Kane, R. R. Ryan, and A. K. Banerjee, "Dynamics of a cantilever beam attached to a moving base," *Journal of Guidance, Control, and Dynamics*, vol. 10, pp. 139–151, March-April 1987.

[4] L. Meirovitch, "State equations of motion for flexible bodies in terms of quasi-coordinates," in *Proc. IUTAM/IFAC Symposium on Dynamics of Controlled Mechanical Systems*, (Berlin), pp. 37–48, Springer-Verlag, 1988.

[5] A. A. Barhorst, "Systematic closed form modeling of hybrid parameter multiple body systems," in *Proceedings of the ASME Winter Annual Meeting*, (New Orleans, LA), November 1993.

[6] J. C. Simo, "Nonlinear dynamics of flexible structures, a geometrically exact approach," in *Proc. of the Workshop on Multibody Simulation*, pp. 235–296, JPL D-5190, April 1988.

[7] M. G. Nasser, *Numerical Methods for Multibody Elastic Systems and Contact.* PhD thesis, The University of Houston, Houston, Texas, 1992.

[8] K. W. Lips and R. P. Singh, "Obstacles to high fidelity multibody dynamics simulation," in *Proc. of the American Control Conference*, pp. 587–594, June 1988.

[9] P. W. Likins, "Multibody dynamics: A historical perspective," in *Proc. of the Workshop on Multibody Simulation*, pp. 10–24, JPL D-5190, April 1988.

[10] K. H. Low and M. Vidyasagar, "A lagrangian formulation of the dynamic model for flexible manipulator systems," *Journal of Dynamic Systems, Measurement and Control*, vol. 110, pp. 175–181, June 1988.

[11] S. Lee and J. L. Junkins, "Explicit generalizations of lagrange's equations for hybrid coordinate dynamical systems," Tech. Rep. 91-0301, Texas A&M University, Aerospace Engineering Department, March 1991.

[12] J. C. Simo and L. Vu-Quoc, "On the dynamics in space of rods undergoing large motions–a geometrically exact approach," *Computer Methods in Applied Mechanics and Engineering*, vol. 66, pp. 125–161, 1988.

[13] T. R. Kane and D. A. Levinson, *Dynamics Theory and Applications.* New York: McGraw-Hill, 1985.

[14] S. Choura, S. Jayasuriya, and M. A. Medick, "On the modeling, and open loop control of a thin flexible beam," *Journal of Dynamic Systems, Measurement and Control*, vol. 113, pp. 26–33, March 1991.

[15] A. A. Barhorst and L. J. Everett, "Obtaining the minimal set of hybrid parameter differential equations for mechanisms," in *Proceedings of the ASME Design Engineering Technical Conference*, (Phoenix, AZ), September 1992.

[16] A. A. Barhorst and L. J. Everett, "Contact/impact in hybrid parameter multiple body systems," in *Proceedings of the ASME 16th Annual Energy-Sources Technology Conference & Exhibition, Dynamics and Vibrations Symposium*, (Houston, TX), January 1993.

[17] A. A. Barhorst, "Closed form modeling of continuous parameter robotic systems-contact/impact and wave propagation," in *Proceedings of the 14th Biennial Conference on Mechanical Vibration and Noise*, (Albuquerque, NM), September 1993.

This is the symbol manipulations for the robotic arm flex model.

Angular Velocity and Acceleration. omega (W__) are the generalized speed.

Newtonian Frame (N)

Orbiter Frame (O)

```
o[1]:=unitVector[O,o,1]
o[2]:=unitVector[O,o,2]
o[3]:=unitVector[O,o,3]
NwO=omega[N,O]=Wo1 o[1] + Wo2 o[2] + Wo3 o[3]
```

```
     ^          ^          ^
Wo1 o   + Wo2 o   + Wo3 o
     1          2          3
```

```
NaO=DvDt[N,NwO]//Simplify
```

```
  .  ^       .  ^       .  ^
Wo1 o   + Wo2 o   + Wo3 o
     1          2          3
```

Manipulator Base Frame (B)

```
b[1]:=unitVector[B,b,1]
b[2]:=unitVector[B,b,2]
b[3]:=unitVector[B,b,3]
OwB=omega[O,B]=Wb1 b[1] + Wb2 b[2] + Wb3 b[3]
```

$$Wb1\ \hat{b}_1 + Wb2\ \hat{b}_2 + Wb3\ \hat{b}_3$$

```
NwB=omega[N,B]=NwO + OwB
```

$$Wb1\ \hat{b}_1 + Wb2\ \hat{b}_2 + Wb3\ \hat{b}_3 + Wo1\ \hat{o}_1 + Wo2\ \hat{o}_2 + Wo3\ \hat{o}_3$$

```
NaB=NaO + DvDt[B,OwB] + NwB >< OwB
```

$$\begin{aligned}
&Wb1\ Wo1\ \hat{o}_1 \times \hat{b}_1 + Wb2\ Wo1\ \hat{o}_1 \times \hat{b}_2 + Wb3\ Wo1\ \hat{o}_1 \times \hat{b}_3 + \\
&Wb1\ Wo2\ \hat{o}_2 \times \hat{b}_1 + Wb2\ Wo2\ \hat{o}_2 \times \hat{b}_2 + Wb3\ Wo2\ \hat{o}_2 \times \hat{b}_3 + \\
&Wb1\ Wo3\ \hat{o}_3 \times \hat{b}_1 + Wb2\ Wo3\ \hat{o}_3 \times \hat{b}_2 + Wb3\ Wo3\ \hat{o}_3 \times \hat{b}_3 + \\
&\dot{Wb1}\ \hat{b}_1 + \dot{Wb2}\ \hat{b}_2 + \dot{Wb3}\ \hat{b}_3 + \dot{Wo1}\ \hat{o}_1 + \dot{Wo2}\ \hat{o}_2 + \dot{Wo3}\ \hat{o}_3
\end{aligned}$$

```
z1=Coefficient[NaB,o[1]><b[1]]
z2=Coefficient[NaB,o[1]><b[2]]
z3=Coefficient[NaB,o[1]><b[3]]
z4=Coefficient[NaB,o[2]><b[1]]
z5=Coefficient[NaB,o[2]><b[2]]
z6=Coefficient[NaB,o[2]><b[3]]
z7=Coefficient[NaB,o[3]><b[1]]
z8=Coefficient[NaB,o[3]><b[2]]
z9=Coefficient[NaB,o[3]><b[3]]
```

Wb1 Wo1

Wb2 Wo1

Wb3 Wo1

Wb1 Wo2

Wb2 Wo2

Wb3 Wo2

N94- 25351

THE ROLE OF VISUAL CONTEXT IN MANUAL TARGET LOCALIZATION

Final Report
NASA/ASEE Summer Faculty Fellowship Program -- 1993
Johnson Space Center

Prepared By:	Susan R. Barry, Ph.D.
Academic Rank:	Assistant Professor
University & Department:	Mount Holyoke College Dept. of Biological Sciences South Hadley, MA. 01075
NASA/JSC	
Directorate:	Space and Life Sciences
Division:	Medical Sciences
Branch:	Space Biomedical Research Institute
JSC Colleague	Jacob Bloomberg, Ph.D.
Date Submitted:	August 31, 1993
Contract Number:	NGT-44-001-800

ABSTRACT

During space flight and immediately after return to the 1-g environment of earth, astronauts experience perceptual and sensory-motor disturbances. These changes result from adaptation of the astronaut to the microgravity environment of space. During space flight, sensory information from the eyes, limbs and vestibular organs is reinterpreted by the central nervous system in order to produce appropriate body movements in microgravity. This adaptation takes several days to develop. Upon return to earth, the changes in the sensory-motor system are no longer appropriate to a 1-g environment. Over several days, the astronaut must re-adapt to the terrestrial environment

Alterations in sensory-motor function may affect eye-head-hand coordination and, thus, the crewmember's ability to manually locate objects in extrapersonal space. Previous reports have demonstrated that crewmembers have difficulty in estimating joint and limb position and in pointing to memorized target positions on orbit and immediately postflight. The ability to point at or reach toward an object or perform other manual tasks is essential for safe Shuttle operation and may be compromised particularly during re-entry and landing sequences and during possible emergency egress from the Shuttle. An understanding of eye-head-hand coordination and the changes produced during space flight is necessary to develop effective countermeasures. This summer's project formed part of a study of the sensory cues used in the manual localization of objects.

To point or reach toward a target, a subject must determine the precise location of the object in extrapersonal space. The position of the target can be determined by using either an egocentric or allocentric reference frame. In an egocentric reference frame, the object is located in relation to the position of the subject's body . In an allocentric reference frame, the object is localized in relation to other objects in the external visual world. The goal of this summer's project was to determine the relative role of egocentric and allocentric cues in pointing movements.

In order to determine the relative importance of egocentric and allocentric cues, subjects were asked to point in the dark to the remembered position of a target. The target was initially seen either against a plain, dark background or against a featured background, that is as part of a rich visual scene. If egocentric cues are used primarily for pointing movements then the presence of the featured background should not affect pointing accuracy. In contrast, if allocentric cues are necessary for accurate pointing movements, then the presence of the featured background will improve pointing performance. The results from this study indicate that the presence of a featured background does not improve pointing accuracy. Therefore, egocentric as opposed to allocentric cues may be used primarily for pointing movements.

INTRODUCTION

During space flight and immediately after return to the 1-g environment of earth, astronauts experience perceptual and sensory-motor disturbances (Young *et al* , 1984) . For example, after flight, crewmembers encounter gait and postural instability. Even two days postflight, astronauts show increased dependence on visual cues to prevent falling (Kenyon and Young, 1986). Sensations of self or surround motion are experienced by crewmembers during voluntary head movements. These perceptual and sensory-motor changes result from adaptation of the astronaut to the microgravity environment of space. During space flight, sensory information from the eyes, limbs and vestibular organs is reinterpreted by the central nervous system in order to produce appropriate body movements in microgravity. This adaptation takes several days to develop. Upon return to earth, the changes in the sensory-motor system are no longer appropriate to a 1-g environment. Over several days, the astronaut must re-adapt to the terrestrial environment.

Alterations in sensory-motor function may affect eye-head-hand coordination and, thus, the crewmember's ability to manually locate objects in extrapersonal space. Previous reports have demonstrated that crewmembers have difficulty in estimating joint and limb position and in pointing to memorized target positions on orbit and immediately postflight (Watt *et al* 1985). The ability to point at or reach toward an object or perform other manual tasks is essential for safe Shuttle operation and may be compromised particularly during re-entry and landing sequences and during possible emergency egress from the Shuttle. An understanding of eye-head-hand coordination and the changes produced during space flight is necessary to develop effective countermeasures. This summer's project formed part of a study of the sensory cues used in the manual localization of objects.

To point or reach toward a target, a subject must determine the precise location of the object in extrapersonal space. The position of the target can be determined by using either an egocentric or allocentric reference frame. In an egocentric reference frame, the object is located in relation to the position of the subject's body (Paillard, 1991; Blouin *et al.*, 1993). Egocentric cues include the direction of gaze and proprioceptive information on the position of the limbs. In an allocentric reference frame, the object is localized in relation to other objects in the external visual world. Thus, the egocentric system is dependent upon internal signals while the allocentric system is dependent upon external cues. The goal of this summer's project was to determine the relative role of egocentric and allocentric cues in pointing movements.

In order to determine the relative importance of egocentric and allocentric cues, subjects were asked to point in the dark to the remembered position of a target. The target was initially seen either

against a plain, dark background or against a featured background, that is as part of a rich visual scene (Figure 1). If egocentric cues are used primarily for pointing movements then the presence of the featured background should not affect pointing accuracy. In contrast, if allocentric cues are necessary for accurate pointing movements, then the presence of the featured background will improve pointing performance. The results from this study indicate that the presence of a featured background does not improve pointing accuracy. Therefore, egocentric as opposed to allocentric cues may be used primarily for pointing movements.

METHODS

Subjects:

Ten subjects, four males and six females, ranging in age from 20 to 50 years, were tested. Six of the subjects were right-handed while four were left-handed.

Experimental setup:

In order to measure pointing accuracy, subjects were seated in a chair located one meter from the center of a screen. The target was illuminated on the center of the screen at eye-level.

A laser for pointing was mounted onto a plastic sleeve which then fit over the subject's index finger . The laser was secured with Velcro straps, and its position on the finger was adjusted along the vertical axis. The subject wore the laser on the preferred hand and held the controls for the laser in the opposite hand. For each test, subjects practiced pointing with the laser at the target on the screen and adjusted the position of the laser along the vertical axis until they were confident that the laser beam projected in the direction that they perceived to be pointing.

The target was initially displayed on a computer monitor and then projected onto the viewing screen using an overhead projector equipped with a special display panel (Proxima Corporation, San Diego CA.). The display panel possessed an auxiliary scanning device that was used to record the laser beam spot on the display screen when the subject pointed with the laser at the remembered target position. The display window has a resolution of 640 units horizontal by 480 units vertical. Software was written both to momentarily display a target on the screen and then dynamically record the coordinates of the laser spot (Figure 2).

Experimental protocols:

After the position of the laser beam was adjusted on the finger, the subject was asked to fixate on but not point at the target on the screen. The lights were then extinguished and the subject was asked to point in

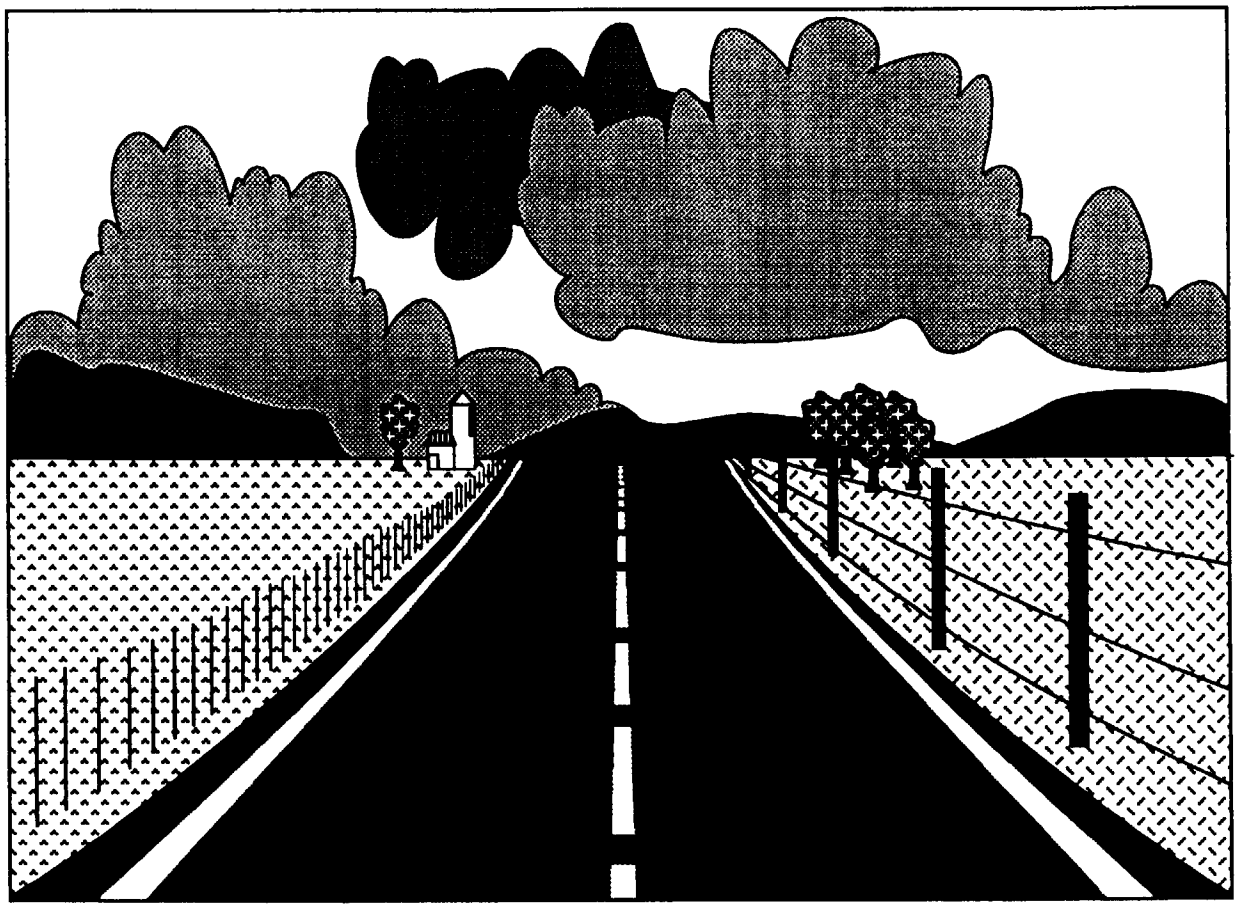

Figure 1.- The featured background. The target is seen here in the center of the visual scene.

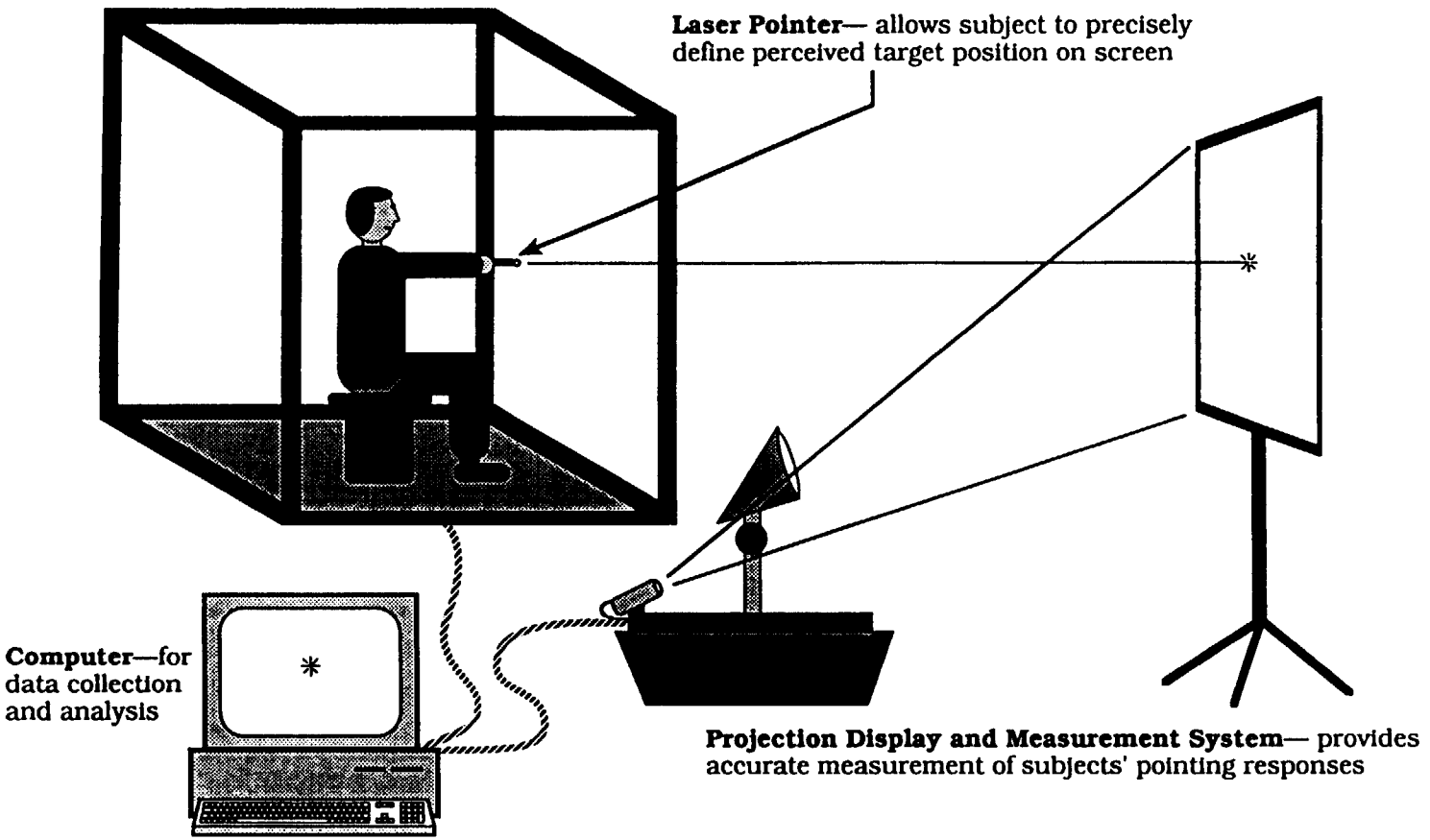

Figure 2.- The experimental set-up.

the dark at the screen to the remembered position of the target. After pointing, the subject lowered his or her arm, the screen was re-illuminated and the target again appeared on the screen for another pointing trial. This procedure was repeated thirty times.

Four different variations of the pointing task were run. For each type of test, the same ten subjects were used. The four variations are described below:

1.) The target consisted of a bright spot always positioned at the center of the screen. The target was seen against a plain, dark background.

2.) The target consisted of a bright spot always positioned in the center of the screen. The target was seen against a featured background, that is within a visual scene (Figure 1). The scene, a landscape of a farm, road and sky, was designed to give the subject cues as to what was up and what was down. The road bisected the scene, and the images on either side of the road were not identical so that the scene contained asymmetrical right and left halves.

3.) The target consisted of a bright spot that was randomly positioned on the screen for each of the thirty trials. The target was seen against a plain background.

4.) The target consisted of a bright spot that was randomly positioned on the screen for each of the thirty trials. The target was seen against a featured background.

For the ten subjects, the order of the tests was always 1 through 4. The time between each test was at least four days. The rationale for the design of the four types of tests is given below.

The subjects were asked to point in the dark so as to eliminate any vision of their limbs while pointing. Vision of the limbs would provide a cue for pointing that is not purely egocentric or allocentric and would thus confound interpretation of the experimental results. By pointing in the dark, the subjects also received minimal feedback of how accurately they had pointed.

If the target was seen against a plain background (tests 1 and 3), then the subject relied on egocentric cues, ie the direction of the gaze and the position of the arm, to help determine where to point. If the target was seen against a featured background (tests 2 and 4), then the subject could use allocentric as well as egocentric cues to help determine where to point. Allocentric cues would include the relationship of the target to other images on the screen.

If the target was always located at the center of the screen (tests 1 and 2) , then with repeated trials, the subject may be able to use the memory of his or her arm position during each trial to help determine

where to point. If the target was found at a different locations with each trial (tests 3 and 4) , then a memory of the arm position used in the former trial will be less useful in determining where to point.

Data analysis:

The resultant deviation in centimeters of the position of the laser beam from actual target position on the screen was determined for each trial. This deviation was considered the pointing error. The values of pointing error for all thirty trials were then averaged. Mean values of pointing error were compared between the four types of tests for a single subject using a Student's unpaired, two-tailed T test. A p value of less than 0.05 indicated a significant difference between the means.

RESULTS

The pointing error from subject to subject ranged from an average of 3.5 cm to 37 cm. No consistent difference was seen between the four left-handed and six right-handed subjects.

The mean pointing error was compared for each subject between tests in which the target was presented at a central spot on the screen against either a plain or featured background (Figure 3). For four of the subjects, the pointing accuracy improved when the target was seen against a plain background; for two of the subjects, pointing accuracy improved when the target was seen against a featured background, while for two subjects, no significant difference was seen in tests using a plain or featured background . Thus, the featured background generally produced no improvement in pointing performance. Since the test involving a plain background was always performed before the test using a featured background, the improvement with a featured background for two of the subjects may simply reflect improvement from practice. When a second test was run on the two subjects using a plain background, no significant difference was seen between the second test using a plain background and the test using a featured background (pointing error for subject G, plain background, test 2: 8.34+/-0.69; featured background: 7.58 +/- 0.73; pointing error for subject H, plain background, test 2: 10.39+/-0.76, featured background: 11.26+/-1.21).

Mean pointing error was also compared for each subject between tests in which the target was randomly located on the screen for each trial either against a plain or featured background (Figure 4). No difference between a plain and featured background was seen in pointing accuracy for six of the ten subjects. Two subjects performed more accurately using a plain background while two subjects performed more

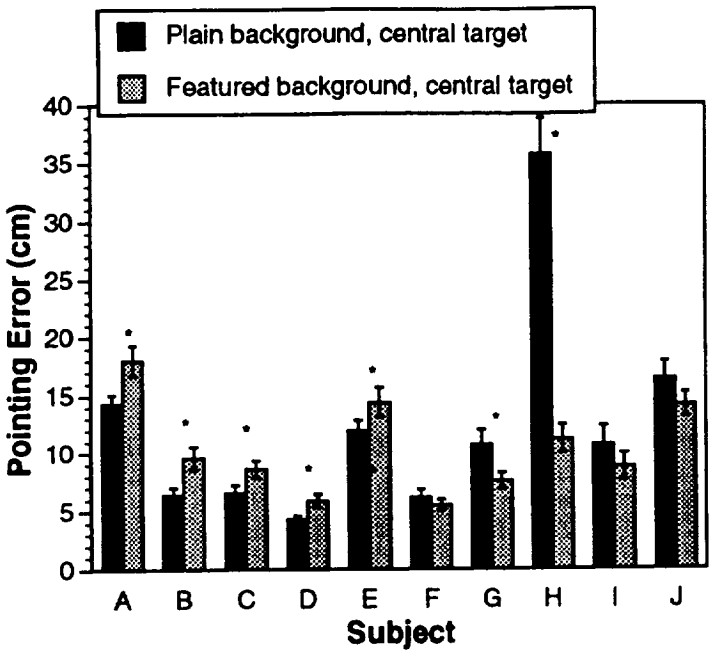

Figure 3.- Error in pointing at a central target seen by the subject against a plain or featured background. Data represent mean +/- S.E.M. of thirty trials. Asterisks indicate significant difference.

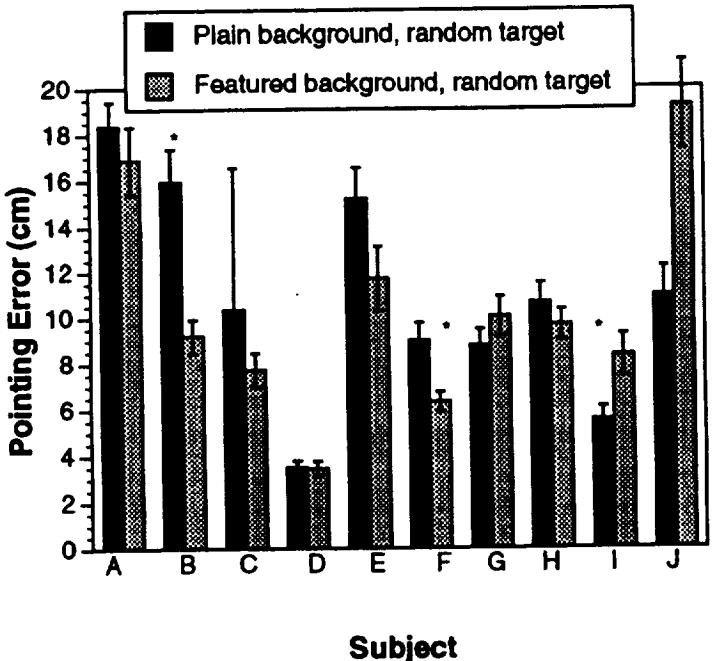

Figure 4.- Error in pointing at a randomly-positioned target seen by the subject against a plain or featured background. Data represent mean +/- S.E.M. of thirty trials. Asterisks indicate significant difference.

accurately using a featured background. As with the tests involving a centrally-located target, the featured background generally did not improve pointing accuracy.

As can be seen in figure 5 and 6, subjects pointed with similar accuracy when the target was centrally-located for all trails as when the target was located at a different position on the screen for each trial. When the target was seen against a plain background (Figure 5), three subjects performed more accurately when pointing at a centrally-located target while three subjects pointed more accurately when the target was randomly-located. No significant differences between centrally- and randomly- located targets were seen for four subjects. When the target appeared against a featured background (Figure 6), one subject performed more accurately with a randomly-located target while two pointed more accurately at a centrally-located target. For the other seven subjects, no significant differences were seen.

DISCUSSION

The experiments performed in this study were designed to test whether or not subjects use egocentric or allocentric cues in pointing at a target. If allocentric cues are used, then the placement of the target in a featured background should enhance pointing accuracy over that seen when the target is placed in a plain background. However, subjects pointed with similar accuracy whether the target was placed in a plain or featured background. This result was seen whether or not the target was located in the same central spot or at a different location with each pointing trial.

One concern in the interpretation of these experiments is the ability of the subjects to perform consistently from day to day. For example, the subjects may learn during the first test how to point more accurately and, therefore, perform better on the second test for reasons unrelated to the changes in target position or type of background. The learning that occurs from test to test is minimized by the fact that the subjects receive no visual feedback during trials of how accurately they pointed. In every test, the subjects pointed in the dark to a remembered location of the target. Furthermore, the test using a featured background was always performed after the test using a plain background. If the subjects had learned to point more accurately from the first test with a plain background, then they should all perform more accurately in the second test using a featured background. Yet, eight out of the ten subjects did not point more accurately on the second, featured-background test. Two subjects did perform more accurately. When they were retested using a plain background, they pointed with the same accuracy as they had in the test with the featured background. Thus,

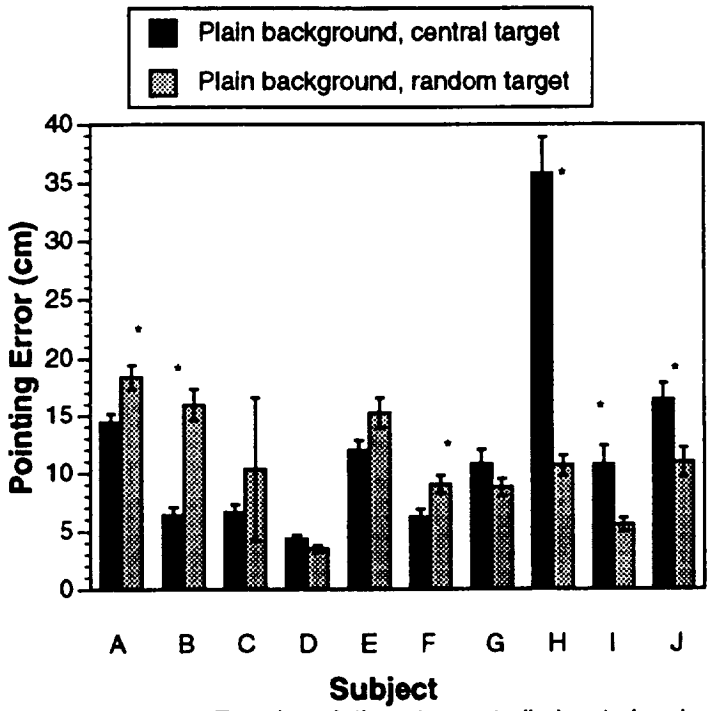

Figure 5.- Error in pointing at a centrally-located and randomly-located target seen by the subject against a plain background. Data represent mean +/- S.E.M. of thirty trials. Asterisks indicate significant difference.

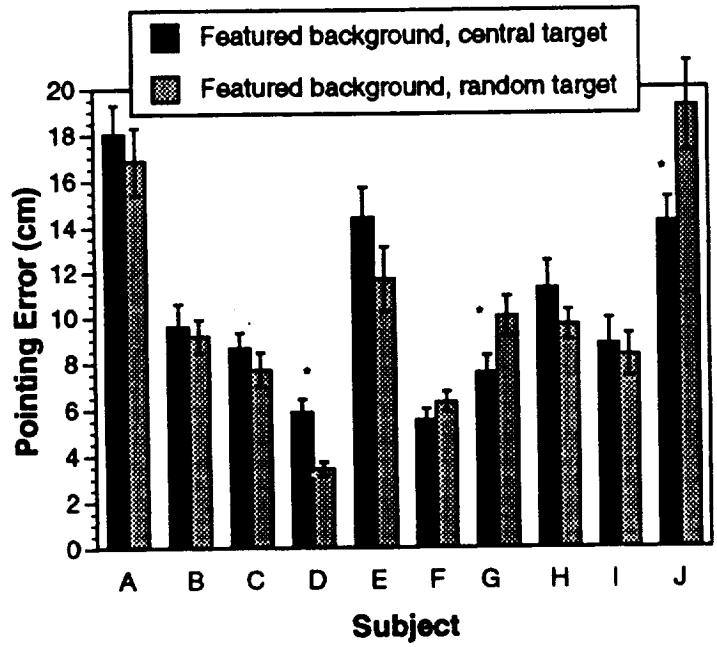

Figure 6.- Error in pointing at a centrally-located and randomly-located target seen by the subject against a featured background. Data represent mean +/- S.E.M. of thirty trials. Asterisks indicate significant difference.

the improvement seen in these two subjects when tested with a featured background may result more from learning how to point more accurately than from the presence of a featured background.

These data strongly indicate that a featured background does not improve pointing accuracy over that seen using a plain background. Thus, egocentric cues, such as the direction of gaze and the position of the limbs, play a much greater role in pointing accuracy than allocentric cues. Subjects determine where to point by the relationship of the target to themselves as opposed to the relationship of the target to other images in the external visual field.

Similar results have been reported by Blouin *et al* ., (1993). These investigators determined that humans point with equal accuracy when the target was seen either in a dark room or in a lighted structured environment. In their experiments, the subject observed the target while pointing. In contrast, in the experiments reported here, the subjects pointed to a remembered location of the target.

Further evidence for an egocentric bias in pointing is seen in the experiments of Stark and Bridgeman (1983). These investigators tested the role of eye position during pointing. They pressed on the subjects eyes during a pointing task in order to send to the central nervous system incorrect information about the position of the eyes. If the target was seen against a featured background, the subjects *perceived* the location of the object correctly. However, they *pointed* to the wrong location in the direction incorrectly given by the eye position signal (Paillard, 1991).

A surprising result from the experiments reported here is that subjects performed with equal accuracy when pointing at target that was centrally-located for each trial as when pointing at a target that was in a different position with each trial. Before each test, the subjects adjusted the position of the laser on their finger by pointing at a centrally-located target at the screen. During this adjustment period, the subjects received visual feedback of how accurately they had pointed. Thus, one might suspect that the subjects would perform better in subsequent tests involving a centrally-located target. Moreover, in tests where the target was located at a central position with each trial, the subject may remember the arm and hand position used in the former trial and use this information as a cue for where to place the arm and hand when pointing in the subsequent trial. Since the majority of subjects performed with equal accuracy in tests involving centrally- and randomly-located targets, other cues, such as eye position, may be more important in determining where to point. This result merits further investigation.

This summer's study not only provided information on the role of egocentric and allocentric cues in manual localization of targets but also provided information for the design of future experiments. One of the major goals of the laboratory is to determine the role of vestibular signals in manual pointing movements. Vestibular input from the

otoliths and semicircular canals provides information on head movements and the position of the head with respect to gravity and thus contributes to the perception of the position of the body in space. While on orbit and following return to earth, astronauts' vestibular responses change. These changes may affect goal-directed pointing movements. To determine the role of the vestibular system in pointing movements, subjects will be asked to point to objects following transient rotational or linear displacement (Bloomberg *et al.*, 1991) . One question in the design of these experiments is whether to place the target in a plain or featured background. The results of this summer's experiments indicate that maximal pointing accuracy can be obtained when the target is placed against a plain, dark background.

During space flight, signals from proprioceptive and vestibular receptors are re-interpreted by the central nervous system. As a result, the egocentric reference frame is altered. Immediately postflight, crewmembers are more dependent than preflight on visual or allocentric cues for maintaining balance and locomotion. The relative importance of egocentric and allocentric cues in pointing movements and other manual tasks may also change postflight. Different results from those reported here may be seen if this study was performed on crewmembers shortly after their return to earth.

REFERENCES

1.) Bloomberg J, Jones GM, Segal B (1991) Adaptive modification of vestibularly perceived rotation. *Exp. Brain Res.* 84: 47-56.

2.) Blouin J, Bard C, Teasdale N, Paillard J, Fleury M, Forget R, Lamarre Y (1991). Reference systems for coding spatial information in normal subjects and a deafferented patient. *Exp. Brain Res.* 93: 324-331.

3.) Kenyon RV, Young LR (1986). MIT/Canadian vestibular experiments on Spacelab-1: 4. Pstural responses following exposure to weightlessness. *Exp. Brain Res.* 64: 335-346.

4.) Paillard J (1991). Motor and representational framing of space. In: Paillared J (ed.) *Brain and Space.* New York: Oxford Univ. Press, pp. 163-182.

5.) Stark L and Bridgeman B (1983). Role of corollary discharge in space constancy. *Perception and Psychophysics.* 34: 371-380.

6.) Watt DGD. Money KE, Bondar RL, Thirsk RB, Garneau M, Scully-Power P (1985). Canadian medical experiments on shuttle flight 41-G. *Can Aeronaut. Space J.* 31:215-226.

7.) Young LR, Oman CM, Watt DGD, Money KE, Lichtenberg BK (1984). Spatial orientation iin weightlessness and readaptation to earth's gravity. *Science.* 225: 205-208.

N94- 25352

PARALLEL PROCESSING METHODS FOR SPACE BASED POWER SYSTEMS

Final Report

NASA/ASEE Summer Faculty Fellowship Program--1993

Johnson Space Center

Prepared By:	F.C. Berry
Academic Rank:	Associate Professor
University & Department:	Department of Electrical Engineering Louisiana Tech University Ruston, Louisiana 71272
NASA/JSC	
Directorate:	Engineering
Division:	Propulsion And Power
Branch:	Power
JSC Colleagues:	Bob Hendrix
	Tom Jeffcoat
Data Submitted:	7-30-93
Contract Number:	NGT-44-001-800

ABSTRACT

This report presents a method for doing load-flow analysis of a power system by using a decomposition approach. The power system for the Space Shuttle is used as a basis to build a model for the load-flow analysis. To test the decomposition method for doing load-flow analysis, simulations were performed on power systems of 16, 25, 34, 43, 52, 61, 70, and 79 nodes. Each of the power systems was divided into subsystems and simulated under steady-state conditions. The results from these tests have been found to be as accurate as tests performed using a standard serial simulator. The division of the power systems into different subsystems was done by assigning a processor to each area. There were 13 transputers available, therefore, up to 13 different subsystems could be simulated at the same time.

This report has preliminary results for a load-flow analysis using a decomposition principal. The report shows that the decomposition algorithm for load-flow analysis is well suited for parallel processing and provides increases in the speed of execution.

INTRODUCTION

A research project, Advanced Electrical Power Management Techniques for Space Systems (ADEPTS), was started at the Johnson Space Center in 1986. The basic goal of ADEPTS was to automate the operations of a space based power system (SBPS) by using the technology of parallel and distributed processing.

From the ADEPTS project, three basic functions were identified which would form the basis of a management system for a SBPS. First was the monitoring of the power system that could be accomplished by the use of state estimation. Second was the scheduling of the generation to meet the required load of the SBPS that could be accomplished by unit dispatch. Third was the solution of the SBPS that could be accomplished by the use of load-flow analysis.

Methods like state estimation, unit dispatch, load-flow analysis, etc., are well-established tools that have been used heavily by the electric power industry since the introduction of the digital computer. However, the use of parallel processing is still relatively new when applied to the area of power systems [1]. In the last few years, a significant amount of research has been done in the area of parallel processing of power system problems. Most of this work has been in the development of algorithms. Actual testing on multiprocessor architectures is still near the beginning stages. The largest uncertainty today is the evolution of the hardware. For example:

1. Pipelined computers in which temporal parallelism is used to calculate overlapped computations. Early Cray-1 and Cyber 205 are good examples of these systems.

2. Array processors in which spatial parallelism is utilized through synchronized arithmetic logical units (ALU). The Illiac-IV is a good example of this system.

3. Parallel processing systems in which asynchronous parallelism is employed at the software level with the Cray X-MP and Cray 2 as typical examples.

Shared-memory and distributed processors are two basic systems of parallel computers that can offer increases in computational power but their acceptability and long term viability is unpredictable [1].

Because parallel algorithm development was much further along, ADEPTS chose to make use of the existing algorithms and focused on tailoring these algorithms to a

specific hardware design. To accomplish this, a hardware platform and software environment had to be decided upon. The INMOS T800 transputer was used as the basic hardware platform. The T800 transputer is a 32 bit reduced instruction set computer (RISC) running at 25 MHz [2]. The T800 transputer can communicate with other transputers or a host computer by a set of four bi-directional channels. By using these channels, a variety of hardware architecture can be investigated. Also, additional transputer modules can be easily added in the future to further enhance the system without making obsolete the existing transputers. Because of the difficulties encountered in developing parallel software, the Express® "operating system" was chosen. The Express package is best classified as a transparent parallel operating system with a set of tools and utilities for developing parallel programs [3, 4, 11].

A preliminary parallel architecture for a management system of a SBPS (Figure 1) was developed and tested using the power system of the Space Shuttle (Orbiter) as a model. The electric power distribution system that is present on the Orbiter is made up of three strings each having a fuel cell that provides DC voltage to those systems that require DC, and the inverters that convert the DC to AC for those elements that require AC. Figure 2 is a block diagram representation of the power system of the Orbiter.

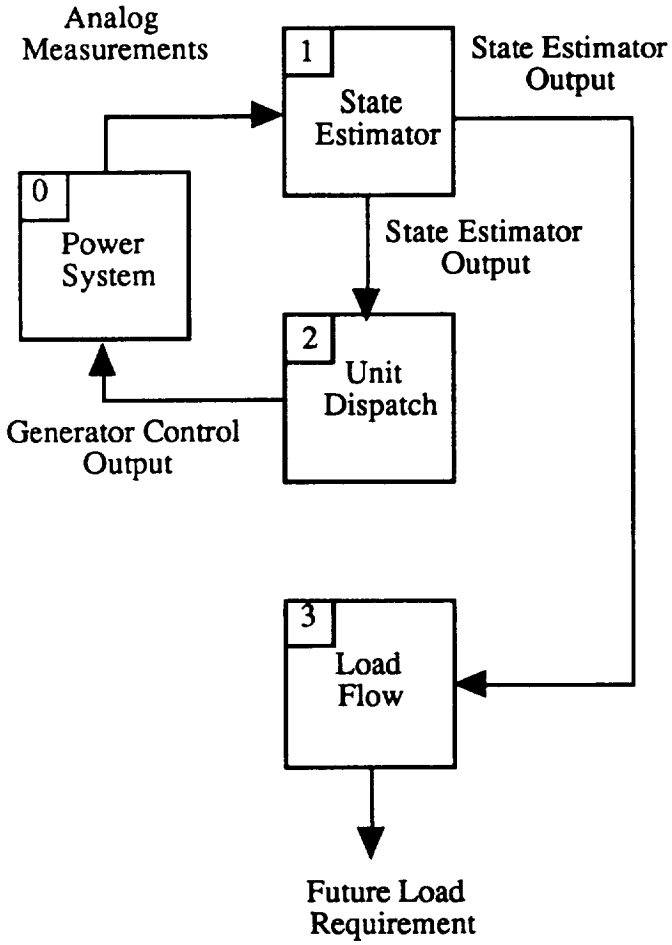

Figure 1: Block Diagram Of A Power Management System.

Preliminary tests of the architecture of Figure 1, using the Orbiter power system, showed that the load-flow program took from 20% to 50% of total processing time depending on the size of the electrical circuit that the load-flow program was solving. To improve the overall performance of the architecture of Figure 1, a different architecture for the load-flow was investigated.

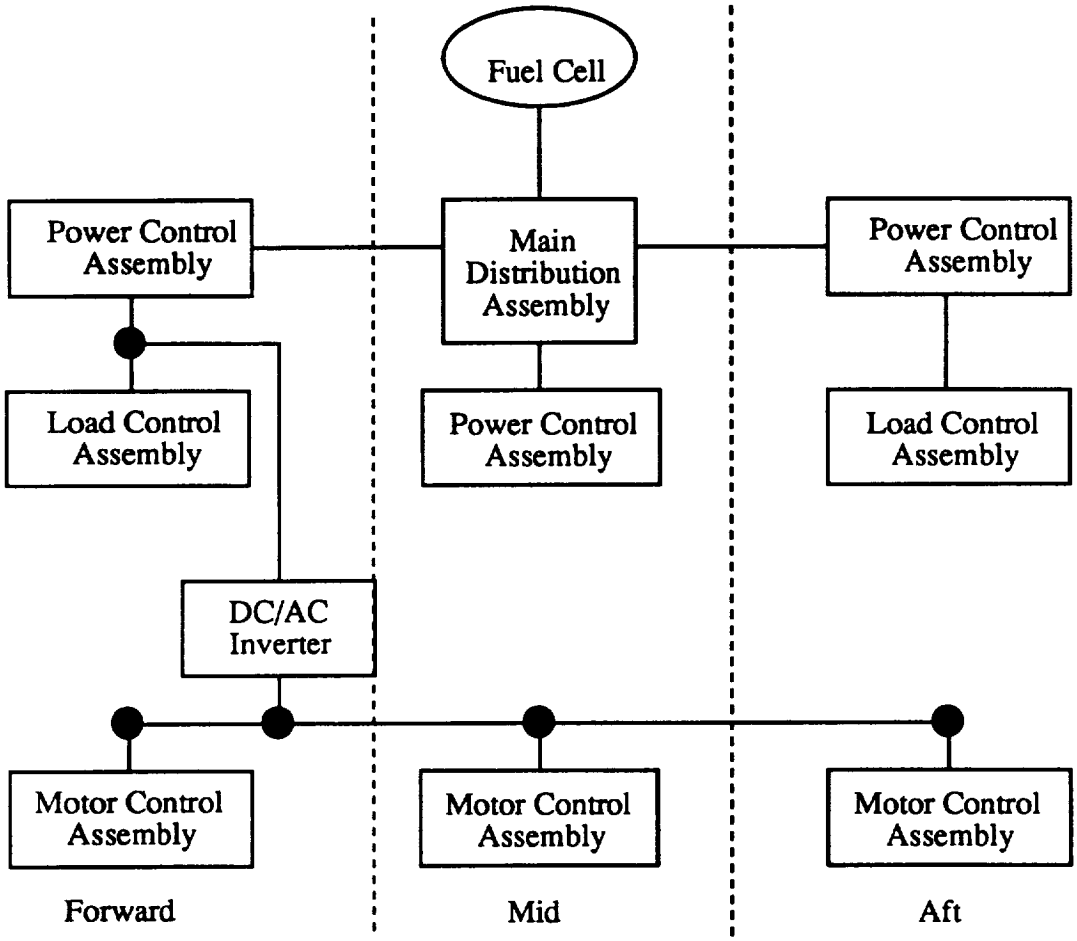

Figure 2: Power Distribution System for the Space Shuttle (1 of 3 Strings).

RELATED RESEARCH

A general definition of load-flow is given: Load-flow is the steady-state solution of equations that describe a power system. These equations can be nonlinear and algebraic. They can be nonlinear because they express powers as a function of voltages. They are algebraic because they describe the steady-state instead of the transient behavior of the power system. [5]

Rafian, Sterling, and Irving [6], presented a method for load-flow analysis for power systems by tearing the network into a number of independent subsystems. These subsystems could then be solved in parallel resulting in a saving of time for on-line control. This method of decomposed load-flow analysis was based on the fast decoupled load-flow algorithm. The decomposed load-flow technique that was presented would

normally give the greatest reduction in time, if the system could be divided such that the subsystems were interconnected only by a few tie lines (separating nodes).

Rafian, Sterling, and Irving [7], present a mathematical technique for the decomposition of a set of nonlinear algebraic and differential equations which result from a corresponding dynamic model of an electric power system. This method of load-flow analysis for power systems again tears the network into a number of independent subsystems. These subsystems could then be executed in parallel. This method of decomposed load-flow analysis was based on the Newton-Raphson load-flow algorithm. It was also shown that this decomposed load-flow algorithm was suitable for implementation on parallel processors with a 32-bit word capability. This decomposition technique resulted in significant savings in the simulation elapsed time.

Wang, Xiang, Wang, and Huang [8], presented two algorithms for a parallel solution of the reduced gradient optimal power flow. The parallel solution method for optimal power flow was accomplished by tearing the network into a number of independent subsystems. These subsystems were then solved in parallel by using what the authors called a two-level computer network.

Berry and Cox [9], presented a coordination decomposition method for load-flow analysis using the Gauss-Siedel algorithm. This coordination decomposition method was accomplished by the tearing of the electrical network into a number of independent subsystems which could then be solved in parallel. However, this load-flow algorithm was only simulated on a serial computer and no true parallel processing took place.

Taoka, Iyoda, Noguchi, Sato, and Nakazawa [10], presented a Gauss-Siedel method for doing load-flow analysis on a hyper cube computer. The algorithm that was presented consisted of solving the power flow equations in an iterative manner in order to minimize the communication between nodes.

LOAD-FLOW

Load-flow is the name given to a network solution that shows currents, voltages, and power flow at every bus in the system. In the load-flow problem, a relationship between voltage and current at each bus exists and the load-flow calculation must solve for all voltages and currents such that these relationships are satisfied. As such, the load-flow gives the electrical response of the transmission system to a particular set of loads and generator unit outputs. Therefore, load-flow is the solution of an electrical network that gives the values of currents, voltages, and power flow at every bus (node) in the electrical power system.

To start the load-flow solution process, a set of linear equations is formulated for an electrical network. This linear set of equations is generally of the node form as represented by equations (1).

$$\begin{bmatrix} I_1 \\ I_2 \\ . \\ . \\ I_i \end{bmatrix} = \begin{bmatrix} Y_{11} & Y_{12} & . & . & Y_{1j} \\ Y_{21} & Y_{22} & . & . & . \\ . & . & . & . & . \\ . & . & . & . & . \\ Y_{i1} & . & . & . & Y_{ii} \end{bmatrix} \begin{bmatrix} E_1 \\ E_2 \\ . \\ . \\ E_i \end{bmatrix} \tag{1}$$

Although currents entering the nodes from generators and load branches are not known, they can be written in terms of P and E.

$$I_i = \frac{P_i}{E_i} \tag{2}$$

Since currents entering the nodes are considered positive, then power flow into the node is also considered positive, and power dissipated in the resistors would be entered as a negative number.

Substituting equation 2 into equation 1 gives the following result.

$$\begin{bmatrix} \frac{P_1}{E_1} \\ \frac{P_2}{E_2} \\ . \\ . \\ \frac{P_i}{E_i} \end{bmatrix} = \begin{bmatrix} I_1 \\ I_2 \\ . \\ . \\ I_i \end{bmatrix} = \begin{bmatrix} Y_{11} & Y_{12} & . & . & Y_{1j} \\ Y_{21} & Y_{22} & . & . & . \\ . & . & . & . & . \\ . & . & . & . & . \\ Y_{i1} & . & . & . & Y_{ii} \end{bmatrix} \begin{bmatrix} E_1 \\ E_2 \\ . \\ . \\ E_i \end{bmatrix} \tag{3}$$

$$\begin{aligned} \frac{P_1}{E_1} &= Y_{11}E_1 + Y_{12}E_2 + \ldots + Y_{1j}E_i \\ \frac{P_2}{E_2} &= Y_{21}E_1 + Y_{22}E_2 + \ldots + Y_{2j}E_i \\ . \quad & . \quad . \quad . \\ . \quad & . \quad . \quad . \\ \frac{P_i}{E_i} &= Y_{i1}E_1 + Y_{12}E_2 + \ldots + Y_{1i}E_i \end{aligned} \tag{4}$$

The set of equations (4) may be solved for E_1 through E_i by the use of an iteration technique.

$$\begin{aligned} E_2 &= \frac{1}{Y_{22}} \left\{ \frac{P_2}{E_2} - [Y_{21}E_1 + \ldots + Y_{2j}E_i] \right\} \\ . \quad & . \quad . \quad . \\ . \quad & . \quad . \\ E_i &= \frac{1}{Y_{ii}} \left\{ \frac{P_i}{E_i} - [Y_{i1}E_1 + \ldots + Y_{(i-1)(j-1)}E_{(i-1)}] \right\} \end{aligned} \tag{5}$$

Note that E_i has been written in terms of itself and the other voltages. Also, one equation has been deleted, this equation or bus is designated as the swing or slack bus. The swing or slack bus is generally a generator that is the first to react to changes in the system. Generally the voltage at the slack bus is specified.

DECOMPOSITION METHOD

The decomposition method for load-flow analysis was started by dividing the electrical power system into a number of smaller systems or subsystems. These subsystems can then be solved independently in parallel [13]. To demonstrate the decomposition method for load-flow analysis, an example will be presented.

The electrical power system of Figure 3 was decomposed by using the admittance matrix (Table 1). The admittance matrix was transformed so that each of the subsystems would appear sequentially; that is, the nodes were renumbered for the electrical circuit. This renumbering caused the network equations for each subsystem to follow the

dynamic equations for that same subsystem. Hence, for the power system of Figure 3 there were 4 different subsystems. In the admittance matrix, the diagonal elements Y_{ii} are the summation of all admittances that surround the ith node, where $Y_{il} = Y_{1i}$ and is the negative of the branch. The admittance for Figure 3 is given in Table 1.

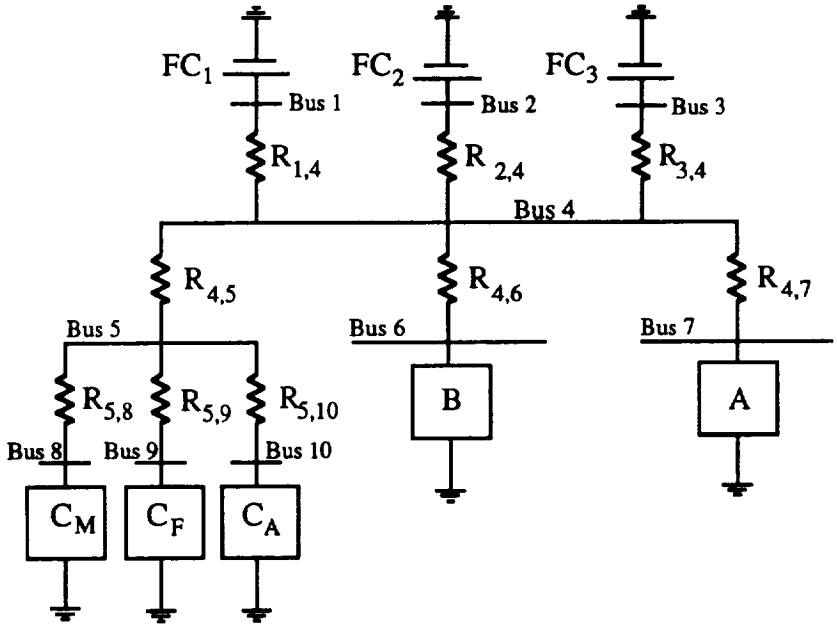

Figure 3: Space Shuttle Power Distribution System.

Table 1: The Admittance Matrix.

	1	2	3	4	5	6	7	8	9	10
1	$Y_{1,1}$			$-Y_{1,4}$						
2		$Y_{2,2}$		$-Y_{2,4}$						
3			$Y_{3,3}$	$-Y_{3,4}$						
4	$-Y_{4,1}$	$-Y_{4,2}$	$-Y_{4,3}$	$Y_{4,4}$	$-Y_{4,5}$	$-Y_{4,6}$	$-Y_{4,7}$			
5				$-Y_{5,4}$	$Y_{5,5}$			$-Y_{5,8}$	$-Y_{5,9}$	$-Y_{5,10}$
6				$-Y_{6,4}$		$Y_{6,6}$				
7				$-Y_{7,4}$			$Y_{7,7}$			
8					$-Y_{8,5}$			$Y_{8,8}$		
9					$-Y_{9,5}$				$Y_{9,9}$	
10					$-Y_{10,5}$					$Y_{10,10}$

After the renumbering of Table 1 is completed the admittance matrix of Table 2 is created. The admittance matrix from Table 2 can be expressed as the sum of two matrices.

$$[Y] = [Y_l] + [Y_c] \tag{6}$$

Where $[Y_l]$ are a number of block diagonal submatrices that represents a matrix for a specific subsystem. From the $[Y_l]$ matrix, it can be seen that four different sets of equations can be produced, one set for each subsystem as shown in Figure 4 and Table 3.

Table 2: The Admittance Matrix Renumbered.

	1	2	3	4	5	6	7	8	9	10
1	$Y_{1,1}$			$-Y_{1,4}$						
2		$Y_{2,2}$		$-Y_{2,4}$						
3			$Y_{3,3}$	$-Y_{3,4}$						
4	$-Y_{4,1}$	$-Y_{4,2}$	$-Y_{4,3}$	$Y_{4,4}$	$-Y_{4,5}$				$-Y_{4,9}$	$-Y_{4,10}$
5				$-Y_{5,4}$	$Y_{5,5}$	$-Y_{5,6}$	$-Y_{5,7}$	$-Y_{5,8}$		
6					$-Y_{6,5}$	$Y_{6,6}$				
7					$-Y_{7,5}$		$Y_{7,7}$			
8					$-Y_{8,5}$			$Y_{8,8}$		
9				$-Y_{9,4}$					$Y_{9,9}$	
10				$-Y_{10,4}$						$Y_{10,10}$

Table 3: The Admittance Matrix $[Y_1]$.

	1	2	3	4	5	6	7	8	9	10
1	$Y_{1,1}$			$-Y_{1,4}$						
2		$Y_{2,2}$		$-Y_{2,4}$						
3			$Y_{3,3}$	$-Y_{3,4}$						
4	$-Y_{4,1}$	$-Y_{4,2}$	$-Y_{4,3}$	$Y_{4,4}$						
5					$Y_{5,5}$	$-Y_{5,6}$	$-Y_{5,7}$	$-Y_{5,8}$		
6					$-Y_{6,5}$	$Y_{6,6}$				
7					$-Y_{7,5}$		$Y_{7,7}$			
8					$-Y_{8,5}$			$Y_{8,8}$		
9									$Y_{9,9}$	
10										$Y_{10,10}$

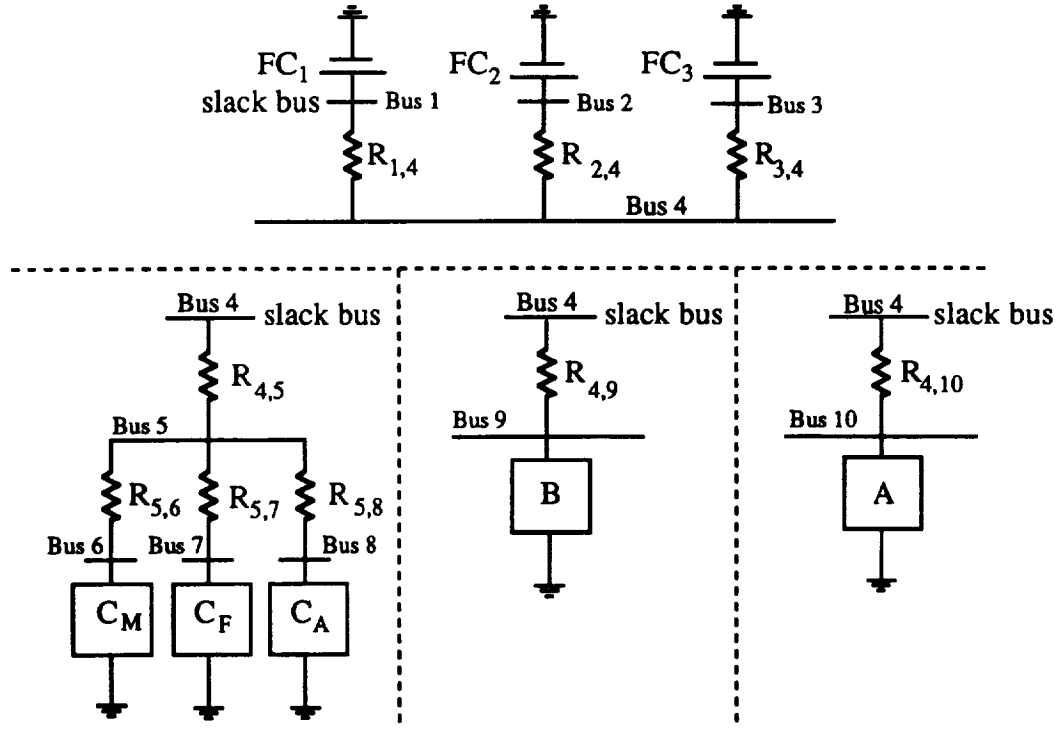

Figure 4: Decomposed Space Shuttle Power Distribution System.

Each of the individual subsystems shown in Figure 4 and Table 3 can be solved independently. These subsystems require their own slack bus and one of these slack buses will serve as the slack bus for the entire system.

The remaining elements, $[Y_c]$ of the admittance matrix are the nonzero off diagonal elements that are the separating nodes of one subsystem with respect to the node voltages in another subsystem. Table 4 shows the $[Y_c]$ matrix.

Table 4: The Admittance Matrix $[Y_c]$.

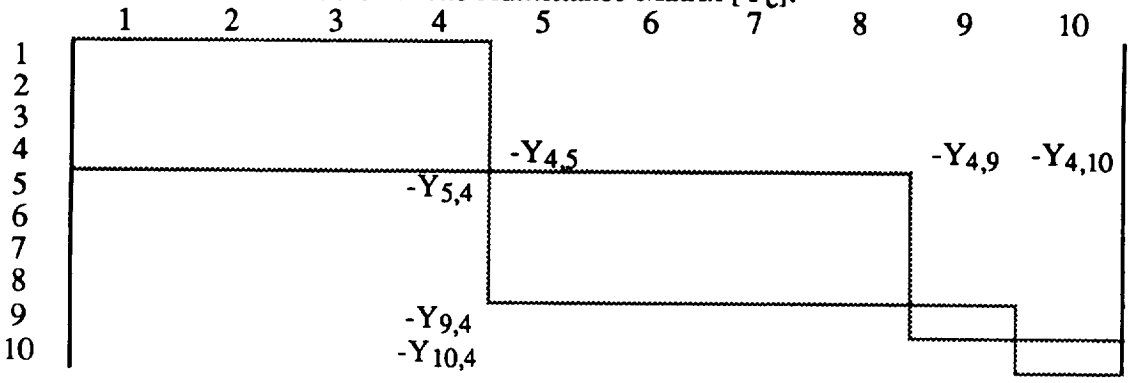

These nonzero off diagonal elements act as sending or receiving nodes for power flow from one subsystem to another. Therefore, these nonzero off diagonal elements can be referred to as voltage and power (EP) separating nodes. Finally, these nonzero off diagonal elements are directly related to the number of common nodes in different subsystems.

From the $[Y_c]$ matrix, it can be seen that at node 4 the system was divided. The $[Y_c]$ matrix is the coordination matrix and generally this matrix will contain the separating nodes. The function of the coordination matrix is to determine the amount of ΔP and ΔE that the separating nodes contribute to each subsystem.

PERFORMANCE ANALYSIS

To test the decomposition method for doing load-flow analysis, simulations were performed on power systems of 16, 25, 34, 43, 52, 61, 70, and 79 nodes. Each of the power systems was divided into subsystems and simulated under steady-state conditions. The results from these tests have been found to be as accurate as tests performed using a standard serial simulator. The division of the power systems into different subsystems was done by assigning a processor to each area. Table 5 provides the results of timing tests for each of the power systems. The times reported in Table 5 are the times associated with the solution of the load-flow problem (Node Time) and part of the host I/O (Host I/O). The Node Time includes internode communication time, calculation time, and part of the host I/O time. The Host I/O time reported in Table 5 is that part of the total host I/O time required to print the result of the load-flow calculation to the screen and the time to create two files, which contains the data of the timing tests that are reported in the following tables.

Table 5: Timing Data

		16 buses	25 buses	34 buses	43 buses
1	Node Time ms	56.77	94.59	146.88	211.9
Transputer	Host I/O ms	115.25	116.35	115.46	119.0
2	Node Time ms	33.41	44.29	51.97	71.6
Transputer	Host I/O ms	112.45	123.20	122.88	113.7
4	Node Time ms	33.02	44.67	48.19	54.9
Transputer	Host I/O ms	102.46	122.82	122.94	123.2
10	Node Time ms	*	*	*	44.4
Transputer	Host I/O ms	*	*	*	128.2
13	Node Time ms	*	*	*	25.9
Transputer	Host I/O ms	*	*	*	110.5

The results of the timing tests that are reported [illegible] running each program 10 times and examining the timi[illegible] recorded when the program finishes [3, 4, 11]. In order to [illegible] like speedup and efficiency, the times reported for the sin[illegible] "best case" and the times reported for the multiprocessor [illegible] By reporting the "best case" times for the single processor [illegible] times for the multiprocessor programs would provide the [illegible] and efficiency for the multiprocessor programs.

Again from Table 5 the Node Times did not change [illegible] these numbers are the actual times. The Host I/O numbers ch[illegible] next. Being consistent with the idea of the "worst case" [illegible] the best "best case" time for the single processor program [illegible] time for the multiprocessor programs. By using the best "[illegible] processor programs and the worst "worst case" time for [illegible] would provide the worst "worst case" for the speed[illegible] multiprocessor programs. This adjustment to Table 5 is give[illegible]

Table 6: Adjusted Time

		16 buses	25 buses	34 buses	43 buses
1	Node Time ms	56.77	94.59	146.88	211.9
Transputer	Host I/O ms	99.84	99.84	99.84	99.84
2	Node Time ms	33.41	44.29	51.97	71.68
Transputer	Host I/O ms	128.26	128.26	128.26	128.26
4	Node Time ms	33.02	44.67	48.19	54.91
Transputer	Host I/O ms	128.26	128.26	128.26	128.26
10	Node Time ms	*	*	*	44.42
Transputer	Host I/O ms	*	*	*	128.26
13	Node Time ms	*	*	*	25.92
Transputer	Host I/O ms	*	*	*	128.26

From Table 6, Table 7 was created. Table 7 is the total "be[illegible] processor program and the total "worst case" time for each m[illegible]

ORIGINAL PAGE IS
OF POOR QUALITY

Table 7: "Worst Case" Total Time

		16 buses	25 buses	34 buses	43 buses	52 buses	61 buses	70 buses	79 buses
1	Node Time ms	56.77	94.59	146.88	211.90	233.02	252.99	275.14	297.28
Transputer	Host I/O ms	99.84	99.84	99.84	99.84	99.84	99.84	99.84	99.84
	Total Time ms	156.61	194.43	246.72	311.74	332.86	352.83	374.98	397.12
2	Node Time ms	33.41	44.29	51.97	71.68	82.68	91.14	98.88	104.38
Transputer	Host I/O ms	128.26	128.26	128.26	128.26	128.26	128.26	128.26	128.26
	Total Time ms	161.67	172.55	180.23	199.94	210.94	219.40	227.14	232.64
4	Node Time ms	33.02	44.67	48.19	54.91	57.92	61.06	63.81	66.24
Transputer	Host I/O ms	128.26	128.26	128.26	128.26	128.26	128.26	128.26	128.26
	Total Time ms	161.28	172.93	176.45	183.17	186.18	189.32	192.07	194.50
10	Node Time ms	*	*	*	44.42	44.99	45.63	49.02	49.54
Transputer	Host I/O ms	*	*	*	128.26	128.26	128.26	128.26	128.26
	Total Time ms	*	*	*	172.68	173.25	173.89	177.28	177.80
13	Node Time ms	*	*	*	25.92	26.56	26.88	26.94	26.82
Transputer	Host I/O ms	*	*	*	128.26	128.26	128.26	128.26	128.26
	Total Time ms	*	*	*	154.18	154.82	155.14	155.20	155.08

Speedup is a measure of the application software utilization of a multiple processor system. However, the original purpose of the speedup was to compare the time of the fastest serial program, T^1, with the time of the parallel equivalent of the same program, T(p). [15] This definition of speedup has a different meaning, e.g.,

$$S(p) = \frac{T^1}{T(p)} \tag{7}$$

The definition of the speedup from equation 7 is rarely used because of the difficulty in measuring T^1. Instead, T(1) is used as an approximation of T^1. Therefore, the speedup is estimated from the measurement for T(1) and T(N) [15] and is defined as follows:

$$S(p) = \frac{T(1)}{T(p)} \tag{8}$$

The speedup of the different multiprocessor programs is given in Table 8. Again these are the "worst case" values for the speedup.

Table 8: Speedup Results

		16 buses	25 buses	34 buses	43 buses	52 buses	61 buses	70 buses	79 buses
1	Total Time ms	156.61	194.43	246.72	311.74	332.86	352.83	374.98	397.12
Transputer	Speedup	NA	NA	NA	NA	NA	NA	NA	NA
2	Total Time ms	161.67	172.55	180.23	199.94	210.94	219.40	227.14	232.64
Transputer	Speedup	0.96	1.12	1.36	1.55	1.57	1.60	1.65	1.70
4	Total Time ms	161.28	172.93	176.45	183.17	186.18	189.32	192.07	194.50
Transputer	Speedup	0.97	1.12	1.39	1.70	1.78	1.86	1.95	2.04
10	Total Time ms	*	*	*	172.68	173.25	173.89	177.28	177.80
Transputer	Speedup	*	*	*	1.80	1.92	2.02	2.11	2.23
13	Total Time ms	*	*	*	154.18	154.82	155.14	155.20	155.08
Transputer	Speedup	*	*	*	2.02	2.14	2.27	2.41	2.56

Processor efficiency measures the contribution of each processor to the parallel solution when p processors are employed. That is, E(p) equals the average efficiency per processor when the problem is run with p parallel processors [15].

$$E(p) = \frac{S(p)}{p} \tag{9}$$

Therefore an efficiency rating of 100% means the program runs in linear speedup time, while an efficiency of 0% means the processor is of no use in solving the problem in parallel [15].

The efficiency of the different multiprocessor programs is given in Table 9. Again these are the "worst case" values for the efficiency.

Table 9: Final Speedup And Efficiency Results

		16 buses	25 buses	34 buses	43 buses	52 buses	61 buses	70 buses	79 buses
1	Speedup	NA	NA	NA	NA	NA	NA	NA	NA
Transputer	Efficiency	NA	NA	NA	NA	NA	NA	NA	NA
2	Speedup	0.96	1.12	1.36	1.55	1.57	1.60	1.65	1.70
Transputer	Efficiency	48.0%	56.0%	68.0%	77.5%	78.5%	80.0%	82.5%	85.0%
4	Speedup	0.97	1.12	1.39	1.70	1.78	1.86	1.95	2.04
Transputer	Efficiency	24.2%	28.0%	34.7%	42.5%	44.5%	46.5%	48.7%	51.0%
10	Speedup	*	*	*	1.80	1.92	2.02	2.11	2.23
Transputer	Efficiency	*	*	*	18.0%	19.2%	20.2%	21.1%	22.3%
13	Speedup	*	*	*	2.02	2.14	2.27	2.41	2.56
Transputer	Efficiency	*	*	*	15.5%	16.4%	17.4%	18.5%	19.6%

FAULT-TOLERANCE

Fault tolerance is a class of methods to achieve dependable and reliable computing systems. Dependability is that property of a computer system that allows reliance to be justifiably placed on the service a system delivers [12, 14]. Fault tolerance is the ability to deliver a service in spite of faults. Fault tolerance is generally obtained from redundancy. This redundancy can be accomplished by masking (static) redundancy or dynamic redundancy [12, 14].

Masking (static) redundancy uses extra components to obscure, or mask, the effect of a faulty component [12, 14]. This technique is regarded as static because once the redundant copies are connected their interconnections remain fixed. The error resulting from faulty components are masked by the presence of other copies of those components. An example of masking redundancy is the computer system for the Space Shuttle. There are four different computers on the Space Shuttle. Three of these computers execute the same program using the same data while the fourth computer runs a different program which performs the same function as the other three. The results of the three computers running the same program are compared or voted on, if any one of the result from one of the computers is inconsistent with that of the others, it is masked out.

The reason that the fourth computer has a different set of software that performs the same function as the other three is to grade against an error in programming. This is a frorm of dynamic redundancy. Dynamic redundancy refers to systems which can be reconfigured in response to a fault. If the fourth computer results were different from the results of the other three computers on the Space Shuttle, the fourth computer would take

over and mask out the others, thereby reconfiguring the computer system from a multiprocessor to a single processor computer system.

Another fault tolerant technique is fault detection, but fault detection provides no tolerance to faults, rather it gives warning when they occur [12, 14].

The reason for this introduction to fault tolerant system was to show how they could be applied to this research. The goal of this research is not to design a fault tolerant computer system but to apply parallel and distributed processing to construct an electric power management system (EPMS) for space based power systems. In the development of this EPMS, two different architectures for doing the decomposition method for load-flow were tested. These results have been presented in Tables 5 through 9. They were the 10 and 13 transputer systems and are presented in Figures 5 and 6.

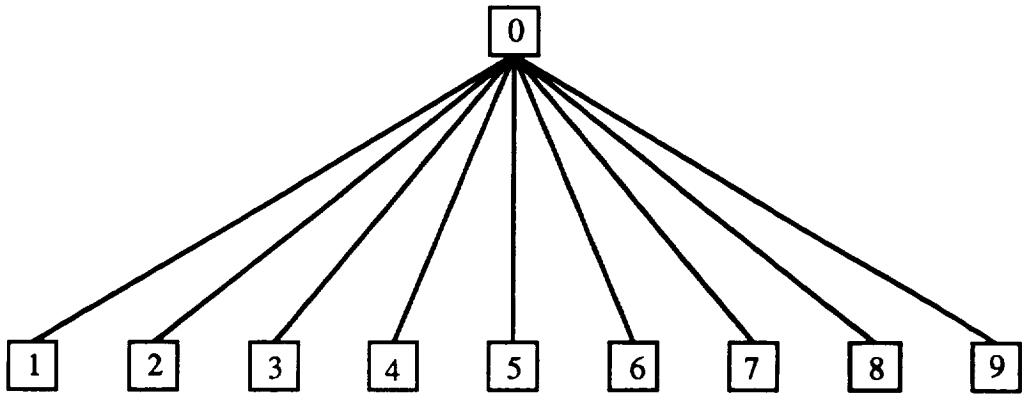

Figure 5: 10 Transputer System

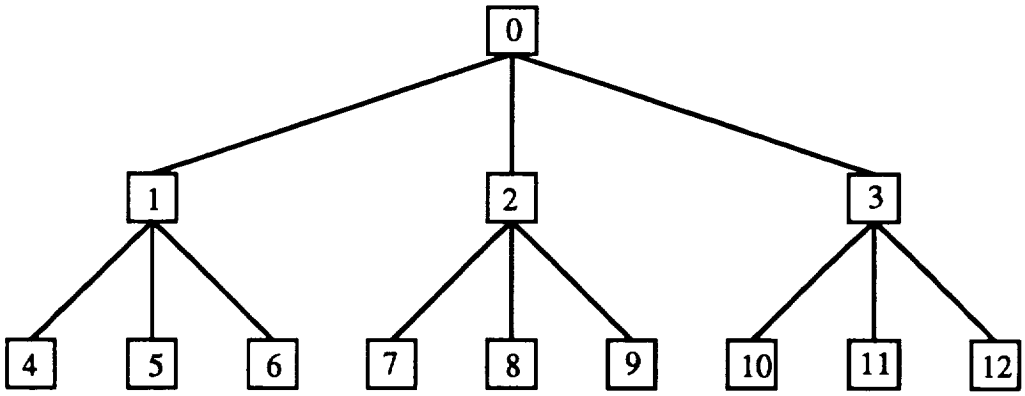

Figure 6: 13 Transputer System

From Figures 5 and 6 it can be seen that processor 0 is the critical processor. If processor 0 were to fail, both systems in Figure 5 and 6 would fail. However if processor 1, 2, or 3 were to fail in Figure 6, the processors which feed into any of these processors would be removed from service. An alternative system which is given in Figure 7 would use 12 processors. The system in Figure 7 would operate the same as the system in Figure 5 with the exception that processors 10 and 11 would perform the same function as processor 0. This would provide a static redundancy for processor 0 and would eliminate the risk of a fault on the middle layer of processors in Figure 6. The system in

Figure 7 was not tested so no timing data are available at this time, but the point is made that fault tolerance can be addressed in this design.

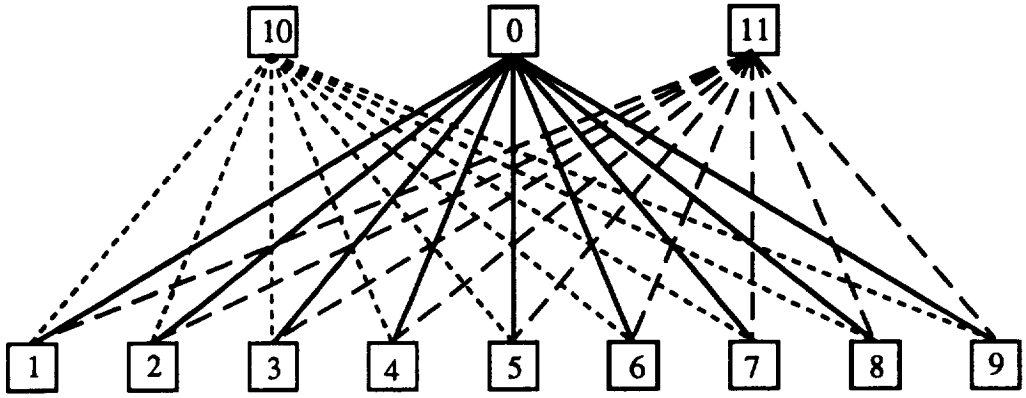

Figure 7: Proposed Fault Tolerant System

CONCLUSIONS

This paper has presented preliminary results for a load-flow analysis using a decomposition principal. It has been shown that the decomposition algorithm for load-flow analysis is well suited for parallel processing and provides increases in the speed of execution. Also two different hardware structures for doing the decomposition method were presented (Figures 5 and 6) and they were analyzed for speedup and efficiency. A fault tolerant design was also proposed (Figure 7) which made use of static redundancy.

Further work will be conducted on the decomposition principal by the addition of more transputers to the present system. This will be done to see whether or not further decomposition by the addition of more processors will be of any benefit. Also with the addition of more transputers, a hyper cube architecture could also be investigated; this approach was presented by Taoka, Iyoda, Noguchi, Sato, and Nakazawa [10].

REFERENCES

[1] IEEE Committee Report, "Parallel Processing in Power Systems Computation," *IEEE Transactions On Power Systems*, Vol. 7, No. 2, May 1992, pp. 629-637.

[2] A.M. Tyrrell and J.D. Nicoud, "Scheduling And Parallel Operations On The Transputer," *Microprocessing and Microprogramming*, Vol 26, 1989, pp. 175-185.

[3] Express 3.0, Introductory, Guide Macintosh, ParaSoft Corporation, 2500, E. Foothill Blvd., Pasadena, CA 91107, 1988, 1989, 1990.

[4] Express 3.0, User's Guide, Version 3.0, ParaSoft Corporation, 2500, E. Foothill Blvd., Pasadena, CA 91107, 1988, 1989, 1990.

[5] Y. Wallach, Calculations And Programs For Power System Networks, Prentice-Hall, Inc., Englewood Cliffs, New Jersey 07632, 1986.

[6] M. Rafian, M.J.H. Sterling, and M.R. Irving, "Decomposed Load-Flow Algorithm Suitable For Parallel Processing Implementation," *IEE Proceedings*, Vol. 132, Pt. C, No. 6, November 1985.

[7] M. Rafian, M.J.H. Sterling, and M.R. Irving, "Parallel Processing Algorithm For Power System Simulation," *IEE Proceedings*, Vol. 135, Pt. C, No. 6, November 1988.

[8] L. Wang, N. Xiang, S. Wang, and M. Huang, "Parallel Reduced Gradient Optimal Power Flow Solution," *Electric Power Systems Research*, Vol. 17, 1989, pp. 229-237.

[9] F.C. Berry and M.D. Cox, "A Technique For Load Flow Analysis On A Power System," *IECEC Proceedings*, Washington, D.C., 1989.

[10] H. Taoka, I. Iyoda, I., H. Noguchi, N. Sato, and T. Nakazawa "Real-Time Digital Simulation For Power System Analysis On A Hyper Cube Computer," *IEEE Transactions On Power Systems*, Vol. 7, No. 1, Feb. 1992, pp. 1-7.

[11] F.C. Berry, "Express, A Tool for Teaching Parallel Processing," *Computers In Education Journal*, Computers In Education Division Of ASEE, Accepted, 1992.

[12] D.P. Siewiorek, "Architecture of Fault-Tolerant Computers: An Historical Perspective," *Proceedings Of The IEEE*, Vol. 79, No. 12, Dec. 1991, pp. 1710-1734.

[13] H.M. Chen and F.C. Berry, "Parallel Load-Flow Algorithm Using A Decomposition Method For Space Based Power Systems," *IEEE Transactions on Aerospace and Electronic Systems*, Accepted, 1993

[14] L.J.M. Nieuwenhuis and G.D. Blom, "Fault Tolerant Computing With Transputers And Occam," *Real-Time Systems With Transputers*, H. Zedan, Ed., 1990, IOS Press, pp. 108-118.

[15] T.G. Lewis and H. El-Rewini, Introduction To Parallel Computing, Prentice Hall, Englewood Cliffs, New Jersey 07632, 1992.

[16] F.C. Berry, R.F. Gasser Jr., and H.M. Chen, "Course Grain Parallel Processing for the Management of a Space Based Power System," *IEEE Transactions on Aerospace and Electronic Systems*, Accepted, 1993.

N94-25353

A PROTOTYPE TO AUTOMATE THE VIDEO SUBSYSTEM ROUTING FOR THE VIDEO DISTRIBUTION SUBSYSTEM OF SPACE STATION FREEDOM

Final Report
NASA/ASEE Summer Faculty Fellowship Program--1993
Johnson Space Center

Prepared By:	Jessie M. Bethly Betz, M.S.
Academic Rank:	Assistant Professor
University & Department:	Southern University & A&M College Department of Computer Science Baton Rouge, Louisiana 70813
NASA/JSC	
Directorate:	Engineering
Division:	Communications and Tracking
Branch:	Systems Engineering
JSC Colleague:	Sally D. Stokes, E.E.
Date Submitted:	August 6, 1993
Contract Number:	NGT-44-001-800

ABSTRACT

The Video Distribution Subsystem (VDS) for Space Station Freedom provides onboard video communications. The VDS includes three major functions: external video switching; internal video switching; and sync and control generation.

The Video Subsystem Routing (VSR) is a part of the VDS Manager Computer Software Configuration Item (VSM/CSCI). The VSM/CSCI is the software which controls and monitors the VDS equipment. VSR activates, terminates, and modifies video services in response to Tier-1 commands to connect video sources to video destinations. VSR selects connection paths based on availability of resources and updates the video routing lookup tables. This project involves investigating the current methodology to automate the Video Subsystem Routing, and developing and testing a prototype as "proof of concept" for designers.

INTRODUCTION

The Johnson Space Center (JSC) is responsible for providing, maintaining, and operating a safe, reliable, and effective National Space Transportation System (NSTS). Further, JSC has significant responsibility for achieving a permanent manned presence in space. This involves creating and operating the Space Station Freedom(SSF) and satisfying a myriad of complex requirements involved in its concept, design and development.[1] The conceptual phase of SSF is complete along with the design and redesign phase, but the total requirements have not been produced for the Video Distribution Subsystem VSR software . VDS provides onboard video communications to SSF. The VDS includes three major functions:

1. External video switching;
2. internal video switching; and
3. sync and control generation.

The external video switching will locate four external video cameras to fourteen locations, controlled remotely through sync and control interface output. The internal video switching will provide viewing for one fixed camera that can be attached to seven internal fixed assemblies. The external camera status is read by status reader in the external switches, and internal camera status by internal switch readers. The internal sync and control generation will allow for a video camera command and status based on the NSTS camera concept.

'The VDS Subsystem Manager Computer Software Configuration Item (VSM/CSCI) is the software which controls and monitors the VDS equipment. It executes in the Standard Data Processor (SDP) and utilizes standard Data Management System (DMS) networking hardware and software. VSM/CSCI operates in conjunction with other customer furnished CSCIs (See Figure 1).

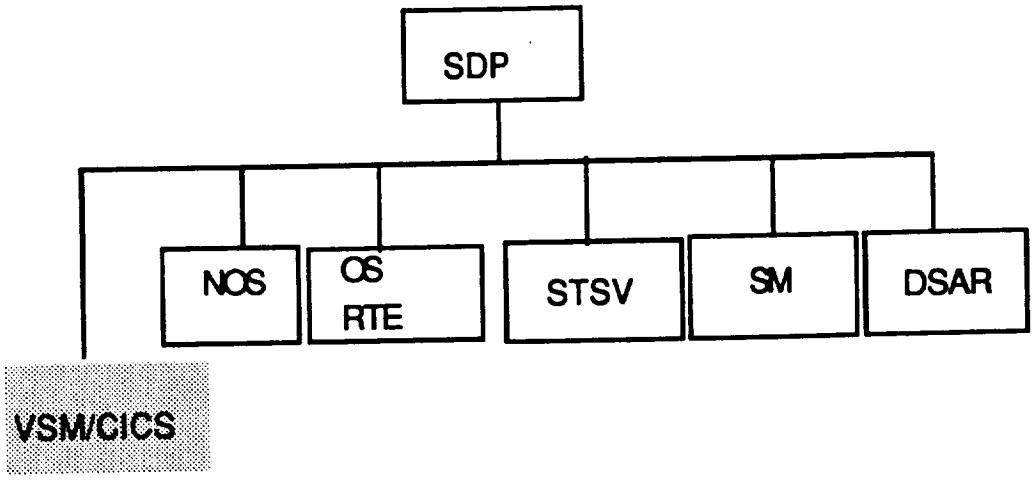

Figure 1.- SDP Overview

NOS:	Network Operating System
OS/RTE:	Operating System/Ada Runtime Environment
STSV:	Standard Service
SM:	System Management
DSAR:	Data Storage and Retrieval

The VSM/CSCI has three major subcapabilities operating under it:
VDS Subsystem Routing (VSR),
External Video ORU Management (EVM), and
Camera Control Input Management (CCIM). (See Figure 2)

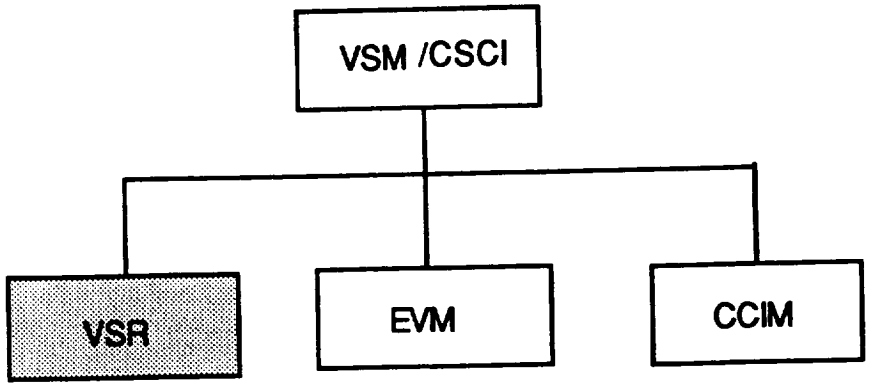

Figure 2.- VSM/CSCI Overview

The Video Subsystem Routing is a part of the VDS Manager Computer Software Configuration Item (VSM/CSCI). It is the responsibility of VSR to activate, terminate, and modify video services in response to Tier-1 commands to connect video sources to video destinations. Teir-1 is the comprehensive term for the coordinated operational command, control, and management of the Space Station. Tier-1 is composed of three major portions:

1. the on-board Integration Station Executive (ISE),
2. the Crew Interface, and
3. the Space Station Control Center. [2].

VSR has the responsibilities of calculating the switch involvement from selected end points; choosing the "best path" from available paths; updating bit strings to reflect the latest selection; and issuing the commands to connect the video source to video destinations. The VSR capability utilizes the following subcapabilities: Command Validation (CV), Video Service Activation (VSA), Video Line Addition (VLA), Video Line Deletion (VLD), Video Service Termination (VST), and Video Table Update (VTU). (See Figure 3).

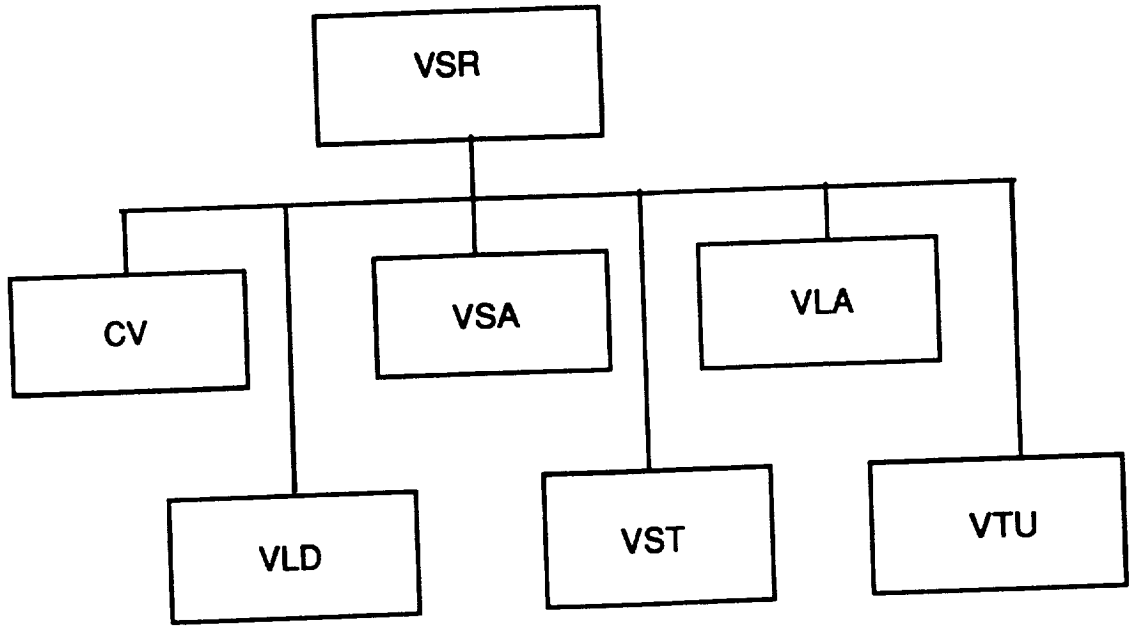

Figure 3.- Video Subsystem Routing (VSR) Capabilities Overview

Command Validation (CV) is the initial receiver for all video commands issued by Tier-1. Each command is checked for syntactic and semantic correctness, then forwarded to the appropriate subcapability to ensure that requested video service is provided. Manual External Video Switch commands are handled exclusively by CV.

Video Service Activation (VSA) accepts Tier-1 initiated Activate Video Service commands from the CV and determines the availability of the requested resources to avoid any conflict. VSA notifies such conflict to Tier-1 by generating a caution and warning advisory message. Once the VSA verifies the resource availability, it creates new video routing paths. If a camera is used as a video signal source, the VSA will initiate a sync connection between the camera and a VSW equipment that hosts the camera. Upon receipt of trunkline status change of the RODB-based VSW Trunkline tables, the VSA updates RODB-based Video Routing Lookup tables.

Video Line Addition(VLA) supports Tier-1 initiated and CV validated Modify Video Service command (Modification Type: Add) which adds another video destination device to an on-going video service without terminating. The Modify Video Service command is passed by CV after validating its semantics and syntactic correctness.

Video Line Deletion(VLD) supports Tier-1 initiated and CV validated Modify Video Service command (Modification Type: Delete) which deletes a video destination device (e.g., video monitor) from an on-going video service without terminating.

Video Service Termination (VST) accepts Tier-1 initiated and CV validated Terminate Video Service command to terminate a video service.

Video Table Update (VTU) updates the RODB-based Video Routing Lookup table, which maintains the source-to-destination video routing path status, by examining the Internal, External or Inter VSW Trunkline tables. VTU also updates the Inter VSW Trunkline table to maintain the VSW trunkline availability status

between any Internal and External VSW Orbital Replaceable Unit (ORU) pair.

A prototype to automate the VSR was investigated with emphasis on the Ada programming language and the top-down structured approach to verify the requirements set forth by the Communications and Tracking Systems Division (TCD) of JSC as found in the Flight System Software Requirements Document (FSSR.) "The FSSR is used by the contractor as the basis for the VSM/CSCI design, implementation, and requirements testing, and by the Government and Prime Contractor to assess whether or not the completed VSM/CSCI complies with its requirements."[3].

The automated prototype was not implemented, but an analysis of the requirements were done with recommended revisions, and justification for the use of Ada versus C++ was also investigated. The advantage the author considered was, Ada is a language that embodies and enforces modern software engineering principles. It contains numerous features to support software engineering principles, such as, data abstraction, information hiding, and strong typing, which are presented as secure, reusable software components for large real-time systems as with VSR.

Ada satisfies the following conditions for prototyping. Prototyping is useful in addition to the design phase because it allows the designers to find out whether the system will solve the problem. [4] "The benefits of using a prototype system during the requirements analysis and definition phase of the software life cycle may be summarized as follows:

1. Misunderstandings between software developers and users may be identified as the system functions are demonstrated.
2. Missing user services may be detected.
3. Difficult-to-use or confusing user services may be identified and refined.
4. Software development staff may find incomplete and/or inconsistent requirements as the prototype is developed.
5. A working, albeit limited, system is available very quickly to demonstrate the feasibility and usefulness of the application to management.

6. The prototype may serve as a specification for the development of a production quality system. " [5]

DISCUSSION:

The system development life cycle methodology applied to the investigation of the prototype was divided into two phases:

- traditional: designing hierarchy charts and pseudocode; and
- non-traditional: utilizing the state-of-the-art method of software engineering (computer aided software engineering tool).

In both methods, the top-down structured methodology was applied and hierarchy charts were developed from the requirements document (FSSR). From these design techniques the traditional pseudocode was written to be translated, after NASA redesign, into Ada code for a Unix Sun Workstation. In the non-traditional method, a software engineering package [6] was reviewed to develop models of Ada application systems using graphic icons that may be used to convert the model to the semantics of the Ada programming language utilizing the Ada Structure Graph Editor. The teamwork/Ada notation is derived from the graphic notation designed for Ada by Dr. R. J. A. Buhr. Buhr supports the structured design feature where the notation provides a one-to-one mapping between a set of graphic elements and the corresponding features of the Ada language. Buhr uses Ada structure graphs (ASGs) instead of conventional program structure charts to model relationships that are specific to Ada systems.

The analysis of the requirements design for both methods of the algorithm, help to modify the subcapabilities. The subcapabilities included such things as, repetition of functions in more than one subcapability, as well as some modules with only one or two lines of instructions.

RECOMMENDATIONS:

The redesign of SSF to Space Station Alpha (SSA) has begun, and the DMS (a VDS software interface) has been eliminated, as well as other

software interfaces, thereby causing necessary modification or redesign of VSR. Once SSA requirements have been released, it is suggested another requirements analysis and prototype be considered. It is imperative that there exist cameras on the Space Station, but how many, how and where they will be located still needs to be addressed. It is suggested that a software engineering package be considered for prototyping versus using the traditional method of coding. This will reduce the amount of time spent on tedious work versus productivity. It is also suggested that Cadre Technologies, Inc. be considered because of the versatility in software engineering. Cadre Technologies, Inc. also supports the creation of real-time system matrices in the form of two packages: State/Event Matrix(SEM) and Process Activation Table (PAT). The SEM maps states to the events which cause a transition from that state. [6]. The PAT is a matrix that presents the rules, or combinatorial logic, by which events enable and /or disable data flow diagrams(DFD). [6] These two processes can also be utilized in the prototyping of the video routing mappings, video routing status table, and various other tasks to activate the video services.

SUMMARY:

Although a working prototype was not completed, much analysis and redesign has been done to enhance the redesign efforts of the SSA team. A draft of the redesign was provide with modifications to the necessary capabilities. The VSR is one of the most important piece of software for SSF and careful consideration should be given to its design and functions.

REFERENCES:

[1] "Johnson Space Center and the University Community: Teamwork for Space Exploration", 1993, page 2,

[2] Flight System Software Requirements (Communications & Tracking System Software Part 1 - Level B) McDonnell Douglas Space Systems Company Space Station Division DR SY-34-1. WP-2. Contract NAS 9-18200. SSP 30606, Vol II Revision A. January 8, 1993. Page 1.4.

[3] Flight System Software Requirements (FSSR). page 3.2.5-5 SSP 300606, Volume II Revision B.

[4] Pfleeger, Shari and Lawrence. Software Engineering. The Production of Quality Software. Macmillan Publishing Company. 1991. 2nd edition. pages 191-192.

[5] Sommerville, I., Software Engineering, 2nd edition, p.36 Addison-Wesley Publishing Company.

[6] teamwork/Ada: User's Guide . Release 4.0 , 1990. Cadre Technologies, Inc. Providence, Rhode Island. pages 1-2.

N94-25354

INVESTIGATION OF HAND CAPABILITIES UNDER A VARIETY OF PERFORMANCE CONDITIONS AND AN ATTEMPT TO EXPLAIN PERFORMANCE DIFFERENCES

Final Report

NASA/ASEE Summer Faculty Fellowship Program-1993

Johnson Space Center

Prepared by:	Ram R. Bishu, Ph.D., and Lisa Bronkema
Academic Rank:	Associate Professor, and graduate student
University and Department	Industrial and Management Systems Engineering Department, University of Nebraska-Lincoln, Nebraska 68588-0518
NASA/JSC Directorate:	Space and Life Sciences
Division:	Man Systems
Branch:	Crew Interface Analysis
Laboratory:	Anthropometry and Biomechanics
JSC Colleague:	Glenn Klute
Date Submitted:	July 20, 1993
Contract Number:	NGT-44-001-800

ABSTRACT

Human capabilities such as dexterity, manipulability, and tactile perception are unique and render the hand as a very versatile, effective and a multipurpose tool. This is especially true for environments such as the EVA environment. However, with the use of the protective EVA gloves, there is much evidence to suggest that human performance decreases. In order to determine the nature and cause of this performance decrement, several performance tests were run which studied the effects of gloves on strength, tactile feedback, and range of motion. Tactile sensitivity was measured as a function of grip strength and the results are discussed. Equipment which was developed to measure finger range of motion along with corresponding finger strength values is discussed. The results of these studies have useful implications for improved glove design.

INTRODUCTION

Human capabilities such as dexterity, manipulability, and tactile perception are unique and render the hand as a very versatile, effective and multipurpose tool. This is especially true for environments such as the EVA environment. Protection of hand and facilitation of extravehicular activities (EVA) to be performed by hand are the objectives of glove design. Gloves are the primary protection device for hands while performing EVA. Numerous articles have been published in the area of the effect of gloves on task performance (for example see Bishu and Klute, 1993a, Bishu and Klute, 1993b, Lyman and Groth 1958, and Cochran et al., 1986). The common finding in all these studies has been that gloves reduce both strength and dexterity performance. Possible reasons for this are the reduction in tactile sensitivity when gloves are donned, and reduction in finger range of motion. Verification of these reasons was the driving force behind research performed this summer. The objectives of this research were to ensure that reduction in tactile sensitivity was in fact causing a reduction in gloved performance, and that with gloves there was a reduction in finger range of motion. Another research project pursued this summer was concerned with the relationship between force and endurance. It has been reported by Bishu and Klute (1993a) that pinch strength of persons is consistent across a range of performance conditions. A corollary to this was the question "How long can a person sustain pinch exertions?"

OBJECTIVES

1. To develop a force time relationship for pinch exertions at different postures.
2. To measure the tactile sensitivity at the hand/handle interface under a variety of performance conditions.
3. To develop equipment for measuring finger range of motion and finger strength.

The objectives were achieved through three experiments described below.

Experiment 1: Force endurance for lateral and pulp pinch (Chapman, Bronkema, and Bishu):

In this study, endurance time was evaluated for three types of exertions (grip, pulp pinch, and lateral pinch), at three different postures (extension, neutral, and flexion). Endurance time was expected to depend on the level of exertion, type of exertion, and on the posture adapted.

Method: Six subjects participated in this study. Three levels of exertion (25%, 50%, 100%) were combined with three types of posture (flexion, neutral, and extension) and three types of exertion (pulp pinch, lateral pinch, and grip force) to yield twenty-seven conditions. The devices used to measure these various strengths were the hand dynamometer and the pinch gauge. Initially the maximal exertions were determined for all the subjects on the first day. The test trials started on the following day. The exertion force for the day was calculated with respect to the maximal exertions. The subjects performed two trials per day, with the order of presentation being randomized. A trial consisted of subjects exerting their condition of the day until they quit voluntarily. The endurance time was recorded and used as a primary dependent variable in analysis.

Results: The data was analyzed with respect to exertion force, and endurance time using SAS software. All the main effects were significant for the endurance force, while exertion

level, expressed as a percentage of maximum voluntary contraction, was the only significant effect. Figure 1 shows the histogram of the type of exertion effect. The grip strength is considerably greater than the two pinch strengths tested here. Figure 2 shows the histogram of the posture effect on exertion. The force exerted at the extended posture of the wrist appears to be more than that exerted at the flexed posture. Figure 3 shows the endurance time plot. As expected, the time the contraction was maintained is the least at 100% exertion level and the most at 25% exertion level.

Discussion: Perhaps the most interesting finding of this experiment is the lack of posture and type of exertion effect on endurance time. A posture effect was definitely expected as was a posture*exertion level interaction. The results suggest that the physiological mechanisms which cause reduction in capabilities due to factors such as posture, gloves, etc. are independent of the mechanisms which cause muscular fatigue. This is a big conjecture and, if proven, has ramifications for the designers. However, the results obtained here suggest just this.

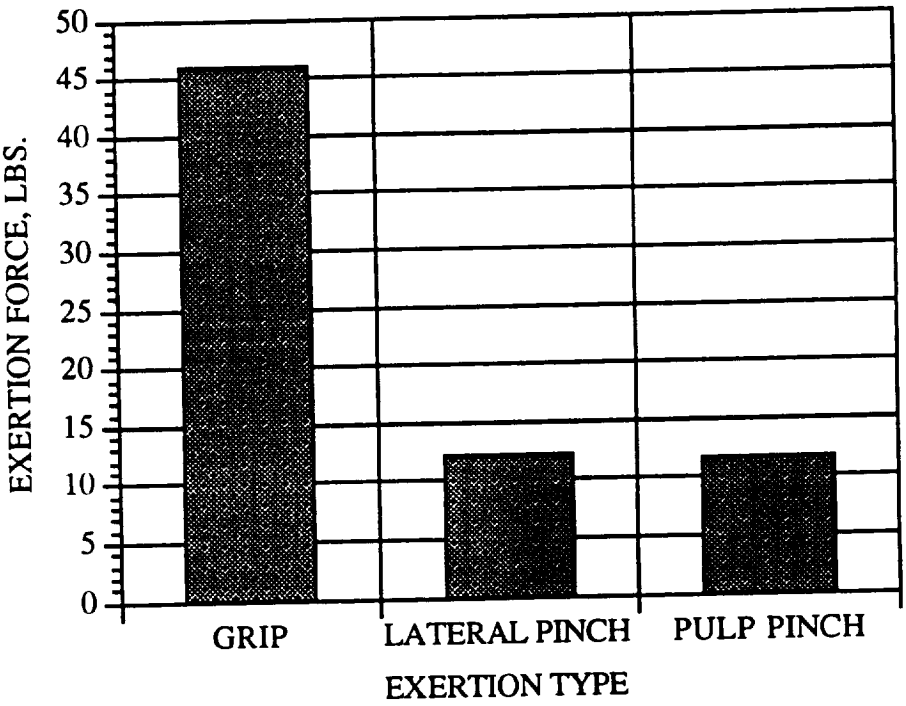

Figure 1.- Exertion type effect on exertion force.

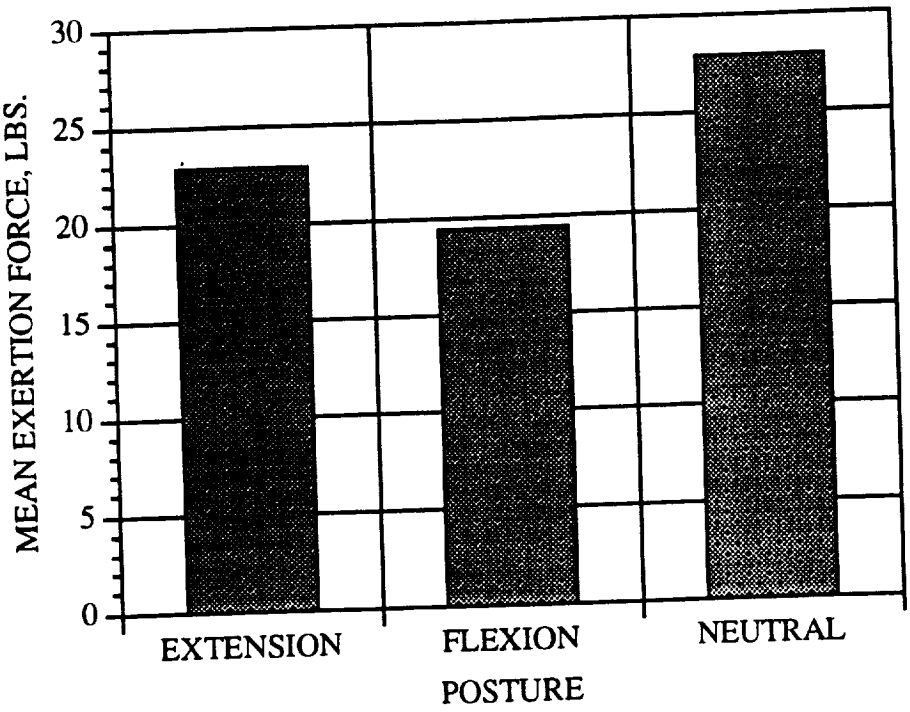

Figure 2.- Posture effect on exertion force.

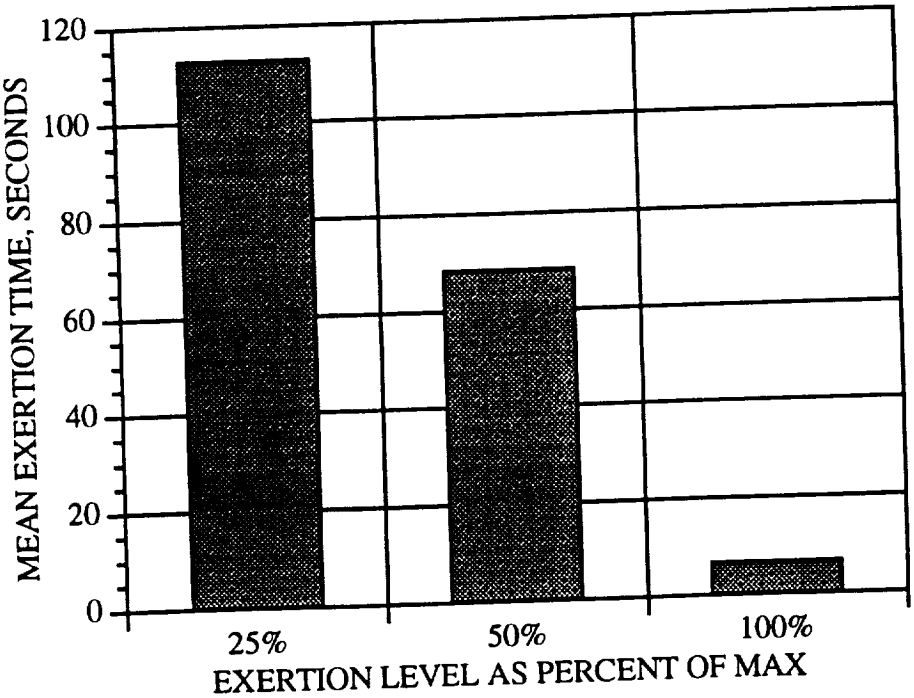

Figure 3.- Exertion level effect on time.

Experiment 2: Tactility as a function of grasp force: the effects of glove, pressure and load (Garcia, Bronkema, and Bishu).

One of the reasons for reduction in performance when gloves are donned is the lack of tactile sensitivity. It was argued that grasping force for a weight to be grasped will be a function of the weight to be lifted and the hand conditions. It was further reasoned that the differences in grasping force for various hand conditions will be a correlate of the tactile sensitivity of the corresponding hand conditions. The objective of this experiment, therefore, was to determine the effects of glove type, pressure, and weight of load, on the initial grasping force and stable grasping force. It was hypothesized that when a person grasps an object, he grasps very firmly initially and then releases his grasp slightly as he realizes what force is needed to maintain a steady grasp. This would seem to be particularly true when a person is wearing a glove and has lost some of his tactile sensitivity and force feedback during the grasp. Therefore, the ratio of initial force and stable force as well as the stable force itself would represent the amount of tactile adjustment that is made when picking up an object, and this adjustment should vary with the use of gloves.

Apparatus: To measure the grasping force, a dynamometer was fabricated and is shown in Figure 4. It consisted of two steel halves, which, when placed together, formed the same elliptical shape of the grab bar on the shuttle payload bay. A small plate was attached to the bottom of the device, so that weights could be added as needed. Between these two halves, at the top and bottom of the device, load cells were placed to measure the horizontal forces applied by the hand along the long axis of the cross section. The output of the load cells was channeled through a real-time data recording system. The data was analyzed using the SAS.

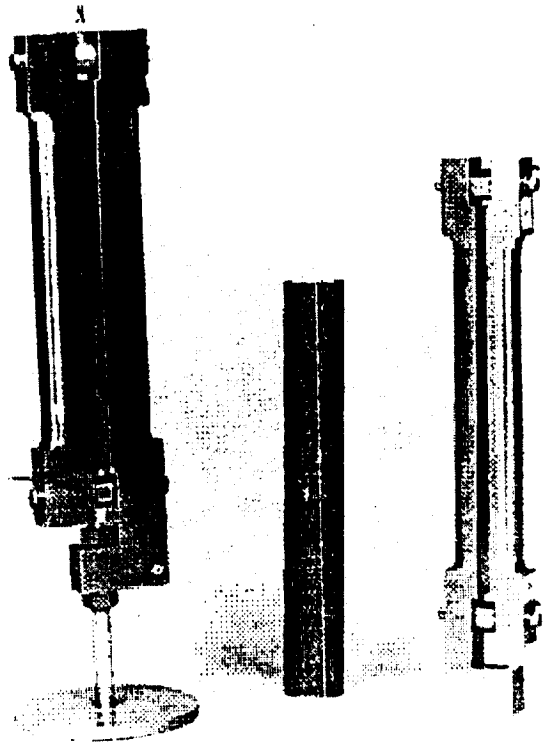

Figure 4.- Dynamometer fabricated and used for this experiment.

Method: The actual performance tests were performed inside a glove box. The independent variables of the experiment were glove type, pressure, load and gender as shown below:

Glove type:	Shuttle, Advanced, and Barehanded
Pressure:	0 PSID, 4.3 PSID, and 8.3 PSID
Load:	3.5 lbs, 8.5 lbs, and 13.5 lbs
Gender:	Male and Female

Eight subjects, four males and four females, participated in this study. For each subject appropriate hand and arm anthropometric dimensions were taken, after which each of the 18 trials were performed, allowing three minutes of rest time between trials. The trial began with adjusting both the weight of the unit and the pressure of the glove box. The subject then donned the glove and adjusted the placement of the grip device so that it was comfortable. After resetting the computer, the subject was asked to grasp and hold the object as he/she normally would of that size and weight. Following a 20 second holding period, the subject was asked to release the grasp as slowly as possible, so that the device

would gradually slip through their hands. The order of the trials was randomized across all the conditions.

Results: Peak force, stable force, and the ratio of peak to stable force were the main dependent variables. Analyses of variance was performed on the data. Among the main factors, load effect and gender effect were significant. Figure 5 shows the plot of the gender effect. Females tended to have a lower stable force than the males. It is possible that the males were over controlling. Figure 6 shows the plot of the load effect. As the load increases so does the grasp force. This was expected. The ratio, although not significant, seems to reduce with increasing load.

Discussion: The results of the study were somewhat counter-intuitive since the only significant effects on the peak and stable grasp force were caused by gender and the weight of load lifted. Neither the gloves nor pressure altered these forces when compared to a barehanded condition as was suspected prior to the test. One reason for this could be that gloves can actually help in holding if they have a large enough coefficient of friction. It is possible that gloves facilitate in holding, due to coefficient of friction while they deter in peak grasp strength. The absence of pressure effect led to the next experiment being performed outside the glove box, and with larger number of conditions.

Experiment 3: Tactility as a function of grasp force: Effects of glove, handle size, orientation, and load (Garcia, Bronkema, and Bishu).

The objective of this experiment was to determine the effects of gloves, handle size, handle orientation, and load lifted on grasp force. The working hypotheses were that grasp force would be a function of all the above mentioned factors.

Method: The same set-up as experiment 2 was used here, but with one exception. A possible reason for the lack of glove and pressure effects in experiment 2 could have been the feedback provided by the visual cue in holding. Therefore, to avoid the visual cue, the subjects lifted and held the load as shown in Figure 7. The other difference was that this experiment was performed outside the glove box. The independent factors were 4 levels of glove (advanced, shuttle, meat packing and bare hand), 3 levels of load (5, 10, and 15 lbs.), 2 levels of orientation (transverse and lateral), and 2 levels of size (large and small). There were 48 conditions in all and 10 subjects (5 male and 5 female) participated in this experiment. The order of presentation was randomized across each subject. The procedure was identical to experiment 2. Stable force, peak force, and ratio of peak to stable force were the dependent measures for analyses. In addition to these, the maximum grasp force at each condition in the lateral orientation was also recorded to determine if maximum grasp was different from holding.

Results: Due to space restrictions, summary analyses are discussed here. The complete report with detailed analyses will be published as a NASA Technical Paper. Among the main factors load, gender, handle orientation, and glove effects were significant. Load effect was similar to Figure 6 with increasing grasp force for increasing loads. The gender effect was again similar to Figure 5 with the female grasping force being 70% of the male

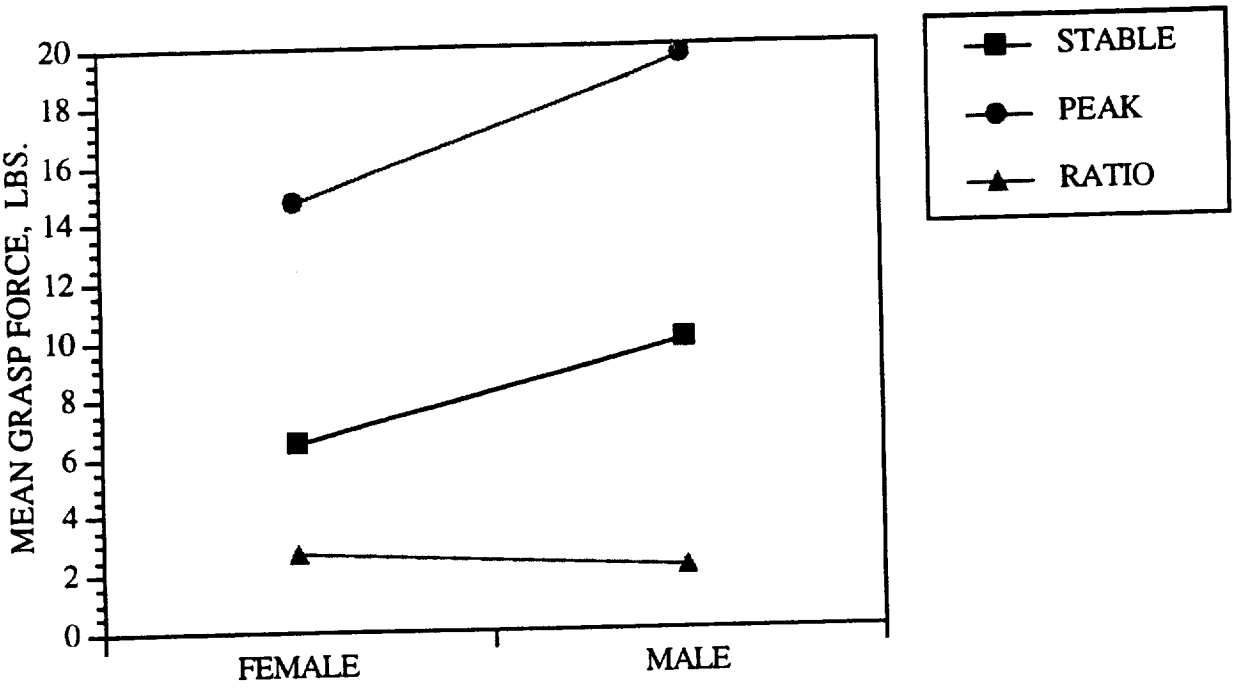

Figure 5.- Gender effect on mean grasp force.

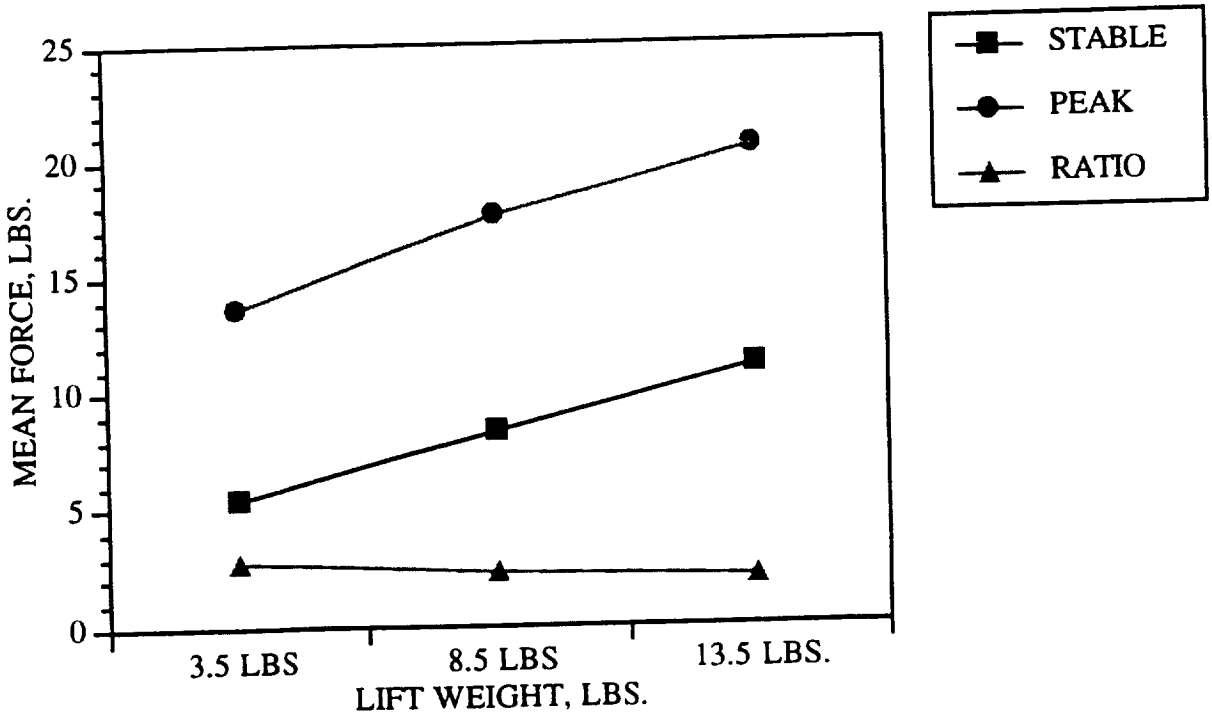

Figure 6.- Load effect on mean grasp force.

Figure 7.- Set-up for Experiment 3.

grasping force. Figure 8 shows the glove effect and it is interesting to note that barehanded and meat packing gloves had significantly larger grasp force than the shuttle and advanced developmental glove. The orientation effect is shown in Figure 9. The lateral position had a greater grasp force than the transverse position. Figure 10 shows the plot of the glove effect on the maximum grasp force. It is very interesting to note that Figures 8 and 10 are similar with bare hand and meat packing showing much higher forces than the advanced and shuttle gloves. The implications of this similarity are far fetched.

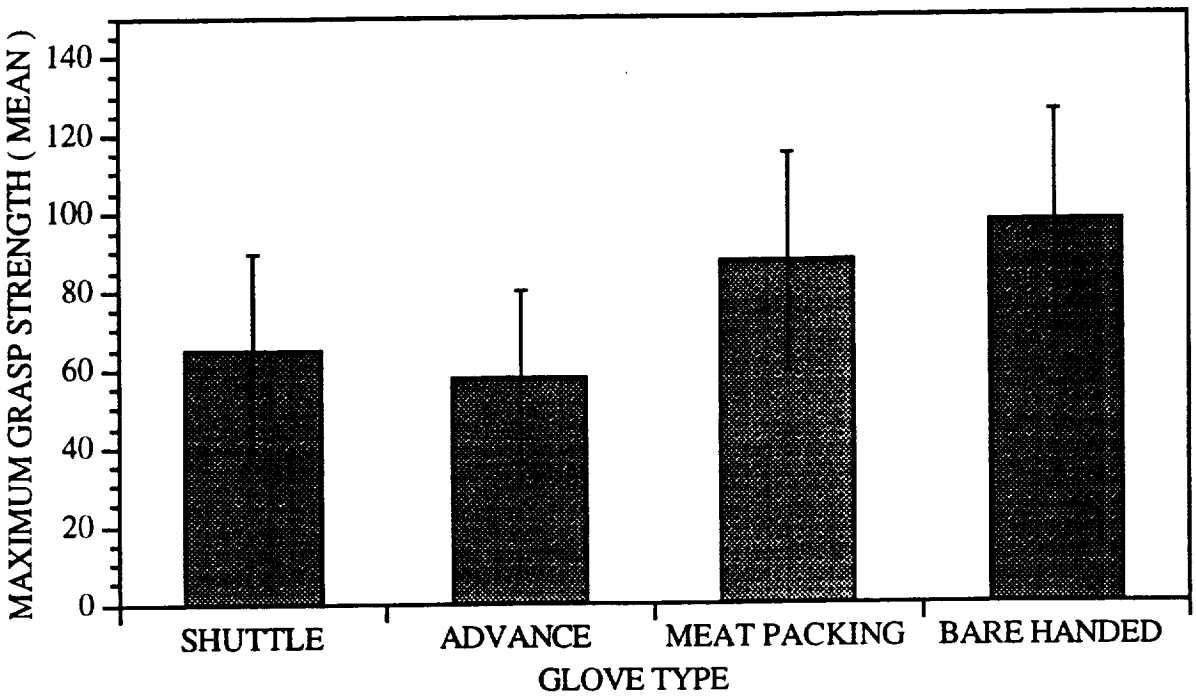

Figure 8.- Glove effect on maximum grasp strength.

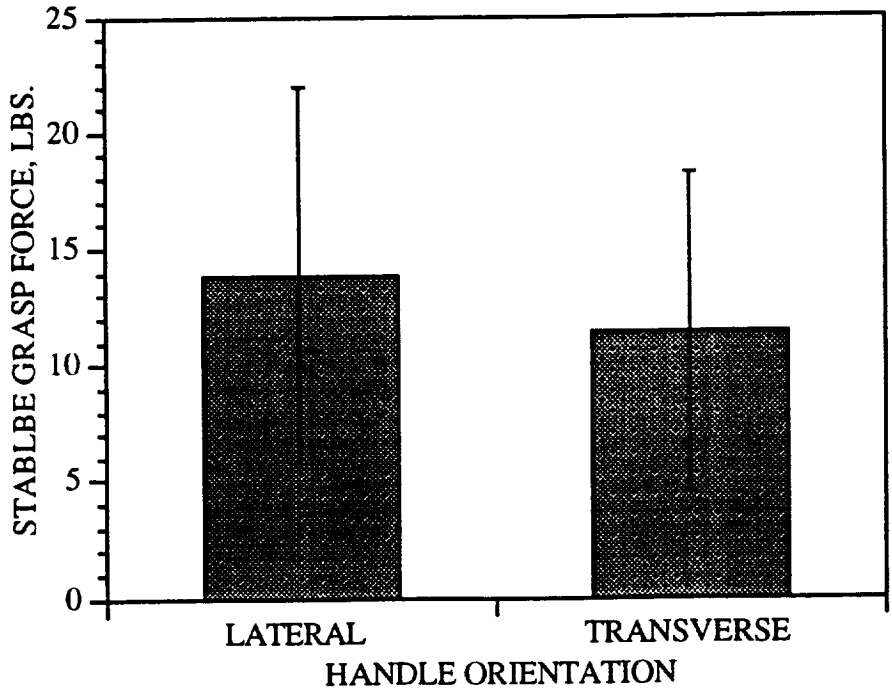

Figure 9.- Handle orientation effect on stable grasp force.

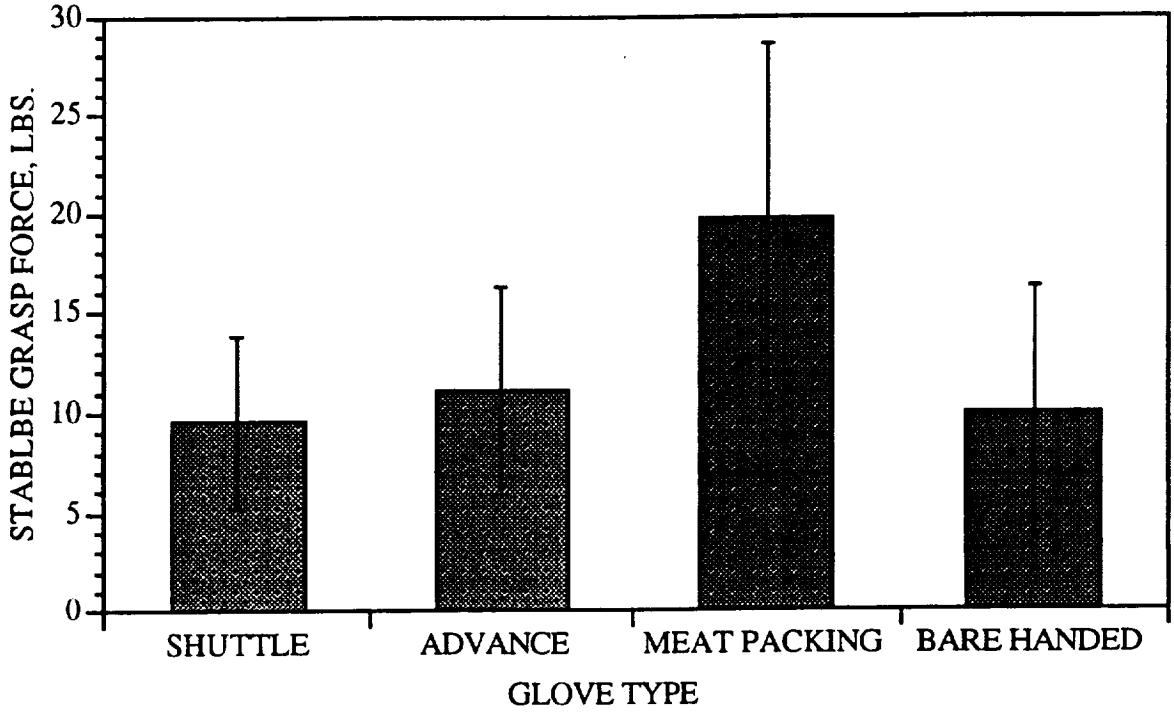

Figure 10.- Glove effect on stable grasp force.

Overall Discussion: It is evident that friction at the glove handle interface impacts the grasping force. This is seen by the reduced grasp force with advanced glove and shuttle glove. There are also indications that the effort exerted by the lower arm musculoskeletal system may be the same for a range of variations in the wrist/fingers/handle configurations. This is evidenced by lack of posture effect in experiment 1, and similarity between Figures 8 and 10. Similarity in glove effect between maximal grasp and stable grasp forces for the three weights tested in experiment 3 indicates that exertion by the musculoskeletal system at the lower arm may be the same, although the force registered by the load cell varied. More research is definitely needed. If this be so, then a tactility index based on the grasp force is possible.

Experiment 4: Isometric strength and range of motion measurement of fingers (Fletcher, Bronkema, and Bishu)

One possible reason for lower dexterity with gloves could be the reduction in finger strength and finger range of motion. It is possible that gloves change the distance between digits and the apparent distance within digits. Considerable need exists for determining the finger strengths and finger range of motion (ROM). The objective of this experiment to design a device to measure the finger strength and ROM.

Apparatus: A literature review revealed the absence of any device for finger strength measurement. Therefore, a device had to be designed and fabricated. The design had to have the capability of restraining digits whose strength was not being measured, and have the capability of motion and strength measurement for the unrestrained digit. A device as shown in Figure 11 was designed and fabricated.

Method: Six subjects participated in this experiment. The isometric strength of the four digits and the metacarpal joint was measured at five different finger angles (0, 15, 30, 45, and 60 degrees). The measurements were done in six different hand conditions (bare hand, advanced glove at 0 psid, advanced glove at 4.3 psid, advanced glove at 8.3 psid, shuttle glove at 0 psid, and shuttle glove at 4.3 psid).

Currently the data is being collected. The complete report of this experiment will be published as a NASA Technical Paper.

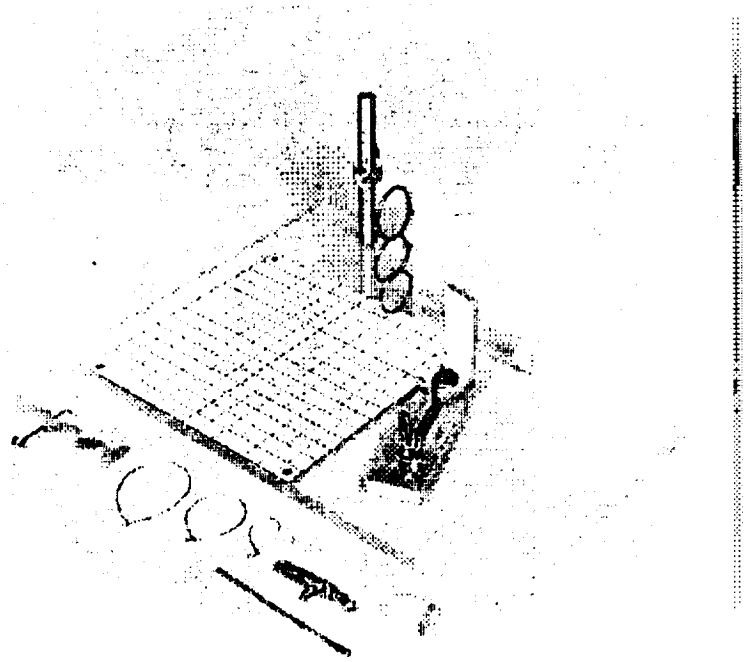

Figure 11.- Device used to measure finger range of motion and strength.

Experiment 5: Ergonomic evaluation of EVA tools (Bronkema and Bishu).

The objective of this project which is currently in progress is to perform an ergonomic evaluation of EVA tools. A short list of EVA tools for evaluation was compiled from astronaut briefings and other NASA documents. From this list, the wrist tether hook was chosen for evaluation, a hook which has historically been difficult and fatiguing to use. Two processes of evaluation were chosen and are being used. The first is a performance evaluation in which six different types of tether hooks are used, ranging in age from the Apollo program to some of the most current developmental hooks. The primary measure of performance in this experiment will be the amount of time needed to perform each of four different types of hooking tasks. The tasks were chosen as a result of suggestions from astronauts and WETF safety divers, and are typical of tasks performed on EVA's. The second process consists of a questionnaire which is administered to each subject following the performance test. It is in a paired comparison format and is designed

to determine the subjects' personal preference of which tools are easiest to use, least fatiguing, and require the least amount of force for activation.

When the data is complete, it will be analyzed to determine the effects that hook, hooking task, gender, and hand size have on performance. Actual performance values will be compared to the preferences voiced in the questionnaire to determine consistencies or inconsistencies in the two types of evaluations. It is expected that a generic procedure for ergonomic evaluation will emerge from this project.

REFERENCES

Will be furnished on request.

N94- 25355

MEASURING TRACK DENSITIES IN LUNAR GRAINS BY IMAGE ANALYSIS

Final Report
NASA/ASEE Summer Faculty Fellowship Program--1993
Johnson Space Center

Prepared By:	George E. Blanford, Ph.D.
Academic Rank:	Professor
University and Department:	University of Houston-Clear Lake School of Natural and Applied Sciences Houston, TX 77058
NASA/JSC	
Directorate:	Space and Life Sciences
Division:	Solar System Exploration
Branch:	Planetary Sciences
JSC Colleague:	David S. McKay, Ph.D.
Date Submitted:	August 6, 1993
Contract Number:	NGT-44-001-800

ABSTRACT

We have developed techniques to use digitized scanning electron micrographs and computer image analysis programs to measure track densities in lunar soil grains. Tracks were formed by highly ionizing solar energetic particles and cosmic rays during near surface exposure on the Moon. The track densities are related to the exposure conditions (depth and time). Distributions of the number of grains as a function of their track densities can reveal the modality of soil maturation. We used a sample that had already been etched in 6 N NaOH at 118°C for 15 h to reveal tracks. We determined that back-scattered electron images taken at 50% contrast and ~49.8% brightness produced suitable high contrast images for analysis. We ascertained gray-scale thresholds of interest: 0-230 for tracks, 231 for masked regions, and 232-255 for background. We found no need to set an upper size limit for distinguishing tracks. We did use lower limits to exclude noise: 16 pixels at 15000x, 4 pixels at 10000x, 2 pixels at 6800x, and 0 pixels at 4600x. We used computer counting and measurement of area to obtain track densities. We found an excellent correlation with manual measurements for track densities below $1x10^8$ cm^{-2}. For track densities between $1x10^8$ cm^{-2} to $1x10^9$ cm^{-2} we found that a regression formula using the percentage area covered by tracks gave good agreement with manual measurements. Finally we used these new techniques to obtain a track density distribution that gave more detail and was more rapidly obtained than using manual techniques 15 years ago.

INTRODUCTION

Solar wind, solar energetic particles, galactic cosmic rays, and meteoroid impacts hit regolith grains on the Moon, asteroids, some planets and satellites, and interplanetary dust particles producing measurable forms of "weathering.". Research has shown that these measurable effects correlate in lunar soils (McKay *et al.*, 1991). Nevertheless, the correlations are very crude because the weathering effects on the Moon are usually measured as a bulk average for a given soil. Most weathering measurements are not very useful for making quantitative predictions of exposure age or even giving a relative measure of maturity for the soil. Furthermore, regolith soils mature by at least two distinct processes: by *in situ* weathering and by mixing. Bulk average measurements cannot distinguish the maturation processes. To improve our understanding of space weathering, we should find these correlations on a grain by grain basis. During the ASEE summer program, we concentrated principally on one form of weathering, the formation of tracks in individual soil grains caused by solar energetic particles and galactic cosmic rays.

Price and Walker (1962) discovered that very ionizing radiation, such as fission fragments and cosmic rays, produces a trail of damage in dielectric materials that can be etched with a reagent to form visible tracks (cf. Fleischer *et al.*, 1975). Their discovery has led to practical applications such as Nuclepore filter paper and cosmic ray dosimeters used by astronauts. Scientific applications include fission track dating of geological samples and, the subject of our research, cosmic ray-solar energetic particle weathering effects on lunar samples. From the beginning quantitative scientific results have followed from counting tracks on micrographs and by micrographically measuring track morphological characteristics. The sophistication and ready availability of image processing software can reduce this tedious labor.

Etching lunar soil grains in a suitable reagent reveals tracks by producing pits at the track locations. We used a scanning electron microscope (SEM) to make digital images of the etched surfaces of polished grain mounts. We developed procedures to rapidly measure track densities with image processing software. We applied these techniques to determine the track density distribution at one level in a lunar core that we compared to measurements made 15 years ago using conventional techniques.

EXPERIMENTAL DETAILS

This summer project concentrated on the development of image processing techniques and not on the techniques of track etching. Consequently we used a lunar soil sample that had been prepared and etched 15 years ago. Although this sample had been returned to the lunar sample curator, it had been rerequested several years ago to show etched tracks to a Japanese film crew and was still in my advisors safe. It was a polished section of an Apollo 16 double drive tube numbered 60009, 6049. Photomicrographs of this sample were available to aid in the location of particular zones of interest. We chose to work at a position that we estimate to be 546 mm below the lunar surface. This sample had been etched for 15 hours in 6 N sodium hydroxide at 118°C. It was also already coated with a vacuum deposited layer of gold to prevent charging in the SEM.

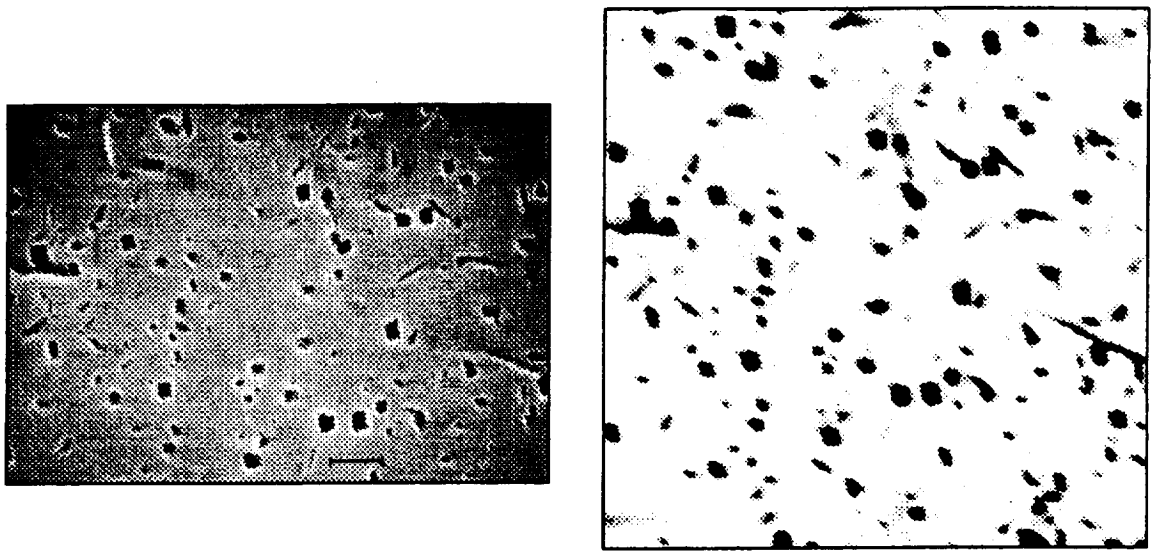

Figure 1. a) The image on the left is a secondary electron image of a lunar plagioclase grain with a track density of 1.7×10^8 cm^{-2}. The bar is 1 μm. b) The image on the right is a digitized back-scattered electron image of the same grain.

We obtained images on an ISI SEM. The sample was oriented perpendicular to the electron beam. The same condenser lens setting and aperture were used for all images. Nevertheless, the microscope is not equipped with a Faraday cup and we could not be sure of reproducing the same beam current exactly for each microscope session. The working distance knob was set at 8 mm, the focus knobs were set at 5 turns clockwise, and the image was brought into focus initially by adjusting the sample height. This procedure assures that magnification and resolution will be consistent from one session to another. We determined magnification calibration with a stage micrometer and verified that it remained consistent within 1.5%. The SEM is capable of making conventional secondary electron images (SEI) and it is also equipped with a back-scattered electron (BSE) detector. Secondary electrons produce a gray scale micrograph that looks very much like a regular black and white photograph (Fig. 1a). If SEI were used, we felt that fairly sophisticated image processing would be necessary to use the computer to distinguish tracks from background. BSE images, however, naturally showed a high contrast between tracks and background. We purposely chose to exploit this property and took digital images that appeared to the naked eye to be almost binary with very little gray (Fig. 1b). Using the computer we could set the contrast and brightness to numerically reproducible settings. We chose a wide variety of contrast settings and adjusted brightness settings visually to reproduce a high contrast image. We could not determine any significant quantitative differences when these images were analyzed for many different contrast settings. We chose to work at a contrast setting of 50%. The brightness setting was at about 49.8%, but it had to be adjusted slightly at different sessions on the SEM, probably because the beam current was not exactly reproducible.

We produced digital images and analyzed them using an eXL computer manufactured by Oxford Instruments, formerly Link Analytical. The computer has a proprietary operating system and software. The system is designed to be used with electron microscopes and it controls energy dispersive x-ray analysis as well as digital imaging. There are a wide variety

of image processing options and analytical options. I will describe only those procedures that were useful to us. Digital images were collected as a Kalman average for 90 sec. The images were 512 x 512 pixels at a 256 gray-scale (8 bit). We consistently worked at 4 different magnifications, 4600x, 6800x, 10000x, and 15000x (we also tried 2200x and 22000x, but found these magnifications to be impractical). After acquiring the image, we created a mask for the image to obscure parts of the image we did not wish to analyze such as areas off the edge of the grain, large cracks, *etc.* We could "paint" the image using this mask to some useful gray-scale level. Masking was not always necessary, but was more necessary at lower magnifications such as 4600x and 6800x. We found two analytical procedures useful. One of these, called "feature scan," actually counts the tracks. The other procedure, called "single image phase analysis," measures areas. Dividing the number of tracks by the area gives the track density.

FEATURE SCAN

The "feature scan" subset of routines is capable of doing many analytical procedures on an image. In future work we will take advantage of some of its capabilities regarding the morphology of "features," but for this work our needs were relatively simple.

A "feature" is defined in terms of connected areas (pixels) within defined limits of gray-scale. Because we took high contrast images, it was relatively simple to define these limits. The lower limit was 0 on the 256 gray-scale. By trial and error the upper limit was set to obtain track counts that were consistent with manual track counts on several standard images. The upper threshold that we finally established was 230. On images that were masked, the masked region was "painted" 231. In addition to setting thresholds, size criteria could also be used. The program counted every connected "feature" within the gray-scale thresholds, but it distinguished some as too big and others as too small. Again trial and error were used to set these size criteria. Eventually it was determined not to set maximum size criteria. The minimum size criteria were set as follows (in pixels): 16 at 15000x, 4 at 10000x, 2 at 6800x, none at 4600x. We also set the "connectivity" to 8 pixels.

With these settings established and set, we simply direct the software to "detect and measure." The image is scanned and each "feature" or track is counted. A cartoon-like image appears on the screen showing and numbering each "feature." The operator can look at this image and make a qualitative judgment about the success of the procedure. The total count is displayed on the screen as well as the counts within the categories of "too big," "too small," and just right.

SINGLE IMAGE PHASE ANALYSIS

The "single image phase analysis" subset of routines prepares a histogram of pixel number versus the image gray-scale levels and allows the user to interactively set thresholds that are color coded. The routine displays the area covered by each threshold region in pixels, in square micrometers (if you have calibrated and set the magnification at the time the image was collected), and percentage of total area. Before we established the threshold level

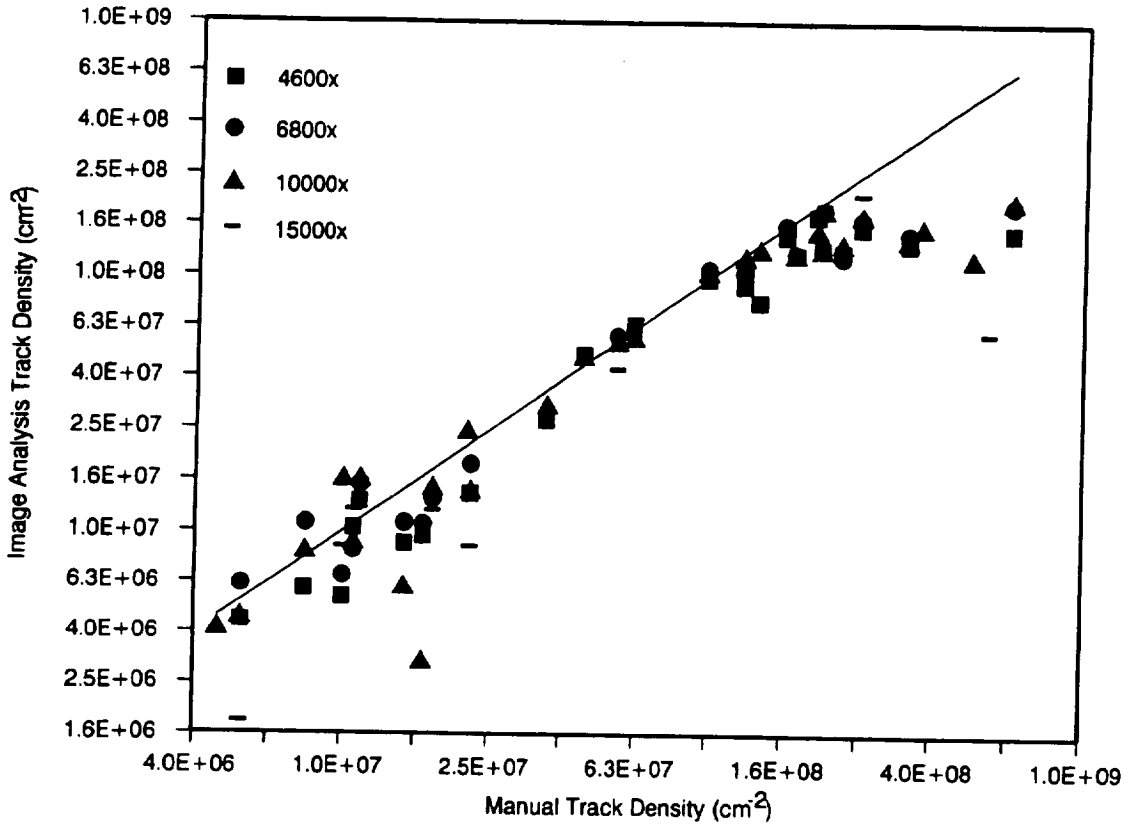

Figure 2. Graph of track densities in lunar soil grains from sample 60009, 6049 at a depth of 546 mm from the lunar surface from images taken at 4600x, 6800x, 10000x, and 15000x. The ordinate has values determined from counts using "feature scan." The abcissa has values determined by manual counting.

of 230 using "feature scan," we examined several different threshold settings on a trial and error basis. The final settings were 0-230 for tracks, 231 for the mask, and 232-255 for background. Using this routine, we could determine the total area of the image, the area of the mask, and the percentage area covered by tracks.

RESULTS

Figure 2 shows a correlation diagram of track density measurements using image analysis with conventional measurements from a photomicrograph. The correlation is excellent for track densities below $1x10^8$ cm^{-2}. Furthermore, the correlation is not sensitive to the magnification used within the range tested (but there is better statistical accuracy for lower track density grains when measured at lower magnifications). However, above track densities of $1x10^8$ cm^{-2} the image analysis technique shows saturation. It is not hard to understand why this is true. In Fig. 3a and b we show images for a point on the far right side of Fig. 2. The human counter can distinguish overlapping tracks to some extent (although this image is approaching the limit for human counting too). The software however lumps many tracks into single "features" on the digital image and the computer

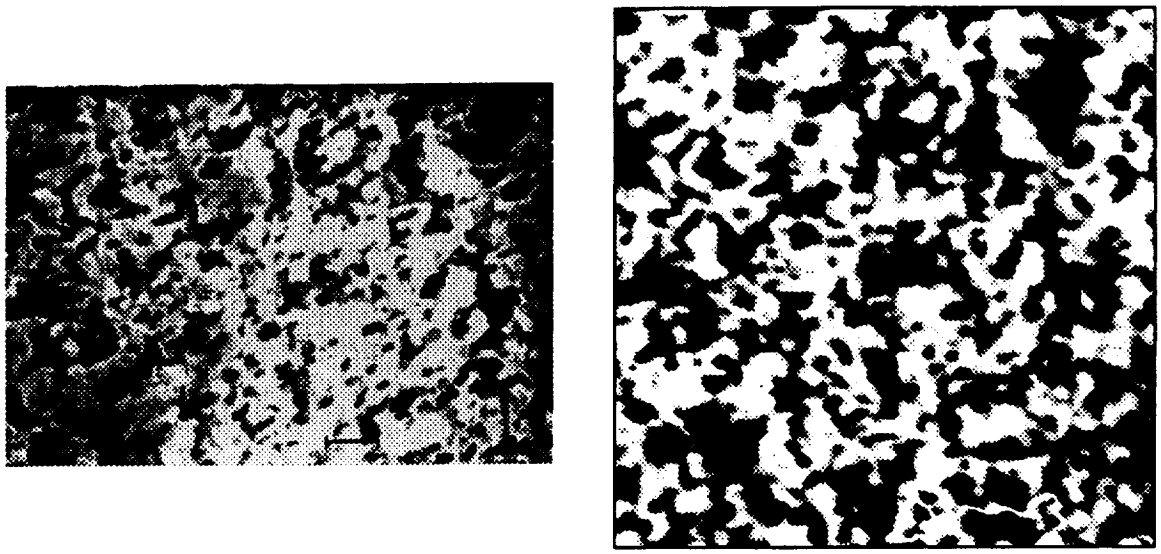

Figure 3. a) The image on the left is a secondary electron image of a lunar plagioclase grain with a track density of 5.6×10^8 cm^{-2}. The bar is 1 μm. b) The image on the right is a digitized back scattered image of the same grain. Tracks are severly overlapped.

under counts. My advisor suggested a way around this problem. The area covered by the tracks should be proportional to the number of tracks. In Fig. 4 we show a graph of track density versus the percentage area covered by tracks for images taken at 10000x that we get from the "single image phase analysis" routines. The linear regression line has a correlation coefficient r=.98. Consequently, we can use this regression line to determine track densities from 1×10^8 cm^{-2} to 1×10^9 cm^{-2}. Even this method is likely to fail at higher track densities. Figure 5 shows the 10000x data from Fig. 2 together with corrected points using the regression formula. The rectangles surrounding each point represent one standard deviation statistical uncertainty.

Although most of the time allotted to this project was spent in establishing the correct conditions for measuring track densities using image analysis software, we wanted to do one practical measurement using our techniques. Because we were using a lunar core sample, we could measure a distribution of the number of grains as a function of track density. Blanford *et al.* (1979) (or McKay *et al.*, 1991) have discussed the relationship of the track density distribution to the modality of soil maturation. They have also measured the track density distribution of the 60009 core at the depth of 546 mm. Using the faster methods of computer image analysis we have remeasured this distribution. We collected 48% of the data for this distribution in only two microscope sessions. We compare the two distributions in Fig. 6. Clearly the distribution using 100 grains that was obtained from computer image techniques shows more detail; it is clearly a bimodal distribution that indicates that the soil at 546 mm in the 60009 core is a mixed soil (Blanford *et al.*, 1979). The disturbing difference between the two distributions is the overall shift to lower track densities for the recently measured distribution. We do not yet understand the reason for this. It has nothing to do with the image analysis techniques. The problem probably arises from one of two sources: a

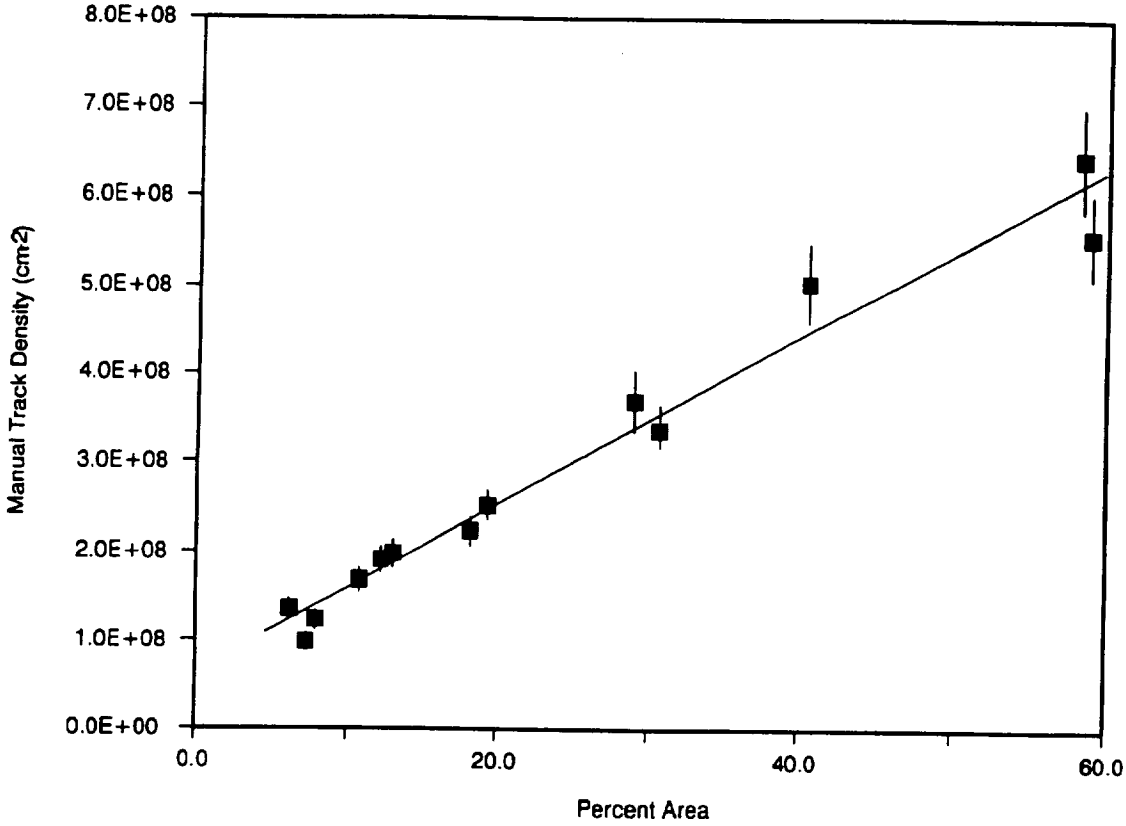

Figure 4. Track densities counted manually versus the percent area of the image covered by tracks. These quantities correlate with a coefficient r=0.98. The line is the linear regression line which best fits the points.

systematic error in magnification for one data set or the other, or a bias against high density grains in this work knowing that they could not be counted using these techniques. It should be noted that the highest density column in the first histogram consists of grains that were deemed uncountable by the observers.

CONCLUSIONS

This summer project has shown that we can measure track densities in lunar grains using image analysis techniques. It is difficult to assess exactly how much more time efficient this method will be. During the course of the study we used 191 digital images most of which have been saved on floppy disks (this procedure is surprisingly slow for this computer). We had ~14 sessions (~6 h each)of microscope time, but it was the last two sessions that we used more or less in the "production" mode of generating scientific data rather than testing and adjusting the procedures. Even during these sessions, however, we keystroked the procedures rather than use macros to speed up the process. In the application

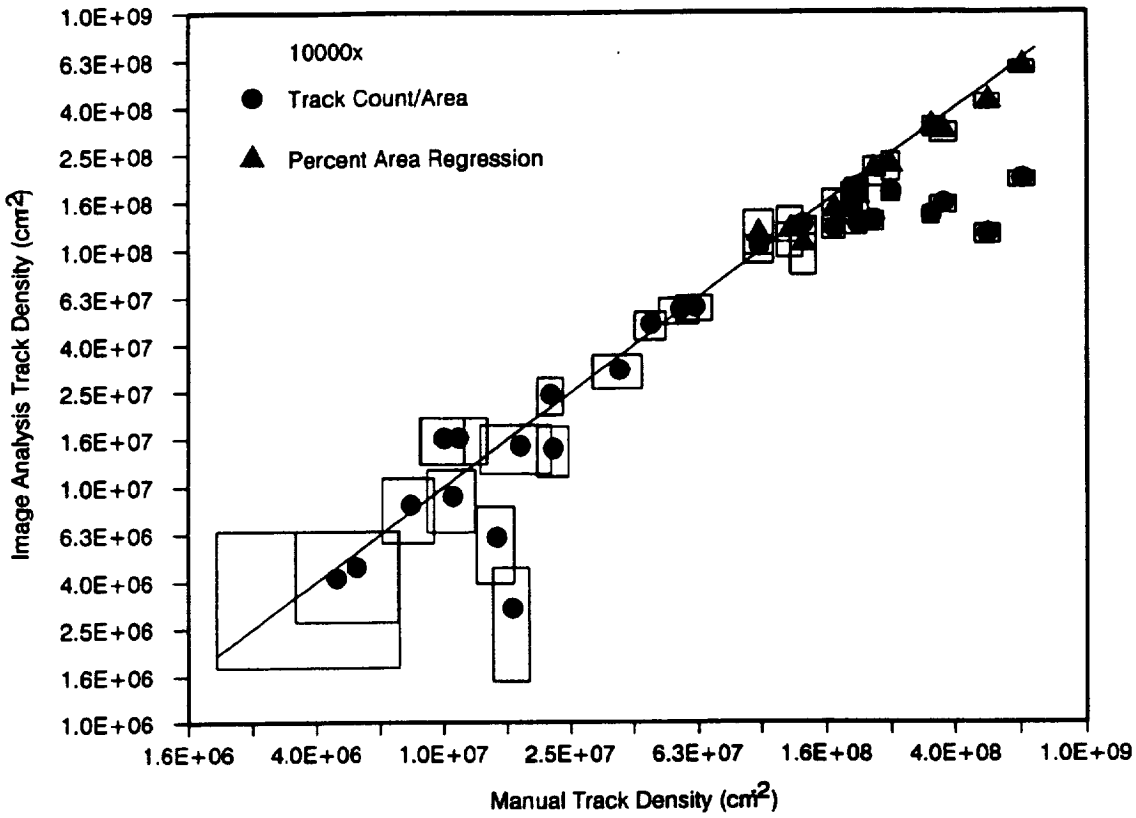

Figure 5. The correlation of manually counted and image analysis determined track densities for data taken at 10000x. Circles represent data obtained using feature scan and triangles represent data using a linear regression formula of the percent area. Rectangles give one standard deviation uncertainty based on counts or the error in the regression formula.

we chose to demonstrate we measured a more detailed distribution than had been reported in the past. An equally valid task would have been to measure distributions at more different depths in the core (the original study measured distributions 12 mm apart except in critical regions (Blanford *et al.*, 1979)). Either task requires making individual measurements on grains at a faster rate which we have shown can be done.

Track morphological characteristics are related to the energy loss rate of the ionizing particle that made the track. Plastics are used as cosmic ray dosimeters by measuring the density and energy loss of ionizing radiation from the tracks it produces (Price and Fleischer, 1971; Fleischer *et al.*, 1975). These measurements are also possible using image analysis techniques and represent a possible future direction of these studies.

REFERENCES

Blanford G.E., Blanford J., and Hawkins J.A. (1979) Irradiation stratigraphy and depositional history of the Apollo 16 double drive tube 60009/10. *Proc. Lunar and Planetary Sci. Conf. 10th*, 1333-1349.

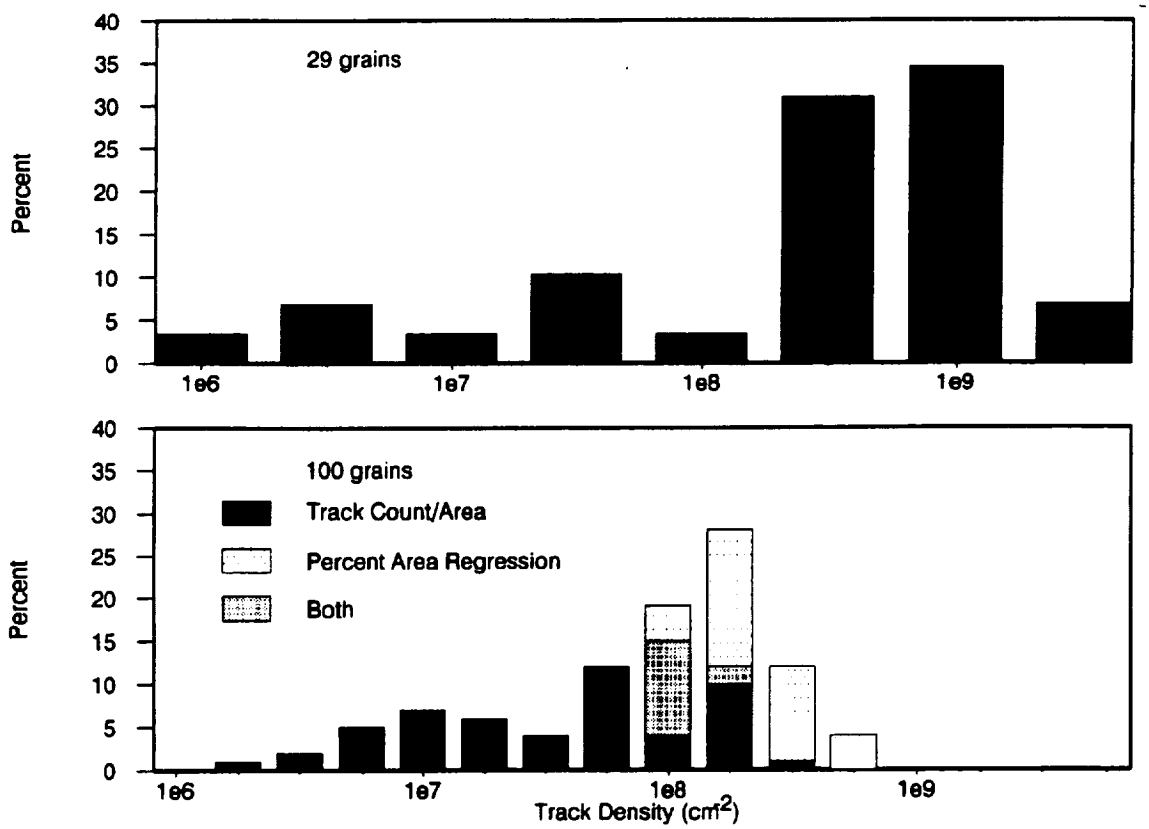

Figure 6. Histograms of the track density distribution at 546 mm below the lunar surface in sample 60009,6049. The upper histogram is based on manual measurements in 29 grains made 15 years ago. The lower histogram is based on 100 grains using image analysis techniques this summer. The bimodal distribution clearly indicates that this soil consists of a mixture of two components with different exposure histories. The distribution based on a larger number of grains is much easier to interpret.

Fleischer R.L., Price P.B., and Walker R.M. (1975) *Nuclear Tracks in Solids: Principles and Applications.* University of California Press, Berkeley, CA.

McKay D.S., Heiken G., Basu A., Blanford G., Simon S., Reedy R., French B.M., and Papike J. (1991) The lunar regolith. In *Lunar Sourcebook: A User's Guide to the Moon* (G. Heiken, D. Vaniman, and B.M. French, ed.), pp. 285-356. (Cambridge University Press, Cambridge).

Price P.B. and Fleischer R.L. (1971) Identification of energetic heavy nuclei with solid dielectric track detectors: Applications to astrophysical and planetary studies. *Ann. Rev. Nuc. Sci.* **21**, 295-334.

Price P.B. and Walker R.M. (1962) Electron microscope observation of etched tracks from spallation recoils in mica. *Phys. Rev. Letters* **8**, 217-219.

N94-25356

UNIFIED APPROACH FOR INCOMPRESSIBLE FLOWS

Final Report
NASA/ASEE Summer Faculty Fellowship Program-1993
Johnson Space Center

Prepared by:	Tyne-Hsien Chang
Academic Rank:	Associate Professor
University & Department:	Texas A&M University at Galveston Maritime System Engineering Galveston, TX
NASA/JSC	
Directorate:	Engineering
Division:	Navigation Control and Aeronautics
Branch:	Aeroscience
JSC Colleague:	C.P. Li, Ph.D.
Date Submitted:	August 10, 1993
Contract Number:	NGT-44-001-800

ABSTRACT

An unified approach for solving both compressible and incompressible flows has been investigated in this study. The difference in CFD code development between incompressible and compressible flows is due to the mathematical characteristics. However, if one can modify the continuity equation for incompressible flows by introducing pseudocompressibility, the governing equations for incompressible flows would have the same mathematical characters as compressible flows. The application of a compressible flow code to solve incompressible flows becomes feasible. Among numerical algorithms developed for compressible flows, the Centered Total Variation Diminishing (CTVD) schemes possess better mathematical properties to damp out the spurious oscillations while providing high-order accuracy for high speed flows. It leads us to believe that CTVD schemes can equally well apply to solve incompressible flows.

In this study, the governing equations for incompressible flows include continuity equation and momentum equations. The continuity equation is modified by adding a time-derivative of the pressure term containing the artificial compressibility. The modified continuity equation together with the unsteady momentum equations forms a hyperbolic-parabolic type of time-dependent system of equations. Thus, the CTVD schemes can be implemented. In addition, the boundary conditions including physical and numerical boundary conditions must be properly specified to obtain accurate solution.

The CFD code for this research is currently in progress. Flow past a circular cylinder will be used for numerical experiments to determine the accuracy and efficiency of the code before applying this code to more specific applications.

INTRODUCTION

GOVERNING EQUATIONS

The two-dimensional incompressible-flow equations are as follows:

$$\frac{\partial u}{\partial x}+\frac{\partial v}{\partial y}=0 \tag{1}$$

$$\rho\left(\frac{\partial u}{\partial t}+\frac{\partial u^2}{\partial x}+\frac{\partial uv}{\partial y}\right)=-\frac{\partial P}{\partial x}+\mu\left(\frac{\partial^2 u}{\partial x^2}+\frac{\partial^2 u}{\partial y^2}\right) \tag{2}$$

$$\rho\left(\frac{\partial v}{\partial t}+\frac{\partial uv}{\partial x}+\frac{\partial v^2}{\partial y}\right)=-\frac{\partial p}{\partial y}+\mu\left(\frac{\partial^2 v}{\partial x^2}+\frac{\partial^2 v}{\partial y^2}\right) \tag{3}$$

where u and v are velocity components in the x and y directions, respectively. P is the static pressure. μ denotes the dynamic viscosity. The incompressible governing equations (1) through (3) are mathematically classified as elliptic partial differential equations while compressible governing equations are hyperbolic partial differential equations. Because of the mathematical difference between the hyperbolic and elliptic partial differential equations, the well-developed numerical schemes for compressible flows can not apply directly to solve incompressible flows. However, if one modifies the continuity equation given in equation (1) by introducing artificial compressibility, the resulting incompressible governing equations are of hyperbolic type. The modified continuity equation is given in equation (4).

$$\frac{\partial p}{\partial t}+\frac{\partial \beta u}{\partial x}+\frac{\partial \beta v}{\partial y}=0 \tag{4}$$

where β is known as the pseudocompressibility constant.

Equations (2) through (4) are transformed into generalized curvilinear coordinates, ξ and η given by

$$\xi = \xi(x,y,t) \tag{5}$$

$$\eta = \eta(x,y,t) \tag{6}$$

The governing equations are then given by

$$\frac{\partial D}{\partial \tau} + \frac{\partial (E - E_v)}{\partial \xi} + \frac{\partial (F - F_v)}{\partial \eta} = 0 \tag{7}$$

where

$$D = \frac{1}{J}\begin{bmatrix} p \\ \rho u \\ \rho v \end{bmatrix} \tag{8}$$

$$E = \frac{1}{J}\begin{bmatrix} \beta(U - \xi_t) \\ \rho uU + \xi_x P \\ \rho vV + \xi_y P \end{bmatrix} \tag{9}$$

$$F = \frac{1}{J}\begin{bmatrix} \beta(V - \eta_t) \\ \rho uV + \eta_x P \\ \rho vV + \eta_y P \end{bmatrix} \tag{10}$$

$$F_v = \frac{\mu}{J}\begin{bmatrix} 0 \\ (\xi_x^2 + \xi_y^2)u_\xi + (\xi_x\eta_x + \xi_y\eta_y)u_\eta \\ (\xi_x^2 + \xi_y^2)v_\xi + (\xi_x\eta_x + \xi_y\eta_y)v_\eta \end{bmatrix} \tag{11}$$

$$E_v = \frac{\mu}{J}\begin{bmatrix} 0 \\ (\xi_x\eta_x + \xi_y\eta_y)u_\xi + (\eta_x^2 + \eta_y^2)u_\eta \\ (\xi_x\eta_x + \xi_y\eta_y)v_\xi + (\eta_x^2 + \eta_y^2)v_\eta \end{bmatrix} \tag{12}$$

U and V are contravariant velocities. Consequently, a chosen numerical scheme developed for compressible flows can be used to solve incompressible flows.

NUMERICAL SCHEME

Numerical algorithms recently developed for high-speed flows have demonstrated the superiority in reducing CPU time while providing the high-order accuracy. The numerical algorithms are based on the finite volume approach. A fourth-order centered scheme (CTVD) developed by Sanders and Li is used to approximate spatial derivatives in the resulting hyperbolic equations. The CTVD differencing proposed in this study has distinctive desired properties in overcoming the spurious oscillations and odd- and even-point decoupling in the solution which are caused by the use of central differencing. In addition, the implementation of these algorithms is simple and no tuning parameters are needed.

By applying the centered differencing to the transformed equations a system of time dependent differential equations is obtained. The system of differential equations can be integrated by a number of methods to obtain a converged solution. In this study, the Runge-Kutta and ADI methods are used in the code development, respectively.

When the algorithms are applied to solve the incompressible flows, a set of corresponding boundary conditions must be specified including analytical boundary conditions and numerical boundary conditions as well. It is crucial to the accuracy of the solution.

The development of numerical code based on CTVD is still in progress. It will take about one year to complete the code development. Numerical experiments will follow when the code is completed. Two-dimensional problems will be investigated first to study the accuracy and efficiency of the numerical algorithms. Then the code will be extensively used to solve three-dimensional incompressible flow problems with application to bay and nearshore circulation, and others.

CONCLUDING REMARKS

The research to develop an accurate and efficient CFD code for incompressible flows using the algorithms that are originally developed for compressible flows is a viable approach. The significant achievements for compressible flows in code development have been providing

a valuable CFD tool for those who are interested in study phenomena of incompressible flows.

N94-25357

NON-INVASIVE OPTICAL DETECTION OF GLUCOSE IN CELL CULTURE NUTRIENT MEDIUM

Final Report
NASA/ASEE Summer Faculty Fellowship Program-1993
Johnson Space Center

Prepared by:	Gerald L. Coté, Ph.D.
Academic Rank:	Assistant Professor
University & Department:	Texas A&M University Bioengineering Program College Station, TX 77843
NASA/JSC	
Directorate:	Space and Life Sciences
Division:	Medical Sciences
Branch:	Biomedical Operations and Research Branch
JSC Colleague:	Glenn F. Spaulding, M.D.
Date Submitted:	August 18, 1993
Contract Number:	NGT-44-001-800

ABSTRACT

The objective of the proposed research was to begin the development of a non-invasive optical sensor for measuring glucose concentration in the output medium of cell cultures grown in a unique NASA bioreactor referred to as an integrated rotating-wall vessel (IRWV). The input, a bovine serum based nutrient media, has a known glucose concentration. The cells within the bioreactor digest a portion of the glucose. Thus the non-invasive optical sensor is needed to monitor the decrease in glucose due to cellular consumption since the critical parameters for sustained cellular productivity are glucose and pH. Previous glucose sensing techniques have used chemical reactions to quantify the glucose concentration. Chemical reactions, however, cannot provide for continuous, real time, non-invasive measurement as is required in this application. Our effort while in the fellowship program was focused on the design, optical setup, and testing of one bench top prototype non-invasive optical sensor using a mid-infrared absorption spectroscopy technique.

Glucose has a fundamental vibrational absorption peak in the mid-infrared wavelength range at 9.6 μm. Preliminary absorption data using a CO_2 laser were collected at this wavelength for water based glucose solutions at different concentrations and one bovine serum based nutrient medium (GTSF) with added glucose. The results showed near linear absorption responses for the glucose-in-water data with resolutions as high as 108 mg/dl and as low as 10 mg/dl. The nutrient medium had a resolution of 291 mg/dl. The variability of the results was due mainly to thermal and polarization drifts of the laser while the decrease in sensitivity to glucose in the nutrient medium was expected due to the increase in the number of confounders present in the nutrient medium. A multispectral approach needs to be used to compensate for these confounders. The CO_2 laser used for these studies was wavelength tunable (9.2 to 10.8 micrometers), however, was to unstable across wavelengths to test the multispectral approach.

From this research further NASA support was obtained to continue the work throughout the year in which a more stable light source will be used at smaller, near-infrared, wavelengths. It is anticipated that a more compact, non-invasive, optical glucose sensor will be realized which can be used with a bioreactor on future space shuttle missions. It is also anticipated that a multispectral optical sensor may be used to determine the concentration of other molecules needed within the NASA bioreactor, such as fructose and galactose.

INTRODUCTION

The NASA Johnson Space Center - Biotechnology Group is currently involved in the development of a new class of cell culture vessel technology [1,2]. The rotating wall vessels are fluid filled cylinders with a silicone membrane oxygenater in which cells and microcarrier beads are horizontally rotated in free suspension resulting in a low shear, quiescent, environment for the culture of these cells. It has been shown that under these simulated microgravity conditions certain cells (i.e. Baby Hamster Kidney (BHK-21), human transitional epithelial bladder carcinoma cell line (T-24), etc.) provides for superior growth, less cellular damage, and less glucose utilization. Currently, the NASA/JSC Biotechnology Group is utilizing a set of *invasive* sensors (i.e. pH, CO_2, O_2, and glucose), off-line, to monitor these samples, to maintain the cells by manually increasing or decreasing the concentration of the various parameters, and to study the effects of feed back control systems on tissue development. As would be expected this approach has the drawbacks of potential contamination and subsequent death of the cells as well as the lack of real-time control. Our work focused on the development of a glucose detection system to overcome the above concerns by providing continuous, non-invasive, sensing of the glucose concentration within the cell culture medium.

Several non-invasive glucose monitoring methods have been proposed and investigated, particularly for blood glucose determination. One approach is polarimetry [3,4,5,6,7] in which a beam of linearly polarized light is directed through the aqueous humor of the eye and due to the chiral nature of the glucose molecule the light polarization rotates in an amount proportional to that of glucose. For this application, since the nutrient medium has a number of optically rotatory confounders, this approach was deemed inadequate. The second approach is a development based on the near infrared (NIR) (750 nm - 1300 nm) spectroscopic absorption of light due to glucose at certain wavelengths. This approach has been used extensively in agricultural food analysis but has been recently applied to blood glucose measurement in which the light is directed through the finger [8,9] and derivative or multivariate analysis techniques are used to quantify the glucose levels. Since NIR bands are due to weak overtones and combinations of fundamental molecular vibration absorption bands which can overlap significantly in a complex medium, such as the one used here, this technique was not initially considered. The last technique is also based on infrared absorption spectroscopy but in the mid-infrared region. Both transmission [10] and attenuated total reflection (ATR) [11,12] techniques have been used in this region. The glucose concentration was found to be directly proportional to the absorption peak at the fundamental vibrations for that molecule. In fact, Mendelson, et.al.[12] reported a resolution in the measurement of glucose concentration in whole blood of 30 mg/dl at the 9.6 μm absorption peak using the CO_2 laser line at that peak. Therefore, using a transmissive optical approach and multiple CO_2 wavelengths it was felt that better than 30 mg/dl could be achieved.

EXPERIMENTAL SYSTEM

The optical path, as shown in Figure 1, began with a Laser Photonics continuous wave CO_2 laser with a maximum power output of 8 Watts. It is linearly polarized 100:1, and is tunable from 9.2 to 10.8 μm using a grating at the output. Power stability of the CO_2 laser is controlled by air-cooling the laser cavity to a desired temperature set point. This also determines the power of a particular CO_2 wavelength at the output. A marginally

stable output of 400 mW at the 9.6 μm wavelength was used in these experiments. The laser and all optics were mounted on a 2 ft by 2 ft optical breadboard for this bench-top system.

The output beam of the laser was reflected off a gold-coated flat mirror and split with a zinc selenite (ZnSe) window into a reference and sample path. The split from the ZnSe window is polarization and thermally dependent but was set at an angle to give a 50/50 split.

Both the reference and sample paths were chopped at a frequency of 300 Hertz by an optical chopper. The blade was precisely positioned with a three dimensional positioner such that when one blade is transmitting the beam from one path, the opposite blade is blocking the beam of the other path. This caused a 180 degree phase difference between the two beams and allowed for the use of a single detector. With the single detector approach the need for detector matching was eliminated and an increase in the signal-to-noise ratio was achieved.

The two beams passed through their respective 20 μm path length ZnSe sealed cells. The reference cell contained double distilled water for on-line subtraction of water absorption in the sample solution. The sample cell contained the glucose solution to be analyzed. Both beams are focused with 4 inch focal length gold-coated spherical mirrors onto a single mercury-cadmium-telluride-arsenic (HgCdTeAs) detector. Since light was continuously incident on the detector from the two paths, a square wave difference signal, resulting from the phase difference, with an offset from zero was obtained. The difference signal represented the different absorptions of the two solutions and the offset was proportional to the power level incident on the detector.

From the detector, the signal was amplified and sent to a band pass filter with a center frequency of 300 Hz to obtain the difference signal and to a low pass filter with a cutoff frequency of .08 Hz to obtain the power signal. The difference signal was passed to a lock-in amplifier which locked into the fundamental frequency. The output of the lock-in amplifier was an offset signal proportional to the magnitude of the difference signal. The output of the lock-in amplifier and of the low pass filter were sampled at 100 Hz by an A/D board to obtain 100 samples for each signal.

The sampled signals were imported into Microsoft Excel for Windows for data analysis. The two signals were averaged individually and then the lock-in amplifier signal was divided by the power signal to remove small laser fluctuations. A linear regression of the signal ratio to glucose concentration was performed and the resolution of the system found.

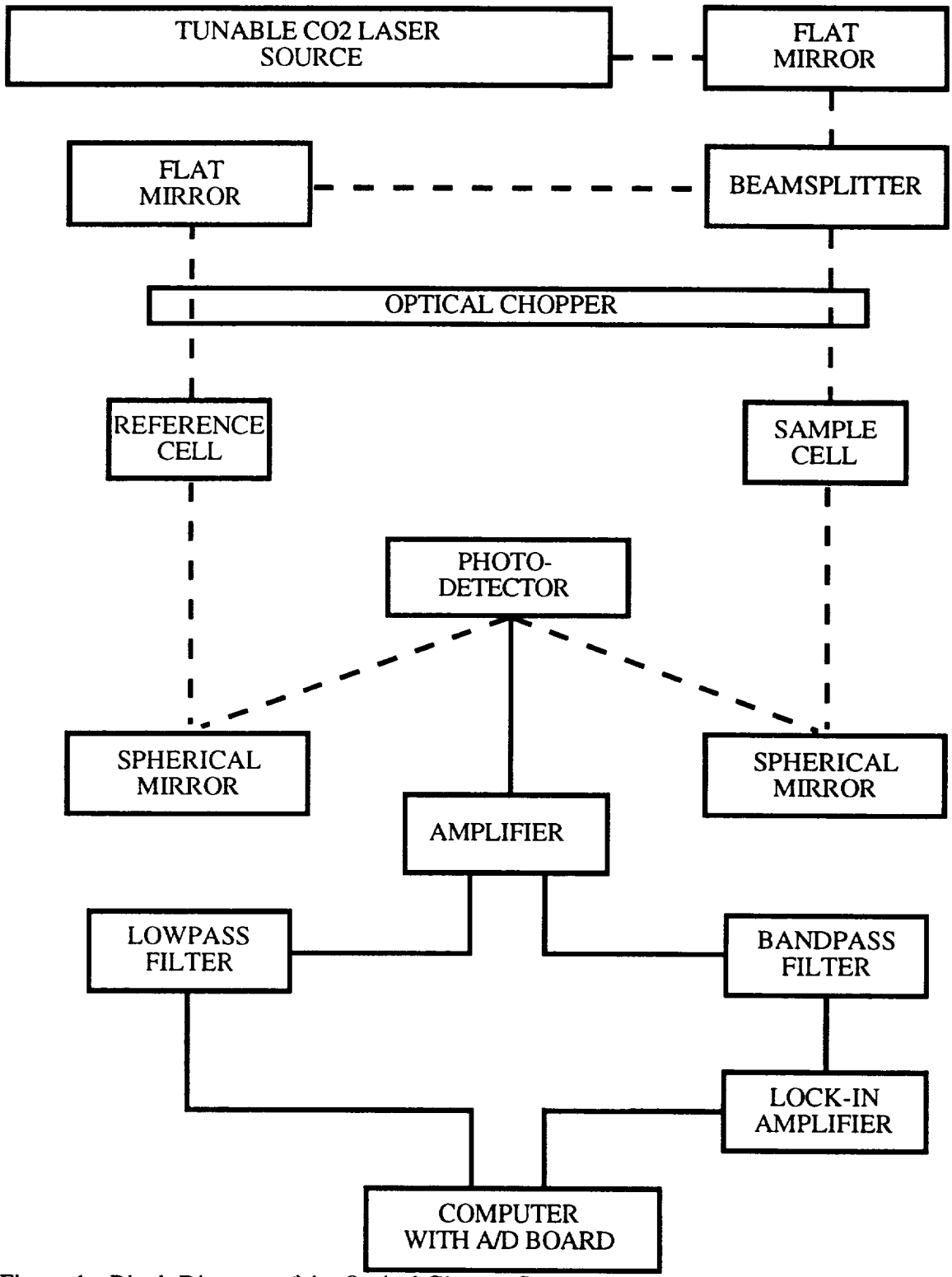

Figure 1.- Block Diagram of the Optical Glucose Sensor Developed for the NASA/JSC Biotechnology Group

RESULTS

The same set of solutions of glucose and water ranging from 100 to 500 mg/dl were analyzed over two consecutive days. The normalized scatter plots of these two runs are included in Figures 2 and 3. A linear regression was performed on the data of Figure 2 and the system resolution was 38 mg/dl. It was discovered, however, that the outlier at 500 mg/dl was due to saturation of the input to the A/D board by the lock-in amplifier. With this point removed the system resolution was found to be 10 mg/dl. A gain adjustment was made to the A/D board and the experiments were repeated the next day. The second run of glucose solutions, shown in Figure 3, showed little repeatability of the system. The obvious difference from the previous data was the decrease in magnitude of the slope. A linear regression was again performed and the system resolution found to be 108 mg/dl. It should be noted that the data had a negative slope which was merely a result of the change in the splitting ratio of the ZnSe window, however this was obviated with normalization. The outlier at 400 mg/dl was due to a momentary shift in intensity to one of the paths off the beam splitter because of laser polarization and power output variations due to thermal effects.

The GTSF solutions with varying concentrations of glucose from 100 to 1000 mg/dl were used in the final experiment. The data is shown in Figure 4 (Again modified to account for negative slope). The linear regression for the data gave a system resolution of 291 mg/dl. The decrease in system resolution was due to the multiple IR absorbing components in solution.

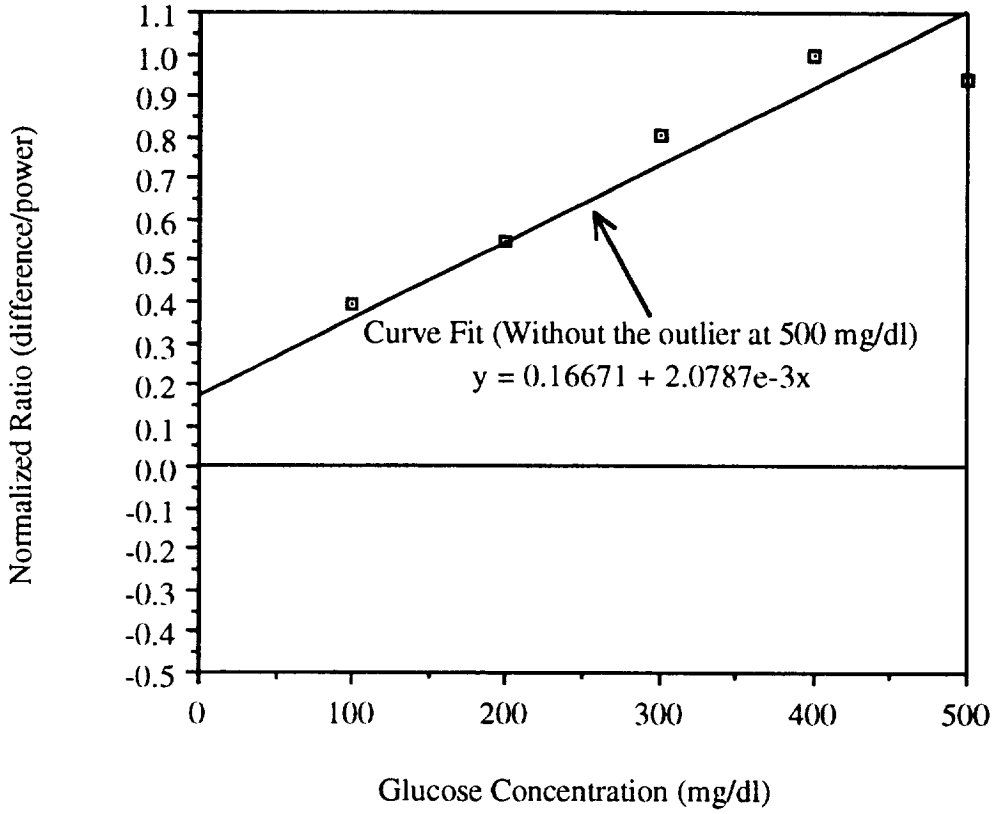

Figure 2.- Initial study of glucose in water showing the normalized ratio of the difference signal as a function of glucose concentration. The outlier at 500 mg/dl was due to saturation of the system.

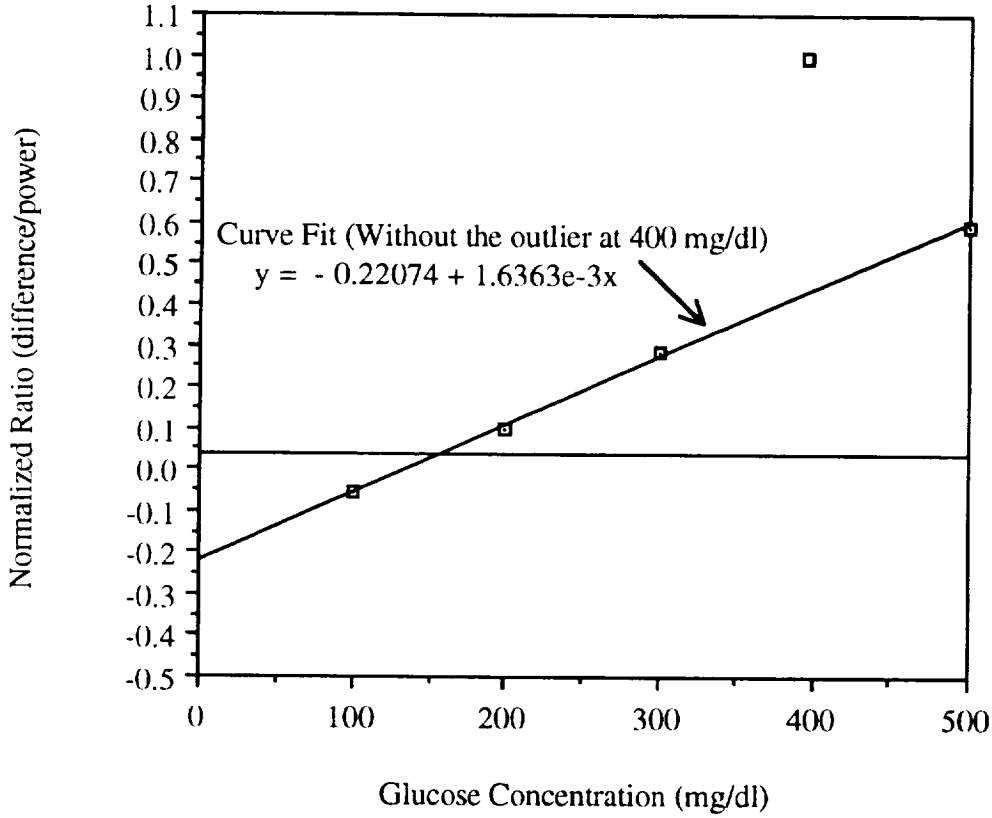

Figure 3.- Repeatability study of glucose in water showing the normalized ratio of the difference signal as a function of glucose concentration from the solutions used for Figure 2, one day later. The outlier at 400 mg/dl was due to shift in intensity of one light path.

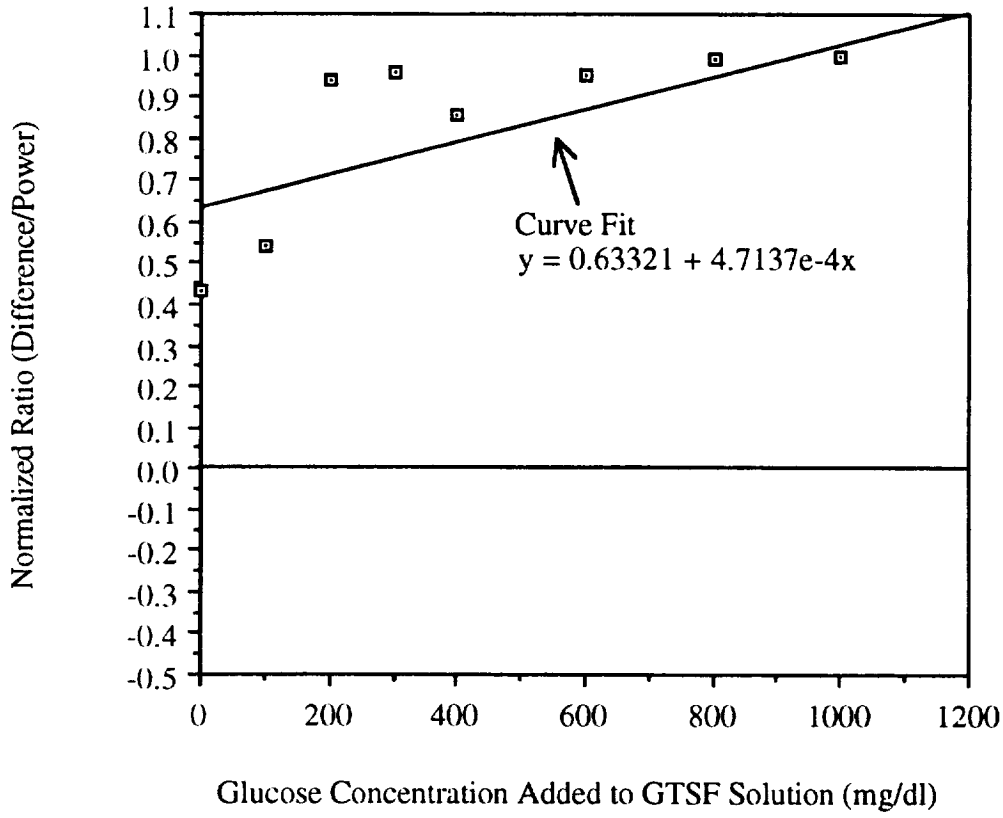

Figure 4.- Study of GTSF nutrient medium showing the normalized ratio of the difference signal as a function of glucose concentration. The result showed a decrease in sensitivity to glucose due to the large number of confounding molecules with overlapping absorption peaks.

CONCLUSIONS

In this report a non-invasive glucose measurement system using a mid-infrared absorption spectroscopy technique that was developed, built, and tested for the Biotechnology Group at NASA/JSC was described. The above results showed the potential for a very accurate glucose measurement system attaining, at times, 10 mg/dl resolution. However, the use of a CO_2 laser as the light source did not allow for repeatable measurements due to its thermal and polarization instability. As anticipated, using a single wavelength, the glucose could only be resolved with good accuracy in the single component (glucose in water) solution but not with the multi-component nutrient medium. It is felt that the use of multiple wavelengths and multivariate analysis would provide the needed 30 mg/dl accuracy in the multiple component cell culture nutrient medium, but the CO_2 laser used here did not show sufficient stability when tuning across wavelengths to perform such analysis.

As indicated, from this research further NASA support was obtained to continue the development of a non-invasive glucose sensor throughout the year in which a more stable light source will be used at smaller, near-infrared, wavelengths. It is anticipated that a more compact, non-invasive, optical glucose sensor will be realized which can be used with a bioreactor on future space shuttle missions. It is also anticipated that a multispectral optical sensor may be used to determine the concentration of other molecules needed within the NASA bioreactor and provide continuous closed loop delivery of various nutrients to the cells.

In addition, this technology, although currently applied to cell culture systems, could also be useful in the non-invasive monitoring of blood chemicals of the astronauts. This will allow for better health care monitoring with less risk to the NASA crew than with contemporary invasive methods such as venipuncture and subsequent analysis by various means following sample preparation. The current monitoring process is time-consuming, requires high to moderate levels of technical expertise, and delivers single time point rather than continuous, real-time data. The development of non-invasive sensors offers significant advantages over current modes. It would reduce the risk of complications due to invasive procedures, increase the availability of critical data with less crew time committed to producing the data, allow real time biomedical analysis and permit telemetry of the data in near real-time to earth stations for medical decision making.

REFERENCES

[1] Prewett, T.L., Goodwin, T.J., and Spaulding, G.F., "Three-Dimensional Modeling of T-24 Human Bladder Carcinoma Cell Line: A New Simulated Microgravity Culture Vessel", J. Tiss. Cult. Meth., 15; pp. 29-36: 1993.

[2] Goodwin, T.J., Prewett, T.L., Wolf, D.A., and Spaulding, G.F., "Reduced Shear Stress: A Major Component in the Ability of Mammalian Tissues to Form Three-Dimensional Assemblies in Simulated Microgravity", J. Cellular Biochemistry, 51; pp. 301-311: 1993.

[3] Rabinovitch, B., March, W.F., and Adams, R.L., "Noninvasive Glucose Monitoring of the Aqueous Humor of the Eye: Part I. Measurement of Very Small Optical Rotations", Diabetes Care, Vol 5, No 3; pp 254-58: May-June 1982.

[4] March W.F., Rabinovitch, B., and Adams, R.L., "Noninvasive Glucose Monitoring of the Aqueous Humor of the Eye: Part II. Animal Studies and the Scleral Lens.", Diabetes Care, Vol 5, No 3; pp 259-65: May-June 1982.

[5] King, T., McNicols, R., Goetz, M., and Coté, G.L., "Closed-Loop Optical Polarimetric Glucose Sensing Using a Multispectral Approach", Optical Engineering, manuscript submitted: August 1993.

[6] Coté, G.L., Fox, M.D., and Northrop, R.B., "Noninvasive Optical Polarimetric Glucose Sensing Using a True Phase Measurement Technique", IEEE Tr. Bio. Eng., V39, N7; pp. 752-56: July 1992.

[7] Goetz, M., King, T.W., and Coté, G.L., " Multispectral Polarimetric Approach to Noninvasive Glucose Sensing", Presented at the Eleventh Annual Houston Conference on Biomedical Engineering Research, University of Houston, Houston TX: Feb. 11-12, 1993

[8] Rosenthal, R.D., Paynter, L.N., Mackie, L.H., "Non-invasive Measurement of Blood Glucose", U.S. Patent #5,028,787: July 2, 1991.

[9] Robinson, M.R., Eaton, R.P., Haaland, D.M., Koepp, G.W., Thomas, E.V., Stallard, B.R., and Robinson, P.L., "Noninvasive Glucose Monitoring in Diabetic Patients: A Preliminary Evaluation", Clin. Chem., V38, N9; pp. 1618-22: 1992.

[10] Zeller, Novak, P., and Landgraf, R., "Blood Glucose Measurement by Infrared Spectroscopy", International J. Artificial Organs, V12, N2; pp. 129-35: 1989.

[11] Heise, H.M., and Marbach, R., "Multivariate Determination of Glucose in Whole Blood By Attenuated Total Reflection Infrared Spectroscopy", Anal. Chem., V61; pp. 2009-15: 1989.

[12] Mendelson, Y., Clermont, A.C., Peura, R.A., and Lin, B.C., "Blood Glucose Measurement by Multiple Attenuated Total Reflection and Infrared Absorption Spectroscopy", *IEEE Trans. Bio. Eng.*, Vol. 37, No. 5; pp. 458-465: May 1990.

N94-25358

A GEOCHEMICAL STUDY OF ACAPULCOITE AND LODRANITE METEORITES

Final Report
NASA/ASEE Summer Faculty Fellowship Program-1993
Johnson Space Center

Prepared by:	Stephen W. Field, Ph.D.
Academic Rank:	Assistant Professor
University & Department:	Stockton State College Dept. of Geology and Environmental Studies Pomona, New Jersey 08240
NASA/JSC	
Directorate:	Space and Life Sciences
Division:	Solar System Exploration
Branch:	Office of the Curator
JSC Colleague:	Marilyn M. Lindstrom, Ph.D.
Date Submitted:	August 20, 1993
Contract Number:	NGT-44-001-800

ABSTRACT

Lodranites and acapulcoites (primitive achondrites) are two classes of meteorites with geochemical signatures similar to chondrite meteorites. Lodranites and acapulcoites, however, have few or none of the chondrules characteristic of the chondrites. Texturally the primitive achondrites appear to have been recystallized though planetary igneous or metamorphic processes. A study of five primitive achondrites; two lodranites, two acapulcoites, and one supposedly intermediate acapulcoite/lodranite were analyzed petrographically and geochemically to determine the igneous and metamorphic processes which have affected them. Acapulcoites show little evidence of melt extraction. The geochemistry of lodranite samples indicates silicate and metal/sulfide melts were removed from the rocks. The mineralogy and geochemistry of the intermediate meteorite suggest the rock is a metal rich acapulcoite and not a lodranite.

INTRODUCTION

Among the objects which have impacted Earth over the past 4.6 billion years are the achondrite meteorites and the chondrite meteorites. Chondrites are generally believed to be fragments of small planetary bodies, possibly asteroids. These meteorites are composed of matter which formed early in the history of the Solar System. These meteorites are characterized by the presence of small round or rounded mineral aggregates called chondrules. Chondrite meteorites show little evidence for high pressure planetary processes such as volcanism or metamorphism. Achondrite meteorites are generally believed to be rocks which have been modified by planetary processes, such as melting, volcanism, or metamorphism. Because the planetary source of achondrites and chondrites is still uncertain and unexplored, the origin and alteration processes that affected these rocks are still ambiguous.

Five achondrite meteorites were analyzed geochemically to determine the igneous or metamorphic processes which may have affected them. The study included reflected light microscope examination, transmitted light microscope examination, electron microprobe analyses of minerals, and instrumental neutron activation analyses (INAA) of major and trace element bulk chemistry.

PRIMITIVE ACHONDRITES

A number of different types of achondrites have been described. The classification of these meteorites is based on characteristics such as oxygen isotopic composition, mineral chemistry, and bulk chemistry. Primitive achondrites are rare rocks which resemble chondrite meteorites in some mineral and bulk chemical characteristics. Some primitive achondrites also contain mineral structures which resemble altered chondrules commonly found in chondrite meteorites. It is generally believed that primitive achondrites are chondrites which have been altered by high temperature and pressure planetary processes, such as igneous melting and metamorphism.

Several subcategories of primative achondrites have been described including winoaites (Prinz et al, 1981), acapulcoites (Palme et al, 1981), and lodranites (Bild and Wasson, 1976). Several unique primitive achondrites have been described but have not been placed into named categories. Acapulcoites and lodranites are two classes of primative achondrites which may be genetically related

(Zipfel and Palme, 1993; McCoy et al, 1992). Acapulcoites are granular rocks composed dominantly of Mg-Fe pyroxene, olivine, plagioclase, Fe-Ni metal, and troilite. Minor amounts of Ca-pyroxene, spinel, and phosphates may be present. Lodranites contain minerals with similar compositions.but contain little or no plagioclase and less troilite than acapulcoites (McCoy et al, 1993). It has also been observed that lodranites are coarser grained than acapulcoites, however, this may be a result of the small sampling population.

PRIMITIVE ACHONDRITE SAMPLES

Five primative achondrites, ALHA 81187, ALHA 81261, MAC 88177, LEW 88280, and EET 84302, were examined in this study. Two samples, ALHA 81187 and ALHA 81261, are classified as acapulcoites and meteorites MAC 88177 and LEW 88280 are classified as lodranites. Meteorite EET 84302 has been suggested as a rock intermediate in mineral and chemical characteristics between acapulcoites and lodranites (McCoy et al, 1993).

PETROGRAPHIC DESCRIPTION

Acapulcoites

ALHA 81187 is an equigranular, fine-grained rock composed of approximately 50 volume % orthopyroxene (opx), 25% olivine (ol), 20% Fe-Ni metal, 5% clinopyroxene (cpx), and less than 1% Cr-spinel. No plagioclase (plag) was found in this sample. The silicate grains are anhedral to subhedral. Patches of metal are common in the sample and fine-grained veins of metal and/or metal oxides and hydroxides rim or partially rim silicates. There are several apparently brecciated sections of the sample and fractures cut through some silicate grains. Metals, oxides, and/or hydroxides fill the fractures and brecciated sections of the sample.

ALHA 81261 is an unbrecciated, granular, fine-grained rock. The silicate minerals appear fresh and unchanged by low temperature alteration. The approximate mineral volume percents are opx 59, plag 15, Fe-Ni metal 10, Troilite 10, cpx 7, apatite 1.5, and merrilite 1.5. Olivine was present only as small round inclusions in enstatite and comprised less than 1 volume percent of the rock. Large subhedral to euhedral opx grains dominate the fabric of the sample.

These grains have straight or smooth slightly curving boundaries. Round inclusions of ol, troilite , and metal are present in some opx grains. Slightly smaller cpx grains are associated with the opx. Plagioclase grains are anhedral and appear to fill void spaces between larger opx grains. Metals and troilite also have anhedral shapes and fill gaps between silicate grains. Phosphates are associated with metal and troilite.

Lodranites

Meteorite MAC 88177 is a coarse-grained granular rock dominated by opx and olivine. The approximate modal percentages are opx 67, ol 21, Fe-Ni metal and troilite 10, cpx 2, Cr-spinel less than 1, and apatite less than 1. Opx and ol are subhedral to euhedral and anhedral metals and troilite fill spaces between these silicates. Small euhedral Cr-spinels and phosphates are associated with the metals and troilite. Some opx grains contain round metal and troilite inclusions. The sample is highly fractured but the fractures are not filled. A few large cpx grains are present. These minerals have concave , scalloped edges when in contact with opx. All of the cpx grains contain abundant exsolution lamellae of opx.

Meteorite LEW 88280 is a coarse-grained granular rock dominated by opx and olivine. Abundant metal and troilite are present interstitial to the silicates. A few large cpx grains are present and these always contain abundant opx exsolution lamellae. Larger rounded opx, ol, metal, and troilite inclusions are also common in the cpx. The inclusions and lamellae are concentrated but not exclusively found in the centers of the pyroxenes. The approximate modal percentages are opx 55, ol 30, metal and troilite 20, and cpx 5.

EET 84302

EET 84302 is a medium- to coarse-grained, metal-rich, granular rock composed dominantly of opx, Fe-Ni metal and Cr-spinel. The rock has some unusual and distinct textures. The Cr-spinel and metal are segregated into distinct domains within the sample. Approximately 1/3 of the sample is composed of silicates + Cr-spinels and the other 2/3 is composed of metal + silicates. Orthopyroxenes have subhedral rounded shapes and contain distinct, generally rectangular patches of rounded to euhedral metal and sulfide inclusions. These patches generally but not always are found in the interiors of the opx grains. The inclusion patches generally occupy only a small fraction (10-20 %) of the pyroxene, and the edges of pyroxenes are usually

inclusion free. Large discrete, anhedral blebs of metals and Cr-spinel are also present. These minerals have concave rounded edges when in contact with silicates. Large cpx grains contain abundant lamellae of opx, large euhedral inclusions of opx, rounded inclusions of metal, and euhedral granular inclusions of plagioclase. Plagioclase is also found as anhedral partial rims or subhedral crystals at the edges of cpx grains. Approximate modal percentages are opx 50, Fe-Ni metal 30, Cr-spinel 10, cpx 5, plag 3, ol 2, and merrilite less than 1.

MINERAL CHEMISTRY

Acalpulcoites

Olivines in the Acapulcoites are Mg-rich. The forsterite composition of olivines in ALHA 81187 are Fo_{95} and the forsterite compositions in ALHA 81261 are Fo_{90}. Orthopyroxenes are Mg-rich in both Acapulcoites. Average compositions in ALHA 81187 are $En_{90}Fs_{6}Wo_{4}$ and $En_{89}Fs_{10}Wo_{1}$ in ALHA 81261. Corresponding cpx compositions are $En_{51}Fs_{2}Wo_{47}$ and $En_{52}Fs_{5}Wo_{44}$. These Ca-rich pyroxenes are diopsides. Average plagioclase compositions in ALHA 81261 are $Ab_{80}An_{17}Or_{3}$. Plagioclase was not detected in ALHA 81187.

Both kamecite ($Fe_{92}Ni_{6}$) and taenite ($Fe_{51}Ni_{49}$) are present in ALHA 81187 but only kamecite ($Fe_{92}Ni_{7}$) was detected in ALHA 81261. Troilite (Fe%=63) was present in ALHA 81261 but not ALHA 81187. Cr-spinel in ALHA 81187 has a Cr/(Cr+Al) ratio of .85. Merrilite in ALHA 81261 contains 2.2 wt% Na_2O and apatite in the same sample contains 0.29 wt% Na_2O. No phosphate was detected in ALHA 81187.

Lodranites

MAC 88177 contains Mg-rich olivine (Fo_{86}) and opx ($En_{84}Fs_{13}Wo_{2}$). Ca-rich cpx has a composition of $En_{50}Fs_{6}Wo_{44}$. Kamecite is variable in composition and ranged from $Fe_{89}Ni_{11}$ to $Fe_{86}Ni_{14}$. Taenite, spatially associated with the kamecite, is generally uniform in composition ($Fe_{63}Ni_{37}$). Spinel in the meteorite is chromium-rich with a Cr/(Cr+Al) ratio of .84. Apatite contains 0.26 wt% Na_2O and troilite contains 63 wt% Fe.

LEW 88280 also contains forsteritic olivine (Fo_{87}) which is similar to olivine in MAC 88177. Opx ($En_{86}Fs_{12}Wo_{2}$) and cpx ($En_{50}Fs_{5}Wo_{45}$) are also similar to corresponding minerals in MAC 88177. Troilite in LEW 88280 contains 61 wt % Fe. Kamecite is compositionally uniform with an average

composition of $Fe_{92}Ni_8$. Taenite, which is spatially associated with kamecite, has highly variable compositions which range from $Fe_{86}Ni_{14}$ to $Fe_{79}Ni_{21}$. The highest Ni contents are present in taenite directly adjacent to kamecite.

EET 84302

EET 84302 contains forsteritic olivine (Fo_{91}), Mg-rich opx ($En_{90}Fs_8Wo_2$), and Ca-rich diopsidic cpx ($En_{51}Fs_4Wo_{45}$). Opx lamellae in the cpx has the same composition as discrete opx. Plagioclase compositions in this meteorite are highly variable and range from $Ab_{68}An_{29}Or_3$ to $Ab_{53}An_{44}Or_3$. This variability is suspect and may be caused by Na migration during the analysis. Average iron contents in this meteorite are 61 wt%. Kamecite has an average composition of $Fe_{92}Ni_8$. The Cr/(Cr+Al) ratio of spinels in this meteorite is .84.

BULK CHEMISTRY

The bulk chemistry of the five primitive achondrites was analyzed with INAA techniques. Among the elements analyzed were the major elements Na, Ca, Fe, and the minor or trace elements Ni, Cr, Eu, Sc, Se, La, Lu, Sm, Yb, Sb, Co, Ir, Au, and As. Other elements were analyzed, however, complete sets of data for the listed elements were obtained for all the primitive achondrites and these data are used for comparisons among the analyzed meteorite compositions. Because the primitive achondrites are thought to have originally had chondritic compositions and because of the need for a common standard, the chemical composition of primitive achondrites are compared to H-chondrite compositions.

The following system is used in this paper to compare primitive achondrite compositions to H-chondrite compositions. Elements in achondrites which have abundances of 0 to 0.30 times chondritic abundances are highly depleted, abundances of 0.31 to 0.70 are moderately depleted with respect to chondritic abundances, abundances of 0.71 to 0.90 are slightly depleted, abundances of 0.91 to 1.10 times chondritic abundance are chondritic, abundances of 1.11 to 1.30 times chondritic abundances are slightly enriched, abundances of 1.31 to 1.70 times chondritic are moderately enriched, and abundances greater than 1.71 times chondritic are highly enriched.

Acapulcoites

The two acapulcoites analyzed contain abundances which deviate only slightly from H-chondrite abundances. ALHA 81261 contains chondritic abundances of Na, Ni, Co, Au, Sc, Sb, and Se. Slightly enriched elements include Eu, La, Sm, and Ir; and moderately enriched elements include Ca, Cr, Lu, Yb, and As. The meteorite contains no elements which are highly enriched relative to H-chondrites. Iron is slightly depleted relative to H-chondrites but no other depleted element is present among the 17 elements used in the comparison.

ALHA 81187 has a similar pattern but some differences do exist. The elements Ir and Sm are chondritic; Ca, Cr, Eu, Sc, Lu, Yb, and Sb are slightly enriched; and Na, Co, Au, As, and La are slightly depleted. The elements Fe, Ni, and Se are moderately depleted relative to H-chondrite abundances.

Lodranites

The two Lodranites analyzed are characterized by a group of highly depleted elements, which clearly distinguishes them from the Acapulcoites. MAC 88177 contains highly depleted concentrations of Na, Eu, Ir, Sm, La, Ni, Co, Au, and As. Moderately depleted elements include Fe, Se, and Sb; and Ca, Lu, and Yb are slightly depleted with respect to H-chondrites. Only Cr and Sc are slightly enriched and no moderately or highly enriched elemental concentrations are present.

LEW 88280 , like MAC 88177, is also highly depleted in elements Na, Eu, Ir Sm, and La. However, unlike MAC 88177 Ni, Co, Au, and As are not highly depleted. The elements Ca, Lu, and Yb are moderately depleted; and Fe, Co, and Au are only slightly depleted with respect to H-chondrites. Chondritic abundances of Ni and Sc are present as are slightly enriched concentrations of As and Se, and moderately enriched concentrations of Cr and Sb. No highly enriched elements are present.

EET 84302

EET 84302 is characterized by a group of slightly depleted, chondritic, and slightly enriched elements and a group of moderately to highly enriched elements. Slightly depleted elements include Na, Sc, Sm, La, and Yb. Calcium abundances are chondritic and Lu abundances are slightly enriched relative to H-chondrite abundances. Moderately enriched elements are Fe, Ni, Eu, and Sb; and highly

enriched elements are Cr, Ir, Au, Co, and As. Cr abundances are approximately 4 times H-chondrite abundances and Ir is approximately 3 times. Au, Co, and As have roughly twice the abundance of H-chondrites.

DISCUSSION

Lodranites and Acapulcoites differ in modal mineralogy, average grain size, and bulk and trace element geochemistry, however, evidence suggests these two types of meteorites are fragments of the same parent body and are genetically linked to one another. Similar isotopic compositions suggest a common parent body (Clayton et al, 1992), and mineral compositions (McCoy et al, 1993), geochemistry of trace and bulk elements (Zipfel and Palme, 1993), and radiometric ages (Bogard et al, 1993) suggest a common and genetically linked ancestry.

The similarity of the chemistry of acapulcoites and H-chondrites lead Palme et al (1981) and Schultz et al (1982) to the conclusion that acapulcoites were originally chondrites that had subsequently been altered to acapulcoites by melting or partial melting. Recent studies by Zipfel and Palme (1993) and McCoy et al (1993, 1992) support an origin by modification of a chondritic parent body through a range of partial to complete melting or solid state recrystallization. McCoy et al (1993) also suggest that lodranites have undergone higher degrees of partial melting than acapulcoites, and that the higher degree of partial melting included physical loss of silicate, metal, and/or sulfide melts from the original rock. Loss of a silicate melt would be reflected by a decrease in the abundance of or loss of plagioclase from the original rock. The acapulcoites may have experienced lower degrees of partial melting and the metal/sulfide melts may not have physically migrated out of the original rock (McCoy et al,1993)

Geochemical data from acapulcoites ALHA 81187 and ALHA 81261 support a chondritic origin for these meteorites. The abundances of most of the major and trace elements examined are roughly chondritic in abundance. Lithophile element (Na, Ca, Eu, etc) abundances suggest little or no silicate melt extraction. Plots of H-chondrite normalized Sm/Sc versus Na/Sc and Sm/Sc versus La/Lu which should indicate silicate loss show no evidence of silicate melt extraction. Conclusions from the geochemical data are supported by the modal mineralogy. Plagioclase is abundant in ALHA 81261, and although no plagioclase was found in our sample of ALHA

81187, it has ben reported in other studies (McCoy et al, 1993). Plots of H-chondrite normalized Au/Co versus Ir/Ni and Se/Co versus Ir/Ni which are indicative of siderophile and chalcophile element behavior show an increase in Ir/Ni ratios and decreases in Se/Co ratios for acapulcoites. This data indicates a metal and/or sulfide melt may have been extracted from ALHA 81187 and ALHA 81261.

Geochemical and mineralogical data from LEW 88280 and MAC 88177 suggest that these lodranites experienced loss of partial melts. Plagioclase is absent in both of these meteorites indicating extraction of a silicate partial melt from the rocks. The low abundance of Na and Eu with respect to H-chondrite abundances also is indicative of plagioclase removal. MAC 88177 is also highly to moderately depleted in Fe, Ni, Co, Au, Ir, As, and Sb with respect to H-chondrites suggesting a metal and/or sulfide melt extraction. Fe, Co, Ni, Au, and As abundances are roughly chondritic in LEW 88280 which suggests silicate melt extraction but not metal/sulfide melt extraction. This does not seem likely as metals and sulfides should melt at lower temperatures than silicates. An alternative explanation is suggested by plots of H-chondrite normalized Se/Co versus Ir/Ni and Au/Co versus Ir/Ni plots. These plots show increased Se/Co ratios and Ir/Ni ratios with respect to H-chondrites. These ratios will increase if a metal/sulfide melt is added to a rock with an initial chondrite composition. Lodranites LEW 88280 and MAC 88177 may have undergone initial metal/sulfide melt extraction along with silicate melt extraction, subsequently, however, another metal/sulfide melt may have invaded the initially depleted rock.

Primitive achondrite EET 84302 is a texturally unique rock which has been called both a lodranite (McCoy et al, 1993) and an acapulcoite (Takeda et al, 1993). Our data indicate EET 84302 is a metal-rich acapulcoite which has experienced little or no silicate melt extraction. Relative to H-chondrites Na, Ca, Sc, Sm, La, Yb, and Lu are roughly chondritic and are close to the abundances of these elements in acapulcoites ALHA 81261 and ALHA 81187. Lodranites LEW 88280 and MAC 88177 are highly depleted in Na, La, and Sm with respect to H-chondrites. Europium is moderately enriched in EET 84302 but is highly depleted in the two studied lodranites. EET 84302 contains moderately to highly enriched abundances of Fe, Ni, Co, Au, Ir, Cr, As, and Sb with respect to H-chondrites and LEW 88280 and MAC 88177 contain depleted and highly depleted concentrations of most of these elements. EET 84302 plots with acapulcoites in lithophile, siderophile, and chalcophile elemental plots, and is clearly separated from lodranite data. The bulk and

trace element data of EET 84302 are more compatible with a alcapulcoite classification than a lodranite classification.

Mineralogy and textures also support an acapulcoite classification for EET 84302, rather than classification as an lodranite. Some textures are seemingly characteristic of lodranites. EET 84302 is coarser-grained than acapulcoites as are most lodranites, and cpx grains in EET 84302 contain opx exsolution lamellae like cpx grains in LEW 88280 and MAC 88177. However, more differences than similarities are present between EET 84302 and lodranites. EET 84302 contains abundant plagioclase, metal is extremely abundant, euhedral plagioclase inclusions are present in cpx, and opx grains are commonly full of metal and sulfide inclusions. Mineral compositions of olivine, opx, and cpx in EET 84302 are Mg-rich and are almost identical to acapulcoite mineral chemistries, whereas lodranites tend to have slightly more iron-rich olivine, opx, and cpx.

There are differences between EET 84302 and acapulcoites. EET 84302 is coarser grained, contains more metal, and contains more Cr-spinel than most acapulcoites. A possible explanation of these characteristics is that EET 84302 may be from a slightly deeper part of the acapulcoite parent body than average acapulcoites. The larger grain size may be a result of higher temperatures or slower cooling associated with a deeper stratigraphic position. Opx grains in EET 84302 contain higher concentrations of Al and Cr than opx grains in ALHA 81261 and ALHA 81187. Increased Al and Cr opx contents are generally suggested to indicate higher pressure and temperature conditions in terrestrial mantle peridotites and the same may be true for non-terrestrial rocks. The higher modal concentration of metal and Cr-spinel may also be a result of a deeper stratigraphic position. If the acapulcoite parent body is large enough to have developed a metal-rich core silicate rocks might have an increasing metal content with increasing depth.

CONCLUSIONS

EET 84302 is an acapulcoite, it contains approximately chondritic abundances of lithophile elements but enriched concentrations of siderophile and chalcophile elements. It contains larger grains, more metal, and more Cr-spinel than average acapulcoites, but these differences may be a result of a deeper stratigraphic position in the acapulcoite parent body. There is no geochemical or mineralogical evidence supporting silicate melt extraction from EET 84302.

Acapulcoites ALHA 81261 and ALHA 81187 are approximately H-chondritic in composition. Lithophile elements show no evidence that a silicate melt was removed from the acapulcoites. Siderophile and chalcophile elements show evidence that a metal/sulfide melt may have been removed from ALHA 81261 and ALHA 81187.

Lodranite lithophile elements suggest a silicate melt was removed from LEW 88280 and MAC 88177, which means lodranites are restites like mantle hazburgites on Earth. Low abundances of Fe, Ni, Co, Au, Ir, and As relative to H-chondrite abundances suggest a metal/sulfide melt may have been extracted from MAC 88177. There is no clear geochemical evidence to suggest metal/sulfide melt extraction from LEW 88280, however, the rock contains very little modal metal or sulfide. H-chondrite normalized Se/Co versus Ir/Ni plots indicate a metal/sulfide melt may have been added to lodranites LEW 88280 and MAC 88177 after initial silicate and metal/sulfide melt extraction.

REFERENCES

Bild, R.W., Wasson, J.T., 1976, The lodran meteorite and its relationship to the urelites. Mineralogical Magizine, v. 40, p. 721-735.

Bogard, D.D., Garrison, D.H., McCoy, T.J., Keil, K., 1993, ^{39}Ar-^{40}Ar ages of acapulcoites and lodranites: Evidence for early parent body heating. Abstracts of the 24th Lunar and Planetary Science Conference, p. 141-142.

McCoy, T.J., Keil, K., Clayton, R.N., Mayeda, T.K., 1993, Classificational parameters for acapulcoites and lodranites: The cases of FRO 90011, EET 84302 and ALH A81187/84190. Abstracts of the 24th Lunar and Planetary Science Conference, p. 945-946.

McCoy, T.J., Keil, K., Mayeda, T.K., Clayton, R.N., 1992, Monument draw and the formation of the acapulcoites. Abstracts of the 23rd Lunar and Planetary Science Conference, p. 871-872.

Schultz, L., Palme, H., Spettel, B., Weber, H.W., Wanke, H., Michel-Levy, M.C., Lorin, J.C., 1982, Allan Hills 77081-an unusual stony meteorite. Earth and Planetary Science Letters, v. 61, p. 23-31.

Takeda, H., Saiki, K., Otsuki, M., 1993, A new Antarctic meteorite with chromite, orthopyroxene and metal with reference to a formation model of S asteroids. Abstracts of the 24th Lunar and Planetary Science Conference, p. 1395-1396.

Wasson, J.T., Kallemeyn, G.T., 1988, Compositions of chondrites. Phil. Trans. R. Soc. Lond. A 325, p. 535-544.

Zipfel, J., Palme, H., 1993, Are acapulcoites and lodranites genetically related? Meteoritics, v28 #3, p.469.

N94-25359

LOADING, ELECTROMYOGRAPH, AND MOTION DURING EXERCISE

Final Report
NASA/ASEE Summer Faculty Fellowship Program-1993
Johnson Space Center

Prepared by:	Fernando Figueroa, Ph.D.
Academic Rank:	Assistant Professor
University & Department:	Tulane University Department of Mechanical Engineering
NASA/JSC	
Directorate:	Space and Life Sciences
Division:	Medical Sciences
Branch:	Space Biomedical Research Institute
JSC Colleague:	Linda C. Taggert, M.D.
Date Submitted:	July 12, 1993
Contract Number:	NGT-44-001-800

ABSTRACT

A system is being developed to gather kineto-dynamic data for a study to determine the load vectors applied to bone during exercise on equipment similar to that used in space. This information will quantify bone loading for exercise countermeasures development. Decreased muscle loading and external loading of bone during weightlessness results in cancellous bone loss of 1% per month in the lower extremities and 2% per month in the calcaneous. It is hypothesized that loading bone appropriately during exercise may prevent the bone loss. The system consists of an ergometer instrumented to provide position of the pedal (foot), pedaling forces on the foot (on the sagittal plane), and force on the seat. Accelerometers attached to the limbs will provide acceleration. These data will be used as input to an analytical model of the limb to determine forces on the bones and on groups of muscles. EMG signals from activity in the muscles will also be used in conjunction with the equations of mechanics of motion to be able to discern forces exerted by specific muscles. The tasks to be carried out include: design of various mechanical components to mount transducers, specification of mechanical components, specification of position transducers, development of a scheme to control the data acquisition instruments (TEAC recorder and optical encoder board), development of a dynamic model of the limbs in motion, and development of an overall scheme for data collection analysis and presentation. At the present time, all the hardware components of the system are operational, except for a computer board to gather position data from the pedals and crank. This board, however, may be put to use by anyone with background in computer based instrumentation. The software components are not all done. Software to transfer data recorded from the EMG measurements is operational, software to drive the optical encoders' card is mostly done. The equations to model the kinematics and dynamics of motion of the limbs have been developed, but they have not yet been implemented in software. Aside from the development of the hardware and software components of the system, the methodology to use accelerometers and encoders and the formulation of the appropriate equations are an important contribution to the area of biomechanics, particularly in space applications.

INTRODUCTION

The principal objective of the project in which the Faculty Fellow was involved was to be able to measure forces on the bones, and forces exerted by individual muscles, during ergometer exercise. This information is necessary to study the mechanism and to suggest solutions to the problem of bone loss experienced by astronauts in zero gravity conditions. In cancellous bone the rate of bone loss is significant even in short durations trips to space (1% per month in the lower extremities and 2% per month in the calcaneous).

The exercise machine to be used is an ergometer, since they are available in the space shuttles for use by the astronauts to maintain their physical integrity. Biomechanic studies of bicycling done by various researchers have been used as reference to define the variables to be measured and their ranges.

This report describes the system developed to measure the forces on bones and the forces exerted by groups of muscles in the lower extremities. The system consists of an ergometer instrumented with load cells in the pedals, angular position encoders in the crank and pedals, and accelerometers attached to the body sections.

SUMMARY OF THE METHODS

To determine forces, the acceleration of the center of mass of each member must be determined, as well as the location of the center of mass, the total mass, and the moment of inertia. The accelerations must be known for every position of the member as it traverses the path dictated by the exercise. The general approach will be to measure the acceleration vector of various points on the member (two points for planar motion) and calculate the acceleration of the center of gravity from these measurements. Newton's Law of motion will then provide equations relating forces and moments applied to the member. Some forces will be measured using load cells, which will allow the determination of forces exerted by groups of muscles and forces at the joints. Forces exerted by particular muscles will be latter separated using EMG signals and possibly other methods such as certain assumptions about the sharing of forces by different muscles, correlations, and minimization/maximization of cost functions.

To determine acceleration of the center of mass, the acceleration vector of two points (for motion on the sagittal plane) will be measured using miniature accelerometers. The acceleration vector will be expressed with respect to a coordinate system attached to the member. The orientation of this coordinate system will be determined using the acceleration of a known point in both coordinate systems (a base coordinate system,and the one attached to the member). The relative rotation of the two coordinate systems will be determined by the equations that relate the orthogonal components of the same acceleration vector expressed in the two coordinated systems rotated with respect to each other.

Using accelerometers on Earth requires that the component of the acceleration of gravity along the direction of the accelerometer axis be factored out[1]. This will be done by considering the hip joint fixed, thus forming a five bar linkage[2] (bicycle crank, foot, calf, thigh, and bicycle body).

Since the position of the leg/foot joint is measured using encoders on the crank and pedal, the position of the knee joint can be calculated. This method provides the orientation of the axes attached to each member with sufficient accuracy to perform gravity compensation on the accelerometers.

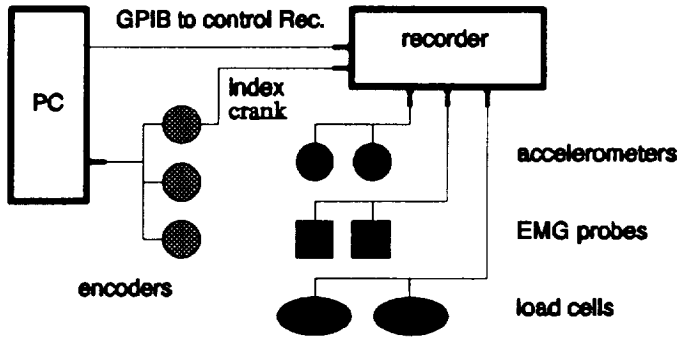

Figure 1 Hardware connections during the experiment

Forces on each member will be determined using Newton's Second Law. Forces on the foot will be measured using a pedal instrumented with load cells. Three equations of motion of the foot will allow determination of three unknowns that may be a force with known direction at the joint, and forces or moments by two other groups of muscles. A similar approach will be used to determine forces at the other joints and forces applied by groups of muscles. Assumptions regarding sharing of force by the various muscles in one group will be used to further identify the force on specific muscles. Further, minimization/maximization of cost functions and EMG signals will be used to identify forces on particular muscles [2,3,4].

Body segment dimensions and mass properties will be determined from X-ray and densitometer image analysis.

DESCRIPTION OF THE HARDWARE

The hardware includes and ergometer, a 28 channel recorder[5], three rotary optical encoders[6], accelerometers[7], load cells[8], 486 class personal computer fitted with three cards, (1) a GPIB interface card to control the recorder[9], (2) a four channel decoder card to read the encoder information[10], and (3) a 32 channel A/D board to digitize data from the recorder. During an exercise

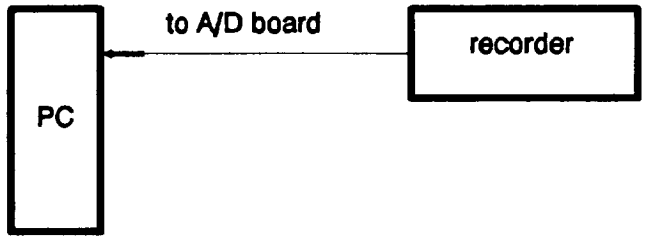

Figure 2 Hardware connections to digitize recorder data prior to their use in the kineto-dynamic formulations.

experiment, data from the accelerometers and EMG probes is recorded in the recorder while position information is digitized using the encoder card. To synchronize the two sets of data, an index pulse generated by the crank encoder in every revolution is also recorded. When the experiment is done, the data is digitized using the A/D board and is synchronized with the data from the encoders before it can be used in the motion equations.

The ergometer was modified slightly so that an encoder could be installed at the crank, and one encoder in each pedal axis. The pedals are fitted with fixtures to hold the load cells that measure force in the sagittal plane. The pedal fixtures were designed by JSC Colleague, Dr. Taggart.

KINEMATIC ANALYSIS

This section describes the methods to determine the acceleration of the center of gravity and the angular velocity and angular acceleration of a section. These variables are needed in the dynamic equations to determine the forces on the section.

Figure 3 shows a schematic of the elements encompassing the system. Five coordinate frames are defined, one inertial frame attached to the ergometer structure at the crank joint ($x_0y_0z_0$), and the others attached to the crank ($x_1y_1z_1$), the pedal and foot ($x_2y_2z_2$), the calf ($x_3y_3z_3$), and the thigh ($x_4y_4z_4$). The frames were defined borrowing a methodology from the area of robotics, according to the Denavit-Hartenberg rules[11]. This notation will help simplify the formulation of the equations and their implementation in MatLab programming environment.

The kinematic equations needed are those that describe plane motion with rotating and translating frames of reference. In Figure 3, the acceleration of a point such as the center of gravity of the calf, knowing the acceleration of the origin of frame $x_3y_3z_3$ is defined by the following equation.

$$a_{g3} = a_{03} + \alpha_3 \times r_{g3} + \omega_3 \times (\omega_3 \times r_{g3}) \qquad (1)$$

where ω_3 is the angular velocity of the section, α_3 is the angular acceleration, and a_{03} is the acceleration of the origin of the coordinate system attached to the calf. Equation (1) may be used to determine the accelerations of the origin of Frame 1, knowing that the acceleration of frame 0 is zero, and that the angular velocity and acceleration of the crank are provided by the crank encoder. Subsequently, the acceleration of the foot/pedal-attachment section (Frame 2) may be calculated using the previously calculated acceleration of the origin of Frame 1, and the angular acceleration and angular velocity of Frame 2 with respect to Frame 1 (pedal encoder). The angular acceleration of Frame 2 is given by the sum of the angular accelerations inferred from the crank and pedal encoders, and the angular velocity of Frame 2 is given by the sum of the angular velocities inferred from the crank and pedal encoders. The specific equations are as follows:

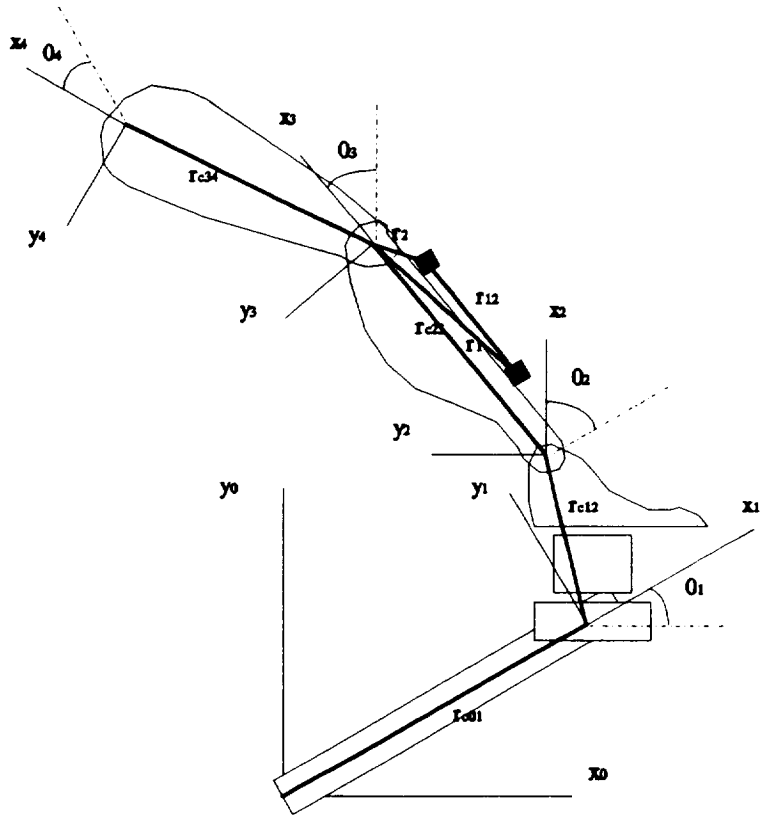

$$\ddot{r}_{c01} = \omega_1 \, x \, (\omega_1 \, x \, r_{c01}) + \alpha_1 \, x \, r_{c01} \tag{2}$$

where ω_1 is the angular velocity, and α_1 is the angular acceleration measured by the crank encoder.

$$\ddot{r}_{c02} = \ddot{r}_{c01} + \omega_2 \, x \, (\omega_2 \, x \, r_{c12}) + \alpha_2 \, x \, r_{c12} \tag{3}$$

where ω_2 is the sum of the angular velocities of the crank and pedal encoders, and α_2 is the sum of the angular velocities measured by the crank and pedal encoders.

At this point, the acceleration of the foot joint has been determined. Next, the angular acceleration and velocity of the calf (Frame 3) will be determined using measurements from the accelerometers. Note that all the accelerometers measure acceleration expressed in Frame 3, but the accelerations are absolute. Therefore, the following formulas will have all the vectors involved expressed in Frame 3 directions. Figure 4 shows the placement of the accelerometers on the calf. Each accelerometer measures acceleration in the x_3 and y_3 directions.

$$\ddot{x}_2 = \ddot{x}_1 + \omega_3 \times (\omega_3 \times r_{12}) + \alpha_3 \times r_{12} \tag{4}$$

where the angular acceleration and velocity vectors are the unknowns. Using the components of the accelerations measured by the accelerometers, the accelerations at the point of placement of the accelerometers can be expressed as follows.

$$\begin{aligned} \ddot{x}_1 &= (a_{x1}, a_{y1}) \\ \ddot{x}_2 &= (a_{y1}, a_{y2}) \\ r_{12} &= (r_x, r_y, r_z) \end{aligned} \tag{5}$$

Expanding the cross products in Equation (4),

$$a_{x2} = a_{x1} + \alpha_y r_z - \alpha_z r_y + \omega_x \omega_y r_y + \omega_z \omega_x r_z - r_x(\omega_y^2 + \omega_z^2) \tag{6}$$

$$a_{y2} = a_{y1} + \alpha_z r_x - \alpha_x r_z + \omega_z \omega_y r_z + \omega_x \omega_y r_x - r_y(\omega_x^2 + \omega_z^2) \tag{7}$$

$$a_{z2} = a_{z1} + \alpha_x r_y - \alpha_y r_x + \omega_x \omega_z r_x + \omega_y \omega_z r_y - r_z(\omega_x^2 + \omega_y^2) \tag{8}$$

For the case of plane motion, the following assumptions are valid: r_z≈0 (acceleration is about an axis perpendicular to the vector joining the accelerometers throughout the entire motion), $\omega_x \approx 0$, and $\omega_y \approx 0$ (no twist or yaw). Applying these assumptions the above equations can be simplified further.

$$\begin{aligned} r_y \alpha_z + r_x \omega_z^2 &= a_{x1} - a_{x2} \\ r_x \alpha_z - r_y \omega_z^2 &= a_{y2} - a_{y1} \end{aligned} \tag{9}$$

System of equations (9) may be solved for the angular accelerations and velocities of the calf section.

Since the acceleration of the foot joint is known, the acceleration of the origin of Frame 3 can be calculated using an expression similar to equation (3), where the angular acceleration and velocity are those determined from equation (9). Also, the same procedure followed to determine the angular acceleration and velocity of Frame 3 may be used to determine these variables for Frame 4. For this, two accelerometers are fixed to the thigh section which can measure acceleration along the directions of the coordinate Frame 4. Once the angular variables are obtained, using the known acceleration of the origin of Frame 3, one may calculate the

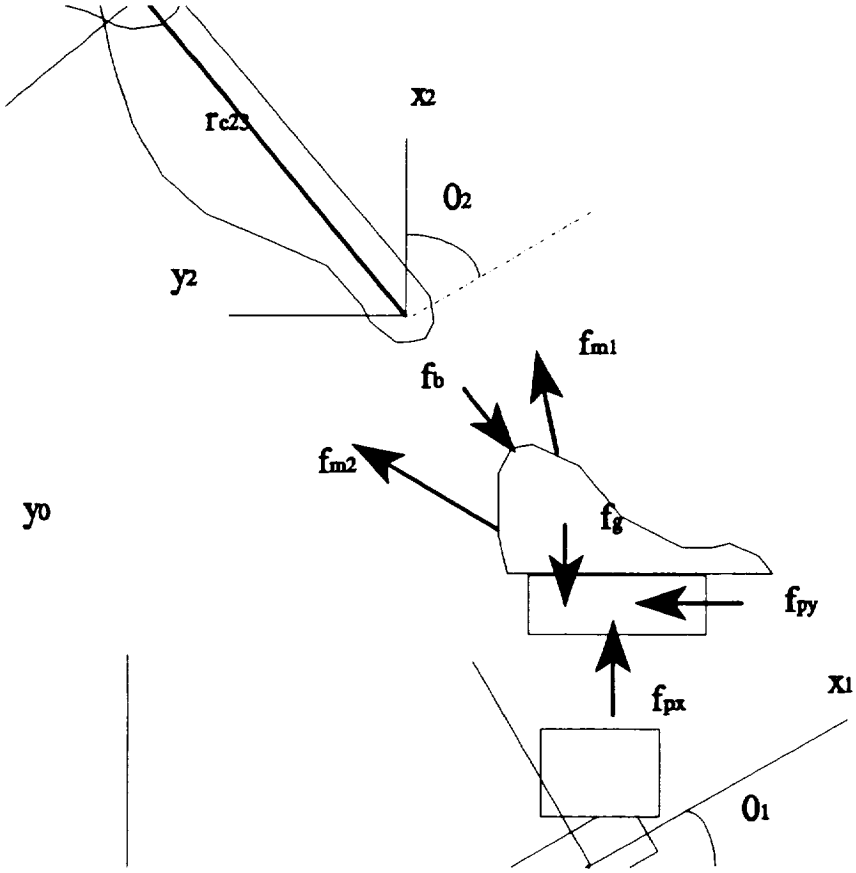

Figure 5 Free body diagram for the determination of forces on the foot/pedal section.

acceleration of the origin of Frame 4.

Finally, knowing the accelerations of all the frame origins, the acceleration of the center of gravity may be calculated using an expression similar to equation (1).

Acceleration Compensation

Accelerometers measure 1-g when oriented in the vertical direction, even when the body where they are fixed is not moving. Therefore, it is necessary to eliminate this bias prior to using the accelerometer data in the kinematic equations. All that is needed is the orientation of each frame at the moment the acceleration is measured. This information may be obtained if one can assume that the hip joint does not move. If this is the case, the frame of the exercise machine , the crank, the foot/pedal, the calf, and the thigh, define a five-bar linkage mechanism.

Knowing the position of the calf-foot/pedal joint (origin of Frame 2), and the distances from the foot/calf joint to the knee joint (r_{23}), and from the knee joint to the hip joint (r_{34}), one can write two equations to determine the angular position of Frames 3 and 4. Let $\mathbf{r}_{02}$ be the vector from

the origin of Frame 0 to the origin of Frame 2, $\mathbf{r}_{23}$ the vector from the origin of Frame 2 to the origin of Frame 3, $\mathbf{r}_{34}$ the vector from the origin of Frame 3 to the origin of Frame 4, and $\mathbf{r}_{04}$ the vector from the origin of Frame 0 to the origin of Frame 4. The following expression relates these vectors.

$$r_{23}+r_{34}=r_{04}-r_{02} \tag{10}$$

Vector equation (10) implies two scalar equations. The vectors on the left hand side may be expressed as $\mathbf{r}_{23}= r_{23}(\cos\theta_3, \sin\theta_3)$ and $\mathbf{r}_{34}=r_{34}(\cos\theta_4, \sin\theta_4)$. Therefore, equation (10) may be solved for the two unknown direction vectors that provide the desired orientations.

DYNAMIC ANALYSIS

Once the accelerations of the center of gravity of each section has been determined, one can apply the equation of motion to each section to determine the forces and torques being borne. Figure 5 shows the free-body diagram corresponding to the foot/pedal section. The equation of motion for this section is given by

$$\begin{aligned} f_p+f_m+f_b+f_g&=ma_g \\ f_pd_p+f_md_m+f_bd_b&=I\alpha_3 \end{aligned} \tag{11}$$

where d_p, d_m, and d_b are the radii of gyration of the corresponding forces.

CONCLUSIONS AND RECOMMENDATIONS

A system to measure forces on bone and forces exerted by muscles during exercise using an ergometer bicycle has been designed and is almost fully implemented. Non-invasive instrumentation and methods have been developed, although further work is necessary to implement software to carry out some of the data collection, and all of the data analysis. The hardware components are compact and do not require much space, in fact, they may be easily adapted for use with the ergometer currently operating in the Space Shuttle. The methods for determination of the forces use data measured by an encoder at the crank, an encoder at the pedal, load cells at the pedal, and accelerometers fixed to the moving section of interest.

Currently the equations apply only to two dimensional motion, but may be easily extended to three dimensions by increasing the number of accelerometers used. Also, complementary methods to determine the force exerted by individual muscles need to be investigated. Some of these methods are mentioned in the introduction.

Further work is needed to describe with adequate precision the motion and forces on the muscles and bones in all the sections of the body during exercise. By making measurements on the same exercise on Earth and on Space, one may determine which exercises are suitable to maintain the astronauts health integrity, as well as synthesize new forms of exercise.

REFERENCES

1. Lawther, A. and Griffin, M. J., "Measurement of ship motion," Human Factors Research Unit, Institute of Sound and Vibration Research, Southhampton University, Southhampton S09 5NH, England.

2. Redfield, R. and Hull, M. L., "Prediction of pedal forces in bicycling using optimization methods," Biomechanics, Vol. 19, No. 7, pp. 523-540, 1986.

3. Harrison R. N., Lees A., and McCullagh P. J. J., "A bioengineering analysis of human muscle and joint forces in the lower limbs during running," Journal of Sports Sciences, Vol. 4, pp. 201-218, 1986.

4. Seireg, A. and Arvikar, R.J., "A mathematical model for evaluation of forces in lower extremities of the musculo-skeletal system," Biomechanics, Vol. 6, 1973, pp. 313-326.

5. 28 channel recorder, TEAC model XR-9000, TEAC America, Inc., Montebello, CA, USA.

6. Rotary optical incremental encoders models:..

7. Accelerometers Model EGAXT-10, Entran Devices, Inc., Fairfield, NJ, USA.

8. Load cells Model ELF-TC1000-250, Entran Devices, Inc., Fairfield, NJ, USA.

9. General purpose interface board Model AT-GPIB, National Instruments Corporation, Austin, TX, USA.

10. Decoder board Model 5312-4, Technology80, Inc., Minneapolis, MN, USA.

11. Spong, M. W. and Vidyasagar, M., *Robot Dynamics and Control*, John Wiley & Sons, Inc., New York, 1989, pp. 65-91.

LOADING, ELECTROMYOGRAPH, AND MOTION DURING EXERCISE

Final Report
NASA/ASEE Summer Faculty Fellowship Program -- 1993
Johnson Space Center

Prepared by:	Fernando Figueroa, Ph.D.
Academic Rank:	Assistant Professor
University & Department:	Tulane University Department of Mechanical Engineering
NASA/JSC	
Directorate:	Space and Life Sciences
Division:	Medical Sciences
Branch:	Space Biomedical Research Institute
JSC Colleague:	Linda C. Taggart, M.D.
Date Submitted:	July 12, 1993
Contract Number:	NGT-44-001-800

Approved By: Linda C Taggart

Date Approved: 13 July 93

N94- 25360

FAILURE DETECTION AND RECOVERY IN THE ASSEMBLY/CONTINGENCY SUBSYSTEM

Final Report

NASA/ASEE Summer Faculty Fellowship Program -- 1993

Johnson Space Center

Prepared by:	Rex E. Gantenbein, Ph.D.
Academic Rank:	Associate Professor
University & Department:	University of Wyoming Department of Computer Science Laramie, Wyoming 82071-3682
NASA/JSC	
Directorate:	Engineering
Division:	Tracking and Communications
Branch:	Systems Engineering
JSC Colleagues:	Sally D. Stokes David A. Overland
Date Submitted:	6 August 1993
Contract Number:	NGT-44-001-800

ABSTRACT

The Assembly/Contingency Subsystem (ACS) is the primary communications link on board the Space Station. Any failure in a component of this system or in the external devices through which it communicates with ground-based systems will isolate the Station. The ACS software design includes a Failure Management capability (ACFM) that provides protocols for failure detection, isolation, and recovery (FDIR).

The author reviews the ACFM design requirements as outlined in the current ACS software requirements specification document. The activities carried out in this review include:

(1) An informal, but thorough, end-to-end failure mode and effects analysis of the proposed software architecture for the ACFM; and

(2) A prototype of the ACFM software, implemented as a C program under the UNIX operating system.

The purpose of this review is to evaluate the FDIR protocols specified in the ACS design and the specifications themselves in light of their use in implementing the ACFM.

The basis of failure detection in the ACFM is the loss of signal between the ground and the Station, which (under the appropriate circumstances) will initiate recovery to restore communications. This recovery involves the reconfiguration of the ACS to either a backup set of components or to a degraded communications mode. The initiation of recovery depends largely on the criticality of the failure mode, which is defined by tables in the ACFM and can be modified to provide a measure of flexibility in recovery procedures.

The failure modes defined for the ACFM are grouped into three major categories:

- pointing vector failures, which indicate a problem in the positioning of the steerable antennae used for high data rate communications;
- hardware failures, which result from internal problems with ACS components; and
- extended losses of command link, which occurs when the ACFM detects a loss of signal but either is unable to isolate the source of the problem or cannot successfully recover communications due to multiple failures.

Other events are also detected by the ACFM, but do not immediately initiate recovery unless coupled with a detected loss of signal or a critical failure mode.

A prototype of the ACFM FDIR protocols, implemented as a set of modules corresponding to the subcapabilities of the ACFM specified by the requirements document, has been constructed and tested to branch coverage using fault injection techniques to demonstrate the behavior specified by the existing requirements document. This document, which is still in draft stage, is missing a number of descriptions relating to events identified in the fault mode and effects analysis. Furthermore, the existing descriptions are often inconsistent or incomplete in their specification of the expected behavior of the ACFM in response to events that can occur in the ACS. These problems need to be resolved before the document can be relied upon for construction of the actual system.

INTRODUCTION

The Assembly/Contingency Subsystem (ACS) is the primary communications link for the Space Station. It provides two-way audio and core data communications and supports ground-based tracking of the Station. The ACS is composed of two encapsulated *strings* of components. The primary components, or Orbital Replacement Units (ORUs), of each string, as shown in Figure 1, are:

- the ACS baseband signal processor (ACBSP), which provides the interface between the ACS and other onboard computer and audio subsystems,
- the ACS transponder (XPDR), which converts ACS information between analog radio frequency (RF) and digital form, and
- the ACS radio frequency group (ACRFG), which provides for transmission and reception of S-band signals between the Station and the ground via the Tracking and Data Relay Satellite System (TDRSS). This group consists of a high-gain and a low-gain antenna and the amplifiers for these antennae.

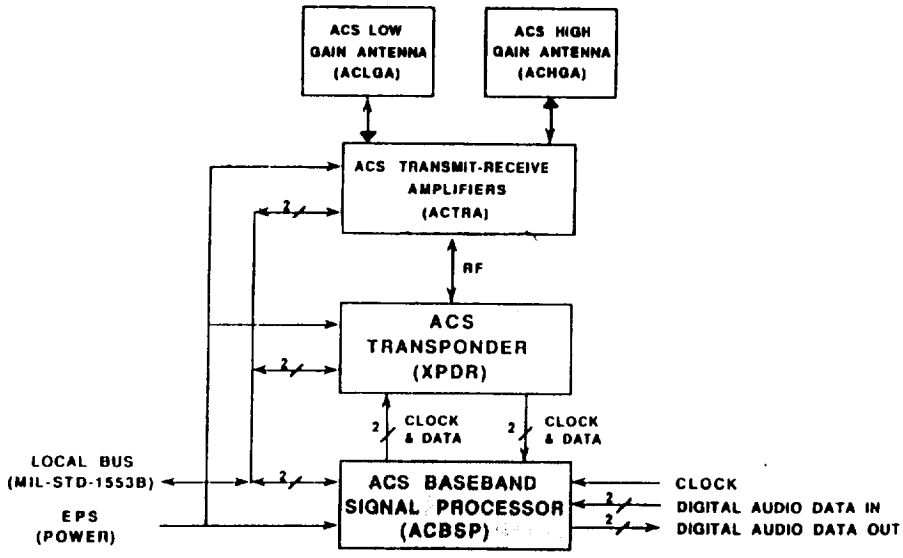

Figure 1.- Block Diagram of the Assembly/Contingency Subsystem (ACS).

Failure in any of the ORUs, or in the external units that provide the connections to both the ground and to other subsystems onboard the Station, have the potential to interrupt the link between the Station and the ground, effectively isolating the Station until such time as the linkage can be restored.

The absence of communications, even for extended periods, is under some conditions an inconvenience, while in other cases, such as extra-vehicular activity, it may be life-threatening. In any event, it is clear that some facility must exist to accomplish failure detection, isolation, and recovery (FDIR) in this subsystem, so that permanent communications loss can be avoided. Furthermore, during the early unmanned stages of the Station's deployment, all control will be initiated from the ground, making it difficult to repair any problems on board without

communications. Even in the manned operational phase, facilities for manual diagnosis and repair of the ACS will be limited, placing continued importance on the system's ability to detect and recover from failures autonomously.

For these reasons, among others, the ACS design includes a Failure Management subsystem (ACFM) for detecting the loss of communications capabilities in the ACS and providing mechanisms by which communications can be restored in the event of failure. The software requirements of this component are described in section 3.2.3.3.2.2 of the ACS Flight System Software Requirements (FSSR) [1]; those requirements state that the ACFM collects equipment status and performance data, and performs failure management functions including equipment and string isolation and redundancy management.

The ACFM itself is composed of three constituent capabilities (also called subcapabilities). Each of these subcapabilities provides a distinct set of services supporting FDIR in the ACS.

- ACFM External Control (ACFXC) is responsible for accepting failure indications from sources external to ACFM and establishes the monitoring mode for failure detection and isolation, determining the behavior of the ACFM in response to detected failures.
- ACFM Failure Detection and Isolation (ACFFDI) collects the raw equipment sensor data and status, and analyzes it to detect and isolate equipment faults within the ACS.
- ACFM Failure Recovery (ACFFR) is responsible for managing the redundant ACS resources at the string level for recovery from a detected failure.

Information used by the ACFM may be generated internally or input from external sources. There are two external sources of information, which may also be updated by the ACFM:

- the Run-Time Object Database (RODB), which maintains system management information from the Station subsystems in a common area and is the primary interface with the Tier 1 system, which provides Station capabilities such as the onboard system executive, the crew interface, and the Station control center, and establishes the operating environment for the ACS; and
- the ACS data base, which maintains ACS information that is not needed outside the ACS.

Additionally, the ACFM may exchange information with the ACS Services Management (ACSS) subsystem, the second subsystem in the ACS, both directly and through the RODB and ACS data base. The relationship among the three subcapabilities of the ACFM and the inputs and outputs for each are shown in Figure 2.

During his 1993 NASA/ASEE Summer Faculty Fellowship at the Johnson Space Center, the author carried out a review of the current design of the ACFM as specified in the FSSR. The purpose of the review was twofold: to evaluate the FDIR protocols proposed for the ACS and to evaluate the FSSR's specification of the ACFM subsystem design.

FAILURE MODE AND EFFECTS ANALYSIS

For review of the FDIR capability of the ACS, an informal Failure Modes and Effects Analysis (FMEA) was initiated on the ACFM design as specified in the FSSR and augmented by conversations with Kent Gaylor of LinCom Corporation. The goal of this work was to analyze the ACFM design on a functional basis, describing and documenting the FDIR system and identifying the expected *failure modes* (the ways in which failures can occur).

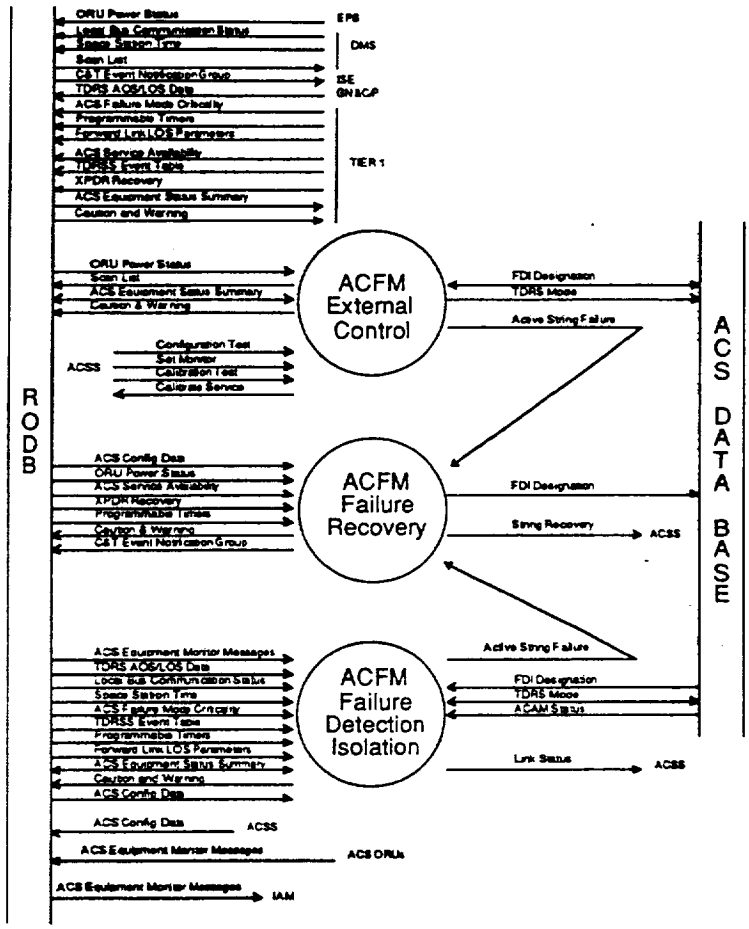

Figure 2.- Subcapabilities of the ACS Failure Management (ACFM) Component.

Failure and Recovery in the ACFM

A number of events have been identified as failure modes for the ACS. These events fall into three major categories, which correspond to the recovery strategies incorporated in the ACFM:

- pointing vectors failures,
- hardware failures, and
- extended loss of command link.

The overall *modus operandi* of the ACFM can be characterized as "if it ain't broke, don't fix it." Even if external or component faults have occurred and are detected in the system, no failure is declared as long as commands are successfully being transmitted and processed on the Station. The reasoning behind this approach is that it is preferable to have communications (even if failures exist within the system) than to attempt recovery that might not succeed. This approach also handles the problem of incorrect sensors triggering an unnecessary recovery.

Loss of signal

An interruption in the information flow between the Station and ground support is termed loss of signal (LOS). Both the forward (ground to Station) and reverse (Station to ground) communications links pass through the Tracking and Data Relay Satellite System (TDRSS). This system consists of two geostationary satellites, TDRS-E(ast) and TDRS-W(est). As shown in Figure 3, the Station passes from the range of one TDRS to the other as it orbits the Earth. Once in each orbit, the interposition of the Earth between the Station and the TDRS satellites, which causes the Station to experience LOS, defines a zone of exclusion (ZOE). Upon emergence from the ZOE, the Station attempts acquisition of the signal (AOS) to reestablish communications.

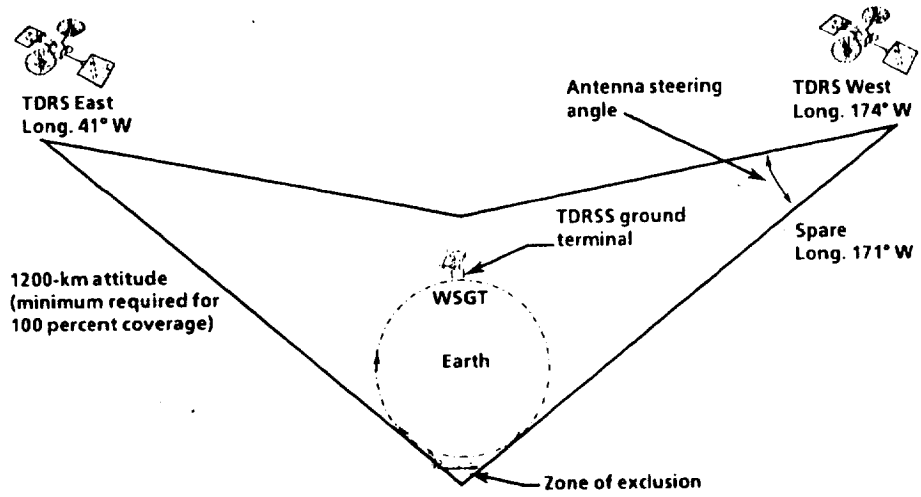

Figure 3.- The Tracking and Data Relay Satellite System (TDRSS).

LOS is detected in the ACFFDI through examination of the TDRS mode and the demultiplexer state, which determines the quality of the forward link. If the TDRS mode is "SEARCH" and the demux state shows "Degraded Frames" continuously for a specified TDRS Search Time, or if the TDRS mode is "ACQUIRED" and the demux state shows "Degraded Frames" continuously for the LOS Declaration Time, then LOS is declared by the ACFFDI. LOS caused by the Station's passing through the ZOE or by other, scheduled competition for use of the TDRSS is not considered a failure in the ACFM. However, LOS in the forward link that is *unscheduled* may result in ACFM declaring a communications failure. A failure may also be declared if the Station is unable to achieve AOS when emerging from the ZOE or passing from the range of one TDRS to the other.

To determine if a detected LOS is scheduled, the ACFM checks the internal TDRS event table, which lists the times when the Station is expected to be in (or near) the LOS period. An uncertainty time is applied to the event times for entering and leaving the period. If no event is found that indicates that the LOS is scheduled, then ACFM declares the LOS to be unscheduled.

The ACFM must also consider the situation in which no event schedule is available. Since the Station will be in long-term orbit, the TDRS event table must be regularly updated.

If such an update fails due to error or inability to communicate with the Station, the events in the table could become outdated in time. Should this occur, the ACFM will use AOS/LOS data in the RODB to see if one of the TDRS satellites is actually in view. This data can be manually confirmed if necessary. If LOS occurs when the event table is exhausted, the ACFM will attempt to determine whether a TDRS is in view. If the AOS/LOS data shows that a TDRS is in view, then such LOS is declared to be unscheduled.

Initiating recovery

The detection of an unscheduled LOS initiates additional effort in the ACFM to isolate the cause of the LOS and to recover communications. The conditions that lead to declaration of failure are described in the following sections. Recovery in the ACS is achieved by switching from one string of ORUs to another. These strings are functionally identical, but receive and transmit on slightly different frequencies to avoid interference. For this reason, the ACFM must keep track of which of the two strings is the *current* or operating string and which is the backup or *alternate* string.

Recovery from communications loss can take place at two levels. At the string level, operations are switched from the current string to the alternate; if successful, the current and alternate indicators are switched so that the current string becomes the backup and vice versa. Recovery may also take place at the data rate level. If external or internal failures make it impossible to use the High Data Rate (HDR) communications facility (which depends on the steerable high-gain antenna) on either the current or alternate string, another configuration, which uses the omnidirectional low-gain antenna, can provide a Low Data Rate (LDR) link.

In order to avoid spurious recovery and unneeded reconfiguration, as well as to provide some flexibility in the recovery actions, all ORU component events in the system have an associated *criticality*. Only an event identified as "CRITICAL" will initiate recovery. The default criticality values for the events in each ORU are defined in the FSSR. This status is maintained through a criticality table in the RODB. This table (which can be modified from the ground) determines whether a failure in a given component will initiate recovery or simply be noted. In the following descriptions of the failure modes, criticality will be mentioned where it affects the behavior of the ACFM.

Pointing Vectors Failure Mode

Once an unscheduled LOS has been declared, the ACFM will attempt to isolate the source of the problem that has caused the failure. One possible problem is that the Guidance, Navigation, and Control / Propulsion (GNC/P) subsystem is unable to correctly position the steerable antenna with respect to the TDRSS. This condition is detected in the ACFM by an unscheduled LOS and the ACS High-Gain Antenna Management (ACAM) subcapability of the ACSS indicating that the ACAM mode is "POINTING" (i.e., using the steerable, high-gain antenna) but ACAM pointing data is not available (this condition is derived by ACAM from AOS/LOS data in the RODB). Under these circumstances, the ACFM will declare an active string failure in the pointing vectors mode. Recovery from this error will be attempted, as described above.

Hardware Failure Modes

Failures due to faults within components of the ACS are broadly categorized as *hardware* failures. Several combinations of faults can result in a failure of this kind. All active string

failures in this mode will initiate an attempt by the ACFM to isolate the failure and recover communication.

Antenna faults

One form of hardware failure occurs when an unscheduled LOS is declared, the ACAM status shows the ACAM position as "NOGO" but the ACAM pointing data as available, and the ACS configuration data in the RODB (which defines the current configuration of the ACS) shows the high-gain antenna in use. This indicates a failure in the high-gain antenna's physical positioning by the ACSS. If the criticality table for the ACRFG component of the active string shows the antenna positioning as a critical event, then an active string failure in hardware mode is declared.

ORU faults

An ORU in the active string may also fail, interrupting the flow of information through the string. The status of the individual units is maintained by the RODB in the ACS Equipment Status Summary. If an unscheduled LOS has occurred, the ACAM pointing data is available, and the ACAM position indicator in the ACAM status is "GO" (meaning that the high-gain antenna is not experiencing problems), then a "NOGO" indicator for any event in the ACBSP, XPDR, or ACRFG on the active string, when matched with a "CRITICAL" entry in the criticality table for that event, will result in an active string failure in hardware mode.

Other hardware faults

Several other circumstances result in the ACFM declaring an active string failure in hardware mode. These are:

- a "NOGO" in a ACRFG BIT summary monitor message from the RODB for either the forward or reverse power indicator, when the indicated ACRFG is in the active string, the SSPA mute is disabled, and the corresponding entry in the ACRFG criticality table is "CRITICAL;"
- a notification from the Electrical Power Subsystem (EPS) through the RODB that an ORU in the active string has been powered off; or
- the ACBSP function status monitor message indicates the multiplexer output is inactive for the ACBSP in the active string, and the corresponding entry in the criticality table is "CRITICAL."

Under each of these three conditions, an active string failure in hardware mode is issued, regardless of whether an unscheduled LOS has been detected.

Extended Loss of Command Link

Under some circumstances, such as malfunction in the transmission system or corruption of transmitted data, it is possible for information to be received by the Station that does not correspond to any known command. Occasional occurrences of this type are not a major problem, since the command can be retransmitted once it is known on the ground that the Station did not respond. However, it is essentially impossible for the ACS to differentiate between corrupt and uncorrupt data, so the ACS may not detect LOS when, in fact, no usable information is being received. This can cause a long-term interruption of information or commands transmitted through the forward link.

To avoid this problem, the Integrated Station Executive (ISE), the software that performs the centralized coordination of the various command and control subsystems on the Station,

includes an "egg timer" that is periodically reset by telecommand. If this timer expires (that is, it is not reset within its expected period), it indicates that the system has experienced extended loss of command link (ELOC). In response, a preset sequence of recovery actions, designed to discover if any path exists through the ACS that will support communications, is initiated. If such a path exists, then communications can be restored.

Obviously, this mechanism would also be invoked if a failure occurs that cannot be diagnosed or recovered by the ACFM, resulting in total loss of communications. Conditions in which ELOC is known to occur due to the inability of the ACFM to respond to a detected failure are:

- an active string failure in pointing vector mode has occurred, but the LDR service on the current (active) string is not available, and an attempt to cycle power to the alternate string fails;
- an active string failure in pointing vector mode has occurred, but neither the current nor the alternate string LDR services are available;
- an active string failure in hardware mode has occurred, but the alternate string is not available and an attempt to cycle power to the current string also fails;
- an active string failure in hardware mode has occurred and the alternate string is indicated to be available, but an attempt to cycle power to the alternate string fails;
- an unscheduled LOS has occurred either while ACAM pointing data is available and either the ACAM status indicates that the ACAM capability of the ACSS is available, or LDR is in use, but no indicator of a critical failure in a component of any ORU exists; and
- an unscheduled LOS has occurred while ACAM pointing data is available, HDR is in use, and the ACAM status indicates that the ACAM position is "NOGO" but the ACAM pointing field is not defined as a critical failure mode by the criticality table.

Under these conditions, the Station will be unable to receive information through ACS until such time as the ELOC recovery procedure is carried out and communications restored.

Other Detected (Non-failure) Events

A number of other events are detected in the ACFM, but these are not immediately declared as failures. In general, they issue warning messages and set flags that, should an unscheduled LOS occur, may be used to isolate the cause and initiate an appropriate recovery action.

Asynchronous ORU events

Asynchronous events in the ACS ORUs involve changes in the ORU. These events, and the ORUs in which they can occur, are:

- BIT Go (ACBSP, XPDR, ACRFG),
- BIT NoGo (ACBSP, XPDR, ACRFG),
- Invalid Command (ACBSP, XPDR, ACRFG),
- Multiplexer Data Lost (ACBSP),
- Demultiplexer Data Lost (ACBSP),
- Pointing Function Status Change (ACRFG), and

- Low-Gain Antenna Switch Request (ACRFG).

As indicated, three of these events can occur in any ORU type. A BIT Go event (which is actually defined for a number of events in each capability) is signaled when a component of the ORU completes either its Power On Self Test (POST) or an Equipment Self Test (EST) or when the Go/NoGo flag in the BIT summary toggles from NoGo to Go. The ACS must report this as a BIT Go asynchronous event and update the appropriate Go/NoGo flags in the BIT summary, update the transmit vector word in the ACS Equipment Monitor, and set a service request bit in the 1553B (bus) status word. Similarly, a BIT NoGo event is reported if the POST or EST complete with failure or if the Go/NoGo flag in the BIT summary toggles from Go to NoGo. Again, the flags in the BIT summary and the 1553B status word are set. An Invalid Command event occurs when the ORU receives a message on the local bus that it doesn't recognize. This event is reported by updating the transmit vector word in the ACS Equipment Monitor and setting the service request bit in the 1553B Status Word (the message itself is discarded).

Two asynchronous ORU events affect only the ACBSP. A Multiplexer Data Lost event occurs when the length of a return link packet received does not match the length contained in the packet header. In this situation, the packet is discarded and the transmit vector word and service request bit are both set as above. A Demultiplexer Data Lost event occurs when data is not being removed from the forward link buffer fast enough to prevent the buffer from overflowing. In response to this event, ACFM again sets the transmit vector word and the service request bit.

Two other asynchronous events are unique to the ACRFG ORUs. A Pointing Function Status Change event occurs when the state of either the beta or alpha gimbals' stop sensors change (indicating that the antenna has passed a software-preset limit). In addition to updating the transmit vector word and setting the service request bit, this event also updates the ACRFG function status monitor message. A Low-Gain Antenna Switch Request event occurs after the ACRFG stops receiving pointing data for the high-gain antenna. Sixteen seconds after such loss, the ACRFG will start a linear extrapolation algorithm based on the last pointing commands. At some later time, if no pointing data has been received, the switch request event occurs; the ACFM reports this by updating the ACRFG function status monitor and the transmit vector word and setting the service request bit.

Internal ORU reset

Occasionally, the ORUs may internally detect a problem and reset themselves. This is done through an internal watchdog timer in the ORU firmware that is periodically reset, approximately every 100 milliseconds. The ACRFG signals this event by toggling the Go/NoGo bit in the ACRFG BIT summary monitor. The XPDR indicates it by the Processor Reset parameter located in the XPDR function status monitor. The ACBSP reports the event through the ACBSP throughput data monitor's ECM Reset since Last Report parameter. In the current ACS design, these events cannot be detected directly; however, if an unscheduled LOS occurred in a critical ORU because of such an event, then a string failure would be declared and recovery initiated. However, this means that some ORU resets may not be detected.

EVALUATION OF THE FDIR DESIGN THROUGH PROTOTYPING

To review the FDIR protocols and their description in the FSSR, the author implemented a prototype of the ACFM design for detecting and recovering from forward link communications failures. This program was written in C and implemented on a SUN workstation running

UNIX in the Control and Monitoring Systems Development Laboratory in Building 44. This section of the report briefly describes the components of the prototype and its implementation and testing.

Components of the Prototype

The prototype was constructed with modularity and testing in mind, using an object-based approach in which the functionality of each of the subcapabilities was encapsulated as a set of source modules corresponding to that subcapability. The interfaces between the modules modeled the ACS data base and the RODB, and all interaction among the subcapabilities used data in those two interfaces. Since the interfaces were designed first, the subcapability designs could be carried out independently.

Each module in the prototype contains code to handle the various FDIR activities specified for the associated subcapability in the FSSR (with extensions for omitted features, as identified by conversations with NASA colleagues and K. Gaylor of LinCom). For example, the ACFXC subcapability handles FDIR associated with events from external sources, such as calibration and configuration tests that are generated by ACSS, the ORU power status changes signaled by the EPS, and so on. The ACFFDI subcapability, which is the most complex of the three, detects failure and, where appropriate, initiates recovery based on a variety of sensor data, such as the ACS equipment status summary, the ORU BIT summary monitors, the pointing data from ACAM, etc. When either of these two subcapabilities detect an error, a number of messages and other indicators are sent through the RODB to other subsystems.

Recovery is initiated when the ACFXC or ACFFDI module declares active string failure. The failure, which will be in either hardware or pointing vectors mode as described above, is then acted upon by the ACFFR module. Given the nature of the failure, reconfiguration at either the current string or data rate level is attempted. If this recovery does not succeed, or if the detection process is unable to isolate the cause of the failure, then the prototype indicates that ACS communication is not available, a condition that would be handled through the ELOC recovery mechanism. The prototype does not simulate ELOC recovery, however, only its detection.

Implementation and Testing

The prototype consists of 23 modules of C code. In addition to the modules for the ACFXC, ACFFDI, and ACFFR subcapabilities, there are support modules for various subtasks not directly related to FDIR, an initialization module, and a number of modules used as test drivers to inject faults into the prototype. The prototype, as it currently is implemented, runs sequentially through a series of test cases. The conditions that activate a particular behavior in the subcapabilities are set in the driver code, then the appropriate detection module is called as a function. In this way, the driver simulates interrupts that would invoke the ACFM when an event or change in state occurs. The detection module looks for the injected fault, issues appropriate messages and updates, then initiates recovery when conditions warrant. The design of this prototype is illustrated in Figure 4.

For each execution of the prototype, the responses of the prototype (implemented as character strings sent to standard output) were collected for validation of the code against the specification. The prototype was tested to branch coverage using this method to ensure that all expected inputs produced the appropriate responses. A combination of black box and white box testing was used to design the test cases. A test plan consisting of 37 tests (some of which

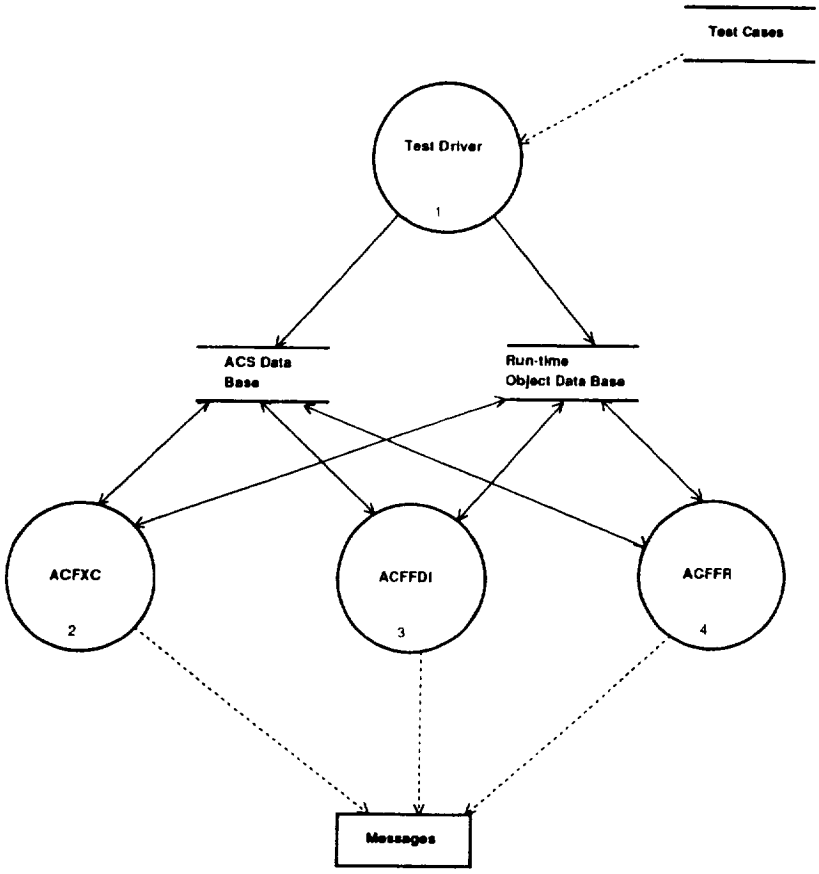

Figure 4.- Design of the ACFM Prototype.

tested multiple cases of the same response: failure and restoration of an ORU, for example) was developed and used to carry out the testing. Where revisions were made due to tests in later stages of the validation, regression testing was used to assure that the changes did not affect any previously validated code.

REVIEW OF CURRENT ACFM DESIGN

The final step in the review of the ACS FDIR capability was to look at the results of the previous analysis and determine what issues were still unresolved or unclear. The FSSR, which is still in a draft stage, is intended to provide both the high-level principal functional requirements as well as the detailed software requirements for the ACS. As such, it is an essential part of the FMEA process and the development of software for the ACS. The previous steps in the review represent preliminary versions of these two activities that exercise and evaluate the FSSR as it is currently defined.

This section of the report addresses two issues. The first part lists the events identified in the FMEA that are either omitted or incompletely addressed in the FSSR. The second part lists ambiguities or inconsistencies found in the document while building the prototype. Caveat: time did not permit a complete review of the FSSR, so the comments that follow are likely

incomplete. Furthermore, some of the items listed as omissions may be handled by subsystems external to the ACFM.

Undefined Events

A number of the events described in the previous sections are not included in the existing ACFM requirements. To address these problems, both the interfaces that provide the detection of these events and the response of the ACFM to them must be determined and added to the FSSR.

TDRS event table exhausted

If the TDRS event table does not contain any events beyond the current time, then the table cannot be used to determine scheduled vs. unscheduled LOS. There is a specification in the ACS FSSR for the activity of the ACS Service Maintenance (ACSM) subcapability of the ACSS when this table is exhausted, but the ACSM specification does not describe the expected behavior of the ACFM. The intent under these conditions is for the ACFM to use data from GNC/P to determine whether a TDRS is actually in view and determine whether a detected LOS is scheduled or unscheduled on that basis. The June 1993 version of the FSSR contains a description of this activity, but this version was not reviewed by the author.

Internal ORU reset

The effect of an ORU reset is not specified in the FSSR. It is assumed that a reset can either succeed or fail, where failure indicates that the ORU does not come back up and is therefore unavailable. There is no specification, however, of what flags should be set by ACFM to indicate detection of either of these events.

Also, the reset event indicators are different for each type of ORU, which makes detection difficult. As currently understood, an ACRFG reset is indicated by a flag in the ACBSP function data throughput monitor, but no such field exists in that data structure as specified. It was also reported by Gaylor that these resets could be handled in the ACS Control and Monitor Software (CMS) if its "Common Failures" parameters were changed, allowing an unsuccessful ORU reset to directly trigger recovery. At this time, however, it is not clear what the ACS's response should be to these events.

Asynchronous ORU events

Some of the asynchronous ORU events (Invalid Command and the ACBSP Multiplexer/Demultiplexer Data Lost events) are described in the ACFM portion of the FSSR. Only the Invalid Command event is completely defined in terms of the interface and response. The responses to the ACBSP Data Lost events are described, but the FSSR shows only that Caution and Warning Messages are issued. Gaylor describes other activities, as discussed in previous sections.

The ACRFG Low-Gain Antenna Switch Request event is shown as one of the possible values in the ACBSP vector word in the interface specifications, but no response to the event is specified. The ACRFG Pointing Function Status Change event is neither shown in the interface nor described in the response specifications. The BIT Go and BIT NoGo events are also omitted in both places for all three ORU types.

If these events are incorporated into the FSSR, the interfaces must also reflect their presence. For example, it appears that a response to an asynchronous ACRFG event would include updating the ACRFG function status monitor, based on comparison with the ACBSP description. However, this structure is not defined, either in the ACFM interface or in the data

structure tables. Similarly, the XPDR function status monitor, which is apparently the source of the XPDR internal reset flag, is not defined in either place.

Extended loss of command link

Recovery from ELOC is not addressed in the ACFM FSSR that was reviewed. It is not clear what capability of the ACS is responsible for either of these activities. The ISE contains the timer that is used to detect ELOC, but the interface between ISE and ACFM is not defined. The algorithm for responding to ELOC and the interfaces are defined in the June 1993 FSSR, but again this version was not reviewed by the author.

It should be noted here that the detection of ELOC when no local response to an unscheduled LOS is defined or possible in the ACFM is shown in the FSSR by the phrase "No additional processing is required." This phrase is also used to indicate the end of a successful mode restoration as well as the detection of recoverable failures. Even if detection of ELOC is the responsibility of some other capability, it would seem appropriate to distinguish the event from "normal" (i.e., non-failure) events in the ACFM description.

Other Comments

In addition to these events that are either omitted or incompletely described, there are several ambiguities and inconsistencies in the ACFM document.

A number of data structures are inconsistently specified among the ACFM context diagram (shown in Figure 2), the summary interface tables in the description of the ACFM, the tables for the individual subcapabilities, and the specifications of the subcapabilities' behavior. These include:

- the ORU FDI designation and the TDRS mode, which are both shown in the ACFM context diagram and in the subcapability tables, but do not appear in the summary tables;
- the ACS equipment summary, which is shown as external input and output in the context diagram, but (a) does not appear as input in the summary tables; (b) appears as external output in the summary and ACFFDI tables; (c) appears as internal input in the ACFFDI table; and (d) appears as internal input and output in the ACFXC tables; and
- the ACS configuration data shown as input to the ACFFDI subcapability includes only the TDRS identifier, while at least two other fields are needed (the SSPA mute field in paragraphs *l* and *m* of the ACFFDI description, and the audio channel status in paragraphs *e* and *f* of the same section).

Other problems arise in the descriptions of the ACFM subcapability. Among those discovered in this review:

- in paragraph *r* of the ACFFDI description, under the case in which the high-gain antenna is in use, the ACAM Position is "NO GO," and the ACS Failure Mode Criticality for Antenna Position is "CRITICAL," the criticality check is redundantly specified;
- in paragraph *p* of the ACFFDI description, the Demultiplexer State is defined to be "DEGRADED FRAMES" if the ACBSP function status monitor is not periodically updated, but no definition of "periodically" is provided; and
- in paragraph *a* of the ACFFR description, it appears that a failure that occurs while the ACS is configured for LDR transmission cannot be recovered by switching to HDR, even if that mode of transmission is available on the current or alternate string. There may be practical reasons that this option is not allowed, but no one with whom the author

consulted could confirm or deny this.

These ambiguities should be reviewed and resolved.

One pervasive problem in the FSSR is the lack of precise terminology to refer to data structures and other information. While the numerous redesigns of the Space Station are no doubt the underlying cause of many of these problems, this review exercise illustrated the difficulty of understanding the relationship between the description of the ACFM capabilities and the interface that provides the information with which they can be implemented. For example, in paragraph *r* of the ACFFDI description, once an unscheduled LOS has been detected, an active string failure in either pointing vectors or hardware mode can be declared. However, the pointing vectors case includes the condition where the ACAM mode is equal to "POINTING" while the first hardware case refers to the high gain antenna being in use. These two conditions are, in fact, exactly equivalent in the existing design. Such inconsistency can only be confusing to the implementor and is a source of potential error.

FUTURE WORK

While all software aboard a spacecraft like the Space Station is critical, the FDIR software must be more trustworthy than any other, since it is responsible for detecting and recovering failures generated elsewhere in the system. Our understanding of the processes and mechanisms that can support this level of reliability in software is still inadequate. For these reasons, the validation and evaluation of the ACFM and similar FDIR software for space-based communications systems are important tasks that require further study.

One immediate project being pursued is to extend this summer's work to a more realistic testbed that can generate events in real time and consider the effects of multiple (concurrent or cascading) failures on the reliability and performance of the system. We plan to port the prototype to a workstation environment at the author's university and create this testbed. We will also develop a test profile for the prototype based on communications outage data from recent Space Shuttle missions that the author has collected this summer. By implementing these real-time test drivers and applying the Shuttle outage data to the prototype, we should be able to measure with reasonable accuracy the error coverage and reliability of the proposed ACFM relative to the Shuttle data. We also hope to look at proposed outage schedules for the Station as well.

Longer range goals involve the exploration of methods by which the reliability, performance, and error coverage in space-based communications systems can be enhanced. In a harsh and still not completely understood environment like space, it is almost impossible to predict what events will and will not occur that may have an adverse effect on communications. Rather than trying to design a system that responds in a predefined manner to a given set of failures, we can look at designs that choose from among several alternatives, using information about the system and environmental state to find the response that has the highest probability of maintaining or restoring communications. Providing this kind of information to an FDIR system might allow a higher degree of reliability than has been previously achievable in communications control systems.

REFERENCES

[1] McDonnell Douglas Aerospace, *Flight System Software Requirements (Communications and Tracking System Software)* SSP 30606, Volume II Revision B (April 5, 1993).

N94- 25361

INTEGRATED RISK MANAGEMENT

Final Report
NASA/ASEE Summer Faculty Fellowship Program - 1993
Johnson Space Center

Prepared By:	J. L. Hunsucker, Ph.D., P. E.
Academic Rank:	Associate Professor
University & Department:	University of Houston Department of Industrial Engineering, Houston, TX, 77204 - 4812
NASA/JSC	
Directorate:	New Initiatives
Division:	Planning and Strategy
Branch:	N/A
JSC Colleague:	Lyn Gordon - Winkler
Date Submitted	August 2, 1993
Contract Number:	NGT 44 001 800

ABSTRACT

The purpose to this report is to first present a basis or foundation for the building of an integrated risk management plan and then to present the plan. The integration referred to is across both the temporal and the hierarchical dimensions. Complexity, Consequence, and Credibility seem to be driving the need for the consideration of risk. Reduction of personal bias and reproducibility of the decision making process seem to be driving the consideration of a formal risk plan. While risk can be used as either a selection tool or a control tool, this paper concentrates on the selection usage. Risk relies on stated purpose. The tightness of the definition of purpose and success is directly reflected in the definition and control of risk. Much of a risk management plan could be designed by the answers to the questions of why, what, who, when, and where. However, any plan must provide the following information about a threat or risk: likelihood, consequence, predictability, reliability, and reproducibility. While the environment at NASA is seen as warm, but not hot, for the introduction of a risk program, some encouragement is seen if the following problems are addressed: no champion, no commitment of resource, confused definitions, lack of direction and focus, a hard sell, NASA culture, many choices of assessment methods, and cost. The plan, itself, is designed to follow the normal method of doing work and is structured to follow either the work break down structure or a functional structure very well. The parts of the plan include: define purpose and success, do initial threat assessment, do initial risk assessment, reconcile threats and parameters, put part of the information down and factor the information back into the decision process as it comes back up, and develop inferences. Two major suggestions are presented. One is to build an office of risk management to be used as a resource by managers in doing the risk process. Another is to form a pilot program to try out the details in the plan and modify the method where needed.

INTRODUCTION

Decision making is becoming more and more difficult as the complexity of society increases and the consequences of bad decisions become more severe. Factors such as these force the consideration of risk into the decision making process. In truth, good managers have always considered risk in their decision making. However, if personal bias is going to be minimized and if the decision making, at least in the consideration of risk, is to be standardized enough to be reproducible by another analyst, then the process must be formalized. Therein lies the basic fundamental purpose of this report., the formalization of the consideration of risk in technological decision making.

Risk, oftimes in the past, has been only considered in the areas of cost, schedule, performance, or safety. The concept of risk is significantly greater than this. In today's society, risk comes from many different sectors such as political risk, societal risk, environmental risk, underfunding risk, just to name a few. The trap here is that we all have a tendency to give the most consideration to those things which are easily measurable, like schedule and cost performance. This is rather similar to the concentration in manufacturing, at least up through recent times, on direct labor in cost reduction even though direct labor usually accounts for around 20% of a products cost while indirect labor and materials cost split the remaining 80% between them. Direct labor is easy to measure. Schedule performance is easy to measure. While both are important, they are not the only important things. Risk management must be as broad as possible.

PROBLEM STATEMENT

The intention of this report is to begin the development of a formalized process of decision making in risk management that is integrated both through the life cycle of the entity at risk and also integrated through the hierarchy of the organization. Part of accomplishing this task will be to develop consistent terms and to formulate a plan that has a reasonable chance of being implemented on a broad basis. As an additional consideration, this report should serve as a beginning point for a follow-on work in risk management.

TERMS AND ASSUMPTIONS

Entity - refers to the program, project or thing to which the risk management program is to be applied.

Threat - Any real or perceived threat against a stated purpose. Threats are not necessarily measurable.

Parameter - A measurable quantity with an acceptable and an unacceptable region and perhaps a gray region. The totality of parameters, if all are in the acceptable region, should reflect that the purpose of the entity is fulfilled or being fulfilled.

Risk - This term is used in two different ways. One is the familiar meaning from everyday life and expresses the likelihood that an unfavorable event will occur. The other is a technical definition and says risk is the mathematical expectation of the parameter in question. Under this definition, risk is a product of likelihood and consequence.

Risk management - Different authorities have defined this slightly differently. Our definition will be that risk management includes risk or threat identification, quantification, inferences, control, and mitigation.

Prodrome - a warning event or sign.

DISCUSSION OF THE LITERATURE

The literature is very extensive on risk management. A quick glance at a paper written by Garland Bauch (unpublished) on Integrated Risk Management shows a discussion of risk management in fourteen different industries that ranges all the way from the construction to the finance industries. There are virtually thousands of papers on risk management in the literature. Many of these papers deal with either safety or with quantification techniques. Here and there, scattered among the rest, are a few which either concentrate on risk identification or provide an overview.

Fortunately, the reading of four or five pieces will provide the interested manger with an adequate background to pursue consideration of risk management. Start with NASA Management Instruction 8070.4 on Risk Management Policy for Manned Flight Programs (effective date Feb. 3, 1988). This document shows that

NASA has been trying to formalize its risk policy for quite some time. Then move to a set of papers by R. G. Batson. One is Risk Analysis Methodology Survey, done as part of the NASA/ASEE Summer Faculty Fellowship Program in 1987 and a follow on piece by the same author, Program Risk Analysis Handbook, 1987. These two will give somewhat of an overview and a fair amount of information on quantification methods. From here, a reading of Bauch's work (available from either me or the author) will provide a nice overview of the literature. This literature review is particularly strong in the risk identification areas. Finishing off with the Defense Systems Management College's manual, Risk Management, Concepts and Guidance, will provide an overview of the entire risk management process. The reader who is pressed for time can do no better than concentrate their efforts on these last two, Bauch's work and the DSMC's manual.

BACKGROUND

Why is this a problem?

The first step in designing new methodology is to determine what problem the new methodology is aimed at solving. In problem solving, the definition of the problem is perhaps the most important and crucial step. Here, this step becomes even more important since the identification of the motivators will, or should, give some indication of the feasibility of introducing a new methodology.

Based on interviews with NASA managers, there seem to be three factors forcing the consideration of a risk management program: complexity, consequence, and credibility. Decision making is becoming significantly more complex. As technology becomes more complex, so must the decisions that shape and mold technology. There is more to know, more to consider, and more to affect a technological decision than ever before. Meanwhile, there may be less resource to enact a decision. So complexity is growing. The consequences of technological decisions have become significantly greater. A wrong decision can have a multi billion dollar impact or even wipe out a whole agency or company. Faced with increasing complexity and consequence, the modern manager is faced with showing upper level management that a good job has been done in the decision making. Some means has to be established to demonstrate credibility. So complexity, consequence, and credibility are driving the consideration of risk.

Since all good managers have always considered risk, the next issue becomes one of why should the program be formalized. One reason is the reduction, or at least the realization, of personal bias. Everyone has their own unique view on risk taking. Some people are risk takers and some are risk avoiders. In decision making, some method must be used so that the other players have some idea of the risks being taken. Another factor pushing formalization of risk management is reproducibility. First, different decision makers should be able to arrive at close to the same decision on risk. Second, the decision process should be reproducible by another analyst. This is required in order to insure that the decision makers are in accord on the treatment of risk. In many industries, and NASA is no exception, managers change jobs rather frequently. Having reproducibility in the risk decision process should help to provide continuity through this management change.

In summary on why should the issue of a formalized risk management program be addressed, perhaps the best answer is that managers are being forced out of their comfort zones. There seems to be a significant amount of managerial unrest and, in some few cases, even paranoia. There is a basic difference between a bad decision and a wrong decision and managers understand the distinction. A bad decision is one based on a faulty decision making process. A wrong decision has a good process which considers everything which should be considered but arrives at a conclusion that leads to difficulty. Most often this difficulty could be that a consequence with a small probability was realized. All of this forces managers out of their comfort zone. Decision making has gotten harder.

Different Aspects of Risk Management: Selection and Control

There are two different uses of risk management. One is to consider risk in the selection among alternatives. In this usage, a manager is considering several different alternatives and uses risk as one criterion to choose a favored alternative to pursue. The other use of risk management is in the control mode. Here an alternative has already been selected and is being pursued. Then the risk must be managed and controlled to ensure that unfavorable consequences do not occur.

As an example, one might consider risk in choosing among different types of propulsion systems. There certainly will be other factors impacting the choice but risk will be one of the factors. This is risk management in the selection mode. Once a propulsion system

is chosen, then risk must be controlled as the propulsion system is designed, manufactured and operated. This is risk in the control phase. As is obvious, the selection mode comes first in the natural development of tasks and then the control mode. As a rule, less will be known about risk in the selection than in the control mode due to the absence of data.

Most of the literature deals with risk in the control mode. There is little distinction in the readings between the two fundamentally different uses of risk management. Since beginning at the beginning has a large amount of appeal in a logical development of a process, this report will concentrate on the selection mode of risk management. However, it is felt that the transition from the selection to the control mode will be natural and relatively easy.

Risk Relies on Purpose

A basic fundamental issue with risk management is the determination of what is at risk. To this end, the entity in question must have a defined purpose. Otherwise there is no way to rationally discuss risk because one cannot answer the question of what is at risk. The tightness of this definition of purpose, to a large degree, determines how tight the risk management can be. Said another way, the strength with which the task is known and understood will be directly reflected in the strength that the risks and threats against a task are understood.

A trap here is the sophomoric attitude that everyone knows and understands safety, cost, and schedule and this is what is at risk. These are just parameters that reflect threats against the basic purpose of the entity. There are no doubt other threats that are not reflected in these parameters. If one does not know the fundamental purpose of an entity, then any discussion of risk can only be at a most superficial level.

Related to this discussion of purpose is the definition of success. If you know the purpose, then you should be able to decide what you consider to be success. If you cannot do so, then, again, risk consideration is, at best, only superficial.

The Real and Perceived Dimensions of Risk

As the definition of success changes, then what is at risk changes and so must the way that risk is managed change. This

thought leads to two major dimensions of risk management and two quasi dimensions of risk management.

As a project or program moves through its life cycle, how success is defined changes. Consider the Shuttle. Before the first flight one major goal was to prove that the design was flight capable. Now that the program has matured, that goal has already been established. Thus the definition of success has changed. Therefore what is at risk has changed and risk management must also change. So risk management has a temporal or time dimension.

The manager at the very lowest level of an organization clearly has a different definition of success than the manager at the very highest level. There will be some commonalty between the two, but there will also be major differences. This means that risk will be different between different levels of an organization. This leads to the hierarchical dimension of risk management.

A minor dimension of risk management is imposed by the consideration of contractors. The way that the contractor views success and the way that the parent organization views success are different, therefore the risk management is different. Another minor dimension is induced by the matrix structure used in many organizations. At NASA, for example, projects and programs are going to view success differently.

So there is a temporal, hierarchical, contractor, and matrix dimension to risk management. The trick is to integrate the management of risk across these dimensions.

The Five W's: Why, What, Who, When, Where?

Much of the above discussion in risk management can be reduced to these five questions.

Why? - Why do a new program such as this?

What? - What is at risk? What is the purpose of the entity?

Who? - Who is at risk, NASA or the contractor?

When? When in the life cycle of the entity is the risk to be managed?

Where? - At what level in the organization is the risk to be considered?

The answers to these five questions will certainly shape a proposed risk management program.

Required Information About A Risk or Threat: Likelihood, Consequence, Predictability, Reliability, and Reproducibility

Once a risk or threat has been identified, the next question is how much information is needed on the threat to factor risk into the decision making process. Likelihood refers to the probability that an unfavorable event will occur. Consequence refers to the outcome or impact of this unfavorable event. These are usual pieces of information associated with risk. Not so usual is the consideration of predictability. Will there be conditions which forewarn the decision maker that an unfavorable event is about to occur or will the event come in an unpredictable or unheralded manner. Predictability relates directly to the amount of control that the manager will have.

Reliability refers to the underlying data or experience that the analyst is relying on to assess the threat. Has there been a lot of experience with threats of this type before? Is there a large data base that is used to assess this threat? Is this a unique experience that has never occurred and one with which no one has much exposure? Is the threat assessment a scientific assessment or is it a reasoned guess?

Closely related to reliability is reproducibility. Would another analyst be able to arrive at the same assessment? Would the same analyst, at a later date, be able to arrive at the same assessment? Reliability and reproducibility are both related to the removal of personal bias from the decision making process. Information on both of these issues is essential to the decision maker.

The Environment

If a program of this sort is being considered, then an assessment of the environment is in order. At NASA, the readiness to accept a program of this sort could at best be described as luke warm. On the negative side, almost no resource has been committed to doing integrated risk management. If the reader is tempted to believe that the rational for this is that the information or the requirement is new, go back and look at the date on the NMI 8070.4 which is 1988 or at the date on Batson's work for NASA which is 1987. There seems to be no great motivation to do risk management at any significant level above the consideration of safety, or any significant catalyst which would increase the desire to accept formal risk management as part of the decision making process. Risk management could at best be described as one of those things that managers feel that they really should do but which they are not ready to commit time or resource to doing.

On the positive side, there seems to be a growing interest in risk management. More than likely, some innovative organization at

NASA will pioneer the use of risk management in decision making and this will open the gates for other organizations to follow. There also seems to be some small indication of interest at upper levels.

Problems

The following is a short list of the perceived problems with implementing a risk management program. For the most part, they are self-explanatory.

1. No Champion - There is no champion, as yet, high enough up in the management structure or respected enough to get others to sign on.

2. No commitment of resources - There does not seem to be any large amount of resource devoted to this issue. To institute a program of this sort will require time, manpower, and money.

3. Confused definitions - Different people have used the terms differently. Many feel they have an adequate risk management program since they do a good job on safety.

4. Lack of direction and focus , absence of overview and strategy - There seems to be a real question about some of the fundamental programs of the agency such as the shuttle and the space station. This in term leads to questions about the fundamental purpose of the agency. Integrated risk management is strongly related to overview and strategy and requires a sense of direction and a tight focus.

5. This will be a hard sell - A program of this sort will change the fundamental way that manager do their business of making decisions. Most of the managers at NASA are older and have established work practices. Getting them to change may be quite difficult.

6. The NASA culture presents a problem - Typically, NASA would assign this problem to a contractor and expect the contractor to bring back a finished product without NASA having much input or doing much of the development on the system. This seems to be the predominant approach used to this point. As a management style for solving problems of the sort discussed here, this, at best, will lead to mediocrity.

7.. Abundance of choices for risk assessment and quantification - There are a large number of methods developed in other agencies and industries to quantify risk. The large amount of choice increases the difficulty of the decision.

8. Cost - As mentioned earlier, a program of this sort will require the expenditure of resource and time. Training must occur in

the usage of such a program.. Tools must be developed. The cost expenditure to introduce integrated risk management throughout the agency would be significant.

RISK MANAGEMENT PLAN BASICS

As stated before, the plan presented will concentrate on the decision mode of risk management as opposed to the control mode. If the process works well at the beginning during the decision phase, then it should evolve handily into the control mode thus providing for temporal integration.

Any plan for risk management must follow the normal way of doing work where possible. For this reason, the plan presented follows the work break down structure or the functional analysis structure equally well. This plan should adapt well to what ever method is used to break down design work into manageable pieces.

Since one of the most difficult parts of risk management is identification, this plan separates risks from threats. Recall that risk is determined by looking at measurable parameters and determining their mathematical expectation. Threats, on the other hand, may or may not be measurable.

THE PLAN

Step 1: Define Both Purpose and Success- The first part of this step is to define the purpose. Recall that the tightness of this definition determines how well focused the risk management plan will be. The second part of this step is to define success. The end result of step one will be two paragraphs, each containing one or two sentences. The first paragraph will be a simple statement of the purpose or function of this entity. The second paragraph will be a sentence that starts, "This entity will be successful if ...". The intent here is to tie success and purpose together in order to assist in focusing the work. This purpose follows the risk management information as it flows down through the organization.

Step 2: Do Initial Threat Assessment -

1. List the threats - Every single threat against the fundamental purpose or function should be listed. Their importance can be decided later. As young doctors learn in medical school, if you don't consider the diagnosis, then you won't make the diagnosis.
2. For each threat, discuss the likelihood. This is done in paragraph form and may or may not include an actual probability.

3. For each threat, discuss the impact or severity should this event occur. This also is done in paragraph form.

4. For each threat, list the prodomal events - The intent with this step is to list the conditions or warning signs that would signal that the threat is about to be realized. This step serves at least two purposes. One, it helps to establish credibility in that the threat has been thought about enough to identify those events leading to a crisis. The other purpose is that it helps the manager to evaluate the strength of the threat and the uncertainty associated with the threat.

5. For each threat, discuss the reliability of the threat assessment. - Identify the basis of the assessment. Give some indication of the strength with which convictions are held.

Step 3: Do Initial Risk Assessment -

1. Determine which parameters to measure - This will not necessarily be an easy task. A good starting place is in the DSMC manual in chapter 3. They start with Technical Risk, Programmatic Risk, Supportability Risk, Cost Risk, and Schedule Risk. The intent here is to identify a broad enough set of parameters such that if they are all in an acceptable region, then the purpose of the entity is, or will be, fulfilled.

2. Develop Measurement/Assessment Methods - This step is, more than likely, going to require some outside assistance. There are numerous methods and most rely on fairly sophisticated statistical methods.

Step 4: Reconcile Threats to Parameters and Conversely - Each threat should be reflected in the parameters and each parameter should be reflected in the threats. If not, then control will be difficult to establish. It may be impossible to find a parameter whose measurement will imply some sort of control or information about a given threat. In this case the threat is moved to a Critical Threat List. Items on the Critical Threat List deserve special attention. They are items surrounded by uncertainty and typify the concept of threat in its rawest form.

Step 5: Down and Back - As the work flows, so flows the risk information. When the work is passed down the organization to the next level of management, the stated purpose is also passed in two forms. One is the upper level purpose. The other is the purpose which is appropriate for this next lower level. This level then does steps 2,3, and 4, i.e., threat assessment, risk assessment, and reconciliation including the Critical Threat List. This is then passed

up the organization for incorporation into their risk model. In order to insure that all relevant threats are identified, it is important that steps 2,3, and 4 be done by the upper level before passing the problem on down to the lower level. If the upper level just waits on lower level information, there is a greater chance that some threat to the program will not be recognized.

Step 6: Develop Inferences - This step relates to the decision making process once all the data is in. The question is one of how threat information will be factored into the decision process. Formal explanations are required at this step if the decision is to be reproducible at a later date.

IMPLEMENTATION

There seems to be two basic ways to implement this program. One is to implement it agency wide. Another is to work a pilot project and iron out the problems and then to go to a wider implementation. Of the two, I would certainly prefer the latter. There are some significant questions that must still be answered but can only be answered in implementation. How much time is required to do a program of this sort? How much resource is required? What form should the data be presented in? These and others require a pilot program.

One concept that is not necessarily clear to NASA but is clear to me is that some sort of support office is going to be required for a program of this sort. Risk assessment requires sophisticated statistical analysis. Most managers at NASA do not have the required background nor do they need it. What they do need is the ability to interpret the statistics generated. This is rather similar to their use of computers. They do not need to be a programmer, but they do need access to some resource on computer programming. In a similar manner, this office could serve as a resource of methods in risk analysis. Another use of the office would be to serve as a storage house of information. A trap here is that some individuals might perceive that this office is intended to do the risk assessment work. This should not be the case. The purpose of the office is to serve as a resource to help the manager do the work.

WHERE TO FROM HERE?

Change Management - Managing change is difficult. The reader is encouraged to read some of the work on change management listed

in the references. The amount of change that will be required of a program of this sort should not be underestimated. When a new program is going to require that work be done in a fundamentally different way, plans need to be laid on how to implement the change.

Champion - This work needs a champion, the higher in the organization, the better. Without a one it will have extreme difficulty.

Support - The support of the champion and of the agency should be both visible and tangible. Otherwise, this program will be treated as if it is just another in a long line of useless programs.

Pilot Program and Pilot Team - Ideally, a team would be formed to work on a pilot project. One possible composition for this team would be a team leader who is both a visionary and a strategist. The purpose of the leader would be to provide direction, focus, and scope to the pilot project. The rest of the team should be composed of two or more young technical types who could do the statistical analysis. The analysts on the team could provide the nucleus of the risk management office discussed above.

Structured in this way, the pilot program should be complete in one to two years. The changes in the plan should be in place by the end of that time. Then training material could be developed for a broader implementation.

REFERENCES

1. Batson, R. G., "Risk Analysis Methodology Survey", NASA/ASEE Summer Faculty Fellowship Program, MSFC, 1987.

2. Batson, R. G., Program Risk Analysis Handbook, NASA Technical Memorandum, NASA TM - 100311, MSFC, 1987.

3. Bauch, Garland T., "Integrated Risk Management", Unpublished, August 1993.

4. Defense Systems Management College, "Risk Management Concepts and Guidance", DSMC, MDA 903-87-C-0781, Ft. Belvoir, VA.

5. Hunsucker, J. L. , Shah, Jaymeen, Santos, D. L. "Strategic Considerations for Planning Major Transitions", Engineering Managemnt J., Vol. 3, , 1991.

N94-25362

STRATEGIES FOR RECRUITING ADDITIONAL AFRICAN AMERICANS INTO THE NASA JSC SUMMER FACULTY FELLOWS PROGRAM

Final Report
NASA/ASEE Summer Faculty Fellows Program--1993
Johnson Space Center

Prepared By:	Ladelle M. Hyman, Ph.D.
Academic Rank:	Professor
University and Department	Texas Southern University Department of Accounting Jesse H. Jones School of Business Houston, Texas 77004
NASA/JSC	
Directorate:	
Division:	None
Branch:	None
JSC Colleague:	Joseph D. Atkinson, Jr., Ph.D.
Date Submitted:	September 27, 1993
Contract Number:	NGT-44-001-800

ABSTRACT

African Americans have participated sporadically in the NASA JSC Summer Faculty Fellows Program--none in 1992 and four in 1993. There is a pool of African Americans who are both qualified to provide services and willing to participate in initiatives which support technologies required for future JSC programs. They can provide human support and handle mission operations, spacecraft systems, planet surface systems, and management tools. Most of these faculty teach at historically black colleges and universities (HBCUs). This researcher will document the current recruitment system, critique it, and develop a strategy which will facilitate the diversification of the NASA JSC Summer Faculty Fellows Program. While NASA currently mails notices to HBCUs, such notices have generated few applications from, and fewer selections of, targeted faculty.

To increase the participation of African Americans in the NASA JSC Summer Faculty Fellows Program, this participant will prepare a strategy which includes a document which identifies HBCU-targeted faculty and enumerates more formally extensive and intensive communication procedures. In addition, an article will be submitted for publication in BLACK ISSUES IN HIGHER EDUCATION. A fifteen-minute panel discussion, which will include a video, will be delivered during the annual meeting of the American Society for Engineering Education (ASEE) to be held in Edmonton, Alberta, Canada June 26-29, 1994. An announcement letter will be mailed to targeted faculty; follow-up telephone calls and personal visits will be made and a checklist flowchart will be completed by key NASA personnel or designee. Although initially limited to NASA JSC's recruitment of African Americans, this strategy may be broadened to include other NASA sites and other targeted minority groups.

INTRODUCTION

The NASA/ASEE Summer Faculty Fellows Program is described in a 1989 NASA report as a cooperative program designed to give

> . . . faculty fellows in various academic disciplines the opportunity to use NASA field centers to perform research.
>
> The program is open to U.S. citizens with teaching or research appointments in universities or colleges; priority is given to applicants with two years of experience.
>
> ASEE sends application packages to more than 50,000 science and engineering faculty members each year. Announcements also appear in ASEE *Journal* and other specialized publications. Field center personnel screen the applications, selecting candidates on the basis of academic record, qualifications, and research interests. Approved applications are then made available to NASA researchers at field centers for final selections.
>
> To date, more than 5,000 faculty members from more than 300 institutions and 35 teaching disciplines have taken part in the program; almost three-fourths of those accepted in the past taught engineering, physics, mathematics/statistics, or chemistry.[1]

Therein lies the core of NASA's recruitment criteria for the Summer Faculty Fellows Program.

The purpose of this research project is to assess recruitment performance and to identify opportunities for improvement. Its objective is to determine if existing application and selection procedures are appropriate in light of the past participation of African American faculty in the JSC Summer Faculty Fellows Program.

1United States. NASA. Educational Affairs Division Program and Services. Washington: NASA Headquarters, June 1989, pp. 18--19.

SCOPE AND PROCEDURES

This researcher conducted a review which consists of a sampling of JSC's recruitment procedures and of the procedures of two other field centers of the NASA Summer Faculty Fellows Program. This researcher reviewed management-selected files and discussed ASEE application and NASA JSC selection practices with NASA personnel, with faculty at investigator-selected universities, and with the three other African American NASA JSC Summer faculty fellows. This researcher also interviewed co-directors of two other NASA Summer Faculty Fellows Programs who described their recruitment activities.

DISCUSSION

Currently, NASA headquarters allocates to JSC twenty-six American Society for Engineering Education summer faculty fellows positions. The nine NASA field centers may gain additional positions through local funding. In the Summer of 1993, JSC had thirty-five faculty fellows. Although the formal application process began in December 1992, the informal, strong pre-selection networking began earlier when candidates spoke informally with key NASA personnel to find a common ground. Some early would-be-fellows do call the university program administrator who in turn can refer them to key NASA personnel.

Each year Dr. Stanley Goldstein, the JSC Director of University Programs, mails to managers within JSC a letter announcing Open House for viewing applications. The letter usually includes a statement about the desirability of selecting minorities and women. The Director reserves a few positions in case minorities are not included by the initial selection process. Subsequently the Director offers these withheld positions to managers within JSC provided they agree to select excluded minorities. However, the Director did not follow this later procedure in 1992 for no African American was selected to participate that year. Figure 1: NASA/ASEE JSC Recruitment Process, (page 5), documents the JSC selection process. In 1993, as applications were received, both the program administrator and the JSC University Director sought to establish an early collegial linkage.

FIGURE 1: NASA/JSC RECRUITMENT PROCESS

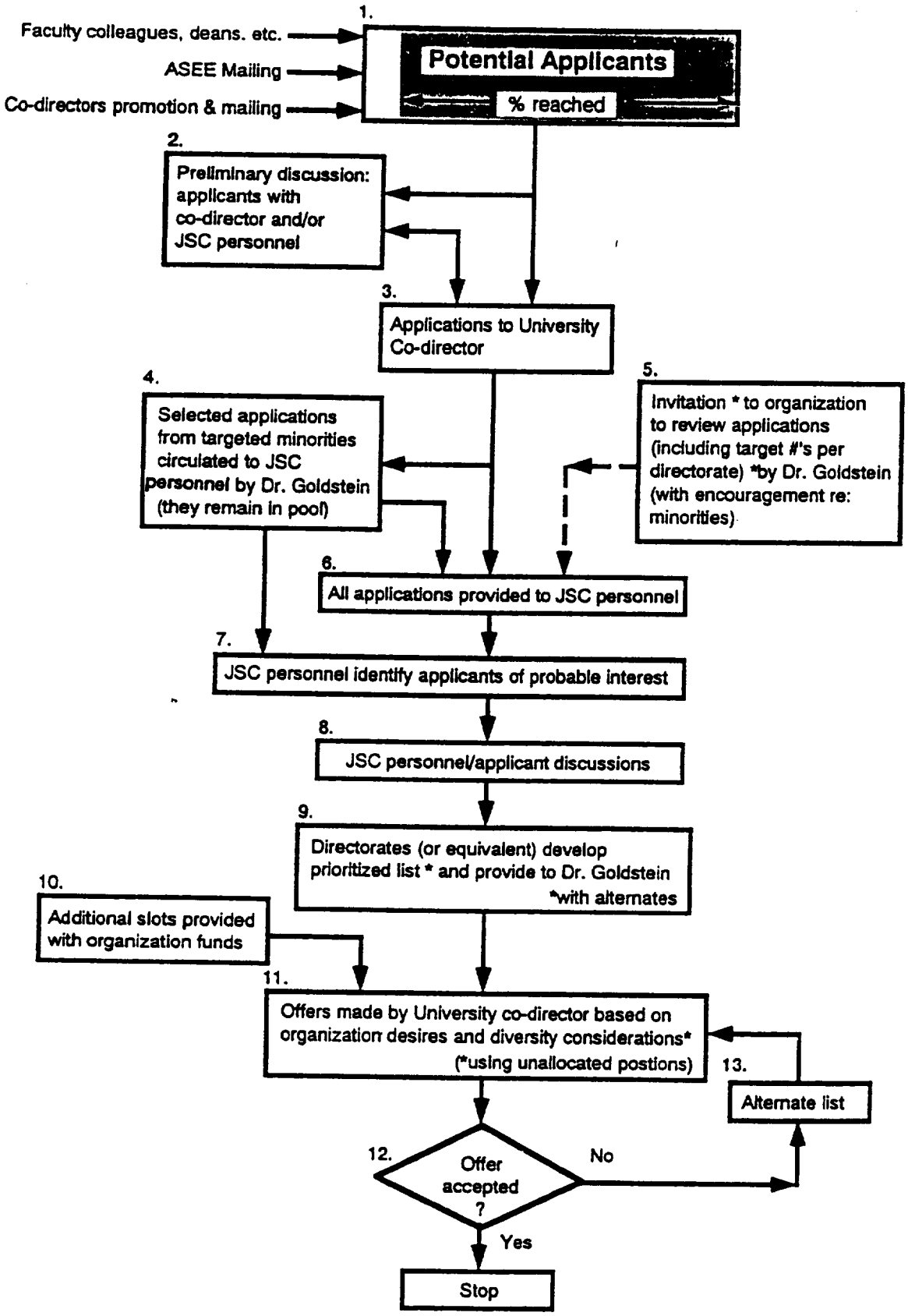

Created by: Dr. William Hyman

Step 2 is crucial in this process but many African American applicants to date seem to be unaware of its decisive role. A remedy is to stress to applicants the necessity of completing this step as indicated. The PI will assume this role and will also follow the steps in Figure 2: Initial and Follow-up Calls and Visits, (page 7). Monitoring the application process in this manner will enhance the quality and fit of the responses to the application line item labeled *Anticipated Research Interests.*

Model

This model requires two activities: identification of targeted faculty and monitoring of the application processes. Each year, the model requires the identification of targeted faculty from the universities listed in Table 1 (page 9). The list is supplemented by names received from others, such as alumni of the 1993 JSC Summer Faculty Fellows program. The activities stated in Table 2 (page 12) are to be performed by the dates indicated. Specifically, said person(s) will fax short documents (or mail longer ones) and will phone and/or visit applicants to provide appropriate follow-up activities. Completion of these activities will insure a steady stream of applicants.

In addition to the above activities, the model incorporates (1) the submission for publication of a NASA/ASEE awareness and recruitment article in the Fall 1993 issue of BLACK ISSUES IN HIGHER EDUCATION (Exhibit A) and to other journals in subsequent years and (2) participation in the June 1994 ASEE annual meeting (See Exhibit A and its related video tape) and at other meetings in subsequent years.

Measurement Criteria

A comparison of the selection activities performed by NASA JSC with those performed by Langley Research Center and with John C. Stennis Space Center revealed no significant differences except for the practice--as opposed to the stated policy--of early collegial bonding prior to the submission of the written application. The rationale is that because JSC is an operational center, rather than a research center, fellows' selections are colleague driven.

FIGURE 2: INITIAL AND FOLLOW-UP CALLS AND VISITS

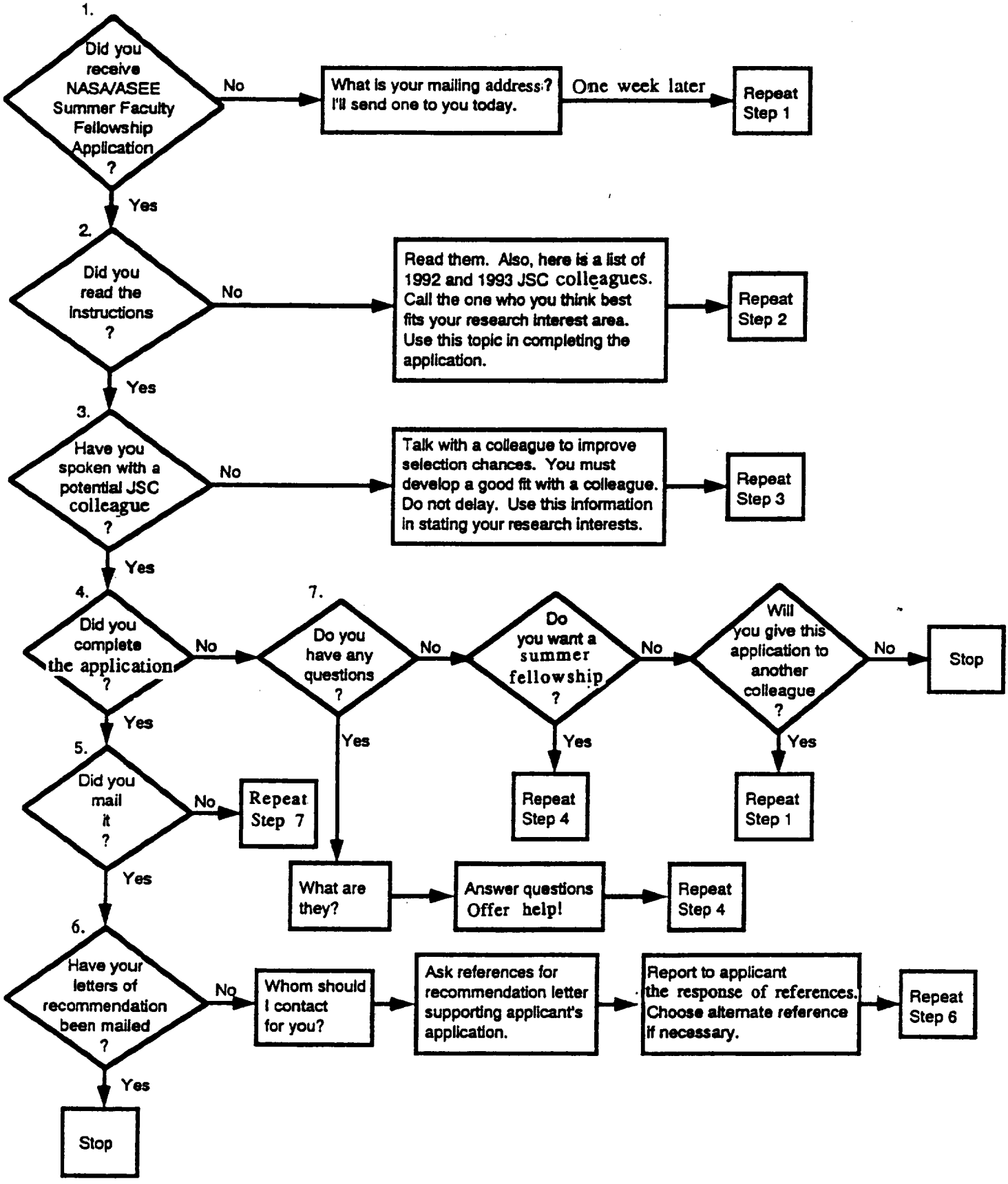

CONCLUSIONS AND RECOMMENDATIONS

The NASA/ASEE Program should consider broadening its scope to reflect recruitment from fields other than science and engineering, as appropriate. The application pool will be considerably greater when other fields are included because there are more African Americans in other fields than in science and engineering. Educators have helped, and can continue to help, complete projects not in science and engineering.

The directors of university programs and co-directors of the JSC Summer Faculty Fellows Program should tell African American applicants that although the formal application process begins in December, the informal, strong preselection networking begins earlier. Applicants speak informally with key NASA personnel (JSC colleagues-to-be) and find common ground **prior** to submission of the written application. (This researcher asked seven first time participants "What steps did you follow in applying for this fellowship?" All had spoken with their JSC colleague-to-be before completing the application.)

The co-directors should inform the summer faculty fellows that they are deemed to be independent contractors. Thus, their $10,000 stipend is both their gross and their net pay. Fringe benefits are excluded.

QUESTIONS FOR FURTHER STUDY

Between 1988 and 1993, the number of African Americans selected at JSC was usually less than half the number of applicants. Specifically, for 1988, 1/7; 1989, 1/unavailable; 1990, 1/5; 1991, 1/2; 1992, 0/4; and 1993, 4/8. (The NASA-wide Center rate is less than 1/3 [2]) Are these low participation ratios a result of articulation deficiencies?

If the applicant receives input from the JSC colleague-to-be **before** completing the written application, will a greater number of the applicants be selected? Performance of this task and subsequent evaluation will determine if this is an effective model for motivating

---

2Ibid., p. 19.

African Americans to consider initiating and completing NASA-type research projects.

Given co-directors' tendency to "look in their own backyards for African Americans," can an African American do a consistently better job of qualifying African Americans for summer faculty fellows selection? To achieve more minority involvement at JSC two choices emerge: create a three-university split in the directorship by including Texas Southern University, or Give one person six of the total JSC slots and have him/her fill them.

The application form should specify where applicants are likely to find placement. Are biologists more likely to be placed at JSC than at any of the remaining centers?

To what extent have JSC alumni continued their NASA-type research activities? For the period, 1985-1993, what is the data on minority participation? What are the numbers of HBCUs and faculty participating?

Are there other appropriate universities and other entry points than those listed in Table 1? How complete and how comprehensive is this listing?

TABLE 1
HBCU DIRECTORY FOR NASA/ASEE PROJECTS

Mr. Burt Allen
Chief Flight Instructor
Alabama Aviation and Mechanical University
Huntsville, Alabama 35672
(205) 774-5113 (X248)

Dr. Linda Chamberlin, Director
Space Life Sciences Training Program
College of Pharmacy
Florida A. and M. University
Tallahassee, Florida 32307
(904) 599-3636

Dr. Clarence Coleman, Chair
Chemistry, Physics, and Engineering Department
Norfolk State University
Norfolk, Virginia 23504
(804) 683-8909

Dr. Joseph Colen, Chair
Department of Mathematics
Jackson State University
Jackson, Mississippi 39217
(601) 968-2161

Dr. Douglas Council, Chair
Natural Sciences, Mathematics, and Computer Science Department
Bowie State College
Bowie,Maryland 20715
(301) 464-6653

Dr. Sylvester Gates, Chair
Department of Physics
Howard University
Washington, DC 20059
(202) 806-6245

Dr. Eddie Hildreth, Chair
Department of Computer Science
Southern University--Baton Rouge
Baton Rouge, Louisiana 70126
(504) 771-4170

Dr. Arthur Jones, Chair
Computer Science
Morehouse University
Atlanta, Georgia 30314
(404) 215-2629

Dr. Joseph Jones,
Vice-President for Research
Texas Southern University
Houston, Texas 77004
(713) 527-7011

Dr. Steve Lai, Director
NASA Center for Aerospace Research
North Carolina A. and T.. State University
Greensboro, NC 27411
(919) 334-7621

Dr. Phil Loretan, Director
NASA Center for Food Production, Processing and Waste Management
Tuskegee University
Tuskegee, Alabama 36088
(205) 727-8011

Dr. Alfred Msezane, Chair
Physics Department
Clark Atlanta University
Atlanta, Georgia 30314
(404) 880-8798

Dr. R. Radha, Chair
Civil Engineering Department
Prairie View A. and M. University
Prairie View, Texas 77446
(409) 857-2418
FAX (409) 857-2222

Dr. Enrique Silberman, Director
NASA Center for Photonic Materials and Devices
Fisk University
Nashville, Tennessee 37203
(615) 329-8620

Mr. John Spencer, Chair
Department of Architecture
Hampton University
Hampton, Virginia 23668
(804) 727-5440

Dr. James Turner, Director (513) 376-6392
Dr. John Hurley, Associate Director (513) 376-6456
Center of Excellence in Applied Mathematics
139-A Jenkins Hall
Central State University
Wilberforce, Ohio 45384

These Table 1 addressees will be monitored in compliance with the Figure 2 dialogue according to the Table 2 timetable.

TABLE 2
ACTIONS AND STRATEGIES

DATE	ACTIVITY
8/15/93-9/15/93	1. Send letters to targeted HBCUs announcing the NASA/ASEE forthcoming applications. Purpose : To establish contact and to motivate participation in NASA-type research projects. **Deliverables: a form letter and a copy of the 1993 application form.** Submit article to BLACK ISSUES IN HIGHER EDUCATION for publication. Contact NAFEO again and arrange to be placed on the March 1994 program.
9/16/93-10/15/93	2. Talk with a contact person (who may or may or may not be the adressee in "1"). Purpose: To locate the names of specific faculty who will apply and to motivate participation in NASA-type research projects. **Deliverables: a copy of the 1993 application form and a list of 1992 and 1993 JSC Colleagues.** 3. Monitor faculty identified in "2" to ascertain their continuing interest in participating and their progress in speaking with a past JSC Colleague.

Purpose: To encourage applicants-to-be to obtain input for purposes of completing the written application and to motivate participation in NASA-type research projects.

12/1/93-1/15/94	4. Monitor the application completion process detailed in *Figure 2*, page 7.
3/23-27/94	5. Register for, attend, and participate in the NAFEO Annual Meeting.

EXHIBIT A

Article for Submission to BLACK ISSUES IN HIGHER EDUCATION for publication.

FOR THE 15-MINUTE PANEL DISCUSSION, IN ADDITION TO PRESENTING THE ARTICLE DATA, ALSO SHOW VIDEO, ANSWER QUESTIONS, INVITE ADDITIONS TO THE CURRENT MAILING LIST, AND DISTRIBUTE COPIES OF THE 1994 APPLICATIONS AS A GUIDE FOR 1995 APPLICATIONS.

EXHIBIT B

FORM LETTER

BIBLIOGRAPHY

Atkinson, Joseph D. Personal interviews 6, 7, 8 June 1993.

Benjamin, Mary. Personal interview. 24 June 1993.

Bethly-Betz, Jessie. Personal interview. 10 June 1993.

Ferguson, Milton. Personal interview. 23 July 1993.

Gilmore, John. Personal interview. 24 June 1993.

Goldstein, Stanley. Personal interviews. 7, 8, 30 June 1993.

Hale, Deborah A. Personal interview. 23 July 1993.

Hathaway, Roger a. Personal interview. 22 July 1993.

Hildrth, Eddie. Telephone interview. 20 July 1993.

Hoskins, Charles. Personal interview. 7 June 1993.

Hyman, William. Personal interviews. 8, 14 June 1993, 6 July 1993.

Massenberg, Samuel. Personal interview. 22 July 1993.

McGee, Sherry. Personal interview. 17 June 1993.

Meade, Andrew. Telephone interview. 13 July 1993.

Proctor, Saundra. Personal interview. 22 July 1993.

Report of the Special Committee on Operational and Management Auditing. Operational Audit Engagements. New York. AICPA, January 1982.

Smith, Albert. Personal interview. 23 July 1993.

Spencer, John. Personal interview. 22 July 1993.

Taylor, Bruce. Telephone interview. 13 July 1993.

United States. NASA. Educational Affairs Division Program and Services. Washington: NASA Headquarters, June 1989.

---. Information Guide to Research and Education Programs. Hampton, VA: Langley Research Center, 1993.

Yang, Bob. Personal interview. 22 July 1993.

N94-25363

IMAGE REMAPPING STRATEGIES APPLIED AS PROTHESES FOR THE VISUALLY IMPAIRED

Final Report
NASA/ASEE Summer Faculty Fellowship Program-1993
Johnson Space Center

Prepared by:	Curtis D. Johnson, Ph.D.
Academic Rank:	Professor
University & Department:	University of Houston College of Technology Houston, TX 77204-4083
NASA/JSC	
Directorate:	Engineering
Division:	Tracking and Communications
Branch:	Tracking Techniques
JSC Colleague:	Richard Juday, Ph.D.
Date Submitted:	August 13, 1993
Contract Number:	NGT-44-001-800

ABSTRACT

Maculopathy and retinitis pigmentosa (rp) are two vision defects which render the afflicted person with impaired ability to read and recognize visual patterns. For some time there has been interest and work on the use of image remapping techniques to provide a visual aid for individuals with these impairments. The basic concept is to remap an image according to some mathematical transformation such that the image is warped around a maculopathic defect (scotoma) or within the rp foveal region of retinal sensitivity. NASA/JSC has been pursuing this research using angle invariant transformations with testing of the resulting remapping using subjects and facilities of the University of Houston, College of Optometry. Testing is facilitated by use of a hardware device, the Programmable Remapper, to provide the remapping of video images.

This report presents the results of studies of alternative remapping transformations with the objective of improving subject reading rates and pattern recognition. In particular a form of conformal transformation was developed which provides for a smooth warping of an image around a scotoma. In such a case it is shown that distortion of characters and lines of characters is minimized which should lead to enhanced character recognition. In addition studies were made of alternative transformations which, although not conformal, provide for similar low character distortion remapping.

A second, non-conformal transformation was studied for remapping of images to aid rp impairments. In this case a transformation was investigated which allows remapping of a vision field into a circular area representing the foveal retina region. The size and spatial representation of the image are selectable. It is shown that parametric adjustments allow for a wide variation of how a visual field is presented to the sensitive retina.

This study also presents some preliminary considerations of how a prosthetic device could be implemented in a practical sense, vis-a-vis, size, weight and portability.

INTRODUCTION

Maculopathy and retinitis pigmentosa (rp) are two forms of human vision defects which are characterized by partial loss of ocular function. In the case of maculopathy the dysfunction is in the foveal region of the retina and thus the area of greatest resolving power. The resulting scotoma or "blind spot" leaves individuals so afflicted with an impaired ability to read and to recognize patterns since both functions involve high resolution visual imagery. They learn to partially compensate by fixating on a spot removed from the focus of attention such that the image falls on the most optimum peripheral retina. Figure 1 illustrates how a sample of written material might appear to a maculopathic individual where the eye is "focused" upon the region directly under the scotoma blocked text. If fixation is made on the center of the circular area the difficulty of character recognition using images falling on peripheral retina can be noted.

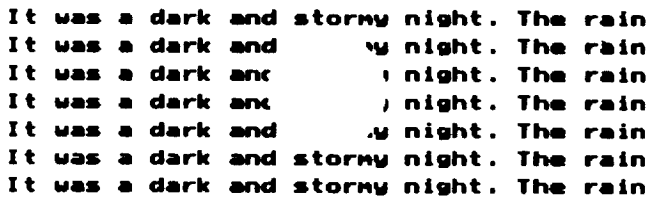

Figure 1. Text viewed with a scotoma

The case of retinitis pigmentosa is the inverse of maculopathy in that it is the peripheral regions of the retina that lose sensitivity while the foveal region remains functional. Individuals afflicted with this "tunnel vision" condition have difficulty in navigation and dexterous activity since loss of peripheral vision disturbs the awareness of local surroundings. Sensitivity to motion detection is also impaired. Afflicted individuals learn to compensate by swinging the head during ambulation to sweep the field of view through the sensitive retinal region.

As part of space activity related research NASA Johnson Space Center has developed considerable expertise in the theory and techniques of visual image warping. The Programmable Remapper[1] (PR) is a hardware device developed by NASA/JSC which is capable of providing specified warping of an input TV image to an output monitor display at better than 30 frames per second. Considerable research has been conducted on how image warping may be applied as a prosthesis for individuals afflicted with maculopathy or rp. The basic concept is to warp the image such that a portion of the lost data is redistributed to remaining sensitive regions of the retina[2-4]. Research thus far has involved remapping of textual material in such a way as to warp the image partially or totally exterior to an assumed scotoma. The warping transformation employed in these initial investigations is an angle invarient shift of the image along radial lines from the center of the scotoma. Figure 2 illustrates the appearance of warped text for which approximately 80% of the image has been remapped outside of an assumed scotoma. Experimental testing

was accomplished by using the PR in conjunction with an eye tracker to provide a warped image for subjects with simulated maculopathy. The results suggest some improvement in reading capacity[5].

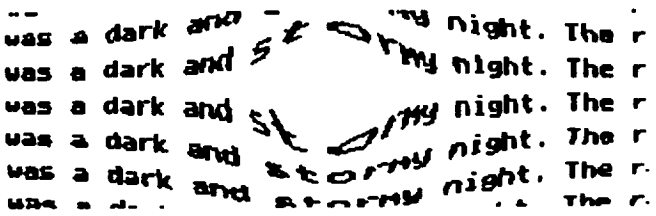

Figure 2. Radial warping of text.

The particular radial transformation employed in the testing and shown in Figure 2 results in considerable distortion of the text characters. This may adversely effect the results of reading rate measurement since, although the image has been warped to a sensitive region of the retina, character distortion hinders recognition.

This paper presents results of two aspects of continued work on the application of warping strategies toward development of a prosthesis for those with maculopathic or rp afflictions. The first aspect involves a study of alternative warping transformations and the second focuses on issues related to the practical and feasible implementation of a prosthesis.

Transformation Formulation

In general a visual image to be remapped consists of a rectangular array of pixels, where each pixel is represented by a two dimensional coordinate and has a "value" which describes the attributes of the pixel. Attributes include such features as intensity and color. The transformation process specifies how a pixel located in the image input plane at (x,y) will be re-mapped to the image output plane at location (u,v). This transformation is specified by equations relating (x,y) to (u,v),

$$u = f(x,y) \quad (1)$$

$$v = g(x,y) \quad (2)$$

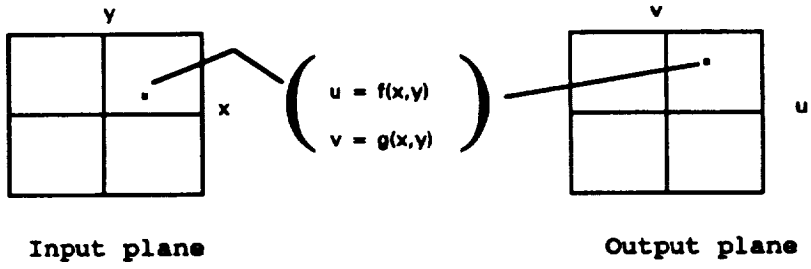

Figure 3. The transformation process

Whereas the process of Equations (1) and (2) is analytically complete it fails to consider the discrete nature of the pixellated image. If the Jacobian of the transformation is greater than unity in some region then a single pixel in the input plane may transform into several output plane pixels. Of course if the Jacobian is less than unity the converse may occur wherein several input plane pixels transform into a single output plane pixel. In these cases interpolation processes must be used to relate un-mapped input and output pixels and the attributes of the input and output plane pixels must be modified to retain image features such as color and contrast.

The Programmable Remapper described earlier includes pixel interpolation and attribute adjustments so that only the analytical features of the transformation need to be developed.

In order to statically test the transformations studied in this work the test text of Figure 1 was employed. The transformation equations were used to recast this image so that the effect of the warping could be examined. Since the objective was to study the effect of transformations on character shape and orientation, only very elementary interpolation and fill-in routines were employed. Therefore the appearance of the test text after warping as shown in this report is is only partially filled and is not to be interpreted as the final representation for actual patient testing.

MACULOPATHIC TRANSFORMATIONS

Study of alternative transformations for maculopathy compensation was confined to those which appeared to be most suitable for enhanced reading skills as opposed to facial recognition. It is not at all clear that the optimum transformation for the first would also be optimum for the second. This choice was made since experimental studies are presently concentrated on measurement of reading enhancement via image warping.

It is assumed that an optimum text warping transformation would be one which:

(1) displaces the text image blocked by the scotoma to sensitive retina just outside the scotoma,
(2) minimizes distortion of the shape of the text characters, and
(3) maximizes preservation of the textual flow of characters as lines are warped around the scotoma.

Of course the true test of a transformation is in its efficacy in improvement of maculopathic reading rate.

A Conformal Transformation - $\sin^{-1}(z)$

A conformal transformation is one which preserves angles between line segments through the transformation. This means that the basic orientational features of characters and lines consisting of characters would be preserved. This is consistent with the optimum transformation objectives. The conformal transformation employed was a two step, complex arcsin/complex sin process.

The first step is to perform a transformation of the form,

$$z' = \sin^{-1}(z) \qquad (3)$$

where $z' = x' + jy'$ is in an intermediate image plane
and $z = x + jy$ is formed from the input image plane
An offset is now added to y',

$$y'' = y' + c \tag{4}$$

so that $z'' = x' + jy''$.

The reverse transformation is used to construct the output image plane,

$$w = \sin(z'') = u + jv \tag{5}$$

It is easy to show that this transformation creates an elliptical void about the origin of the (u,v) plane with dimensions shown in Figure 4. Essentially the transformation expands the line from (0,-1) to (0,+1) in the input image plane into the indicated ellipsoidal shape. Thus images in the input plane will be warped into the output image plane such that all input image pixels are remapped into the space surrounding the elliptical void.

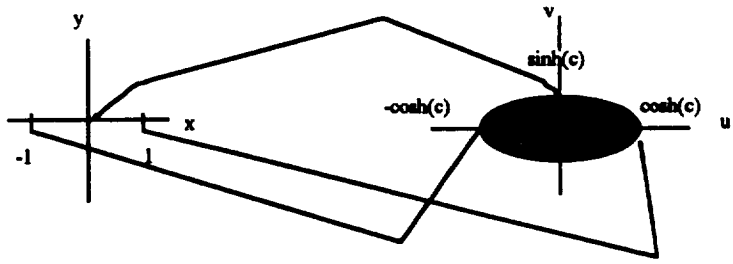

Input plane Output plane

Figure 4. Conformal remapping by arcsin/sin

Since unity points play an important role in this remapping, proper normalization of the input image must be included. To test this transformation for maculopathy a circular scotoma of radius r_s is assumed, as shown in Figure 1. The input image is then normalized to some radius, r_n, about the scotoma site, to define the unity points. If the entire scotomal area is to be remapped then the origin in the input image plane must map to the edge of the scotoma on the output image plane. In general one may wish to remap some fraction, α, of the scotoma blocked region of the input image to unblocked regions of the output image. This defines the value of the transformation displacement, c, through the relation,

$$\sinh(c) = \alpha(r_s/r_n) \tag{6}$$

Thus two parameters determine the features of the remapping. The fraction of image recovery, α, and the normalization radius, r_n.

The transformation was tested using $\alpha = 0.8$. Figure 5 shows the result for the case $r_s/r_n = 0.5$, which means that the unity points lie outside of the scotoma.

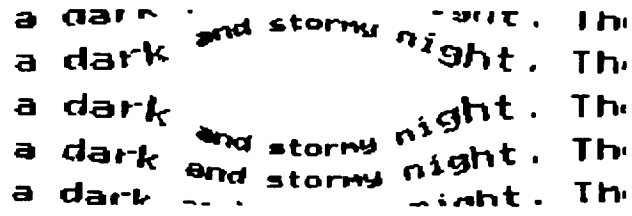

Figure 5. Conformal transformation, 80% and $r_s/r_n = 0.5$

Notice the way the characters flow around the scotomal area while retaining their effective shape and orientation. Also the process of displacement in the transformed domain results in a magnification. Figure 6 shows the remapping which results from a remapping with $r_s/r_n = 1.0$ and Figure 7 for $r_s/r_n = 1.5$. Note the increased magnification in each case.

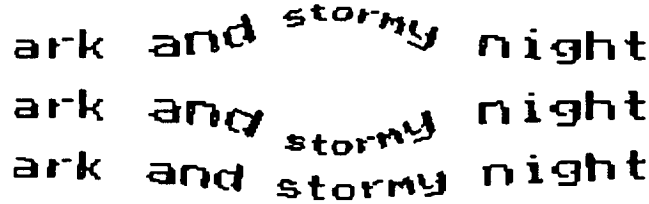

Figure 6. Conformal transformation, 80% and $r_s/r_n = 1.0$

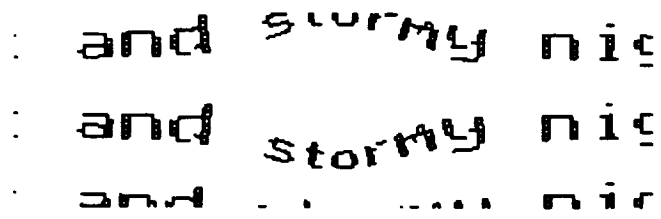

Figure 7. Conformal transformation, 80% and $r_s/r_n = 1.5$

The above examples assume that the fixation point of the observer is between lines of text. The effect of scanning the fixation point down across the lines of characters can be seen in Figure 8.

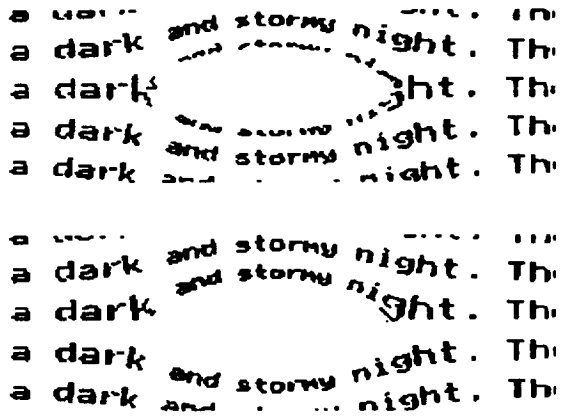

Figure 8. Effect of changing fixation point on warping
(80%, r_s/r_n = 0.5)

Experimental study of the efficacy of this conformal transformation on reading enhancement is presently underway at the University of Houston, College of Optometry.

Hyperbolic Secant Transformation

Another transformation studied which has many of the desired features for the optimum transformation is defined by the following equations:

$$u = x \tag{7}$$

$$v = y + a(\mathrm{sech}(bx)) \tag{8}$$

The effect of this transformation is such that the y space of the input plane is warped such that an approximately ellipsoidal void, similar to the conformal, is produced. Figure 9 shows how the test text is warped by this transformation.

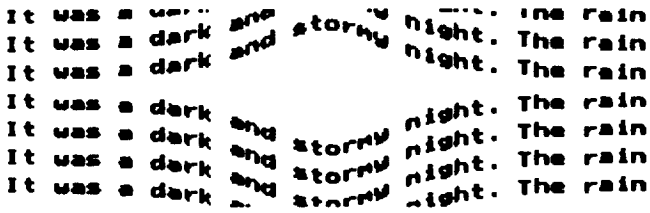

Figure 9. Secant transformation

The x space is unchanged. Thus the transformation pushes characters up but does not totally preserve the shape of letters. Unlike the confromal transformation there is no magnification associated with the warping, although this can be added. Variation of parameters allows for changing the roll-off of character lines and the vertical extent of the warping. Experimental studies of this transformation will be conducted at the College of Optometry of the University of Houston.

RETINITIS PIGMENTOSA TRANSFORMATIONS

Transformations for retinitis pigmentosa (rp) are required to remap the input plane into a smaller field of view centered on the fovea. This kind of transformation leads one to consider transformations which map a Cartesian system into the unit circle as suggested in Figure 10.

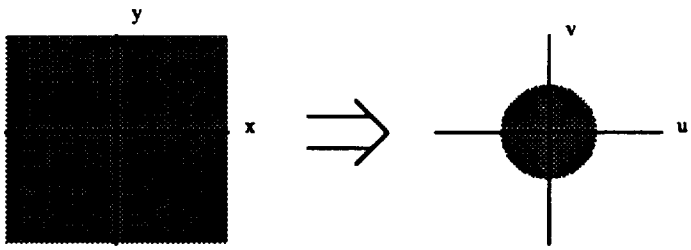

Figure 10. RP Transformation

During this project a radial transformation was studied which maps the entire world view into a circular region of variable radius. By variation of transform parameters it is possible to vary not only the radius of the output plane image but also the region of the input plane which appears relatively undistorted in the output plane. The transformation equations are given by:

$$r = [x^2 + y^2]^{1/2}$$

$$u = [1 - e^{-gr}]x/r \qquad (10)$$

$$v = [1 - e^{-gr}]y/r \qquad (11)$$

Figures 11, 12 and 13 show three samples of how the test text would appear following transformations given by Equations (10) and (11). Note that the entire field of Figure 1, without the scotoma overlay of course, is included in these image views. The original image has been compressed toward the edges in a circularly symmetric way.

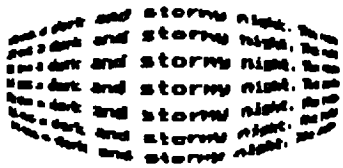

Figure 11. RP image for wide vision

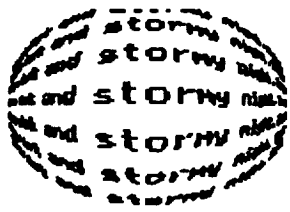

Figure 12. RP image for intermediate vision

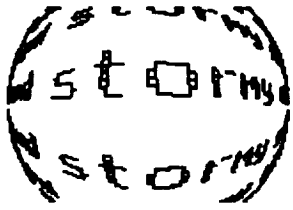

Figure 12. RP image for narrow vision

Although these show the effect of the remapping it should be noted that the real test of rp transformations lies in pattern recognition. The next phase of this work will be to implement transformations such as that presented here in a portable viewing system. This will study the efficacy of the system for enabling a person afflicted with rp to navigate, locate and retrieve objects. It will be necessary to be able to switch the rp correction system to provide various views such as for enhanced near-field vision or far-field vision.

IMPLEMENTATION CONSIDERATIONS

There were two issues explored during the project period with respect to implementation of a practical prosthesis using transformations. The motivation for study of this problem is the need for a portable, "heads up" system for practical use by a visually impaired individual. Although the Remapper is able to provide up to 30 frames per second, it consist of a large, heavy computer system with associated power supplies, monitors and so forth. The need is for a process by which a system could be head mounted, with associated video camera(s) and miniature display(s).

The first issue was to consider the construction of a sensor at the front end of the system which could perform part of the transformation in a hardware sense. The concept here is that variation of the size and physical geometry of the sensor pixel array could effect part of the required transformation[6]. Discussions were held with industrial representatives from Texas Instruments regarding the feasibility of building such a sensor. It appears that there are significant obstacles to such a device although similar sensors have been fabricated. This is an area for further study.

The second study regarded the possibility of implementation of an effective sensor using optical, distorted fiber bundle technology. In

this case consideration was given to the use of a fiber-optic bundle which has been tapered. Such a device is commonly employed to provide a magnified or reduced image. In the case of a low vision prosthesis for maculopathy the die forming the original bundle would have a central hollow core as shown in Figure 14. When heated and drawn the core would normally reduce in proportion to the fiber bundle major radius. It may be possible however to draw down the heated bundle such that the core radius reduces to zero as the whole bundle is drawn. This would result in a structure similar to that in Figure 14. It is clear that if an image is presented to the reduced area surface it will be projected onto the larger radius surface with a void in the central region, where the scotoma would be located. In this way the image is warped around the scotoma.

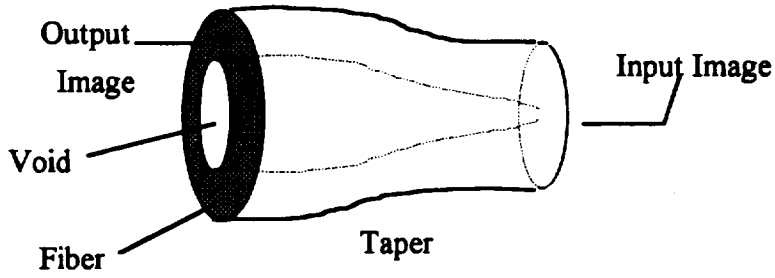

Figure 14. Taper glass fiber sensor

Whereas there is some technical reason to believe this process would work, the resulting remapping does not have good features with respect to providing a readable image. Further consideration will be given to this process and possible modifications to provide for useful transformations.

1. Fisher, Timothy E. and Richard D. Juday, "Programmable video image remapper," Proceedings of the SPI E 938, 122-128 (1988).
2. Juday, Richard D. and David S. Loshin, "Some examples of image warping for low vision prosthesis," Proceedings of the SPIE 938, 163-168 (1988).
3. Loshin, David S. and Richard D. Juday, "The Programmable Remapper: Clinical applications for patients with field defects," Optometry & Vision Science Vol. 66, No. 6, 389-395 (1989).
4. Juday, Richard D. and David S. Loshin, "Quasi-conformal remapping for compensation of human visual field defects: Advances in image remapping for human field defects," Proceedings of the SPIE 1053, 124-130 (1989).
5. Loshin, David S., Janice Wensveen and Richard D. Juday, "Design of a reading test for low vision image warping,"
6. Juday, Richard D., "Patterned Sensors for Human Low Vision," NASA Internal communication, September, 1992.

N94-25364

NEAR SURFACE ANALYSIS

Final Report
NASA/ASEE Summer Faculty Fellowship Program-1993
Johnson Space Center

Prepared by:	Gordon G. Johnson, Ph.D.
Academic Rank:	Professor
University & Department:	University of Houston Department of Mathematics Houston, TX 77004
NASA/JSC	
Directorate:	Software Technology
Division:	Information Technology
Branch:	Information Systems
JSC Colleague:	Lui Wang
Date Submitted:	August 23, 1993
Contract Number:	NGT-44-001-800

Abstract

This is a study to assist in the understanding of earth near surface structure. Higher order moments are used to detect the density distribution as well as to seek patterns found in geological structures. It is shown how higher order moments at points outside a mass structure are determined as well as how to recover the mass distribution from the higher order moments. It is interesting to note that the first moment at a point P outside the mass structure, $V_0(P)$, is the entire mass and the second moment, $V_1(P)$, is the potential at P due to the mass structure. Usually only the mass and the potential function are used to determine the density distribution in a body. In this study an infinite function sequence $\{V_n(P)\}_{n=0}^{\infty}$ is required to uniquely determine the density distribution.

Density Determination

Suppose that A is a material body, i.e., not a point mass, that is modeled by assuming that there is a non negative continuous function g defined on a closed and bounded subset K of euclidean three space E, where K is a geometric approximation of A and g is an approximation to the density function of A. Note that K need not be connected, i.e., K need not be "in one piece".

We shall denote the real number line by R, and the euclidean inner product on by $< \cdot , \cdot >$ which induces a norm $\| \cdot \|$. If r is a positive number and P is a point in E, then

$$S_r(P) = \{ Q \text{ is in } E: \| P - Q \| \leq r \}$$

and $$\text{Bdry}S_r(P) = \{ Q \text{ is in } E: \| P - Q \| = r \}.$$

Since K is bounded there is a number $r>0$ and a point C, the geometric center, of K such that K is contained in $S_r(C)$. Let D denote the complement of $S_r(C)$ in E.

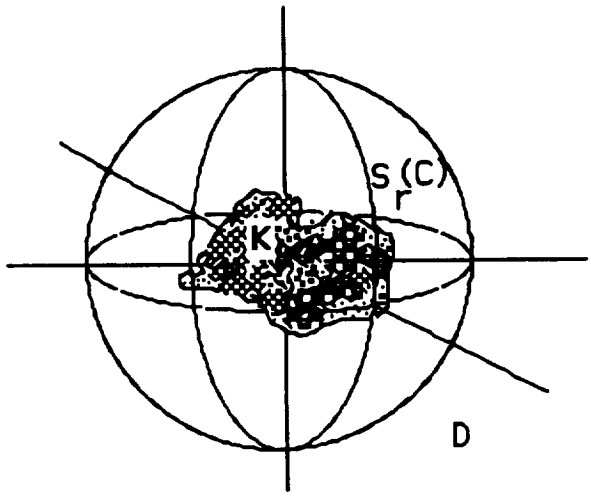

For each non negative integer n, V_n is the real valued function defined on D by

$$V_n(P) = \int_{S_r(C)} \frac{g(Q)}{\| P - Q \|^n} \, dQ \quad \text{for P in D.}$$

The above integral is a triple integral. Notice that $V_0(P)$ is the mass of K, and $V_1(P)$ is the Newtonian potential at P due to the mass K.

Suppose g is a non negative continuous function defined on E, S_1 is a ball containing K centered at the geometric center of K, S_2 is a ball properly containing S_1 that is concentric with S_1 and also g is zero on the complement of S_2.

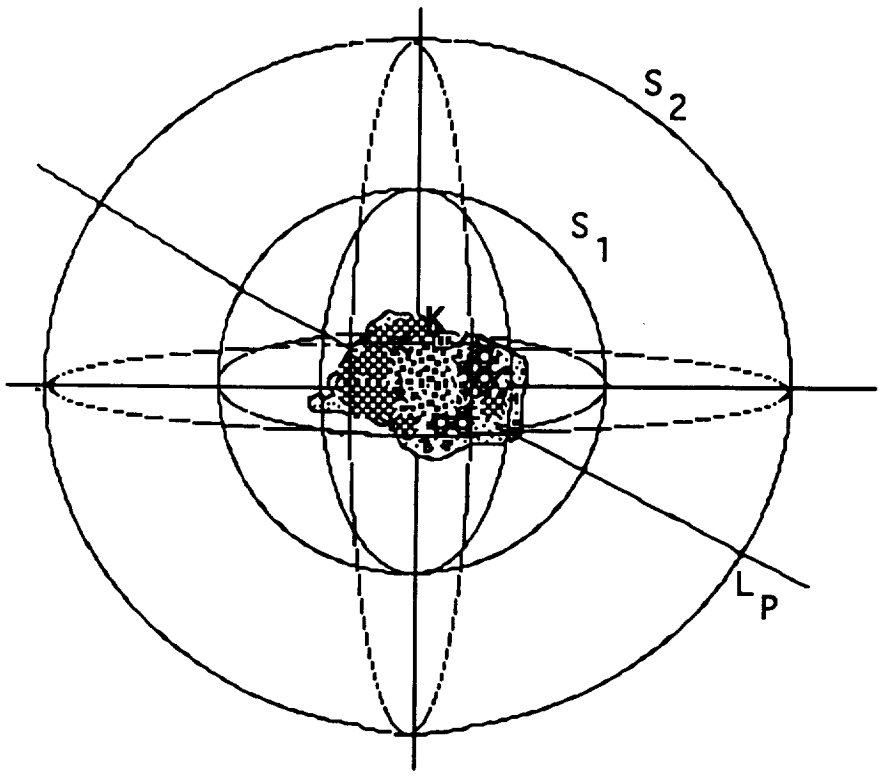

There is a one-to-one correspondence between the set
$V = \{ \{ V_n(P) \}_{n=0}, P \text{ is in the complement of sphere } S_2 \}$
and g, moreover g can be constructed from the set V.

Suppose P is in D. Let m_P be the mass function defined on the real line R by

$$m_P(x) = 0 \text{ if } x \leq 0$$

and $$m_P(x) = \int_{S_x(P)} g(Q)\, dQ \text{ if } x > 0.$$

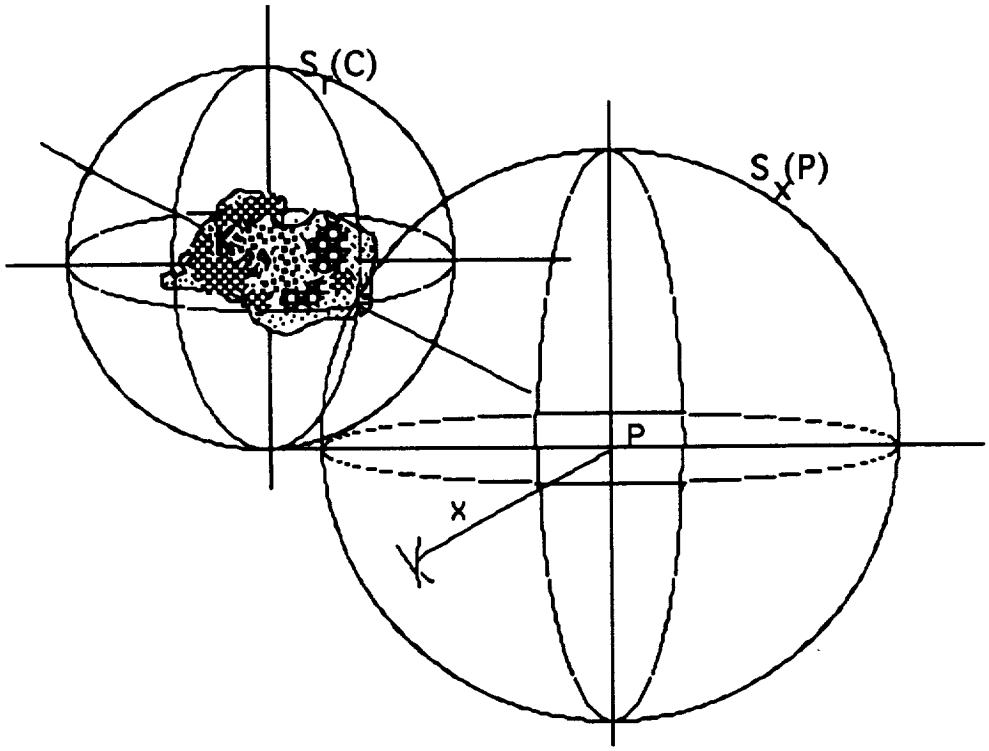

Observe that for each point P in D, m_P is a real-valued, non decreasing continuous function on R, which has a continuous derivative and hence is of bounded variation on R. (Recall that m_P is constant except on a finite interval of the line.)

$m'_P(x) = 0$ if $x \leq 0$,

$m'_P(x) = \int_{S_r(C) \cap \text{Bdry}S_x(P)} g(x,z)\, dz$ if $S_r(C)$ intersects $\text{Bdry}S_x(P)$, and

$m'_P(x) = 0$ if $x > 0$ and $S_r(C)$ does not intersect $\text{Bdry}S_x(P)$.

If P is a point, then

$$u_P = \inf \{ \| P - Q \| : Q \text{ is in } S_r(C) \} = \| P - C \| - r$$
$$v_P = \sup \{ \| P - Q \| : Q \text{ is in } S_r(C) \} = \| P - C \| + r.$$

Observe that $V_n(P) = \int_{u_P}^{v_P} (1/t^n)\, dm_P(t)$ for n = 0,1,2, . . .

Making a change of variables $s = 1/t$ for $u_P \le t \le v_P$, we have

$$V_n(P) = \int_{u_P^{-1}}^{v_P^{-1}} s^n \, dm_P(1/s) \quad \text{for } n = 0,1,2, \ldots$$

Define for each point P in D

$$A_P = v_P^{-1}, \qquad B_P = u_P^{-1}$$

and $$M_P(x) = M - m_P(1/x) \qquad A_P \le x \le B_P.$$

Note that $M_P(A_P) = 0$, and $M_P(B_P) = M$,
hence extend M_P to $(0, B_P)$ by defining $M_P(x) = 0$ for $0 \le x \le A_P$.
Finally
$M'_P(A_P) = m'_P(1/A_P)(1/A_P^2) = 0$ and hence M_P has a continuous derivative on $(0, B_P)$.
We now have

$$V_n(P) = \int_0^{B_P} x^n \, dM_P(x) \quad \text{for } n = 0,1,2,3 \ldots,$$

$M'_P(B_P) = m'_P(1/B_P)(1/B_P^2) = 0,$
and the sequence $\{V_n(P)\}_{n=0}$ satisfies the Hausdorf conditions (See appendix 1).

Suppose for each point P on the surface of S_2, where S_2 is a sphere properly containing and concentric with the sphere S_1 which contains K, with center C, (the geometric center of K), the sequence

$$\{ V_n(P) \}_n^{\infty} \quad \text{is known.}$$

For each such point P consider the line L_P containing P and C the center of S_1.

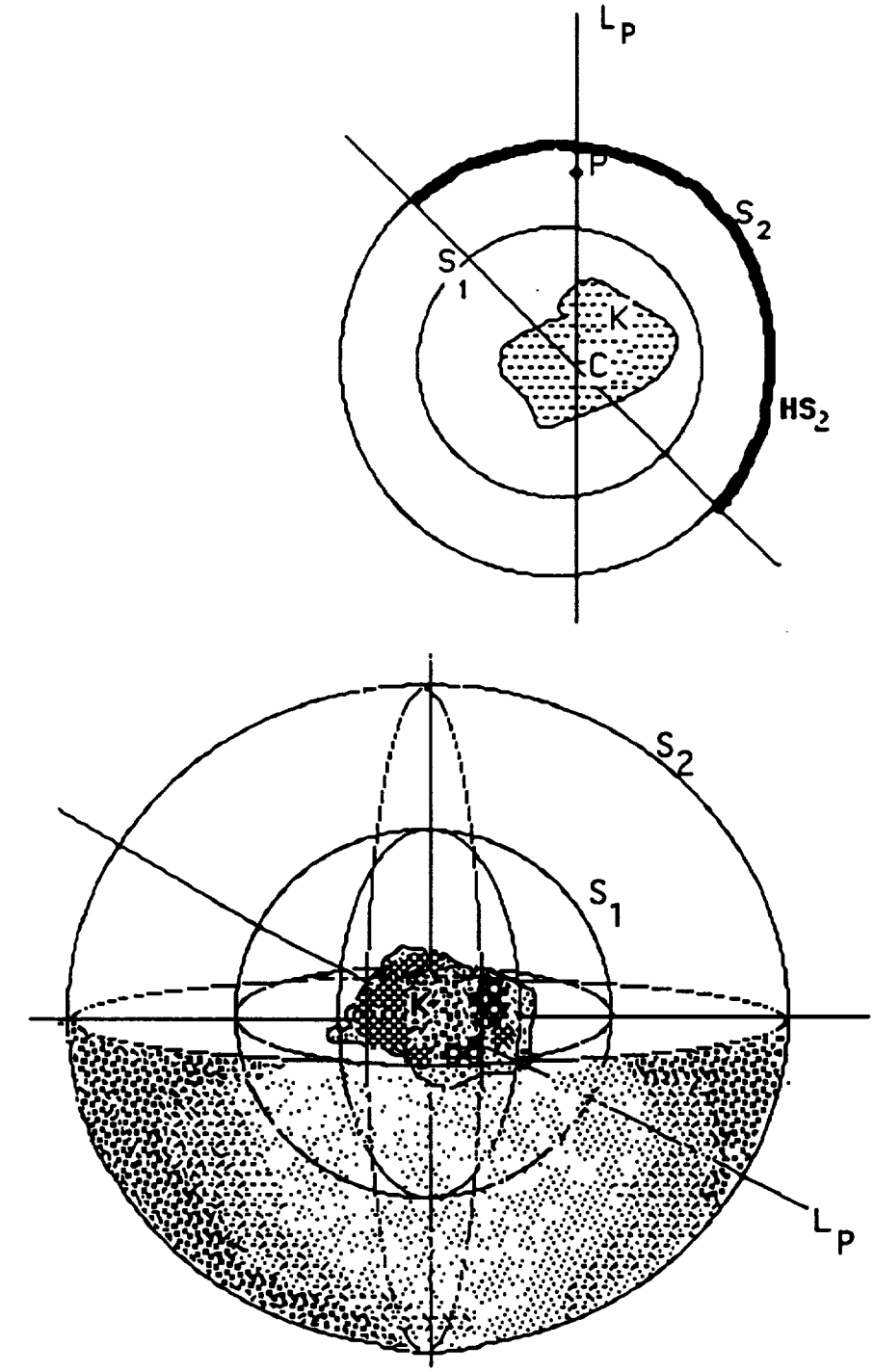

From the sequence $\{V_n(P)\}_n^{\infty}$ we can recover (see A1) the function m_P. Hence for each point P on S_2 we have m_P, then using the method of bilinear forms we may recover (see appendix 2) the function g.

APPENDIX A1

Suppose that the number sequence $\{C_n\}_{n=0}^{\infty}$ is known and satisfies the Hausdorf Condition i.e., there is a positive number H such that

$$\sum_{t=0}^{n} B(n,t) \left| \sum_{s=0}^{n-t} B(n-t,s)\,(-1)^s\, C_{t+s} \right| < H \qquad \text{for } n = 0,1,2,\ldots$$

where B(n,t) is the binomial coefficient $n!/(t!\,(n-t)!)$.

For each non negative in n and each number x in the number interval [0,1] define

$$g_n(x) = \sum_{t=0}^{w} B(n,t) \sum_{s=0}^{n-t} B(n-t,s)\,(-1)^s\, C_{t+s} \quad \text{if } w/n \le x < ((w+1)/n).$$

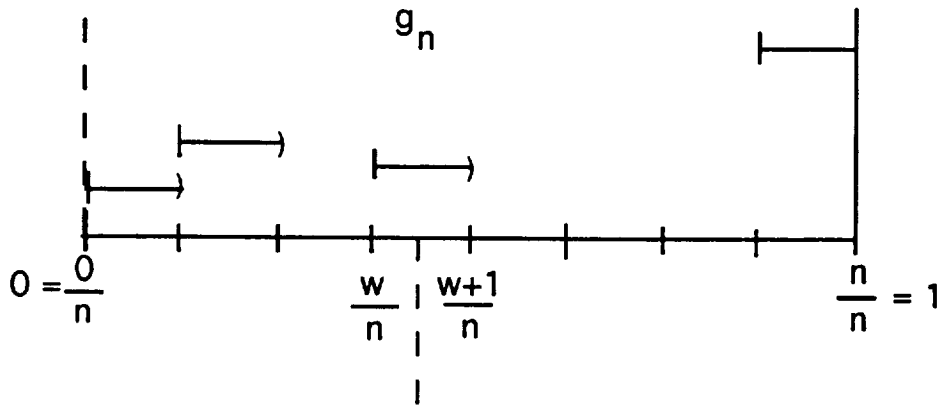

The function sequence g_n then converges pointwise to a function g on [0,1]. The function g is of bounded variation on [0,1] with total variation not exceeding H and has the property that

$$\int_0^1 x^n \, dg(x) = C_n \qquad \text{for } n = 0,1,2,\ldots .$$

APPENDIX A2

If for each point P on the surface of a hemisphere we know $M_P(x)$, then we can determine g on K in the following manner.

A sequence of functions is created that will converge pointwise to g, on a dense subset of S_2 (**g** is the restriction of g to the dense subset). Since g is continuous, we can extend **g** to g on S_2 .

We define for each positive integer n a function f_n on the three dimensional normalized grid G_n.

$$f_n(x, y, z) = \sum_{i=1}^{n} \sum_{j=1}^{n} \sum_{k=1}^{n} \Phi_i(x)\, \Phi_j(y)\, \Phi_k(z)\, w_{ijk} \quad \text{for the point } (x,y,z)$$

in the grid G_n where n +1 is the number of grid points on a side and h is 1/n. The problem is to determine w_{ijk} for $1 \le i,j,k \le n$.

Below is a two dimensional schematic to suggest the three dimensional case.

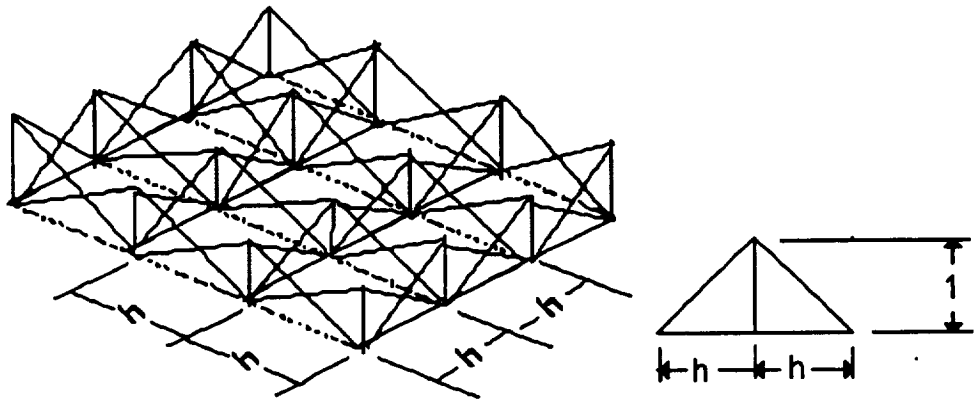

Φ function on grid Typical Φ function

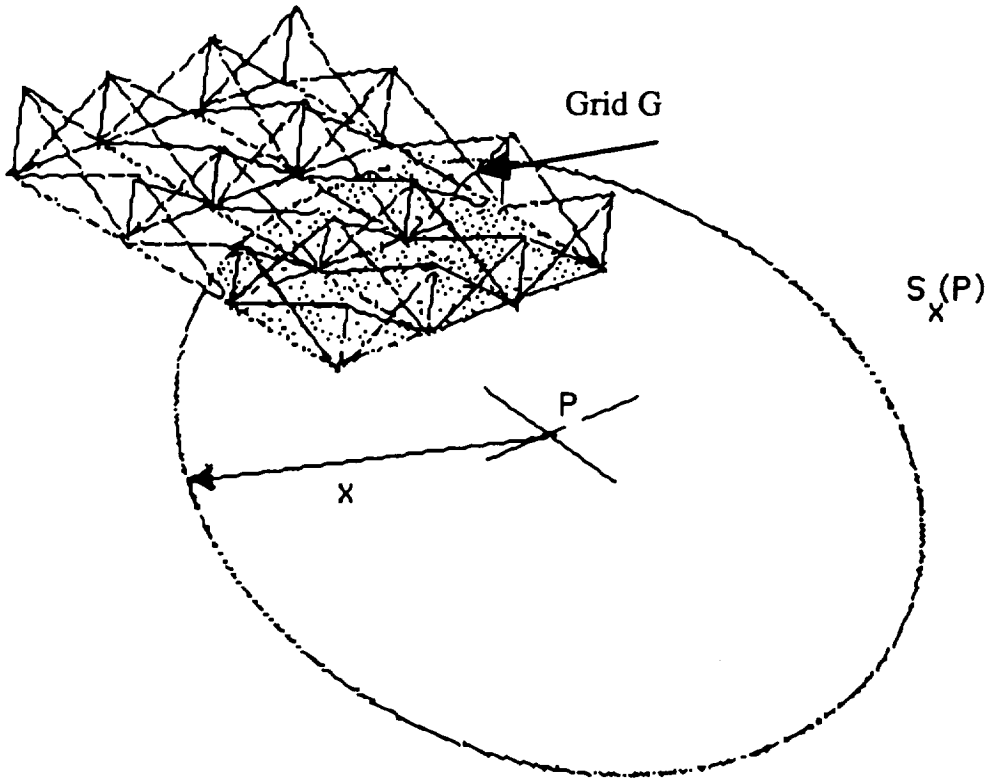

The function f_n is integrated over the same portion of the grid as is intersected by the sphere centered at a point P of radius r (see schematic figure below) and set equal to $m_P(r)$, which was constructed from the sequence $\{V_n(P)\}_n$. By selecting various points P and various radii we have a system of linear equations in w_{ijk} that we can solve and thus determine the function f_n. As stated before, the sequence $\{f_n\}_n$ converges pointwise on dense subset to **g**, which is then extended to the function g.

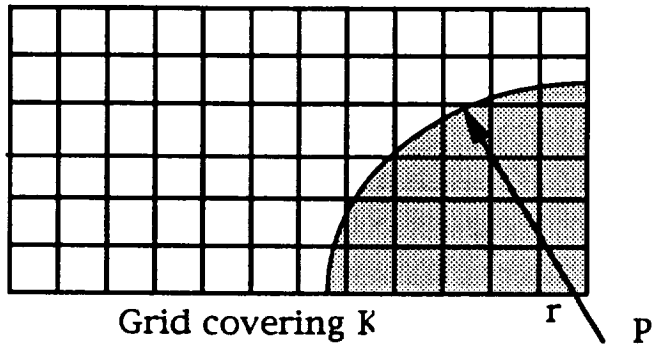

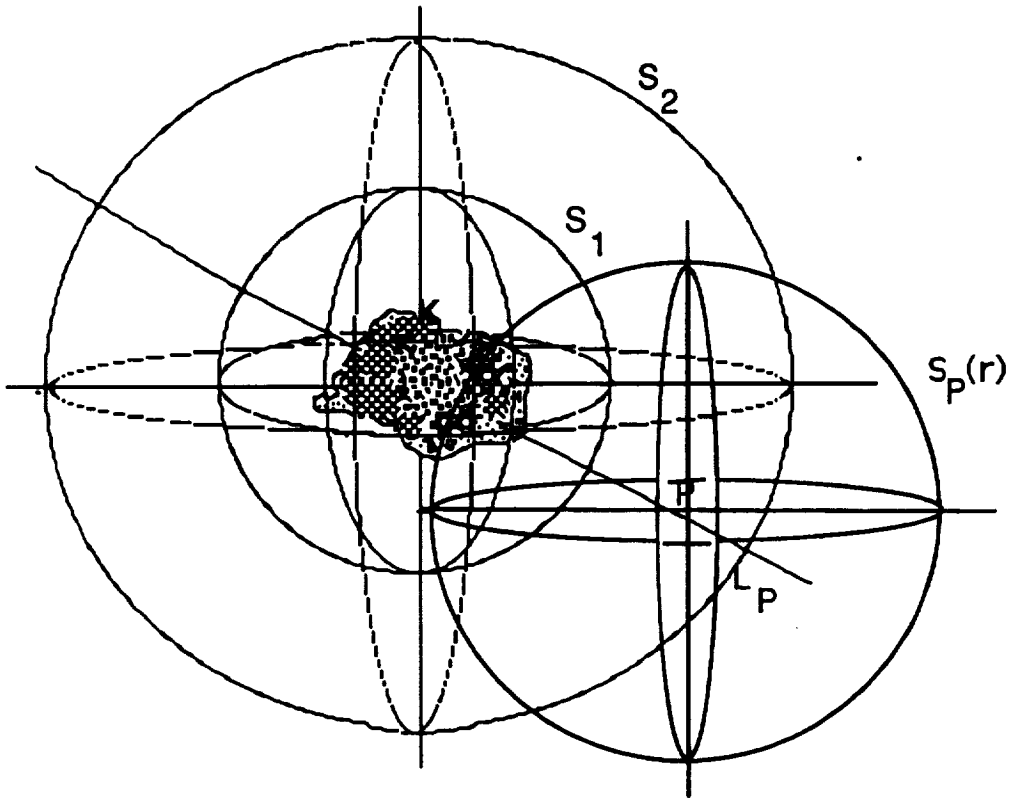
S_2
S_1
$S_P(r)$
P
L_P

N94- 25365

INFLUENCE OF TEST CONFIGURATION ON THE COMBUSTION CHARACTERISTICS OF POLYMERS AS IGNITION SOURCES

Final Report

NASA/ASEE Summer Faculty Fellowship Program -- 1993

Johnson Space Center

Prepared By:	Howard L. Julien
Academic Rank:	Associate Professor
University & Department:	New Mexico State University Mechanical Engineering Dept. Box 30001/Dept. 3450 Las Cruces, NM 88003-0001
NASA/JSC	
Directorate:	White Sands Test Facility
Division:	Laboratories Office
JSC Colleague:	Harold D. Beeson
Date Submitted:	August 10, 1993
Contract Number:	NGT-44-001-800

ABSTRACT

The experimental evaluation of polymers as ignition sources for metals has been accomplished at the NASA White Sands Test Facility (WSTF) using a standard promoted combustion test. These tests involve the transient burning of materials in high-pressure oxygen environments. They have provided data from which design decisions can be made; data include video recordings of ignition and non-ignition for specific combinations of metals and polymers. Other tests provide the measured compositions of combustion products for polymers at select burn times and an empirical basis for estimating burn rates. With the current test configuration, the detailed analysis of test results requires modeling a three-dimensional, transient convection process involving fluid motion, thermal conduction and convection, the diffusion of chemical species, and the erosion of the sample surface. At the high pressure extremes, it even requires the analysis of turbulent, transient convection where the physics of the problem are not well known and the computation requirements are not practical at this time.

An alternative test configuration that can be analyzed with a relatively-simple convection model was developed during the summer period. The principal change constitutes replacing a large-diameter polymer disk at the end of the metal test rod with coaxial polymer cylinders that have a diameter nearer to that of the metal rod. The experimental objective is to assess the importance of test geometries on the promotion of metal ignition by testing with different lengths of the polymer and, with an extended effort, to analyze the surface combustion in the redesigned promoted combustion tests through analytical modeling of the process. The analysis shall use the results of cone-calorimeter tests of the polymer material to model primary chemical reactions and, with proper design of the promoted combustion test, modeling of the convection process could be conveniently limited to a quasi-steady boundary layer analysis where the economical solution of parabolic equations is involved.

The products for the summer period are: (1) a conceptual-level redesign of the test apparatus, and (2) the development and use of an approximate integral boundary layer analysis to demonstrate the influence of geometry changes prior to testing. A computer code STAN5, an accurate numerical boundary layer model whose earlier versions were developed for the NASA Lewis Research Center by the Fellow, also was installed and validated on the WSTF and New Mexico State University computer systems as a starting point in the development a more detailed fluid mechanics and combustion model.

INTRODUCTION

The standard promoted combustion tests performed at the White Sands Test Facility (WSTF) have been used by NASA, DOD and industry to select materials for oxygen systems where polymer materials are used for seals, seats, etc. The burning of metals in the presence of various burning polymers can be ranked with the data obtained. However, there is not a clear understanding of the importance of the test configuration on the test results or the possible influence of the configuration in the oxygen system of primary interest.

A redesign of the test configuration to facilitate a more convenient analysis of the test geometry and the combined fluid mechanics/combustion processes near the surface of the burning material was undertaken. The objectives for the summer period were to identify design changes and to demonstrate through a preliminary approximate boundary layer analysis that configuration dependent parameters must be considered.

An overview of the results of the investigation are described in this report, with specific details being available to the reader upon request. The design changes in the standard test are first described. This is followed by an outline of the approximate integral boundary layer analysis and the numerical results obtained for one representative polymer. Then, the more accurate numerical model STAN5 that was installed on the WSTF and New Mexico State University computer systems for future investigations is described. Conclusions and recommendations for future work are presented at the end of the report.

SYMBOLS

A	Surface area, m^2
b	Blowing parameter, defined in Eq. (8)
c_p	Specific heat at constant pressure, J/(kg K)
C_f	Friction factor, defined in Eq. (9)
F	Constants, defined in Eqs. (10)-(12)
g_c	Conversion constant in Newtons Second Law, kg m/s^2N
Gr_x	Local Grashof number, based on position x
i	Enthalpy, J/kg
i^*	Stagnation enthalpy, J/kg
J	Conversion constant, work equivalent of energy
k	Thermal conductivity, $W/(m^2 K)$
m''	Mass flux, kg/m^2
m_j	Mass concentration of component j, kg per kg of mixture
P	Pressure, Pa
Q	Heat transfer rate, W
q''	Heat flux, W/m^2
r	Radial distance in cylindrical coordinates, m
T	Temperature, K
u	Velocity in x-direction, m/s
u'	Instantaneous value of fluctuating velocity component in x-direction, m/s
u_l	Characteristic velocity, m/s
v	Velocity in y-direction, m/s
v'	Instantaneous value of fluctuating velocity component in y-direction, m/s
X	Body force in x-direction, N

x	Distance along surface of body, m
y	Distance normal to surface of body, m
β	Volumetric coefficient of thermal expansion, K^{-1}
γ_j	Mass diffusion coefficient for substance j in a mixture, kg/(m s)
δ	Boundary layer thickness, m
ϵ	Emissivity of polymer surface
μ	Dynamic viscosity, (N s)/m^2
ν	Kinematic viscosity, m^2/s
ρ	Density, kg/m^3
σ	Stefan-Boltzmann constant, $W/(m^2 K^4)$
τ	Shear stress, Pa
ψ	Parameter, defined in Eq.

Subscripts:

e	Refers to entrained fluid at edge of the boundary layer
o	Refers to value at surface
R	Refers to radiation
∞	Refers to position outside boundary layer

DESCRIPTION OF TEST GEOMETRY AND THE PROPOSED CHANGES

Figure 1 is a sketch of the modified test chamber with the test samples shown. The changes made to the test chamber included:

- Addition of a top view port to analyze cumulative products of combustion for the purpose of calibrating and confirming the boundary layer analysis

- Addition of a quartz cylinder to collect and direct products of combustion to top view port.

The selection of instrumentation required for chemical analysis has not been made and the experimental evaluation of possible problems associated with gas collection in a quartz tube and the possible condensation of metals making the tube opaque have not been made. With these minimal changes, the test chamber should continue to provide for testing with gas pressures up to 69 MPa.

Another major change in the test involves replacing the flat disk polymer sample with a cylindrical polymer sample that is nearer the diameter of the metal rod sample. Figure 2 compares the current configuration with a proposed "carrot shape" configuration based on the integral boundary layer analysis performed. The proposed shape reflects a variable burning rate for the polymer that after a period of time will result in coaxial polymer and metal cylinder samples of equal diameter; at that particular instant in time, a quasi-steady boundary layer flow can be assumed and modeled. With this change, the effects test configuration can be evaluated by testing polymer samples of different length giving different thermal conditions at the polymer-metal interface.

Average burning rates were estimated for a polyethylene sample using measured burning rates for a disk sample recently tested by Shelly et al. (1993). The test samples

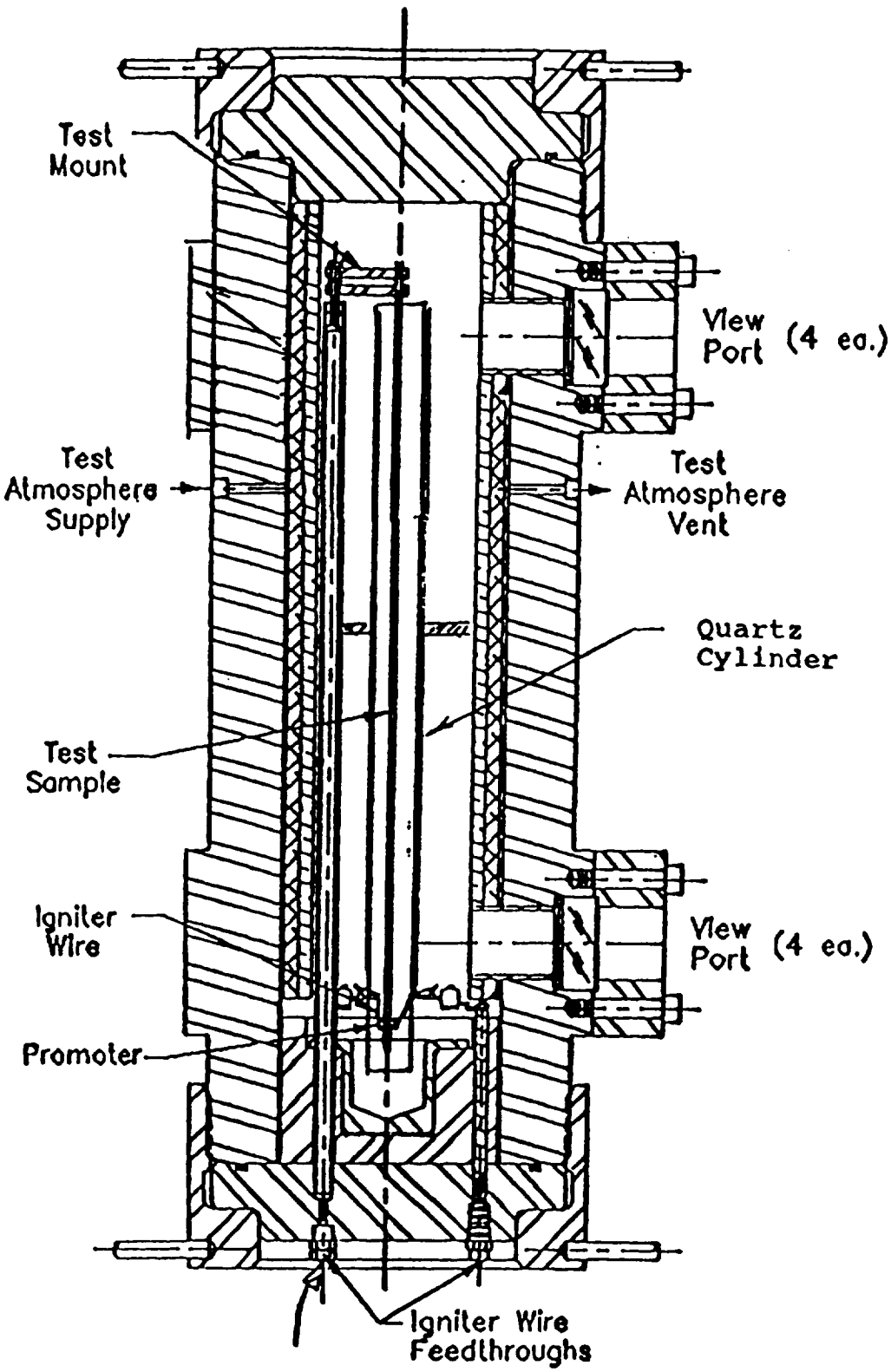

Figure 1. - Modified Test Chamber for Promoted Igntion Tests.

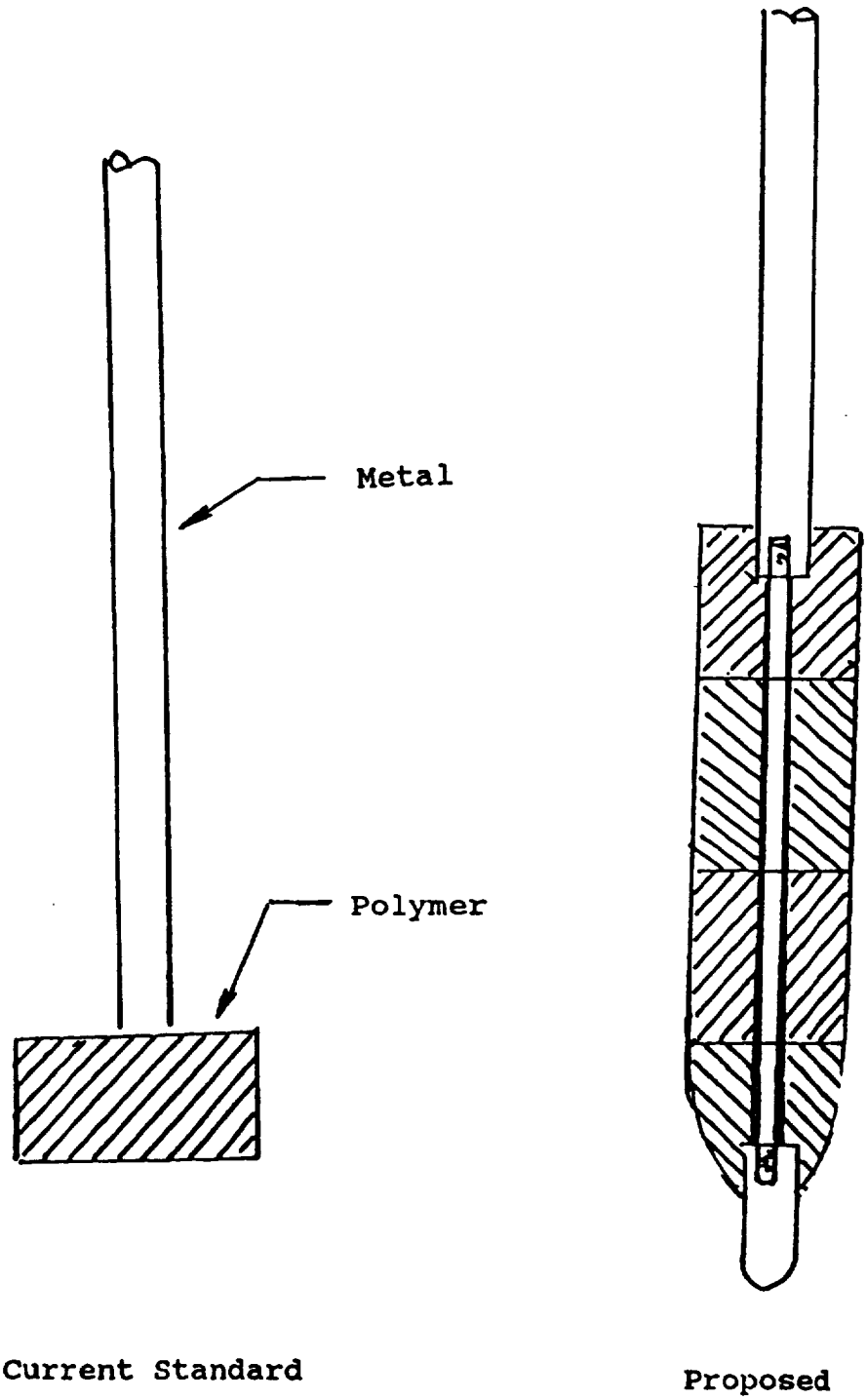

Figure 2. - Comparison of Proposed Polymer Sample Shape with Current Standard Disk Shape.

compared in Figure 2 were calculated to have the same total burn times, assuming the surface burn rate is uniform with the disk sample. However, this estimate is considered to be inaccurate based on recent simulations made with the numerical boundary layer code STAN5 and the actual shape of the polymer required to achieve a well-defined boundary layer flow must be determined experimentally.

At a minimum, the proposed configuration provides for a convenient mathematical model to sort and analyze the effect of test configuration with an analysis of a natural convection boundary layer flow. Even the approximate integral boundary layer analysis of this flow already explains some of the different burning behavior of polyethylene and teflon observed by Shelly.

APPROXIMATE INTEGRAL BOUNDARY LAYER ANALYSIS

An approximate solution to the boundary layer equations can be obtained by integrating the equations across the thickness of the boundary layer and incorporating profile shapes for velocity and temperature. Following a procedure first used by Eckert and Jackson (1950), an integral analysis of this type was performed for assumed turbulent natural convection at the surface of a burning polymer in the proposed test configuration.

Integral Equations of the Boundary Layer

The integral equations considered are those used by Eckert and Jackson with an additional term added to the energy equation to account for convected energy at the surface due to the release of combustion products. The equations solved are:

$$-\tau_o = -g\beta\int_0^{\infty}\rho(T-T_\infty)dy + \frac{1}{r}\frac{d}{dx}\left(r\int_0^{\infty}\rho u^2 dy\right) \tag{1}$$

$$q_o'' = \frac{c_p}{r}\frac{d}{dx}\left(r\int_0^{\infty}\rho u T dy\right) - m_o'' c_p T_o \tag{2}$$

The radius r is constant in this application and, consequently, it does not appear in the equations actually solved.

The assumed profiles shapes for velocity and temperature are typical 1/7th power profiles for turbulent flow:

$$\frac{u}{u_1} = \left(\frac{y}{\delta}\right)^{1/7}\left[1-\frac{y}{\delta}\right]^4 \tag{3}$$

$$\frac{T-T_\infty}{T_o-T_\infty} = 1-\left(\frac{y}{\delta}\right)^{1/7} \tag{4}$$

The solution provides algebraic expressions for the boundary layer thickness δ and characteristic velocity u_1 used in these equations.

Shear, Heat Flux, and Mass Transfer at the Polymer Surface

The procedure used by Eckert and Jackson to represent surface exchange parameters τ_o and q_o'' in the integral equation was adopted. Correlations developed for forced convection are used with the free-stream velocity replaced by the characteristic velocity u_1; the resulting correlation for convective heat transfer was found by Eckert and Jackson to agreed reasonably well with experiment. Specific correlations for wall shear and heat flux are:

$$\tau_o = 0.0225\rho u_1^2 \Psi \left(\frac{\nu}{u_1 \delta}\right)^{1/4} \tag{5}$$

$$\frac{q_o''}{\rho c_p u_1 (T_o - T_\infty)} = 0.0225 \Psi \left(\frac{\nu}{u_1 \delta}\right)^{1/4} \tag{6}$$

Here, the term Ψ is a modification to account for mass transfer at the surface; it is defined:

$$\Psi = \frac{b}{e^b - 1}, \tag{7}$$

where b is a blowing parameter,

$$b = \frac{m_o''/\rho u_1}{(C_f/2)_o} . \tag{8}$$

The denominator in Eq. (8) is the friction factor for the case of no blowing at the wall, i.e.,

$$(C_f/2)_o = \left(\frac{\tau_o}{\rho u_1^2}\right)_o . \tag{9}$$

The reader is referred to Kays and Crawford (1993) for a complete development of this correlation for turbulent forced convection with moderate surface blowing.

General power functions of the position x along the surface are assigned to δ and u_1; then, the exponents are determined by substitution of the assumed profiles and these correlations into the integral equations. The wall shear and heat flux must necessarily vary as a power of x;, and, by analogy, the mass transfer at the polymer surface must have the same power relationship. The resulting rate equations are:

$$\tau_o = F_f\, x^{0.2} \tag{10}$$

$$q_o'' = F_q\, x^{0.2} \tag{11}$$

$$m_o'' = F_m\, x^{0.2} \tag{12}$$

The constants F_f, F_q, and F_m are determined from the solutions for δ and u_1. The "carrot shape" shown in Figure 2 corresponds to Eq. (12) with the constant F_m determined for polyethylene.

Solutions for δ and u_1

The solutions for δ and u_1 are:

$$\delta = C_\delta\, x^{0.5}, \qquad u_1 = C_u\, x^{0.7} \tag{13}$$

where the constants C_δ and C_u are determined from the aforementioned substitution of profiles and correlations into the integral equations. The thermal boundary conditions and overall mass transfer rates adopted were established using measured burning rates and a convenient surface combustion model.

Surface Combustion Model

Stoichiometric combustion at the surface of the polymer is assumed for the estimated surface burning rates. The corresponding oxidant-to-fuel ratio on a mass basis is 4.51 for polyethylene and 0.32 for teflon.

Surface combustion temperatures were calculated using adiabatic flame temperatures obtained by Shelly et al. (1993) with the Gordon and McBride code (1971) and a correction for radiation losses to the chamber based on a small body in a large enclosure model. The radiation correction is:

$$Q_R = \epsilon A \sigma \left(T_o^4 - T_\infty^4\right) \tag{14}$$

Numerical Results

Table 1 presents numerical results obtained for polyethylene in oxygen at five test pressures. Four observations are:

- The flame temperatures are shown to be a strong function of test pressure; this is a result of the burning rates increasing with pressure and the radiation correction having a relatively smaller effect.

- The high flame temperatures at the higher pressures exceed the ignition temperatures of some metals.

- At all test pressures, the blowing parameter b is shown to be high in comparison to a value of 4 corresponding to "blowoff" and boundary layer separation; hence, the assumption of moderate blowing is violated and a need for a more accurate model is indicated.

- The last column is the ratio of oxidant entrained in the boundary layer to the mass of polymer burned at the surface. In all cases, this ratio is below the stoichiometric oxidant-to-fuel ratio of 4.51 and the achievement of surface combustion only cannot be met; another violation of a model assumption. However, this result is corroborated by the data of Shelly et al. where a wide diffusion flame with combustion in the boundary layer was observed.

TABLE 1. - RESULTS OF INTEGRAL BOUNDARY LAYER CALCULATIONS.

P (Mpa)	T_f (K)	C_δ	C_u	b	m_e''/m_o''
3.4	2022	0.1034	4.8673	3.48	3.48
6.9	2204	0.0805	4.5150	2.87	3.24
20.4	2610	0.0636	4.5969	2.60	3.32
34.4	3043	0.0751	4.7239	3.63	3.11
68.9	3294	0.0565	4.7304	1.60	3.25

The assumption of turbulent natural convection was confirmed by the calculated Grashof numbers Gr_x at x equal to 10 mm. Values range between 10^6 at the lowest test pressure to 10^{11} at the highest test pressure.

Velocity and temperature profiles constructed from these numerical results vary in both magnitude an extent beyond the polymer surface as the boundary layer develops. It follows that different thermal and flow conditions can be achieved at the interface of the polymer and metal rod samples by simply extending the length of the polymer test sample.

Numerical results were not obtained for teflon. However, the mass ratios for teflon are expected to be comparable to those calculated for polyethylene and the achievement of a stoichiometric mass ratio of 0.32 at the surface is considered quite feasible. This result is also corroborated by the observations of Shelly et al. where near surface combustion was observed with the teflon samples.

STAN5 - A NUMERICAL COMPUTER MODEL

The inability to validate model assumptions made in the integral analysis indicated that a more detailed model accounting for combustion in the boundary layer flow is needed. The computer code STAN5, previously developed for NASA by Kays et. al. [Julien (1969, 1971), Kays and Crawford (1976)] at Stanford University, was acquired from the NASA Lewis Research Center for this purpose. It is a version of a general purpose boundary layer calculation code developed by Patankar and Spaulding [Patankar and Spaulding (1967, 1970),

energy and the diffusion equations for any number of species; in particular, the equations solved are:

$$\frac{\partial}{\partial x}(r\rho u) + \frac{\partial}{\partial y}(r\rho v) = 0 \tag{15}$$

$$\rho u\frac{\partial u}{\partial x} + \rho v\frac{\partial u}{\partial y} = g_c X - g_c\frac{dP}{dx} + \frac{1}{r}\frac{\partial}{\partial y}\left[r\left(\mu\frac{\partial u}{\partial y} - \rho\overline{u'v'}\right)\right] \tag{16}$$

$$\rho u\frac{\partial i*}{\partial x} + \rho v\frac{\partial i*}{\partial y} = \frac{1}{r}\frac{\partial}{\partial y}\left(r\left[\frac{k}{c}\frac{\partial i*}{\partial y} - \rho\overline{i*'v'} + \sum_j \gamma_j\frac{\partial m_j}{\partial y}i_j + \frac{\mu}{g_c J}\frac{\partial}{\partial y}\left(\frac{u^2}{2}\right)\right]\right) + \frac{uX}{J} \tag{17}$$

$$\rho u\frac{\partial m_j}{\partial x} + \rho v\frac{\partial m_j}{\partial y} = \frac{1}{r}\frac{\partial}{\partial y}\left(r\left[\gamma_j\frac{\partial m_j}{\partial y} - \rho\overline{v'm_j'}\right]\right) + \dot{m}_j''' \tag{18}$$

This computer program has been installed on both the WSTF and NMSU computer systems in preparation for future more detailed analysis. Test runs have been made and some initial modeling of boundary layer flows on a burning polymer sample has been accomplished; but, combustion in the boundary layer flow and species transport were not considered.

The analysis of the boundary layer flow with combustion does require detailed thermodynamic data for the test polymers. To obtain these data, a test program involving the use of a cone-calorimeter developed by Hshieh et. al. (1993) is being considered as a possible parallel research activity at WSTF.

CONCLUSIONS

1. The revised promoted combustion tests should provide for the evaluation of configuration specific parameters on test results. Different thermal and flow conditions can be achieved near the metal sample by simply changing the length of the polymer sample in the new test configuration.

2. An approximate integral boundary layer analysis demonstrated the capability to evaluate configuration specific parameters in the revised test and did explained some of the visual test observations made by Shelly et. al. in recent promoted combustion tests. However, basic assumptions of moderate mass injection and stoichiometric combustion at the polymer surface were found not to be valid.

3. A numerical boundary layer prediction code STAN5 has been made available and it is capable of analyzing more accurately and in greater detail the revised promoted combustion tests. And the required thermodynamic data to address combustion within the boundary layer flow can be obtained in a parallel test program at WSTF.

RECOMMENDATION

Continuation of this research activity through Academic Year 93/94 and Summer 1994 is recommended. This should be accomplished in parallel with the test program to obtain requisite thermodynamic properties of polymers. And, it should be followed by the modification of the test chamber and development of the revised promoted ignition test.

REFERENCES

Eckert, E. R. G. and T. W. Jackson. "Analysis of Turbulent Free-Convection Boundary Layer on Flat Plate." *NACA Technical Note 2207* (Superseded by NACA Report 1015). Washington, D.C., 1950.

Gordon, S. and B. J. McBride. "Computer Program for Calculation of Complex Chemical Equilibrium Compositions, Rocket Performance Incident and Reflected Shocks, and Chapman-Jouguet Detonations." *NASA SP-273*, Washington, D.C., 1971.

Hshieh, F. Y., S. E. Motto, D. B. Hirsch, and H. D. Beeson. "Flammability Testing of Materials in Oxygen-Depleted and Oxygen-Enriched Environments Using a Controlled-Atmosphere Cone Calorimeter." Presented at the *Intl. Symposium on Heat Release and Fire Hazard*, Intl. Heat Release Assoc., Tsukuba, Japan, 1993.

Julien, H. L. *The Turbulent Boundary Layer on a Porous Plate: Experimental Study of the Effects of a Favorable Pressure Gradient*. PhD. Thesis, Dept. of Mechanical Engineering, Stanford University. Stanford, CA, 1969.

Julien, H. L., W. M. Kays, and R. J. Moffat. "Experimental Hydrodynamics of the Accelerated Turbulent Boundary Layer With and Without Mass Injection." *ASME J. of Heat Transfer*, Vol. 93, New York, NY, 1971.

Kays, W. M. and M. E. Crawford. "STAN5 - A Program for Numerical Computation of Two-Dimensional Internal and External Boundary Layer Flows." *NASA Contractor Report 2742*, Washington, DC, 1976.

Kays, W. M. and M. E. Crawford. *Convective Heat and Mass Transfer*, 3rd Ed. New York, NY: McGraw-Hill Book Co. 1993.

Patankar, S.V. and D. B. Spaulding. *Heat and Mass Transfer in Boundary Layers*, 1st Ed. London, England: Morgan-Grampian, 1967.

Patankar, S.V. and D. B. Spaulding. *Heat and Mass Transfer in Boundary Layers*, 2nd Ed. London, England: International Textbook Company Ltd., 1970.

Shelley, R. M., D. B. Wilson, and H. D. Beeson. "Combustion Characteristics of Polymers as Ignition Promoters." *Flammability and Sensitivity of Materials in Oxygen-Enriched Atmospheres: Sixth Volume, ASTM STP 1197*. J.M. Stoltzfus and D. Janoff, Eds. Philadelphia, PA: American Society for Testing and Materials, 1993.

Spaulding, D. B. "A General Computer Program for Two-Dimensional Boundary-Layer Problems." *Report HTS/73/48*, Dept. of Mechanical Engineering, Imperial College of Science and Technology. London, England, 1973.

N94- 25366

CONSIDERATIONS REGARDING THE DEPLOYMENT OF HYPERMEDIA AT JSC

Final Report
NASA/ASEE Summer Faculty Fellowship Program - 1993
Johnson Space Center

Prepared By:	Charles J. Kacmar, Ph.D.
Academic Rank:	Assistant Professor
University & Department:	Florida State University Department of Computer Science Tallahassee, Florida 32306

NASA/JSC

Directorate:	Engineering
Division	Automation and Robotics
Branch:	Intelligent Systems
JSC Colleague:	Jack Bacon
Date Submitted:	July 30, 1993
Contract Number:	NGT-44-001-800

ABSTRACT

Electronic documents and systems are becoming the primary means of managing information for ground and space operations at NASA. These documents will utilize hypertext and hypermedia technologies to aid users in structuring and accessing information. Documents will be composed of static and dynamic data with static data consisting of traditional objects such as text, graphics, audio and video and dynamic data consisting of user-defined annotations and hypermedia links.

The report consists of three major sections. First, it provides an overview of hypermedia and surveys the use of hypermedia throughout JSC. Second, it briefly describes a prototypical hypermedia system that was developed in conjunction with this work. This system was constructed to demonstrate various hypermedia features and to serve as a platform for supporting the electronic documentation needs for the MIDAS system developed by the Intelligent Systems Branch of the Automation and Robotics Division [Pac92]. Third, it discusses emerging hypermedia technologies which have either been untapped by vendors or present significant challenges to the Agency.

INTRODUCTION

The purpose of this document is to provide a brief overview and assessment of hypermedia[1] use at the Johnson Space Center. Due to the variety of applications which utilize, behave like, or plan to incorporate hypermedia, it is not the purpose of this document to argue a specific set of requirements. However, this document will discuss some of the primary and advanced hypermedia capabilities that relate to ongoing work at JSC.

The concepts in this document are a result of many interactions with groups throughout JSC. The author worked closely with staff of and contributed specifically to the Electronic Documentation (EDP) and HYPERMAN projects. Although many systems were viewed and a prototype was constructed, this report will not focus on any particular hypermedia model or system.

Organization

This report consists of three major sections. The first section will present an overview of hypermedia and establish terminology which will be used throughout the remainder of the report. Included in this section are small scenarios and discussions of capabilities that are characteristic of hypermedia systems. Section two presents a very brief overview of a prototype hypermedia system which demonstrates hypermedia features and provides a platform for supporting electronic documentation. Section three discusses features which are important to JSC but do not appear to be adequately addressed by vendors. Thus, systems which lack these features may not be sufficient to meet some of the current and especially the future needs of the Center. The lack of support for these features also indicates areas for future research and further investigation.

BACKGROUND

Hypermedia

Hypermedia is a methodology for storing and accessing information by association. It allows relationships to be defined among information objects to provide access to those objects by navigation.

For the purpose of this document we define the basic components of hypermedia to be *nodes, objects, anchors, links,* and *link markers*[2]. Nodes are objects which contain other objects, i.e. a container, including other nodes. An object is an entity which has content or substance such as a text string with attributes and values. An object may be composed

[1] The terms *hypertext* and *hypermedia* will be regarded as synonymous in this document [Nel65].

[2] Actual terminology used at JSC for these entities is slightly different. A *link* is an action that associates two objects. There are two basic types of links: a *traversal link* which causes the user to traverse to another location, and an action link which links to an action. A *markup* is a visible modification to the text on a page of a document [which includes links]. The term *hyper-link* means: a markup object which connects to another markup or to an action. An *icon anchor* is a markup represented by an icon. Even though differences exist in terminology, it is assumed that the reader can relate the two sets of terms [NAS93].

of other objects. An anchor relates nodes and objects to links. A link relates anchors.

The anchor-link-anchor relationship exists for the purpose of defining associations among objects in the hypermedia information space. An association is defined, informally, as a tuple consisting of

(nodes:objects, Anchors, Links, Anchors, nodes:objects)

In other words, a node, object, or collection of nodes and objects are related by the existence of anchors and links. A link may connect one or more nodes and objects at the source end of the link to one or more nodes and objects at the destination end of the link. An object or node may be associated with multiple anchors and links.

The visual manifest of a link on the user display is called a *link marker*. Link markers may appear in different ways such as icon, enclosed text string, a text string in a special font, or as an object which is displayed in a different color. Although links may exist without the need for link markers, in most situations, a link marker will appear at the source end of the link.

A link is *uni-directional* if it is navigable only from the source to the destination. A link which is navigable in both directions, from the source to the destination and from the destination to the source, is said to be *bi-directional*. Bi-directional links are normally accompanied by link markers which are visible at both ends of the link. Systems which provide both types of link directionality are preferred.

To be consistent with the literature, we allow the possibility of links connecting to other links thus forming a "strap"-like relationship. Navigating from the source of a strap-link to the strap will cause the ends of the strap to be activated thus providing a 1-to-N type of relationship. Although links are normally viewed and used to define 1-to-1 relationships, the implementation of links may provide M-to-N relationships in either their basic form or through the use of strap links.

Nodes, objects, anchors, links, and link markers are all assumed to be accompanied by appropriate functionality to support their existence, persistence, and operation. This functionality may reside in one or more components of the application - the application's interface, the body of the application, or the application's data management component. The placement of functionality is arbitrary and is beyond the scope of this report.

Granularity

Many organizations, including JSC, require the hypermedia system to operate in parallel with a paper document environment. The hypermedia system must mimic paper documents by presenting information in page-sized chunks. Though this strategy is effective for certain documents, a paper-based metaphor for accessing and managing electronic documents may in fact be counterproductive to user activity since the "page" may be too small or too large for certain information. The electronic environment increases the flexibility of presentation by allowing the *granularity* of information which is displayed to a user to be changed. Thus, information is viewed in terms of "chunks" rather than pages. The quantity of material in a chunk is variable and may depend upon

the complexity of the material, the display surface on which it is viewed, and level of user sophistication.

Another issue regarding granularity concerns the size of objects which may be associated with a link. Some hypermedia systems provide an object-like model in which the size of an object is determined by the user. If the user creates an object which is the size of a paragraph, the smallest identifiable unit of the object is the entire paragraph. Systems which provide character and pixel-level support may seem to provide greater flexibility but this is questionable due to the manner by which the information is used and amount of information which the user needs to associate with links. Of more importance to NASA is the ability to define link endpoints consisting of words or phrases which are embedded within textual information as well as portions of graphical objects. The critical issues here concern the association of link endpoints with their intended information and the maintenance of those relationships across subsequent versions of the document.

Annotations

Annotations provide a mechanism for personalizing documents with textual comments, graphical objects, drawings, and user-defined links. The two common methods of supporting annotations are popup notebox and marginalia (writing in the margins).

A popup notebox is requested by the user into which comments are placed. The notebox can be connected or associated with the original document in several ways but is usually done so with a link. The tool which supports the note may be the same as or different from the hypermedia system. The content of the notebox may be stored separately from the hypertext.

After entering comments into a notebox, the box is closed and the user returns to normal activities. The notebox is displayed when the user activates the notebox link or icon by clicking on it with the mouse.

Notebox tools have traditionally had limited functionality as compared to the primary application. They rarely allow the user to create links to reference other notes or allow users to create noteboxes on noteboxes in a recursive-like manner. These limitations can be very confusing since users expect the same functionality to be available. It is highly recommended that the notebox facility be an extension of the hypermedia document environment.

Another facility which is important to JSC is marginalia. A marginalia approach allows the user to write directly "on top of" documents, without invoking another tool or opening another window. Comments are normally placed in the margins of the document, but when necessary, can be placed directly on top of the information which is being displayed. This is especially valuable to support annotation of figures and drawings.

A marginalia approach employs a spatial interface metaphor whereby objects "stick" to the display wherever they are placed. This interface behavior is found in paint programs and is not characteristic of hypermedia environments. In fact, the only commercial system which supports this type of functionality is KMS [AMY88].

Both the notebox and marginalia approaches are important and necessary in the JSC environment to support user annotation. Further, systems must assist in the management of annotations by keeping track of the author of the annotation and allowing users to select or filter annotations to be displayed, printed, or edited. Such a capability also will allow users to see annotations of other users, assuming appropriate permissions are provided.

Union and intersection operations are important to support the annotation space. For example, a user could request a display of annotations created by a specified set of users as compared to being limited to seeing either all or only one user's annotations. In this regard, color can be used to distinguish among the various users.

Link Markers

Link markers are the visual manifest of a link on the user's display. They provide the initiation point for activating a link and can act as the termination point at the link's destination.

When a link is followed and the destination is reached, color can be used to focus the user's attention to the object(s) which constitute the destination. Depending on the granularity of the destination, it may be appropriate to omit coloring the destination objects in a special way. For example, if the destination is a node, coloring the entire node may be very distracting. Instead, the node's border could be colored to indicate that the link connects to the entire node. If the destination is an object in a node, the individual object may be displayed in a different color to distinguish it from the other objects in the node. The choice of color is rarely a problem in this case unless the object is extremely large.

A final issue regarding color concerns the directionality of links and the status of the objects at the destination. If the link is bidirectional, the objects at the destination may be both destinations and sources of the same link. In the case of a uni-directional link, the object(s) may be the destination of one link and the source of a different link. The basic cases that must be delineated are listed below.

- not associated with a link
- source of a link
- destination of a link
- source of one link and destination of another link
- source and destination of multiple links

Identification

A fundamental issue in hypermedia concerns the ability to identify document components in order to relate the components through links. Users must be permitted to create links which connect to specific paragraphs, sentences, or phrases. Moreover, these relationships must be maintained when new versions of the same document are released. To provide this capability, a hypermedia system must identify objects in some manner. An identification mechanism, such as that proposed by Khoshafian and Copeland [KhC86], is appropriate for supporting hypermedia for different levels of object

granularity. When this model is applied to a document environment, it requires that a unique identifier be assigned to each object and used throughout the object's life. Implementing such a mechanism in the extremely large and diverse environment of NASA will be difficult due to the problem of controlling object identifiers. Thus, an alternative approach might be to use a combination (concatenation) of the document's identifier, JSC number, and a within-document identifier. This scheme appears to be sufficient for most needs except when the same object is used in multiple documents. In this case, the identity of the object must permit reference and containment in multiple documents. Additionally, links associated with the object must maintain the context of the link, that is, relative to the document in which the reference is made.

Another problem concerns document accessibility with respect to database issues. In many cases, it is highly desirable to provide access to objects without requiring the "opening" of an entire document which contains the object. Opening an entire document from which only a small part is needed results in overhead which is generally unnecessary. Thus, objects should be viewed as entities which may exist within or separate from their associated documents.

Finally, an object identification policy must provide the ability for crew and staff to alias or name objects using slang. Generally, object identification is viewed as a system level function and is of no concern to the end user. However, maintaining an aliasing facility which is unique to individual users is both costly in terms of document storage and configuration management. Regardless, aliased object identification has been expressed on several occasions and is viewed as a necessary part of the electronic document environment. The reader can consult the final report for DTO-1209 [NAS92] concerning formal requests from crew for aliasing services.

Links

The traditional view of linking is one of the user clicking with the mouse on an icon and either the current window's contents change to display new information or another window appears with the information. This example demonstrates a 1-1 relationship between objects but also demonstrates that the view provided to the user can be implemented differently. Either the current window's contents are replaced or a new window is displayed. Both mechanisms should be supported with the user being able to control which view is provided. Alternatively, the author of the link could specify the behavior during navigation of the link. For additional information concerning the importance of link arrival and departure, the reader should consult Slatin [Sla88].

Links may be associated with objects of various sizes including entire nodes, paragraphs, sentences, words, characters, figures, video clips, rules, sounds, and so on. Due to the diversity of the information that might be associated with links, links should support arbitrary object granularity. This would allow links to connect simple, complex, or node objects. For example, a word in a sentence could be linked to a video.

Multi-endpoint links are important and should be provided. This allows an author to create a link which connects two or more objects at the source end of the link with two or more objects at the destination of the link. The objects to which the link may be attached can be of the same or different types. This would allow the user to follow a link into a

document at which time a block of text, video clip, and sound byte appear and are played simultaneously. Such a scenario would be valuable for crew training or when information from multiple documents containing objects of different types must be accessed at the same time.

The user should be allowed to define links that can be initiated automatically or manually. The traditional view of hypermedia requires that the user initiate all navigation. This view is limiting in that it requires user intervention for all linking services. It is suggested that links be viewed as functional entities which support the document viewing environment. Links may be implemented to automatically "fire" at a certain time, under certain conditions, or when other links are navigated. A system which exhibits some of this functionality is described in [StF89].

HYPERMEDIA VIEWER

A prototypical hypermedia system to support the viewing of on-line documentation for the MIDAS [Pac92] system was constructed. The viewer supports full color text, graphic, and image objects on Unix, Sun[3], workstation environments. The viewer is optimized for handling small documents and supports two "types" of documents -- a "roff-like" document construction language to facilitate document presentation and ASCII files.

There are many features of the system which are important to JSC and NASA. Some of the more notable features include spatial and notebox annotation, full-color highlighting, simple and complex boolean search, catalog management with subclassing, user customization, and integration with existing systems. A supporting component provides users with the ability to parse and extract table of contents information from documents, creating a hypertext which provides non-linear access to the document. Another support component parses incoming electronic mail and builds a multi-level hypertext relative to the day and order that messages were received. The mail component embeds hypermedia buttons into messages to facilitate replies to the sender or to delete messages that are no longer valuable.

Four types of links are supported. The types delineate the placement, appearance, and functionality of the link. Links may be spatially placed *on* a document if identification of objects in the document is not possible. Links may be *embedded within* the document to provide linking services in the event that changes to the document affect the position of an object or if links are to "travel" with the document to support distribution. Links may be used to initiate applications, including the viewer itself. They can be packaged with search arguments to assist the user in locating information through a single mouse click. Automatic links allow the user to identify words or phrases which are defined across all documents and provide access to a document, perform a search, or initiate a process.

Links persist in both embedded and non-embedded forms and are managed by a hypermedia data management component. Users can create links which are maintained in a personal link space and are unavailable to other users. The linking mechanism also

[3] Sun is a trademark of Sun Microsystems, Inc.

allows multiple users to share a common set of links over a document space.

The embedded link mechanism permits users to place links within documents so that links travel with and are maintained as part of the document content. In this case, the link is not associated with a particular user since user identification is not supported. The link is therefore a *public* entity and is accessible by all users of the document. One of the advantages of the embedded link mechanism is that it allows the creation of hypermedia documents by non-hypermedia components. For example, a background process could create a document containing embedded links and initiate the viewer to provide non-linear navigation over the document. Moreover, the process could run continually, affecting the content and structure of the hypertext dynamically. Such a process would not have to concern itself with interface, navigation, or search issues since all of these services are provided by the hypermedia viewer.

CHALLENGES AND UNTAPPED ISSUES

There are many challenges which face the use of hypermedia throughout NASA as well as other organizations. Some of these challenges are being addressed in current research while others remain virtually unexplored. In this section we present a few issues which have the potential of offering enhanced access or presentation features to the electronic environments at JSC, or which appear to present a significant challenge to the successful deployment of hypermedia throughout the Agency.

Cross-vendor compatibility

It is obvious that several systems must exist in order to support the various operations at NASA. Many of these systems utilize a proprietary format for storing information or exchanging information between components and are designed to operate on a unique computing platform. These limitations result in systems which are incompatible with others even though they may be implemented for the same computing platform. This lack of compatibility and interoperability is well documented in the literature and is regarded as a major limitation in hypermedia system design [Eng78, Eng82, Mey89, BoR90, Ril90].

Systems which exist as "islands" and which are unable and incapable of sharing information and procedures with other systems are inappropriate for the long-term goals of JSC. Since it is impossible for a single system to meet every need of JSC and NASA, multiple systems must exist within the framework of a larger environment. This requires vendors to cooperate and develop systems which are capable of interacting and exchanging information, especially in a sense much broader than the dynamic data exchange (DDE) services which some systems provide. This necessitates an overall plan of integration whereby systems coexist in a seamless manner to support ground and space operations.

An interoperable framework offers many benefits, one of which is the ability to add new components. Another benefit is the ability to migrate to new or updated systems which provide increased capabilities. Migration can be accomplished without requiring transformations of information or loss of functionality if systems utilize a compatible data

substrate. Achieving this level of interoperability will empower users by providing them with a collection of tools that can be used and tailored to meet specific needs. Therefore, an important task is to establish a framework for the interchange and sharing of information, and the integration of diverse systems within the NASA computing environment.

A related issue concerns a much broader view of the migration concept. This view is only now being considered within the scope of hypermedia systems but in fact has been an issue which has been addressed in other disciplines. The issue concerns the migration of processes to support computation.

The earlier paragraphs presented the issue of migration as one involving the movement of information, i.e. documents, around an information space. If one views the software components as "information", the migration issue equally applies. This perspective provides for the migration of processes among workstations to improve performance and distribute the workload. It also allows for recovery of a process if a workstation fails. To plan for the long-term needs of the Center, it is important to consider systems which utilize such architectures, allowing their components to be distributed and migrated without a negative effect on user activity.

Composition and Computation

The hypermedia research community has been exploring issues of *composition* and *computation* [Hal88] for quite some time. Composition is the construction of objects from other objects in the information space while computation involves dynamic, "on the fly", determination of object content and structure.

The incorporation of these capabilities into hypermedia systems appears to be very important to the immediate and long-term goals of electronic documentation at NASA for several reasons. First, hypermedia systems have traditionally employed a monolithic architecture and static data model [Mey89]. The monolithic (single process) architecture inhibits interoperability, as described in the previous section, and the static data model requires all links to be defined prior to the time of access. Clearly, the costs of manually defining every link is prohibitive given the enormous number of documents which exist in the NASA environment. Therefore, methods must be used to create links automatically and reliably on demand.

Second, users have different document access needs and for this reason it is important for a hypermedia system to construct links based on specifications from or information about a user. In order for this to be accomplished in a hypermedia framework, the content and the structure of objects must be determined on the fly.

Third, information can be a reusable resource in that it may be used in multiple documents. To support reusability in most existing hypermedia systems, information must be duplicated. Duplication is not cost effective given the tremendous number of documents which will exist in electronic form within the NASA community.

Systems which support referential and inclusion links and utilize a non-embedded hypermedia data model offer the greatest potential for supporting computability and

composition. Multiple link types based on reference and inclusion-style linking allow the user to construct hypertexts that can be used more effectively to tailor the presentation of information. Non-embedded links allow the system to determine link destinations without accessing the underlying documents. This allows the hypermedia engine to service the needs of multiple applications within a single computing environment. This type of design expands the scope of hypermedia by provides linking services "across" applications rather than limiting services to a single or selected class of applications. Further, this design allows the hypermedia engine to play an active role in support exploratory access from a structural perspective. For example, the hypermedia engine could construct and display a graphical map of the document space based on the current contents and relationships which exist among the documents. As another example, the engine could provide a list of all documents which contain a particular object and which is linked to a specific document and which consists of at least 4 chapters.

Finally, it is important not to confuse the issue of computation with that of automatic linking. Computation involves much more, specifically, the construction of the objects to be displayed as well as the construction of links that are associated with the object. In contrast, automatic linking can be implemented over a static data space and not involve any *computation* on the part of the hypermedia engine or application.

Distribution

The enormous number of documents and potential users necessitate an efficient and accurate distribution system throughout NASA. Unfortunately, no hypermedia system or research effort has addressed this issue. For this reason we identify this as an important issue and one that deserves special consideration.

There are various ways to think of document distribution which include the distribution of the underlying document, public and private links, and user-defined annotations. Obviously, the goal of a distribution system is to permit timely and easy access to documents. We identify and outline a few specific scenarios to demonstrate some of the possible responsibilities of a distribution system.

New document. A new document is released to the organization. The document has zero or more links. A list of target users, i.e. a distribution list, identifies a preliminary set of users to send the document and its links.

The potential problems concerning the distribution of a new document relate to the links which are associated with the document. More than likely, the links associated with this document will reference other documents in the information space. If the user is not on the distribution list for any one of the destination documents, the links which provide the reference are invalid for that user. This requires the hypermedia engine to coordinate document distribution and access lists with link visibility to avoid incorrect presentation of links when the document is viewed. Alternatively, links may serve as a specification for adding users to a document's distribution list and distributing the document to the user automatically.

Updated document. The release or versioning of a document incurs many of the same problems as those associated with a new document but also has the problem that any user-

defined links and annotations must be merged into the new release. Various mechanisms can be used to relate annotations and links with their intended positions, but depending on the degree of change to the document, some mechanisms may not adequately preserve these relationships. This usually results in dangling objects and links, or objects which must be discarded because their relationship to the new version cannot be determined. Clearly, the number of objects which must be discarded must be minimized in the NASA environment.

Cross platform and system. Users who conduct activities on multiple computing platforms or use multiple software systems risk inconsistency in versions of the same document. For example, if a user has access to a document on a personal computer and access to the "same" document on a workstation, the annotations and links defined by the user on their personal computer will probably not carry over to the workstation environment or vice versa, unless of course the two systems are networked and the document is shared between the systems or the user transports a copy of the document between the systems on a backup device (e.g. floppy disk). Clearly, requiring the user to manage documents and their distribution manually would involve significant time commitments for users given the number of documents to which they might refer. The networked solution is therefore more appropriate but requires the distribution system to have access to all computing platforms used by an individual and to maintain the annotations made to a document. This requires that all annotations and links be in the same format, a mapping operation occur to convert annotations made on one machine to a form which can be used on another, or all machines store and access annotations from a central repository.

Informal sharing. A final problem concerns the informal sharing of documents and annotations among users. In this case, a user shares a document with another user without the distribution system being informed of this activity. The new user proceeds to create annotations and links for this document in isolation and remains dependent on their friend for information about updates. This is problematic if the distribution system provides the mechanism for coordinating updates with user-defined annotations and links. Since the informal user is not on the distribution list, their annotations will not be merged into the new version. Although this may not be a problem for the first few releases of a document, it is probable that the informal user will eventually cease updating the versions with their annotations. Thus, the informal user eventually becomes completely out of sync with the release of the document due to their inability or unwillingness to maintain annotations and links.

SUMMARY

Electronic documents and systems are becoming an important means of managing information for ground and space operations at NASA. Hypertext and hypermedia technologies will play a strategic role in the management of information by allowing users to structure and access information by navigation.

This report has outlined some of the uses and problems facing the implementation and deployment of hypermedia systems at JSC. It also presents a brief description of a hypermedia system that was developed to support and demonstrate hypermedia capabilities for on-line documentation. Finally, the report discusses some hypermedia

technologies which have either been untapped by vendors or present significant challenges to the Agency.

REFERENCES

[AMY88] R. Akscyn, D. McCracken, and E. Yoder, "KMS: A distributed hypermedia system for managing knowledge in organizations," *Commun. ACM* **31**(7), 820-835 (July 1988).

[BoR90] J. Bornstein and V. Riley, "Hypertext interchange format," *Proceedings of the Hypertext Standardization Workshop*, pp. 39-47 (January 1990).

[Eng78] D. C. Engelbart, "Toward integrated, evolutionary office automation systems," *Proceedings of of the International Engineering Management Conference*, pp. 63-68 (October 1978).

[Eng82] D. C. Engelbart, "Integrated, evolutionary, office automation systems," pp. 298-315 in *Emerging Office Systems, Proceedings of the Stanford International Symposium on Office Automation.*, ed. R. Landau, J. Bair, and J. Siegman,Ablex Publications Corporation, Norwood, NJ (1982).

[Hal88] F. Halasz, "Reflections on NoteCards: Seven issues for the next generation of hypermedia systems," *Commun. ACM* **31**(7), 836-852 (July 1988).

[KhC86] S. Khoshafian and G. Copeland, "Object identity," *Proceedings of the Conference on Object-Oriented Programming Systems, Languages, and Applications - OOPSLA '86, Sigplan Notices* **21**(11), 406-416 (November 1986).

[Mey89] N. Meyrowitz, "The missing link: Why we're all doing hypertext wrong," 107-114 in *The Society of Text: Hypertext, Hypermedia, and the Social Construction of Information*, ed. E. Barrett,The MIT Press (1989).

[NAS92] NASA/JSC-DTO1209, "Development Test Objective (DTO) 1209 Advanced Portable Computer Evaluation - Final Report," NASA JSC Report #JSC-25588, Johnson Space Center, Houston, TX (December, 1992).

[NAS93] NASA/JSC-EDP, "Electronic Documentation Project (EDP):Level A requirements," NASA JSC Report #JSC-TBD, Johnson Space Center, Houston, TX (June, 1993).

[Nel65] T. H. Nelson, "A file structure for the complex, the changing, and the indeterminate," *Proceedings of the 20th National ACM Conference*, pp. 84-100 (1965).

[Pac92] G. Pack, "Application of Automation and Intelligent Software to Analysis of Engineering Space Shuttle Systems - Mission Evaluation Room (MER) Intelligent Diagnostic and Analysis System (MIDAS)," 1992 JSC Research and Development Accomplishments Report (RADAR) Inputs Schedule, IA4, Chief Technologist, New Initiatives Office, Johnson Space Center, Houston, TX (1992).

[Ril90] V. A. Riley, "An interchange format for hypertext systems: The intermedia model," *Proceedings of the Hypertext Standardization Workshop*, pp. 213-222 (January 1990).

[Sla88] J. Slatin, "Toward a rhetoric for hypertext," *Hypermedia '88 Conference*, (August 1988).

[StF89] P. D. Stotts and R. Furuta, "Petri-net based hypertext: Document structure with browsing semantics," *ACM Trans. Off. Inf. Syst.* 7(1), 3-29 (January 1989).

REPORT DOCUMENTATION PAGE

Form Approved
OMB No. 0704-0188

Public reporting burden for this collection of information is estimated to average 1 hour per response, including the time for reviewing instructions, searching existing data sources, gathering and maintaining the data needed, and completing and reviewing the collection of information. Send comments regarding this burden estimate or any other aspect of this collection of information, including suggestions for reducing this burden, to Washington Headquarters Services, Directorate for information Operations and Reports, 1215 Jefferson Davis Highway, Suite 1204, Arlington, VA 22202-4302, and to the Office of Management and Budget, Paperwork Reduction Project (0704-0188), Washington , DC 20503.

1. AGENCY USE ONLY (Leave Blank)	2. REPORT DATE	3. REPORT TYPE AND DATES COVERED
	Dec/93	Contractor Report

4. TITLE AND SUBTITLE
National Aeronautics and Space Administration (NASA)/American Society for Engineering Education (ASEE) Summer Faculty Fellowship Program - 1993, Volumes 1 and 2

5. FUNDING NUMBERS

6. AUTHOR(S)
William A. Hyman* and Stanley H. Goldstein, Editors

7. PERFORMING ORGANIZATION NAME(S) AND ADDRESS(ES)
Johnson Space Center
Houston, Texas 77058

8. PERFORMING ORGANIZATION REPORT NUMBERS

9. SPONSORING/MONITORING AGENCY NAME(S) AND ADDRESS(ES)
National Aeronautics and Space Administration
Washington, D.C. 20546-0001

10. SPONSORING/MONITORING AGENCY REPORT NUMBER
CR 188271

11. SUPPLEMENTARY NOTES
* Texas A&M University, College Station, Texas

12a. DISTRIBUTION/AVAILABILITY STATEMENT
unclassified/unlimited
Available from the National Technical Information Service, 5285 Port Royal Road, Springfield, VA 22161 (703) 487-4600.

Subject Category: 99

12b. DISTRIBUTION CODE

13. ABSTRACT *(Maximum 200 words)*

The JSC NASA/ASEE Summer Faculty Fellowship Program was conducted by Texas A&M University and JSC. The objectives of the program, which began nationally in 1964 and at JSC in 1965, are (1) to further the professional knowledge of qualified engineering and science faculty members; (2) to stimulate an exchange of ideas between participants and NASA; (3) to enrich and refresh the research and teaching activities of participants' institutions; and (4) to contribute to the research objectives of the NASA centers. Each faculty fellow spent at least 10 weeks at JSC engaged in a research project in collaboration with a NASA/JSC colleague. This document is a compilation of the final reports on the research projects completed by the faculty fellows during the summer of 1993.

14. SUBJECT TERMS
information transfer, research , research projects, urban research, engineering, science, universities, university program

15. NUMBER OF PAGES
488

16. PRICE CODE

17. SECURITY CLASSIFICATION OF REPORT	18. SECURITY CLASSIFICATION OF THIS PAGE	19. SECURITY CLASSIFICATION OF ABSTRACT	20. LIMITATION OF ABSTRACT
unclassified	unclassified	unclassified	UL